

DUAL FUNCTIONALIZED COCONUT SHELL  
BIOADSORBENT WITH CHLORELLA MICROALGAE AND  
MAGNESIUM OXIDE FOR ENHANCED CO<sub>2</sub> CAPTURE

NURADILA ZAHIRAH BINTI MOHD AZMI

FACULTY OF ENGINEERING  
UNIVERSITI MALAYA  
KUALA LUMPUR

2025

**DUAL FUNCTIONALIZED COCONUT SHELL  
BIOADSORBENT WITH CHLORELLA MICROALGAE  
AND MAGNESIUM OXIDE FOR ENHANCED CO<sub>2</sub>  
CAPTURE**

**NURADILA ZAHIRAH BINTI MOHD AZMI**

**THESIS SUBMITTED IN FULFILMENT OF THE  
REQUIREMENTS FOR THE DEGREE OF DOCTOR OF  
PHILOSOPHY**

**FACULTY OF ENGINEERING  
UNIVERSITI MALAYA  
KUALA LUMPUR**

**2025**

**UNIVERSITI MALAYA**  
**ORIGINAL LITERARY WORK DECLARATION**

Name of Candidate: Nuradila Zahirah binti Mohd Azmi

Matric No: s2022703/1

Name of Degree: Doctor of Philosophy

Title of Thesis: Dual Functionalized Coconut Shell Bioadsorbent with  
Chlorella Microalgae and Magnesium Oxide for Enhanced CO<sub>2</sub> Capture

Field of Study: Advanced Materials & Technology (NEC 524: Chemical and Process)

I do solemnly and sincerely declare that:

- (1) I am the sole author/writer of this Work;
- (2) This Work is original;
- (3) Any use of any work in which copyright exists was done by way of fair dealing and for permitted purposes and any excerpt or extract from, or reference to or reproduction of any copyright work has been disclosed expressly and sufficiently and the title of the Work and its authorship have been acknowledged in this Work;
- (4) I do not have any actual knowledge nor do I ought reasonably to know that the making of this work constitutes an infringement of any copyright work;
- (5) I hereby assign all and every rights in the copyright to this Work to the Universiti Malaya ("UM"), who henceforth shall be owner of the copyright in this Work and that any reproduction or use in any form or by any means whatsoever is prohibited without the written consent of UM having been first had and obtained;
- (6) I am fully aware that if in the course of making this Work I have infringed any copyright whether intentionally or otherwise, I may be subject to legal action or any other action as may be determined by UM.

Candidate's Signature

Date: **10/4/2025**

Subscribed and solemnly declared before,

Witness's Signature

Date: **10/4/2025**

Name:

Designation:

# **DUAL FUNCTIONALIZED COCONUT SHELL BIOADSORBENT WITH CHLORELLA MICROALGAE AND MAGNESIUM OXIDE FOR ENHANCED CO<sub>2</sub> CAPTURE**

## **ABSTRACT**

The increasing carbon dioxide emissions resulting from industrial and human activities require the implementation of effective carbon capture systems. Adsorption using solid adsorbents, such as activated carbon has emerged as the most preferred among other technologies due to its simplicity and wide range of applications for CO<sub>2</sub> adsorption and utilization. Nevertheless, conventional solid adsorbents have limitations such as the need for complex regeneration processes, poor efficiency, dependence on non-renewable resources, and high energy consumption for production. Hence, this study aims to develop a green bio-adsorbent from coconut shell (CS) which is a type of agricultural waste, to capture CO<sub>2</sub>, aligning with the principles of the circular economy. CS was chosen as a precursor for the synthesis of a bio-adsorbent due to its abundant access, with a worldwide production of 63.7 million metric tonnes annually. However, raw CS exhibits low adsorption efficiency due to lower carbon-to-surface ratio and surface area availability. To overcome this limitation, potassium hydroxide was used to activate the carbonised CS, hence promoting the development of a porous structure in an energy-efficient and alkaline environment. Further enhancement involved dual-functionalisation using *Chlorella* microalgae and magnesium oxide (MgO) to introduce nitrogen and metal oxide functional groups, enhancing CO<sub>2</sub> capture further due to basicity. The characterisation revealed the successful development of the ternary composite bio-adsorbent, functionalised with microalgae and MgO (HCS-N-Mg), with specific surface area of 1045 m<sup>2</sup>/g, which is as high as the conventional activated carbon, and containing nitrogen and MgO functional groups. XRD analysis of HCS-N-Mg reveals crystalline peaks at 36.8°, 42.9°, and 62.4°, confirming the successful impregnation of MgO. The

CO<sub>2</sub> adsorption experiments were conducted using High-Pressure Volumetric Analysis, examining the effects of temperature and pressure using a design of experiments. The dual functionalised CS with microalgae and MgO, HCS-N-Mg, exhibits 50% higher CO<sub>2</sub> adsorption capacity (2.63 mmol/g) than pristine bio-adsorbent, HCS (1.75 mmol/g). Statistical analyses suggest that the adsorption capacity of HCS-N-Mg is influenced by pressure, temperature, and their interaction. Adsorption isotherms show that the non-linear Sips model best describes the CO<sub>2</sub> adsorption onto HCS-N-Mg, indicating multilayer adsorption with surface heterogeneity of  $n=2.3$ , providing various adsorption sites for CO<sub>2</sub> binding. Additionally, thermodynamic analysis confirms the chemisorption and stability of HCS-N-Mg at 25-75°C, with an enthalpy of -20.45 kJ/mol, compared to -13.23 kJ/mol for HCS, with stable adsorption at 25-50°C, indicating higher stability at elevated temperatures. Density functional theory (DFT) was applied to determine the CO<sub>2</sub> adsorption mechanism onto bio-adsorbent surfaces. DFT result demonstrated that the dual-functionalisation enhances the binding interactions between the carbon surface and CO<sub>2</sub>. Compared to conventional adsorbent, HCS-N-Mg outperforms by 40%, highlighting the potential of microalgae and MgO in advancing carbon capture technology and addressing environmental challenges.

**Keywords:** Metal oxide, Hydrothermal carbonisation; Biomass adsorbent; Design of experiment, Gas selectivity

**DWI-PENGFUNGSIAN BIOADSORBEN DI OLAH DARI TEMPURUNG  
KELAPA DENGAN MIKROALGA CHLORELLA DAN MAGNESIUM  
OKSIDA BAGI PENINGKATAN PENYERAPAN CO<sub>2</sub>**

**ABSTRAK**

Kepesatan ekonomi serta aktiviti industri dan manusia menyebabkan peningkatan pelepasan karbon dioksida, menjurus kepada keperluan system penangkapan karbon yang efisien. Antara kaedah yang popular ialah penangkapan CO<sub>2</sub> melalui penyerapan gas-pepejal dengan menggunakan penyerap bersifat pepejal kerana kesederhanaannya dan boleh digunakan melalui pelbagai cara untuk menyerap dan menggubah CO<sub>2</sub>. Walau bagaimanapun, keberkesanan penyerap bersifat pepejal yang konvensional adalah terhad kerana keperluan proses regenerasi yang kompleks, kecekapan yang rendah, kebergantungan pada sumber tidak boleh diperbaharui, dan penggunaan tenaga yang tinggi untuk penghasilan bahan penyerap. Oleh itu, kajian ini bertujuan untuk menghasilkan bio-adsorben hijau daripada sisa biojisim tempurung kelapa (CS) untuk menyerap CO<sub>2</sub>, selaras dengan prinsip ekonomi pekeliling. CS dipilih sebagai bahan mentah bagi penghasilan bio-adsorben kerana ketersediaannya yang meluas, pengeluaran global sebanyak 63.7 juta metrik tan setiap tahun. CS yang tidak diolah menunjukkan kecekapan penyerapan yang rendah kerana nisbah karbon-ke-permukaan yang rendah dan kawasan permukaan yang terhad. Kalium hidroksida digunakan untuk mengaktifkan CS yang dikarbonkan, seterusnya menggalakkan penghasilan struktur berliang dalam persekitaran beralkali yang cekap tenaga. Seterusnya, pengfungsian secara dwi terhadap bio-adsorben dengan menggunakan mikroalga *Chlorella* dan magnesium oksida (MgO) dilaksanakan bagi memperkenalkan kumpulan fungsian nitrogen dan oksida logam, seterusnya meningkatkan penangkapan CO<sub>2</sub> kerana kebiasaan. Ciri-ciri fisiokimia seperti morfologi permukaan, kumpulan berfungsi, serta perlakuan terma bagi bahan mentah dan bio-adsorben berasaskan CS telah dianalisa.

Pencirian mendedahkan keberjayaan dalam penghasilan komposit bio-adsorben ternari, difungsikan dengan mikroalga dan MgO (HCS-N-Mg), dengan kawasan permukaan spesifik 1045 m<sup>2</sup>/g, serupa dengan karbon teraktif konvensional, dan mengandungi kumpulan berfungsi nitrogen dan MgO. Analisis XRD HCS-N-Mg menunjukkan keberadaan puncak kristal pada 36.8°, 42.9°, dan 62.4°, yang mengesahkan keberjayaan pengfungsian MgO. Kajian penjerapan CO<sub>2</sub> dijalankan dengan menggunakan Analisis Volumetrik Tekanan Tinggi bagi mengkaji kesan suhu dan tekanan dengan menggunakan *Design of Experiment*. Tempurung kelapa berdwi-fungsi dengan mikroalga dan MgO, menunjukkan kapasiti penjerapan CO<sub>2</sub> yang 50% lebih tinggi (2.63 mmol/g), berbanding dengan bio-adsorben asal (1.75 mmol/g). Analisis statistik mendapati bahawa kapasiti penjerapan HCS-N-Mg dipengaruhi oleh tekanan, suhu, dan interaksi antara kedua-dua pembolehubah. Isotherma penjerapan menunjukkan bahawa model isotherma Sips dengan regresi tidak linear paling sesuai dalam menerangkan penjerapan CO<sub>2</sub> ke atas HCS-N-Mg, dimana penjerapan berbilang lapisan dengan heterogenitas permukaan n=2.3, menyediakan pelbagai tapak penjerapan untuk pengikatan CO<sub>2</sub>. Selain itu, analisis termodinamik mengesahkan kemisorpsi dan kestabilan penjerapan HCS-N-Mg pada 25-75°C, dengan entalpi -20.45 kJ/mol, berbanding -13.23 kJ/mol bagi HCS, dengan penjerapan stabil pada 25-50°C, menunjukkan kestabilan yang lebih tinggi pada suhu yang lebih tinggi. Teori fungsi ketumpatan (DFT) digunakan untuk menentukan mekanisme penjerapan CO<sub>2</sub> ke atas permukaan bio-adsorben. Keputusan DFT menunjukkan bahawa pengdwi-fungsian meningkatkan daya ikatana antara permukaan karbon dan CO<sub>2</sub>. Berbanding dengan adsorben konvensional, prestasi penjerapan HCS-N-Mg 40% lebih tinggi, menonjolkan potensi mikroalga dan MgO dalam memajukan teknologi penjerapan karbon dan menangani pencemaran alam sekitar.

**Kata kunci:** *Oksida logam, Karbonisasi hidroterma; Adsorben biojisim; Reka bentuk eksperimen, Kecenderungan gas*

## ACKNOWLEDGEMENTS

Alhamdulillah. Praise be to Allah the Almighty God, the most gracious and the most merciful, for granting me the strength, patience, and perseverance to complete this PhD journey. First and foremost, I am profoundly grateful to my supervisors, Professor Ir. Dr. Abdul Aziz Abdul Raman, Ch.M. Dr. Archina Buthiyappan and Dr. Muhammad Fazly Abdul Patah for their continuous efforts in guiding and encouraging me as well as their patience during the course of conducting the research and completing this thesis. Their never-ending compassion and willingness of guidance are indeed crucial for me to finish this research on time and the right track. I am grateful for their contributions and kindness. I also extend my gratitude to University Teknologi Petronas, Dr. Surianti and Dr. Adilla, for their assistance during the research.

To my family, whose love and encouragement have been my constant source of strength, thank you. To my parents, Dr. Mohd Azmi Mohd Lila and Mrs. Rohani Maidin, thank you for your endless support and for believing in me even when I doubted myself. To my siblings, Farhana, Danial, and Loqman, your encouragement and understanding have meant the world to me. I am also grateful to my colleagues at Universiti Malaya for creating a stimulating and supportive environment. Special thanks to Miss Tan Yan Ying, Mrs. Fathimath Afrah, Mrs Zainab, Mr. Zhang Xinggang, Mrs. Jayaprina Gopalan, Miss Amy Aynee Chan and Mr. Pu Wei for your camaraderie, collaboration, and for making this journey more enjoyable.

My sincere appreciation goes to the Fundamental Research Grant Scheme (FRGS) FP095-2022, for financially supporting this research work. Lastly, I am indebted to all the participants, collaborators, and anyone who contributed directly or indirectly to this work. Your contributions have been invaluable, and this thesis would not have been possible without your support.



## TABLE OF CONTENTS

Abstract .....	iii
Abstrak .....	v
Acknowledgements .....	vii
Table of Contents .....	viii
List of Figures .....	xiii
List of Tables.....	xvii
List of Symbols and Abbreviations.....	xix
<b>CHAPTER 1: INTRODUCTION.....</b>	<b>1</b>
1.1 Background study .....	1
1.2 Problem statement .....	3
1.3 Research questions.....	5
1.4 Aim and objectives .....	6
1.5 Scope of the study.....	7
1.6 Thesis outline.....	7
<b>CHAPTER 2: LITERATURE REVIEW.....</b>	<b>10</b>
2.1 Carbon capture utilisation and storage .....	10
2.2 CO <sub>2</sub> adsorption.....	12
2.2.1 Physisorption and chemisorption .....	15
2.3 Porous adsorbent for carbon dioxide adsorption .....	16
2.3.1 Challenges and limitation of conventional adsorbents.....	18
2.3.2 Adsorbent from waste materials.....	21
2.3.2.1 Coconut shells as biomass adsorbent precursor for carbon capture .....	26

2.3.2.2	Limitation of unmodified bio-adsorbent derived from coconut shell .....	28
2.4	Synthesis methods of adsorbent from waste material.....	30
2.4.1	Carbonisation.....	31
2.4.2	Activation .....	31
2.4.2.1	Physical activation.....	32
2.4.2.2	Chemical activation.....	33
2.5	Operating parameters affecting the synthesis process of adsorbent.....	36
2.5.1	Effect of activating agent.....	36
2.5.2	Effect of holding temperature.....	39
2.5.3	Effect of impregnation ratio .....	40
2.6	Functionalisation of carbon materials.....	42
2.6.1	Heteroatoms.....	42
2.6.2	Metal oxides .....	45
2.7	Significant physicochemical characteristics of adsorbent .....	46
2.7.1	Porosity and surface area.....	46
2.7.2	Surface chemistry .....	49
2.7.3	Thermal stability.....	50
2.8	Recent advances in adsorption prediction for practical application .....	51
2.9	Summary.....	54
<b>CHAPTER 3: METHODOLOGY.....</b>		<b>56</b>
3.1	Overall methodology .....	56
3.2	Materials and chemicals .....	58
3.3	Synthesis of adsorbent .....	58
3.3.1	Carbonisation process.....	60
3.3.2	Chemical activation of the adsorbent .....	62

3.3.3	Functionalisation of bio-adsorbent with magnesium oxide .....	62
3.3.4	Functionalisation of bio-adsorbent with microalgae .....	63
3.4	Adsorbent characterisations.....	64
3.5	Design of experiment.....	65
3.6	Carbon dioxide adsorption study .....	65
3.6.1	Sample preparation.....	67
3.6.2	Sample Degassing .....	68
3.6.3	HPVA II analysis.....	69
3.7	Adsorption mechanism .....	71
3.7.1	Adsorption isotherm .....	71
3.7.2	Adsorption thermodynamics .....	73
3.8	Quantum chemical calculation .....	74
3.9	Safety precautions.....	75
<b>CHAPTER 4: RESULTS AND DISCUSSION .....</b>		<b>78</b>
4.1	Introduction.....	78
4.2	Optimisation of bio-adsorbent synthesis from coconut shell .....	78
4.2.1	Coconut shell bio-adsorbent.....	79
4.2.1.1	Statistical analysis .....	79
4.2.1.2	Effect of operating condition on the hydrochar yield, bio-adsorbent yield and CO <sub>2</sub> adsorption capacity.....	88
4.2.1.3	Modelling optimisation of synthesis process .....	109
4.2.2	Coconut shell bio-adsorbent functionalised with magnesium oxide.....	111
4.2.2.1	Effect of impregnation method on CO <sub>2</sub> adsorption.....	111
4.2.2.2	Optimisation of concentration of magnesium oxide .....	113
4.2.3	Bio-adsorbent functionalised with microalgae.....	116

4.2.3.1	Effect of functionalisation method of microalgae on the CO <sub>2</sub> adsorption capacity.....	116
4.2.3.2	Effect of microalgae concentration on the CO <sub>2</sub> adsorption capacity.....	118
4.2.3.3	Comparison CO <sub>2</sub> adsorption capacity of raw microalgae, hydrochar microalgae, pyrochar microalgae and coconut shell bio-adsorbent functionalised with microalgae .....	119
4.2.4	Selection of adsorbents based on the bio-adsorbent yield and CO <sub>2</sub> adsorption capacity.....	131
4.3	Physicochemical characteristic of adsorbent.....	132
4.3.1	Surface area and porosity .....	133
4.3.2	Surface chemistry .....	136
4.3.3	Crystallographic structure .....	139
4.3.4	Surface morphology .....	142
4.3.5	Elemental analysis .....	147
4.3.6	Thermogravimetric analysis .....	149
4.3.7	Comparison of physicochemical properties of pristine and functionalised coconuts shell-based bio-adsorbents .....	152
4.4	Carbon dioxide adsorption capacity evaluation.....	154
4.4.1	Statistical analysis .....	158
4.4.2	Effect of operating parameters on the CO <sub>2</sub> adsorption capacity .....	163
4.4.2.1	Adsorption temperature.....	163
4.4.2.2	Adsorption pressure.....	168
4.4.3	Optimisation and validation study of CO <sub>2</sub> adsorption performance .....	170
4.4.4	Adsorption performance evaluation of different types of functionalised bio-adsorbent based on published literature .....	172

4.5	Isotherm analysis .....	174
4.6	Thermodynamic analysis .....	178
4.7	Mechanism study .....	179
4.8	Molecular modelling and simulation .....	181
4.8.1	Electrostatic potential analysis .....	181
4.8.2	Highest occupied and lowest unoccupied molecular orbital .....	186
4.8.3	Adsorption energy and binding distance analysis .....	190
4.9	CO <sub>2</sub> /N <sub>2</sub> selectivity of bio-adsorbent .....	196
4.10	Reusability study .....	199
4.11	Comparison of adsorption performance of hybrid CS-bio-adsorbents with various activated carbon .....	200
4.12	Commercialization prospects of dual-functionalised bio-adsorbent relative to pristine bio-adsorbent and with commercial activated carbon .....	203
4.12.1	Economic analysis .....	203
4.12.2	Environmental analysis.....	206
4.12.3	Feasibility of industrial upscaling of dual-functionalised bio-adsorbent .	208
<b>CHAPTER 5: CONCLUSION AND RECOMMENDATIONS .....</b>		<b>211</b>
5.1	Conclusion .....	211
5.2	Significance of the study .....	213
5.3	Knowledge contributions and novelty .....	214
5.4	Potential Application .....	215
5.5	Recommendation for future work.....	216
References .....		218
List of Publications and Papers Presented .....		253

## LIST OF FIGURES

Figure 1.1: Global activated carbon market forecast .....	2
Figure 1.2: Desirable characteristics of adsorbent for CO <sub>2</sub> capture.....	3
Figure 2.1: Adsorption and desorption process of gas molecules into carbon surface ...	13
Figure 2.2: Statistics of studies on adsorbent precursor from biomass (2013-2020).....	21
Figure 2.3: Synthesis process of activated carbon .....	30
Figure 2.4: Pore structure of an activated carbon .....	47
Figure 2.5: Classification of (a) isotherm based on N <sub>2</sub> physisorption, and, (b) types of hysteresis .....	48
Figure 3.1: Flow diagram representing the overall methodological approach of the study .....	57
Figure 3.2: (a) Granulator and (b) table grinder.....	59
Figure 3.3: (a) Raw CS at the collection stage, (b) Raw CS after cleaning, washing and granulation, and (c) Raw powdered CS .....	59
Figure 3.4: High Pressure Volumetric Analyser (HPVA II).....	66
Figure 3.5: Schematic diagram of HPVA II.....	67
Figure 3.6: (a) Sample chamber, (b) housing, and (c) filter gasket .....	68
Figure 3.7: Manual control screen of HPVA II.....	69
Figure 4.1: Diagnostic plot of model adequacy: (a-c) normal probability plot of Y <sub>1</sub> , Y <sub>2</sub> and Y <sub>3</sub> ; (d-f) predicted vs. actual response of Y <sub>1</sub> , Y <sub>2</sub> and Y <sub>3</sub> .....	85
Figure 4.2: Contour plot of carbonisation time (X <sub>1</sub> ) and carbonisation temperature (X <sub>2</sub> ) vs. response Y <sub>1</sub> .....	89
Figure 4.3: Contour plot of carbonisation time (X <sub>1</sub> ) and carbonisation temperature (X <sub>2</sub> ) vs. Y <sub>2</sub> .....	91
Figure 4.4: Contour plot of carbonisation time (X <sub>1</sub> ) and carbonisation temperature (X <sub>2</sub> ) vs. Y <sub>3</sub> .....	92
Figure 4.5: Contour plot of carbonisation temperature (X <sub>2</sub> ) and carbonisation time (X <sub>1</sub> ) vs. hydrochar yield (Y <sub>1</sub> ) .....	94

Figure 4.6: 3D surface plots of Carbonisation time ( $X_1$ ) and carbonisation temperature ( $X_2$ ) vs. response $Y_1$ .....	95
Figure 4.7: 3D surface plots of Carbonisation time ( $X_1$ ) and solid weight % ( $X_3$ ) vs. response $Y_1$ .....	96
Figure 4.8: Energy dispersion x-ray spectroscopy of hydrochars.....	98
Figure 4.9: Van Krevelen diagram of hydrochar at different HTC condition .....	99
Figure 4.10: Response surface plot of carbonisation time ( $X_1$ ) and carbonisation temperature ( $X_2$ ) vs. response bio-adsorbent yield ( $Y_2$ ) .....	101
Figure 4.11: Effect of carbonisation temperature on (a) $Y_1$ , (b) $Y_2$ , and (c) $Y_3$ . .....	102
Figure 4.12: Contour plot of solid weight percentage ( $X_3$ ) and carbonisation time ( $X_1$ ) vs. response $Y_1$ .....	104
Figure 4.13: Contour plot of solid weight percentage ( $X_3$ ) and carbonisation temperature ( $X_2$ ) vs. response $Y_2$ . .....	105
Figure 4.14: Contour plot of solid weight percentage ( $X_3$ ) and carbonisation temperature ( $X_2$ ) vs. response $Y_3$ . .....	106
Figure 4.15: Perturbation plot for response (a) hydrochar yield ( $Y_1$ ), (b) bio-adsorbent yield ( $Y_2$ ), and (c) $CO_2$ adsorption capacity ( $Y_3$ ).....	108
Figure 4.16: Effect of MgO functionalisation method onto $CO_2$ adsorption capacity of HCS.....	112
Figure 4.17: Effect of MgO concentration onto $CO_2$ adsorption capacity of HCS.....	114
Figure 4.18: TGA Analysis (a) raw microalgae, (b) hydrochar-microalgae, (c) pyrochar-microalgae, and (d) activated hydrochar derived from microalgae .....	122
Figure 4.19: Fourier Transform Infrared Spectroscopy of microalgae and corresponding treatment.....	128
Figure 4.20: Functional groups of pristine and functionalised HCS.....	137
Figure 4.21: Crystalline structure of (a) HCS, (b) HCS-Mg, (c) HCS-N, and (d) HCS-N-Mg .....	140
Figure 4.22: Field Emission Scanning Electron Microscope image of raw coconut shell .....	143
Figure 4.23: Field Emission Scanning Electron Microscope image of coconut shell hydrochar.....	143

Figure 4.24: Field Emission Scanning Electron Microscope image of pristine bio-adsorbent (HCS).....	144
Figure 4.25: Field Emission Scanning Electron Microscope image of MgO functionalised bio-adsorbent (HCS-Mg) .....	144
Figure 4.26: Field Emission Scanning Electron Microscope image of raw magnesium oxide.....	145
Figure 4.27: Field Emission Scanning Electron Microscope image of microalgae functionalised bio-adsorbent (HCS-N) .....	146
Figure 4.28: Field Emission Scanning Electron Microscope image of dual-functionalised bio-adsorbent (HCS-N-Mg) .....	147
Figure 4.29: Thermal degradation of developed adsorbents.....	150
Figure 4.30: Carbon dioxide adsorption capacity of pristine and functionalised HCS at standard temperature and pressure .....	155
Figure 4.31: Pore width distribution of HCS, HCS-Mg and HCS-N-Mg.....	157
Figure 4.32: 2D contour plot of CO <sub>2</sub> adsorption capacity of HCS for temperature and pressure interaction .....	165
Figure 4.33: 2D contour plot of CO <sub>2</sub> adsorption capacity of HCS-Mg for temperature and pressure interaction .....	165
Figure 4.34: 2D contour plot of CO <sub>2</sub> adsorption capacity of HCS-N for temperature and pressure interaction .....	166
Figure 4.35: 2D contour plot of CO <sub>2</sub> adsorption capacity of HCS-N-Mg for temperature and pressure interaction.....	167
Figure 4.36: Nonlinear isotherm plots for HCS at 25 °C.....	176
Figure 4.37: Nonlinear isotherm plots for HCS-N-Mg at 25 °C.....	176
Figure 4.38: FTIR of clean HCS-N-Mg and CO <sub>2</sub> -saturated HCS-N-Mg.....	180
Figure 4.39: Crystalline structure of HCS-N-Mg before and after adsorption .....	181
Figure 4.40: Electrostatic potential of (a) CO <sub>2</sub> , and, (b) (MgO) <sub>4</sub> models .....	182
Figure 4.41: Electrostatic potential (a) HCS, and, (b) HCS-N-Mg models .....	183
Figure 4.42: (a) HOMO of MgO, (b) LUMO of MgO, (c) HOMO of HCS, (d) LUMO of HCS, (e) HOMO of HCS-N, and (f) LUMO of HCS-N .....	187



Figure 4.43: Top-view of optimised structure of HCS-N-Mg .....	189
Figure 4.44: Molecular interactions of HCS surface with CO <sub>2</sub> .....	191
Figure 4.45: Molecular interactions of MgO surface with CO <sub>2</sub> .....	192
Figure 4.46: Molecular interactions of HCS-N-Mg surface with CO <sub>2</sub> .....	193
Figure 4.47: Side-view of interaction between CO <sub>2</sub> and HCS.....	195
Figure 4.48: Side-view of interaction between CO <sub>2</sub> and HCS-N-Mg.....	196
Figure 4.49: CO <sub>2</sub> and N <sub>2</sub> adsorption isotherm onto HCS and HCS-N-Mg at 25°C.....	198
Figure 4.50: Selectivity of CO <sub>2</sub> /N <sub>2</sub> on HCS and HCS-N-Mg at 25°C .....	199
Figure 4.51: Cyclic CO <sub>2</sub> adsorption at 25°C and 1 bar. ....	200
Figure 4.52: Comparison of commercial AC, HCS and HCS-N-Mg at different temperatures (1 bar) .....	202
Figure 4.53: Process water from HTC consists of coconut shells and microalgae as precursors .....	210

## LIST OF TABLES

Table 2.1: Common adsorbent performance on CO <sub>2</sub> adsorption .....	11
Table 2.2: Properties of physisorption and chemisorption processes .....	16
Table 2.3: Advantages and limitation of CO <sub>2</sub> adsorbent.....	19
Table 2.4: Compositional elements associate with different precursors.....	22
Table 2.5: Comparison between conventional and hydrothermal carbonisation .....	31
Table 2.6: Characteristics of physical and chemical activation .....	34
Table 3.1: RSM-CCD design for the synthesis process of coconut shell bio-adsorbent through hydrothermal carbonisation and KOH activation .....	61
Table 3.2: RSM-CCD design for adsorption condition of bio-adsorbents .....	65
Table 3.3: Structural and molecular properties of adsorbent and adsorbate .....	75
Table 3.4: Safety precautions during the experiment.....	76
Table 4.1: RSM-CCD design matrices with actual and predicted responses of synthesised bio-adsorbent precursor coconut shell .....	81
Table 4.1: RSM-CCD design of coded equations for HTC process condition for synthesis of coconut shell bio-adsorbent .....	82
Table 4.3: ANOVA analysis of hydrochar yield (Y <sub>1</sub> ), bio-adsorbent yield (Y <sub>2</sub> ), and CO <sub>2</sub> adsorption capacity (Y <sub>3</sub> ).....	84
Table 4.2: Model fit summaries for bio-adsorbent precursor coconut shell .....	88
Table 4.3: Optimisation parameters and validation of hydrothermal carbonisation.....	110
Table 4.4: Structural properties of pristine HCS and functionalised with MgO.....	115
Table 4.5: Effect of various concentration of microalgae during co-carbonisation on bio-adsorbent yield and CO <sub>2</sub> adsorption performance. ....	119
Table 4.6: Nomenclature for each optimised sample.....	132
Table 4.7: Surface area and pore properties of bio-adsorbents .....	133
Table 4.8: EDX analysis (in wt.%) of bio-adsorbent materials .....	148
Table 4.9: Comparison of physicochemical properties of developed bio-adsorbents ..	153

Table 4.10: Multiple regression analysis and ANOVA used to fit the quadratic model to the CO <sub>2</sub> adsorption capacity .....	158
Table 4.11: Model fit summaries for adsorption conditions of bio-adsorbents .....	162
Table 4.12: Optimised operating conditions of HCS and HCS-N-Mg .....	171
Table 4.13: Comparison of carbon dioxide adsorption capacity on adsorbent obtained from biomass at 25°C and 1 bar .....	173
Table 4.14: Adsorption isotherm constant and R-square values for carbon dioxide adsorption on bio-adsorbents .....	175
Table 4.15: Thermodynamic Analysis Results .....	178
Table 4.16: Highest occupied and lowest unoccupied molecular orbital of HCS, HCS-N, MgO and carbon dioxide.....	186
Table 4.17: The binding distance and adsorption energy of CO <sub>2</sub> for pristine and dual-functionalised bio-adsorbent .....	190
Table 4.18: Isotherm analysis of N <sub>2</sub> adsorption on HCS and HCS-N-Mg.....	197
Table 4.19: A comparison study of maximum CO <sub>2</sub> adsorption capacity (mmol/g) on various adsorbents (activated carbon).....	201
Table 4.22: Comparison of economic analysis of dual functionalised bio-adsorbent ..	205
Table 4.20: Environmental impact of synthesis of bio-adsorbent, waste valorisation and treatment.....	207

## LIST OF SYMBOLS AND ABBREVIATIONS

### List of Abbreviations

Adj	:	Adjusted
AC	:	Activated Carbon
AC1	:	Norit® SX2 Activated Carbon
ACMA	:	Bio-Adsorbent Derived from Microalgae
AH	:	Activated Hydrochar
ANOVA	:	Analysis of Variance
AP	:	Adequacy Precision
BET	:	Bruneaur, Emmet and Teller
CCD	:	Central Composite Design
cm	:	Centimetre
CO	:	Carbon Monoxide
CO <sub>2</sub>	:	Carbon Dioxide
CV	:	Coefficient of Variance
dTG	:	Derivative Thermo-Gravimetric
EDX	:	Energy Dispersive X-Ray
etc.	:	Et cetera
exp.	:	Experiment
FTIR	:	Fourier Transform Infrared
GHG	:	Greenhouse Gases
GWP	:	Global Warming Potential
H <sub>2</sub>	:	Hydrogen
HCl	:	Hydrochloric Acid
HCS	:	Bio-adsorbent derived from Coconut Shell

HCS-N	:	Microalgae Functionalised Bio-adsorbent
HCS-Mg	:	Magnesium oxide Functionalised Bio-adsorbent
HCS-N-Mg	:	Dual Functionalised Bio-adsorbent
HOMO	:	Highest Occupied Molecular Orbital
H <sub>3</sub> PO <sub>4</sub>	:	Phosphoric Acid
HPVA II	:	High Pressure Volumetric Analyzer
hr	:	Hour
IAST	:	Ideal Adsorption Solution Theory
IUPAC	:	International Union of Pure and Applied Chemistry
K <sub>2</sub> CO <sub>3</sub>	:	Potassium Carbonate
kJ	:	Kilojoule
KOH	:	Potassium Hydroxide
LCA	:	Life Cycle Analysis
LUMO	:	Lowest Unoccupied Molecular Orbital
m	:	Metre
min	:	Minute
mL	:	Millilitre
mm	:	Millimetre
mmol	:	Millimole
MOF	:	Metal Organic Framework
N <sub>2</sub>	:	Nitrogen
NASA	:	National Aeronautics and Space Administration
nm	:	Nanometre
ppm	:	Parts Per Million
Pred	:	Predicted

PRESS	:	Predicted Error Sum of Square
rpm	:	Revolution Per Minute
RSM	:	Response Surface Methodology
SD	:	Standard Deviation
TGA	:	Thermogravimetric Analyzer
$\mu\text{m}$	:	Micrometre
FESEM	:	Field Emission Scanning Electron Microscopy
wt.%	:	Weight Percentage
XRD	:	X-Ray Crystallography
ZnCl <sub>2</sub>	:	Zinc Chloride

Universiti Malaya

## List of Symbols

Symbol	Nomenclature	Unit
$\Delta G^\circ$	: Change in Gibbs free energy	kJ/mol
$\Delta H^\circ$	: Change in enthalpy	kJ/mol
$\Delta S^\circ$	: Change in entropy	kJ/mol.K
$K_s$	: Sips Affinity Constant	bar <sup>-1</sup>
$K_F$	: Freundlich constant	mmol/g·bar <sup>1/n</sup>
$K_L$	: Langmuir constant	bar <sup>-1</sup>
$K_T$	: Temkin constant	L/g
$n_s$	: Heterogeneity Coefficient (Sips)	
$n_F$	: Freundlich Factor/Coefficient	
$P_{s1}$	: Pressure of Sample after Dosing	mmol/g
$q_e$	: Equilibrium Adsorption Capacity	mmol/g
$q_m$	: Maximum Monolayer Adsorption Capacity	kJ/mol
$q_t$	: Adsorption Capacity at Time t	mmol/g
$R$	: Ideal gas constant	J/mole·K; cm <sup>3</sup> ·bar/mole·K
$R^2$	: Coefficient of Determination/ Regression Coefficient	
$S_{BET}$	: BET surface area	m <sup>2</sup> /g
$S_{meso}$	: Mesopore Surface Area	m <sup>2</sup> /g
$S_{micro}$	: Micropore Surface Area	m <sup>2</sup> /g
$t$	: time	min
$T$	: Absolute temperature	Kelvin (K)

## CHAPTER 1: INTRODUCTION

### 1.1 Background study

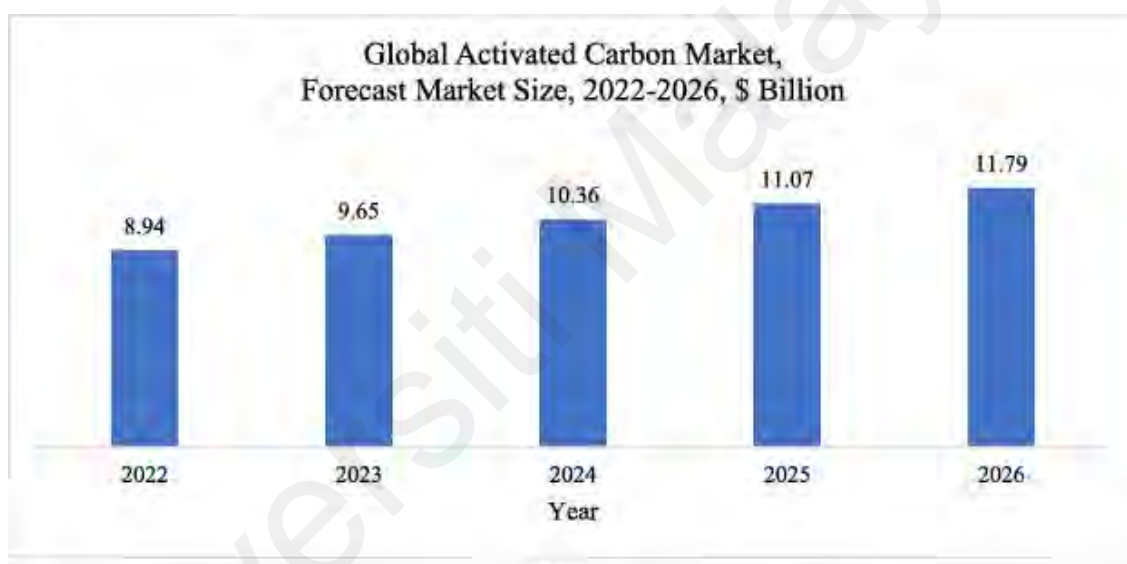
The industrial revolution has been primarily responsible for the prominent increment of atmospheric carbon dioxide (CO<sub>2</sub>) at a rate of 0.17 percent each year. The National Aeronautics and Space Administration (NASA) reported that the atmosphere has 427 parts per million (ppm) of CO<sub>2</sub> as of the June 2024. The value reveals an increment of roughly 50 % compared to before the industrial revolution and the addition of 13 % of CO<sub>2</sub> since 2000. The plethora of research shows that the increment in CO<sub>2</sub> emission is mainly due to industrial activities and the burning of coal and petroleum (Azevedo et al., 2018; Cheng et al., 2023; Crippa et al., 2019). Industries such as petroleum refining, cement, steel and iron manufacturing, and power plant processing have complex systems, processes, and requirements. Although green technology may appear far-fetched because CO<sub>2</sub> emissions contribute to climate change and threaten human health, effective and acceptable solutions such as carbon capture, storage and utilisation (CCUS) is needed.

Solid-gas adsorption has been recognised as one of the effective carbon capture methods. Among commercial adsorbent, carbon-based adsorbent such as charcoal and activated carbon (AC) are the most promising adsorbent proposed to capture CO<sub>2</sub> as it is known to have highly enhanced physio-chemical, mechanical, high thermal and chemical stability. Activated carbon specifically exceeds zeolite and metal organic framework (MOF) performance in humid environments, lower cost, wider range of available resources (Idrees et al., 2018). In addition to its high concentration of micropores and large surface area, chemical properties at the surface of activated carbon can be easily modified with various functional groups depending on the need of the application. Other features such as size and volume of pores, surface area, and pore distribution can easily be tailored by altering the amount and type of activation condition and activating agents.



Existence of micropores in activated carbon is favorable in enhancing adsorption process due to high availability of binding sites.

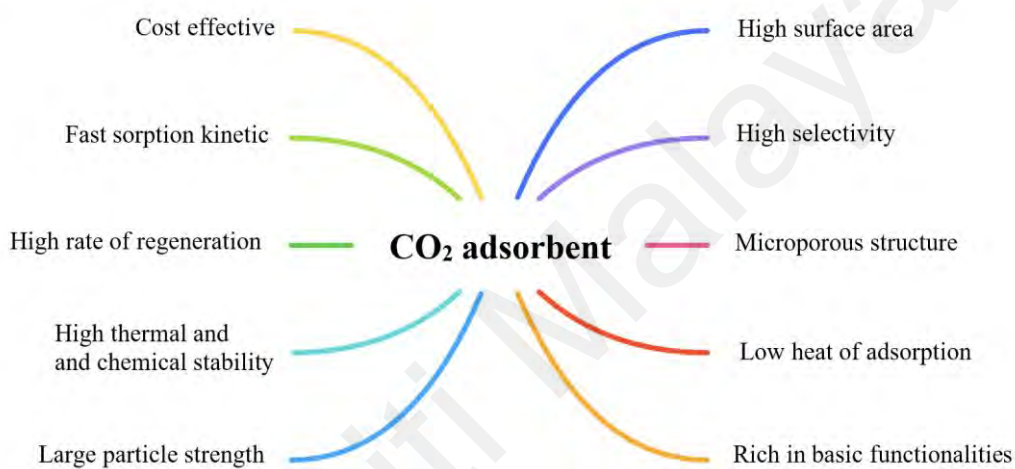
In the industry, AC function is at a wide range; purification of gas, water and gold, sewage treatment, metal extraction, decaffeination, medicine and many other applications. The market size for AC worldwide increases dramatically each year as shown in Figure 1.1. Market forecasts indicate that the worldwide market for activated carbon is projected to experience substantial growth, increasing from an estimated value of \$4.47 billion in 2020 to \$8.49 billion by the year 2025.



**Figure 1.1: Global activated carbon market forecast**

Coal, a major source of activated carbon, is a finite, non-renewable resource that undergo rapid depletion of which is inevitable given current consumption rates. To address both present and projected demand, researchers are now seeking alternative precursors for AC derived from more affordable and sustainable materials while ensuring these alternatives meet the essential criteria for effective CO<sub>2</sub> adsorption, as illustrated in Figure 1.2. Currently, there is a growing trend in using various types of waste materials as adsorbent precursors. Waste from agricultural residues, lignocellulosic biomass, industrial by-

products, food waste, and industrial sludge are considered good raw materials for adsorbent development due to their high carbon content and mechanical strength (Om Prakash et al., 2020). Utilising waste as adsorbent precursors contributes to waste management and environmental conservation by minimizing waste that needs to be disposed of. This approach also has the added benefit of indirectly reducing greenhouse gas emissions, aligning with the principles of a circular economy.



**Figure 1.2: Desirable characteristics of adsorbent for CO<sub>2</sub> capture**

## 1.2 Problem statement

The efficiency of raw bio-adsorbent and simple activated bio-adsorbent in capturing CO<sub>2</sub> is restricted due to their lack of selectivity and poor adsorption stability – primarily depending on physisorption which directly related to availability of surface area, hinders their applicability in industrial applications (Boonpoke et al., 2011). Ullah et al. (2024) highlighted that activated carbon derived from bio-adsorbent exhibits low mechanical strength and low adsorption affinity due to a lower carbon-to-surface ratio, surface area availability and lack of binder. To address these issues, it is crucial to prioritize on the modification of the bio-adsorbent surface by introducing functional groups. This enhancement can improve the selectivity and efficiency of the bio-adsorbent, particularly

for target substances like carbon dioxide. By modifying the surface characteristics, the bio-adsorbent can achieve better adsorption performance and mechanical stability, thereby overcoming the limitations associated with its raw form. Moreover, functionalisation plays a significant role in ensuring that CO<sub>2</sub> adsorption is being carried out effectively (Sharma et al., 2021).

The study by Das and Meikap (2021); Karbalaie Mohammad et al. (2020); Khoshraftar and Ghaemi (2022) have revealed the potential of N-containing functional group adsorbents using urea, melamine, chitosan, and amine in enhancing carbon dioxide adsorption. Functionalisation of the nitrogen heteroatom onto adsorbent assists the CO<sub>2</sub> adsorption through the reaction between carbon dioxide and amine to produce carbamate (Eq. (1.1) and (1.2)) as it resulted in production of N-containing functional group adsorbent. The improvement in adsorption capacity is attributed to the development of a high surface area through the activation process, as highlighted by Shi et al. (2022). However, these microporous structures are brittle and sensitive to high temperatures, resulting in a significant performance decrease at high temperatures. In addition, the production and disposal of amine-doped activated carbon are detrimental to the environment, especially during the process of regeneration, and leaching can occur and produce harmful and poisonous byproducts that result from secondary pollution (Gunawardene et al., 2022).

Aside from nitrogen functionalisation, utilisation of metal oxide as CO<sub>2</sub> adsorbent showed promising results, especially at high temperatures. According to Duan and Sorescu (2010) and Madzaki et al. (2018b), alkaline metal oxides are suitable materials to enhance AC performance in CO<sub>2</sub> adsorption due to the formation of OH<sup>-</sup> functional groups and alkaline nature that react with acidic CO<sub>2</sub>. In addition, metal oxides have abundant availability, inexpensive cost, and high stability. The incorporation of metal oxide onto porous carbon was conducted by Isahak et al. (2018), and it was concluded

that metal-oxide functionalised adsorbent has a lower surface area but stable CO<sub>2</sub> adsorption at higher temperatures.



In recent years, several studies have investigated significant enhancements in CO<sub>2</sub> adsorption by modifying untreated biomass adsorbents with metal oxides or nitrogen heteroatoms. Limited studies have explored the synergistic effects of dual functionalisation with metal oxides and nitrogen in enhancing adsorbent stability and reducing surface area loss at high temperatures. Therefore, in this study a dual-functionalised bio-adsorbent using coconut shell (CS) as substrates and *Chlorella s.p.* microalgae with magnesium oxide (MgO) as the nitrogen heteroatoms and metal oxide precursor was developed.

### 1.3 Research questions

This study aims to address the following four key research questions:

1. Could a bio-adsorbent derived from coconut shells be effectively functionalised with both microalgae and magnesium oxides?
2. How does the microalgae and magnesium oxide functionalisation alter the physiochemical properties of the bio-adsorbent?
3. How do adsorption operating conditions (temperature and pressure) affect the CO<sub>2</sub> adsorption capacity of pristine and functionalised bio-adsorbents, and what are the optimal conditions for maximizing their performance?

4. How do the isotherms, thermodynamics and mechanisms properties of CO<sub>2</sub> adsorption change when using the dual-functionalised bio-adsorbent compared to pristine bio-adsorbent?
5. How does the dual-functionalisation of coconut shell bio-adsorbent with *Chlorella* microalgae and magnesium oxide influence its quantum adsorption properties for CO<sub>2</sub>?

#### **1.4 Aim and objectives**

The study aims to develop bio-adsorbent from coconut shell for CO<sub>2</sub> adsorption through green process. The process utilises green precursors, including coconut shell and microalgae, and, hydrothermal carbonization as a green synthesis method. The specific objectives of this study are as follows:

1. To synthesise a novel bio-adsorbent from activated coconut shell, functionalised with microalgae and metal oxide to enhance the CO<sub>2</sub> adsorption performance.
2. To characterize the physiochemical properties of coconut shell-based bio-adsorbents, including surface morphology, elemental composition, functional groups, surface area, crystallography and thermal stability, to evaluate their potential for enhanced adsorption performance.
3. To optimise the CO<sub>2</sub> adsorption performance of developed bio-adsorbents from coconut shells by investigating the effects of operating pressure and temperature, with a focus on their suitability for post-combustion carbon capture applications
4. To analyse the CO<sub>2</sub> adsorption behavior of the bio-adsorbent by evaluating adsorption isotherms, including Langmuir, Freundlich, Sips, and Temkin models, thermodynamic parameters of the adsorption process, such as enthalpy ( $\Delta H$ ), Gibbs free energy ( $\Delta G$ ), and entropy ( $\Delta S$ ), and mechanism of the CO<sub>2</sub> adsorption process of the bio-adsorbent.

5. To investigate the synergistic effect of dual-functionalised bio-adsorbent on CO<sub>2</sub> adsorption performance through quantum chemical molecular modelling

## **1.5 Scope of the study**

The bio-adsorbent precursor coconut shell was synthesised through a two-step activation process by utilising hydrothermal treatment and pyrolysis in the absence of air. The incorporation of activating agents through solid-solid mixing was investigated. The physicochemical characteristics of both pristine and functionalised bio-adsorbents were examined through Brunauer, Emmett and Teller (BET) surface area, pore size distribution, surface functional groups, surface morphology, thermal stability, elemental composition, and crystalline structure. The effect of operational parameters, including pressure and temperature, on CO<sub>2</sub> adsorption performances was also investigated.

## **1.6 Thesis outline**

This thesis dissertation adheres to a conventional structure which starts with an abstract that provides an overview of the research, followed by five chapters, each detailing out different aspects of the research. The dissertation concludes with a complete list of references and the presentation of research findings, highlighting the contributions of the work.

### **Chapter 1: Introduction**

The first chapter of this report provides a comprehensive overview of biomass wastes and carbon dioxide. It also provides an outlook on adsorbents from biomass wastes and on developing adsorbents from coconut shells and microalgae to capture carbon dioxide from the atmosphere. Additionally, the chapter addresses the limitations associated with current biomass-based adsorbents and explores strategies to overcome these challenges.

The chapter concludes by clearly defining the research problem, outlining the study objectives and scope, and providing an overview of the structure of the report.

## **Chapter 2: Literature Review**

This chapter focuses on the recently published literature that provides materials on the carbon dioxide adsorption process, various types of solid adsorbents, and the limitation/challenges of the adsorption process using conventional commercial adsorbent. It also includes the synthesis methods for low-cost bio-adsorbents, modification of bio-adsorbents, and functionalisation of the bio-adsorbents. In addition, the literature review also highlights recent results on the performance of activated carbon precursor biomass waste on the adsorption of carbon dioxide and the operational parameters for different waste adsorbents.

## **Chapter 3: Methodology**

In this chapter, the methodology of the research activities used to obtain the objectives of the study is described. A flowchart illustrating the methodology, the chemicals employed, and the step-by-step process for preparing adsorbents is presented in this section. Furthermore, the experimental design, techniques for evaluating adsorption performance, the computational methodology employed, and essential safety considerations are also covered within this section. Adsorption isotherm and thermodynamic analysis were also discussed in this chapter. Additionally, the characterisation of the samples using FESEM-EDX, FTIR, TGA, BET and XRD is also elaborated in this chapter.

## **Chapter 4: Experimental Results and Discussion**

In chapter 4, the results obtained from the experiments and the discussion regarding the physical and chemical characteristics of developed bio-adsorbents and their performances in carbon dioxide adsorption capacity are presented. This chapter also provides detailed information regarding the effect of microalgae and magnesium oxide

functionalisation on the CO<sub>2</sub> adsorption capacity of developed adsorbents. Additionally, the experimental findings from the CO<sub>2</sub> adsorption, isotherm and thermodynamic analyses, and molecular modelling through DFT studies were discussed. The comparison of developed pristine and dual-functionalised bio-adsorbent with commercial activated carbon was evaluated along with their selectivity CO<sub>2</sub>/N<sub>2</sub> reusability potential.

### **Chapter 5: Conclusion**

This chapter summarizes the overall experimental findings with respect to the research objectives. This chapter concludes by proposing recommendations for future investigations aimed at refining and extending the scope of the research.

Universiti Malaysia



## CHAPTER 2: LITERATURE REVIEW

### 2.1 Carbon capture utilisation and storage

According to Global Carbon Capture and Storage (CCS) Institute, Carbon Capture, Utilisation and Storage (CCUS) technologies have emerged as a prominent approach for mitigating climate change while generating economically valuable products. CCUS is a technology of capturing carbon dioxide, either from the atmosphere or directly from factories, then transferring the gases to storage facilities such as underground reservoirs, where the gases are securely stored to prevent their release back into the atmosphere, or, using the captured carbon dioxide to facilitate process and as precursor. Based on Elhenawy et al. (2020), absorption, cryogenic separation, membrane separation, and adsorption are competent methodologies for capturing CO<sub>2</sub> in the atmosphere. According to Raganati et al. (2021), the most efficient approach to capturing CO<sub>2</sub> is adsorption, as it is cost-effective. Commercially, the medium used for adsorption of gases is activated carbon (Sarwar et al., 2021), silica gel (Park et al., 2020), metal-organic framework (MOF) (Elhenawy et al., 2020), zeolite (Kim et al., 2022), activated alumina (Mohammad et al., 2019), and polymeric adsorbents (Peng et al., 2019). The common adsorbent respective to their CO<sub>2</sub> adsorption performance is represented in Table 2.1

Table 2.1 demonstrates that CO<sub>2</sub> adsorption capacities are influenced by temperature. Among them, zeolites and activated carbon have the highest CO<sub>2</sub> adsorption capacity at 25°C. However, utilisation of zeolite in the humid condition is limited. This can be supported by Purdue and Qiao (2018) and Panda et al. (2020). Activated carbons (AC) are the most promising adsorbent proposed to capture CO<sub>2</sub> as it is known to have highly enhanced physio-chemical, mechanical, high thermal and chemical stability.

**Table 2.1: Common adsorbent performance on CO<sub>2</sub> adsorption**

<b>Adsorbent</b>	<b>Temp. (°C)</b>	<b>CO<sub>2</sub> adsorption capacity (mg/g)</b>	<b>Ref.</b>
Alumina	25	30	Chen and Ahn (2011)
Zeolite 13X	25	231	
Amine-MCM-41	25	40	
Activated carbon – coal	25	250	Labus et al. (2014)
Hydrotalcites – Mg	200	35	Wang et al. (2011)
Zeolites 13X	25	118	Garshasbi et al. (2017)
Activated alumina	20	88	Mohammad et al. (2019)
Activated anthracite	30	58	Maroto-Valer et al. (2005)
Organic polymer	0	183	He et al. (2015)
Silica gel	25	20	Zhao et al. (2012)
Metal oxides	30	30	Alkadhem et al. (2020)
Boron nitride	0	308	Kamran et al. (2019)
MOF	0	162	Ma, Li, Chen, Wang, Li and Li (2018)
MOF-5	30	38	Lu et al. (2010)
Porous silica	25	149	Cecilia et al. (2016)
Polymeric adsorbent	30	157	Kong et al. (2015)

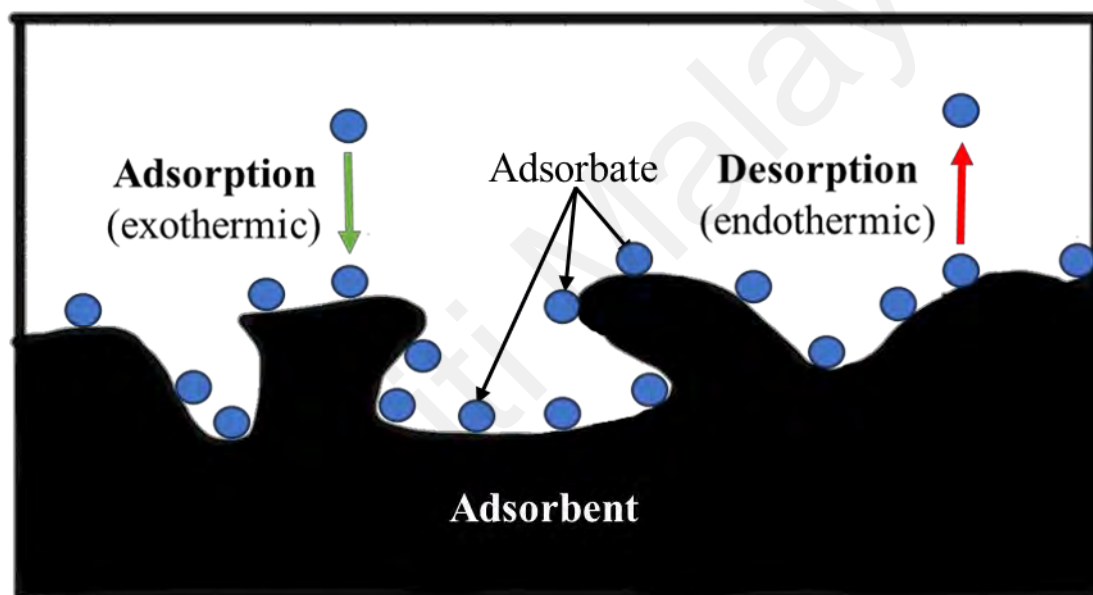
Once captured, CO<sub>2</sub> can be converted into valuable products through chemical, electrochemical, or biological pathways. Catalytic hydrogenation, such as the Sabatier reaction, enables the conversion of CO<sub>2</sub> and hydrogen into methane or methanol using transition-metal catalysts (Ravanchi & Sahebdehfar, 2021). Electrochemical reduction, powered by renewable electricity, produces valuable chemicals such as ethylene, ethanol, and formate, with advances in copper-based catalysts significantly enhancing efficiency (Karapinar et al., 2021). Additionally, biological methods utilize engineered microorganisms or algae to ferment CO<sub>2</sub> into biofuels (e.g., ethanol) or bioplastics (Karishma et al., 2024). Another promising utilization route is mineral carbonation, which reacts CO<sub>2</sub> with alkaline industrial waste or minerals to form stable carbonates. This process is already being commercialized for concrete production by companies like CarbonCure (Sandeep, 2021). Emerging technologies such as photochemical systems

and hybrid approaches, including the integration of direct air capture (DAC) with renewable hydrogen production, further expand the range of CO<sub>2</sub> utilization strategies. The shift in perspective towards CO<sub>2</sub> has led to significant changes in industrial standard operation procedures and practices, recognizing it as a valuable resource rather than waste. This transformation has given rise to numerous opportunities for the production of fuels, chemicals, construction materials, and consumer goods. Carbon capture technologies have become a crucial component of sustainable industrial practices, enabling industries to reduce their carbon footprint while also creating new revenue streams through the utilization of CO<sub>2</sub>.

## 2.2 CO<sub>2</sub> adsorption

Adsorption is a process in which gas or liquid molecules from a mixture adhere to the surface of a porous solid material. The gas or liquid molecule that the material is actually adsorbing is referred to as the "adsorbate" in this situation. The "absorption" process, in which molecules enter the lattice (bulk) of a solid absorbent, is the opposite of this phenomena. During the adsorption process in an isolated system, the adsorbent's weight increases as the gas pressure decreases upon exposure to the adsorbate. This implies that a certain amount of gas has been adsorbed by the adsorbent. Adsorption scenarios usually have an exothermic behaviour that is simply described by fundamental thermodynamic laws (Ferrer, 2016). Since spontaneous adsorption implies a negative free energy change ( $\Delta G_{\text{ads}} = \Delta H_{\text{ads}} + T\Delta S_{\text{ads}}$ ), its enthalpy ( $\Delta H_{\text{ads}}$ ) must also be negative, making it an exothermic process. Therefore, desorption ought to be endothermic, as presented in Figure 2.1. Weight and gas pressure balanced and remained constant after a particular amount of time, which denotes an equilibrium state. The amount of gas adsorbed is calculated using either a volumetric (by a decrease in pressure as measured by a manometer or transducer gauge) or gravimetric (via an increase in solid weight as

monitored by a spring balance) technique. The binding of the adsorbate's atoms, molecules, and ions to the solid surface allows gas to adsorb at the surface of the adsorbent. Depending on the nature of the forces involved in the process, adsorption can be classified into two primary categories, which are physisorption and chemisorption. Due to the limitations of current technology, it is crucial to explore alternative methods for mitigating CO<sub>2</sub> emissions under post-combustion conditions (298 K and 1 bar (Raganati & Ammendola, 2024)).



**Figure 2.1: Adsorption and desorption process of gas molecules into carbon surface**

Desorption or regeneration is the method of removing adsorbed compounds from the surface layer of adsorbent components. Different techniques, which are pressure-swing adsorption, electric-swing adsorption, temperature-swing adsorption, and vacuum pressure-swing adsorption, can be used to promote desorption (W. Liu et al., 2022). In temperature-swing (TSA), gas adsorption occurs at a lower working temperature, followed by a desorption process at a higher temperature. TSA is effective for gases with strong adsorption bonds that are difficult to desorb by pressure changes alone. This

method is suitable for oxy-combustion processes where high-temperature flue gases can be used to regenerate the adsorbent, making TSA energy efficient. However, the high attrition rate of the adsorbent caused by the considerable energy and time required to achieve complete desorption limits the use of this technique. Electric-swing adsorption (ESA) has been proposed as an alternative for this temperature-swing procedure. By creating the Joule effect and running electricity through a conductor inside the adsorption column, the heating mechanism, in this case, heats the column considerably more quickly. In a TSA cycle, the adsorption column is typically heated using hot gases or steam. The primary distinction between the electric-swing method and conventional temperature-swing adsorption lies in the heating mechanism. In the electric-swing method, the column is heated rapidly, and the temperature increases without the introduction of an external gas, minimizing potential interference during the adsorption process (Verougstraete et al., 2024). However, the high cost of conductive adsorbents and the need for sophisticated control systems limit ESA widespread adoption.

Pressure-Swing Adsorption (PSA) is a widely used method based on cycling between high and low pressures. During high-pressure conditions, the adsorbent captures the pollutant gas from the feed stream, and when the pressure of the system decreases, the captured gas molecules are released, regenerating the adsorbent for reuse. This method is particularly suitable for applications where the gas mixture has significant differences in adsorption affinities at varying pressures, making it highly efficient for the removal of CO<sub>2</sub> from natural gas, hydrogen purification, and other industrial gas separations. PSA is often employed in post-combustion carbon capture systems due to its capability in handling substantial gas volumes and its inherent scalability. The effectiveness of PSA in achieving desorption through pressure reduction has been extensively documented, and it is used on a large scale across various industrial separation processes (Abd et al., 2023; Abd et al., 2022; Huang et al., 2023).

Vacuum-swing adsorption (VSA/VPSA) has a similar mechanism to pressure-swing adsorption, which involves spontaneous desorption that takes place at pressures lower than atmospheric pressure. This approach enhances desorption efficiency by reducing the partial pressure of the adsorbed gas, facilitating its release from the adsorbent. VPSA is advantageous when a higher purity of the desorbed gas is required or when lower energy consumption for the desorption phase is desired. It is particularly useful in pre-combustion applications where syngas purification is necessary before combustion, ensuring higher hydrogen recovery. However, VPSA involves desorption at pressures lower than atmospheric pressure, which can be costly due to the need to compress the flue gas stream to high pressures (Krishnamurthy, 2022). While vacuum pressure-swing adsorption is the process that is commonly used in the industrial operation for gas separation and purification (Sakanaka et al., 2023), VPSA is not viable for the adsorption study in this work since it utilised adsorption pressure of 0.1-5 bar. This is because using VPSA would escalate costs significantly due to the substantial energy required, making it impractical for the given conditions. Overall, in contrast to the release of adsorbed gas, CO<sub>2</sub> adsorption on activated carbon adsorbent is typically based on exothermic activity, favouring high pressure and low temperature (Hong et al., 2016).

### **2.2.1 Physisorption and chemisorption**

The adsorption process depends on the complex interactions between adsorbate molecules and the adsorbent surface, influencing the efficiency and mechanism of adsorption. There are two primary mechanisms in adsorption, which are physisorption and chemisorption, distinguished by the energy and strength of the interaction that binds the adsorbate molecules to the surface of the adsorbent (Table 2.2). Physisorption or physical adsorption occurs due to the interaction of weak intermolecular forces, such as dispersion forces or van der Waals, arising from induced dipole-dipole interactions. In

contrast, chemisorption or chemical adsorption involves the formation of strong chemical bonds, akin to covalent or metallic bonds (Atif et al., 2022).

**Table 2.2: Properties of physisorption and chemisorption processes**

<b>Property</b>	<b>Physisorption</b>	<b>Chemisorption</b>
<b>Specificity towards adsorbate</b>	Non-selective, accommodates various gases	Highly selective, specific to certain gases
<b>Temperature and pressure dependence</b>	Favoured at lower temperatures and higher pressures	Can occur at a wider range of pressure and temperature
<b>Adsorption rate</b>	Typically rapid	May be slow
<b>Reversibility</b>	Readily reversible	Can be irreversible or reversible, depending on bond strength
<b>Heat of adsorption</b>	Low (2-3 times the latent heat of evaporation)	High (>3 times the latent heat of evaporation)
<b>Adsorbate-adsorbent interaction</b>	Weak van der Waals or dispersion forces, possible adsorbate polarization	Strong chemical bonds (covalent or metallic) often with adsorbate dissociation and electron transfer
<b>Adsorbate layer formation</b>	Can form monolayers or multilayers	Typically forms monolayers only
<b>Surface requirement</b>	Can occur on activated or non-activated surfaces	Can occur on activated or non-activated surfaces
<b>Average value for enthalpy</b>	< 20 kJ/mol	> 80 kJ/mol

Instead of relying solely on chemisorption, most separation processes utilise physical adsorption. The reversibility of physisorption allows for easier adsorbent recycling, making it a more practical choice in many applications.

### **2.3 Porous adsorbent for carbon dioxide adsorption**

According to Raganati et al. (2021), the core of the adsorption process is a solid adsorbent, therefore choosing the right adsorbent is crucial to deciding how well the process works as a whole. Solid adsorbents for the carbon dioxide capture at post-

combustion system should meet certain important criteria, including good mechanical strength, facile regeneration, high chemical/thermal stability, high selectivity towards CO<sub>2</sub>, high kinetics of CO<sub>2</sub> adsorption, and low cost. Majd et al. (2022) also stated that the adsorption isotherm should be used as the basis for adsorbent qualities. For the post-combustion CO<sub>2</sub> adsorption, Sevilla et al. (2013) mentioned that a temperature region of 0 to 25 °C and operating pressure ranging between 0 to 1 bar have been recognized to be the standard condition. Since N<sub>2</sub> and CO<sub>2</sub> comprise the majority of the gas pollutants in the post-combustion approach, the adsorbent utilised in the system must exhibit high selectivity for CO<sub>2</sub> as distinguished to other gas components such as nitrogen. According to Chen et al. (2018), it has been proven that having a high CO<sub>2</sub>/N<sub>2</sub> selectivity is important for an adsorbent to be used in flue gas separation. Additionally, minimal regeneration is possible to increase the sturdiness and recyclability of the specific adsorbent throughout the multiple adsorption-desorption cycle.

Among the various types of adsorbents used for carbon capture in post-combustion systems, activated carbon shows high potential due to its cost-effectiveness, ease of preparation, and tuneable pore structures. AC also offers a large surface area, is highly stable, and simplicity of regeneration with low energy requirement. Moreover, activated carbon exhibits low affinity for water vapor present in flue gas, making it particularly effective in such applications. This hydrophobic characteristic further enhances its suitability for carbon capture (Rehman & Park, 2018). AC is derived from carbonaceous substances such as petroleum coke, wood and peat. These high carbon content raw materials will undergo chemical and physical activation to remove volatile matter, allowing more micropores and mesopores readily available for adsorption. Activated carbon outperforms other adsorbents in various ways. It exceeds zeolite and MOF performance in humid environments, lower cost, a more comprehensive range of available resources (Idrees et al., 2018). In addition to its large surface area, chemical



properties at the surface of activated carbon can be easily modified with various functional groups depending on the need of the application. Other features such as size and volume of pores, surface area and pore distribution can easily be tailored by altering the amount and type of activation condition and activating agents. Micropores in activated carbon are favourable in enhancing the adsorption process due to the high availability of binding sites. AC is also known to have a large inner surface. According to the literature, the surface area of one gram of activated carbon varies between 950 m<sup>2</sup>/g up to 2000 m<sup>2</sup>/g, in comparison to zeolite at 600-800 m<sup>2</sup>/g (González-Domínguez et al., 2017; Roberts et al., 1997). To simplify, a teaspoon (~2 g) of activated carbon corresponds to approximately 4000 m<sup>2</sup> of surface area, which almost is equivalent to the size of a football field. Furthermore, the use of activated carbon is cost-effective because it can be regenerated and thus suitable for the removal of environmentally harmful substances in the air and water.

### **2.3.1 Challenges and limitation of conventional adsorbents**

Table 2.3 summaries the advantages and limitation of conventional and non-conventional CO<sub>2</sub> adsorbents. Due to the complex parameters involved in synthesising AC and adsorption condition, determination of the best CO<sub>2</sub> adsorbent is limited due to dissimilarities in research data. It is biased to evaluate the potential of waste products as CO<sub>2</sub> adsorbent by just comparing the CO<sub>2</sub> adsorption capacity at the same condition. This is because the characteristics of AC produced are mainly dependent on the synthesis process, which differs between literature. Most of the literature does not portray the actual adsorption system as they investigate the efficiency of CO<sub>2</sub> removal without including potential competitive adsorbate such as CO, N<sub>2</sub> and CH<sub>4</sub>. Aside from cost, operation complexity, potential of regeneration, sources availability, and impact on the environment need to be considered when making suitable adsorbent.

**Table 2.3: Advantages and limitation of CO<sub>2</sub> adsorbent**

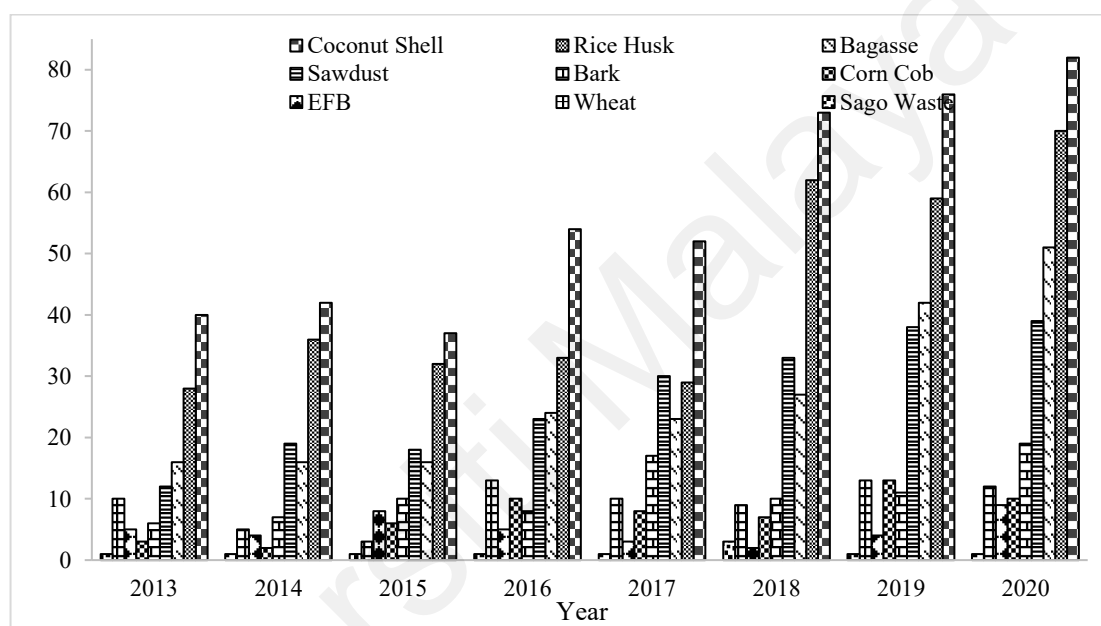
<b>Adsorbent</b>	<b>Features/mechanisms/ advantages</b>	<b>Limitation/disadvantages</b>	<b>Ref.</b>
Commercial activated carbon	The most efficient adsorbent	Initial cost of the carbon and non-renewable resources	Labus et al. (2014)
Zeolites	High surface area, thermal stability and low heat required to regenerate	Efficiency reduce with existence of moisture and impurities	Zukal et al. (2017), Azmi and Aziz (2019)
Commercial polymeric and synthetic organic resins		Originated from petroleum-based materials	Varghese and Karanikolos (2020)
Silica	High surface area and good mechanical and thermal stability	High regeneration energy requirements	R. Wang et al., 2012, Cecilia et al. (2016)
Metal organic framework (MOF)	High surface area and physiochemical stability	Costly and difficult to produce for industrial scale	Bhatta et al. (2015), Ma, Li, Chen, Wang, Li and Li (2018)
Waste products	Renewable sources, low cost and abundant	High variance in CO <sub>2</sub> adsorption depending on the material, the preparation and treatment conditions and the physicochemical properties	Hidayu and Muda (2016), Ogungbenro et al. (2020), Han et al. (2019)
Metal oxides	Abundant availability and low toxicity	High regeneration energy requirements	Duan and Sorescu (2010), Azmi and Aziz (2019)

**Table 2.3, continued**

<b>Adsorbent</b>	<b>Features/mechanisms/ advantages</b>	<b>Limitation/disadvantages</b>	<b>Ref.</b>
Industrial by- products	Highly available and low-cost precursor	Varies adsorption strength depending on the precursor	de Andrés et al. (2013)
Agricultural wastes	Low cost and abundant	Performance varies depending on the precursor	Yang et al. (2011), Parshetti et al. (2015)
Biomass	Plenty resources with high adsorption capacity, low cost and effective technology	In study/experimental stage	Hao et al. (2013), Alabadi et al. (2015)
Biochar	Plenty resources with high adsorption capacity, low cost and effective technology	Low CO <sub>2</sub> uptake compare to AC	Salem et al. (2021)
Peat	Low cost, abundant and widely available bio-adsorbent	Low mechanical strength	Varila et al. (2017)
Shrimp shells/Chitosan	Plentiful, renewable, biodegradable, and environmentally friendly resource	Low surface area	Karaer and Kaya (2016), Banu et al. (2019)
Activated alumina	Relatively well-known and commercially available	High cost of adsorbent	Chen and Ahn (2011), Mohammad et al. (2019), Fashi et al. (2019),

### 2.3.2 Adsorbent from waste materials

To meet current and projected demand, researchers are looking for AC precursors from more affordable materials. One of the approaches is the synthesis of bio-adsorbent by using the waste materials that keep piling on the wasteland each year. By doing so, the industry can reduce the raw material problem and environmental issues associated with wasteland.



**Figure 2.2: Statistics of studies on adsorbent precursor from biomass (2013-2020)**

This raw material, also known as biomass, can be categorized into two groups; conventional and non-conventional waste. Conventional wastes are defined as waste materials that have a high lignocellulosic content. These typically include biomasses from agriculture and the wood industry, such as wood, palm kernel shell, coconut shells, saw dust, bagasse and rice straw. At the same time, non-conventional wastes are by-products from municipal and industrial activities such as plastic, sugarcane bagasse, citrus peel and tires. Figure 2.2 shows some of the popular projects conducted towards potential precursors from waste products over the years. The most popular precursor

being investigated is coconut shells due to the inherent high carbon content and mechanical strength, which the compositional analysis in Table 2.4 can support. A comparative study by Khalil et al. (2013), Das (2014), and Jasni et al. (2018) confirm that the adsorption capability as well as the practicality of AC precursor coconut shell. Based on the literature, a comprehensive understanding of the carbon content and composition of potential raw materials is crucial, as these factors directly influence the properties of the resulting adsorbent developed. The most common indicator for determining the effect of carbonisation and porosity development are fixed carbon and volatile matter contents. Theoretically the, carbonisation stage resulted in mobility and reduction of volatile matter, thus facilitating the formation of additional pores within the material.

**Table 2.4: Compositional elements associate with different precursors. NR = not reported**

Raw Materials	Element analysis (wt.%)					Ref.
	C	N	H	O	Ash	
Olive stone	47.10	0.21	6.23	46.46	0.45	Fadhil and Kareem (2021)
Date stone	48.43	0.67	6.44	44.46	1.58	
Apricot stone	48.45	0.44	6.03	45.08	1.68	Abbas (2021)
Algae	50.20	7.20	6.80	35.00	6.70	Masoumi and Dalai (2020)
Shrimp shell	42.07	24.81	5.74	NR	NR	Boonyoung et al. (2017)
Crab shell	10.23	3.94	2.82	NR	NR	
Douglas fir	47.90	0.08	6.55	45.57	0.21	Huo et al. (2020)
Wheat straw	41.52	0.61	5.76	36.24	NR	Zhao et al. (2019)
Pinewood sawdust	49.09	0.33	6.05	44.53	NR	Gao et al. (2018)
Rice husk	36.52	0.86	4.82	41.10	16.70	Boonpoke et al. (2011)
Sugarcane bagasse	41.55	0.03	5.55	52.86	6.20	
Walnut shell	54.40	3.20	5.60	36.80	1.00	Wu et al. (2018)

**Table 2.4, continued**

Raw Materials	Element analysis (wt.%)					Ref.
	C	N	H	O	Ash	
Rice straw	40.67	0.80	5.73	32.30	NR	Zhao et al. (2019)
Cherry stone	49.00	0.24	6.37	44.15	0.24	González-Domínguez et al. (2017)
Macadamia nut shell	53.19	0.29	5.78	40.68	0.30	Wongcharee et al. (2018)
Almond shell	51.40	0.30	6.10	41.60	1.30	Plaza et al. (2010)
Peanut shell	41.10	1.05	5.90	51.59	3.71	Gueye et al. (2014)
Peanut shell	46.82	0.80	6.58	37.64	8.61	S. Wang et al. (2020)
Pecan shell	47.53	0.33	5.53	45.97	NR	Kaveeshwar et al. (2018)
Sea mango	58.50	0.00	NR	36.67	NR	Zulkurnai et al. (2017)
Coconut shell	49.62	0.22	7.31	42.75	0.80	Iqbaldin et al. (2013)
Cotton stalk	38.96	1.01	3.56	56.47	6.03	Pramanik et al. (2021)
Citrus peel	41.87	0.58	5.49	51.62	2.86	Weng et al. (2019)
Hemp straw	48.40	0.30	6.40	44.90	1.80	Lupul et al. (2015)
Wheat straw	39.90	0.65	5.75	41.97	12.30	Zubkova et al. (2019)
Waste palm shell	51.00	3.00	7.00	39.00	4.00	Yek et al. (2019)
Barley straw	45.40	0.70	6.10	41.92	5.00	Pallarés et al. (2018)
Empty fruit bunch	43.89	0.52	5.33	54.32	3.72	Onochie et al. (2017)
Soybean straw	41.50	0.28	5.52	41.39	8.87	Leng et al. (2020)
Cassava peel	47.21	1.35	7.74	43.70	1.92	Fonseca et al. (2018)

**Table 2.4, continued**

Raw Materials	Element analysis (wt.%)					Ref.
	C	N	H	O	Ash	
Sunflower straw	52.90	1.38	6.58	35.90	3.00	Skoulou and Zabaniotou (2007)
Oat straw	46.00	1.13	5.91	43.50	4.90	
Cassava peel	47.21	1.35	7.74	43.70	1.92	Fonseca et al. (2018)
Lemon peel	38.48	1.21	4.98	NR	3.68	Herrera-Barros et al. (2020)
Cassava peel	38.34	2.08	6.13	38.55	4.32	Cruz et al. (2021)
Coconut shell	40.33	0.72	2.78	51.57	4.18	Liu et al. (2021)
Palm kernel shell	47.88	0.94	5.15	42.69	0.69	Onochie et al. (2017)
Palm fibre	42.20	0.92	5.21	42.34	7.90	

Table 2.4 shows the element analysis for different precursors. By referring only to carbon content, nutshell, coconut shell, algae, and sea mango has higher carbon content as compared to the average of the sample which is 44.95. As a result, it is suggested that the wastes are more desirable for AC production as the high concentration of carbon in precursor is associated with a higher yield of adsorbent. As reported by Onochie et al. (2017), Pallarés et al. (2018) and Hao et al. (2013), higher yield of AC were reported as high concentration of carbon precursor was utilised. This is due to the high carbon content which assist in creation of microporous structure.

In addition to high carbon composition, algae, walnut shell and waste palm shell also has higher nitrogen content compared to the other sample. The average nitrogen composition of the sample is 1.67% while algae, walnut shell and waste palm shell is 7.20%, 3.20% and 3.00% respectively. Even though percentage of carbon in raw materials play a huge role in precursor selection, studies by Chen et al. (2015) and Yang et al. (2018) discovered that high concentration of nitrogen in precursor increase the adsorption and selectivity of CO<sub>2</sub> despite the carbon composition. It is reported by Boonyoung et al.

(2017) that low carbon content in the precursor resulted in low surface area of AC produced. However, recent study by Nazir et al. (2021) found that addition of heteroatoms rich materials during carbonisation and activation of AC derived from shrimp increases the surface area of AC produced as well as the carbon yield. It was reported that addition of melamine, sodium thiosulfate and KOH doubled the AC yield due to improvement of thermal stability.

An excellent precursor for the production of adsorbent should be low in ash content (Hidayu & Muda, 2016). The lowest ash content recorded in this review was 0.21% (Table 2.4) for Douglas fir which is lower than the average of 4.12%. A high ash content, of 6.70%, was obtained for algae and 16.70% for rice husk. The results obtained suggest that Douglas fir will make a better adsorbent since it has a lower ash content. Although ash content, particularly those containing alkaline earth metals like CaO and MgO, can form stable carbonates that facilitate CO<sub>2</sub> adsorption, high ash content in biomass can lead to the formation of unwanted compounds that compromise the quality of the final product, including its surface area and pore size, ultimately affecting its performance. Additionally, ash content does affect the properties of adsorption through the formation of inactive sites.

In addition, further understanding of the dominant lignocellulose structure is required as different waste products have different lignocellulose compositions. By comparing the literature from Wu et al. (2018), Zhang et al. (2019), Masoumi and Dalai (2020) and Pramanik et al. (2021) it can be assumed that precursor contains higher lignin content are subjected to spherical porous structure formation during AC synthesis while precursor dominated by cellulose structure will be procured cylindrical pore structure AC. Similar finding also reported by Olivares-Marín et al. (2011) in which the type of precursor play important roles in the development of AC texture. Therefore, the ideal activated carbon for CO<sub>2</sub> adsorption is challenging to be prepared by using single waste materials due to



the diversity of composition properties of the same waste originated from different suppliers.

Among all the waste-based synthesis activated carbon, agricultural wastes such as coconut shells, rice husks and bagasse are the most common precursor studied for CO<sub>2</sub> adsorbent. These biomasses are preferred due to rich in fixed carbon content, high availability, and low ash content. It is essential to analyse the precursor to ease the synthesis process of AC into a suitable CO<sub>2</sub> adsorbent. Aside from large surface area and high microporosity concentration, the waste-based synthesis AC need to be cost-effective, rich in basic functionalities, low heat adsorption, high CO<sub>2</sub> selectivity and subject to manufacture for industrial usage. To emphasis, the compositional content of waste products is crucial as it define the quality of AC produced. In addition, different values in the ultimate analysis with the same type precursor was also obtained in Table 2.4 which indicate that vary in the results will lead in inconsistent of AC performance.

### **2.3.2.1 Coconut shells as biomass adsorbent precursor for carbon capture**

Coconut shells (CS) are increasingly recognized by researchers as a valuable biomass waste for adsorbent production due to their abundant availability. In 2019, the global plantation of coconut trees resulted in 62.5 million metric tons production of coconut, mainly contributed by South America and Asia. These coconuts are processed into various consumable products such as coconut oil, nata de coco, coconut milk, desiccated coconut, fibre-based coconut and including cosmeceuticals. Malaysia, for instance, ranked 10<sup>th</sup> globally with 0.54 million metric tons of coconut production in 2019 (Hoe, 2018). Within the country, Selangor recorded the highest coconut production at 99,674 tons annually, followed by Johor at 95,677 tons, and Perak at 87,890 tons in 2016. This significant coconut production also generates considerable amounts of waste including coconut shell.

Traditionally, the CS were often incinerated, which is environmentally detrimental, contributing to the greenhouse effect and depletion of ozone layer (Baby et al., 2019). However, this biomass can be valorised into other materials due to its high carbon content and lignocellulosic components. Thus, coconut shells offer a sustainable alternative for AC production, given their high carbon content, which interacts with activators to form pores. CS is also rich in lignin (15%-47%), hemicellulose (12%-27%), and cellulose (21%-40%) (Bello, 2016; Sangian & Widjaja, 2018). Coconut shells contain functional groups like hydroxyl and carboxyl, which improve their capacity to adsorb pollutants such as CO<sub>2</sub> (Emahi et al., 2019). Additionally, the presence of carbonyl (C=O) promotes pollutant adsorption through various interactions, including hydrogen bonding,  $\pi$ - $\pi$  interactions, and electrostatic interactions (Gunawan et al., 2022).

Furthermore, coconut shells possess distinct physical and chemical properties, including high content of fixed carbon, low ash content, good thermal stability, and high density, contributing to their structural strength and durability (Itodo, 2010). For instance, studies have shown that raw coconut shells contain 41% carbon, 70.8% volatile matter, 1.8% ash, 5.6% moisture, and have a density of 412.0 kg/m<sup>3</sup> (Kabir Ahmad et al., 2022). Similarly, Itodo (2010) reported low ash content of CS at 2.96 wt.%, reduced to 1.49 wt.% post-development into AC. The relatively low ash content in CS is beneficial, as it reduce the tendency of fouling which can negatively impact adsorption capacity (Maniarasu et al., 2021).

Research by Ahmad et al. (2021) has indicated that CS possesses both amorphous and crystalline structures, contributing to the production of homogeneous adsorbents via thermal and chemical modifications. Moreover, these structures highly contribute to the mechanical strength and thermal stability, making CS a promising candidate for bio-adsorbent development. Additionally, high fixed carbon content of CS (47.6%) reported by Dongardive et al. (2019) further supports its potential for creating thermally stable

carbon materials. Based on these attributes, coconut shells appear to be a promising material for synthesis of bio-adsorbents specifically designed for CO<sub>2</sub> capture.

### **2.3.2.2 Limitation of unmodified bio-adsorbent derived from coconut shell**

Utilisation of CS biomass in the development of adsorbents has gained attention due to its sustainability and cost-effectiveness. However, raw CS-based adsorbent has lower adsorption efficiency due to limited surface area and active functional groups, tailored to adsorb CO<sub>2</sub>. Untreated coconut shell typically subjected to low surface area and pore volume, restricting the available binding sites for pollutants and affecting its overall adsorption capacity. Additionally, the inherent functional groups, while present, might lack the diversity and abundance to effectively capture a wide range of pollutants, limiting their use in diverse wastewater treatment applications. Furthermore, the pore size distribution in raw coconut shell can be heterogeneous and often not ideal for capturing specific pollutant molecules, leading to lower adsorption rates and reduced efficiency. While raw CS has moderate thermal stability, untreated coconut shells are not chemically and thermally stable for robust enough for applications involving high temperatures or harsh conditions, potentially leading to degradation and a shortened lifespan for the adsorbent.

Several studies have compared the properties of raw and modified CS-based adsorbents in terms of alteration of surface area, carbon content, pore volume, functional groups and ash content. Techniques like carbonisation, activation, and impregnation play a crucial role in enhancing the physical and chemical properties and characterisation of CS-based adsorbent, leading to better adsorption performance. For instance, C. Wang et al. (2021) studied the effect of thermal degradation on the structural properties of raw coconut shell (CS) using gasification. They found that gasification significantly enhance the surface area and formation of porous structure of the material, approximately 78 times

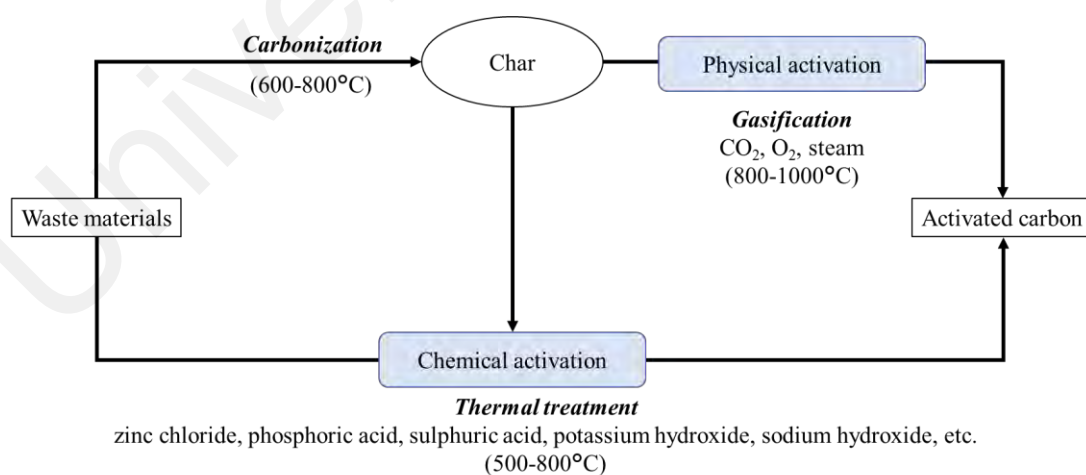
compared to raw CS, indicating larger active sites for adsorption which allow deeper penetration of adsorbates into pores and thereby increasing adsorption efficiency (Saleem et al., 2019). Additionally, gasified-CS has higher microporous structure, pore volume and homogenous pore structure. Recent study also found that thermally treated biomass resulted in reduction of ash content from 2.6% to 0.9%, indicating the potential of CS as promising precursor for adsorbent development (Dongardive et al., 2019). Moreover, the study concluded that precursors with reduced ash content possess fewer non-functional sites and a greater availability of active sites, contributing to enhanced adsorption efficiency. Study by Yağmur and Kaya (2021), also reported that chemical activation by using zinc chloride ( $ZnCl_2$ ) enhance the untreated coconut shell biomass surface area from  $3 \text{ m}^2/\text{g}$  to  $935 \text{ m}^2/\text{g}$ , highlighting the efficacy of this chemical in enhancing pore development and overall surface characteristics.

The effect of modifications on the structural properties of developed adsorbents were reported by Tan et al. (2017). Their research compared non-modified CS-based activated carbon with HCl-functionalised AC. The results indicated that AC treated with HCl has a higher total pore and microporous volume, and BET surface area at  $0.291 \text{ cm}^3/\text{g}$ ,  $0.272 \text{ cm}^3/\text{g}$ , and  $525 \text{ m}^2/\text{g}$  respectively, compared to the non-modified AC at  $0.229 \text{ cm}^3/\text{g}$ ,  $0.218 \text{ cm}^3/\text{g}$ , and  $436.0 \text{ m}^2/\text{g}$ . Although activation is typically associated with oxygen-rich agents like KOH or  $ZnCl_2$ , HCl plays a different role in enhancing the physicochemical properties of bio-adsorbents. As a strong acid, HCl protonates the carbon sphere surface, leading to the formation of carboxylic acid and other functional groups. These functional groups undergo further reactions, facilitating pore formation and increasing the number of active sites. Additionally, the acidic environment created by HCl aids in the removal of impurities and volatile matter, contributing to pore enlargement and improved surface area. This observation suggests that acidic treatment enhances the overall adsorption capacity of bio-adsorbents by optimizing their structural

and chemical properties (G. Liu et al., 2022). Prior research has established that unmodified bio-adsorbents generally display less favorable adsorption properties. Therefore, modifications such as impregnation with other materials, chemical functionalisation, and chemical treatment are commonly utilised to enhance the physical and chemical properties which directly improve the adsorption capabilities of these bio-adsorbents.

#### 2.4 Synthesis methods of adsorbent from waste material

The choice of raw materials and activation method influences the distribution of pore size and the adsorption capability of the activated carbon. Rich carbon content materials such as coal and charcoal have some adsorption capacity. However, to ensure more utilisation of the resources, the precursors are suggested to the activation process to enhance the capacity adsorption. As a result, there are two primary phases in the conventional synthesis of AC; carbonisation and activation. Figure 2.3 illustrate the procedures for the synthesis of AC.



**Figure 2.3: Synthesis process of activated carbon**

From Figure 2.3, waste products are subjected to carbonisation to remove volatile matter, eliminate moisture, and produce char. Next, the char will undergo an activation

process through incorporating an activating agent with the materials. Although further activation resulted in an in reduction of yield AC, it is favorable due to more formation of pores. Activation can be done using two approaches; physically, which is also known as thermal activation, and chemical activation.

#### 2.4.1 Carbonisation

Table 2.5 summarises some differences in conventional pyrolysis and hydrothermal carbonisation (HTC) obtained through reviewing Binti Mohd (2017), Duran-Jimenez et al. (2017), Prathiba et al. (2018), and Haeldermans et al. (2020) work. The speciality of hydrothermal carbonisation over the conventional method is the heating mechanism. In addition, HTC utilised pressure which resulted in major reduction of heat energy required to carbonise the waste materials. Hydrothermal carbonisation has a better reputation compared to traditional pyrolysis due to energy-efficient, fast and time-saving procedures as the system can process wet feedstock (Lam et al. (2015), Liew, Chong, et al. (2018)).

**Table 2.5: Comparison between conventional and hydrothermal carbonisation**

<b>Parameters</b>	<b>Conventional Pyrolysis</b>	<b>HTC</b>
<b>Temperature (°C)</b>	750-1000	150-250
<b>Pressure (bar)</b>	Atmosphere	20-25
<b>Residence time (min)</b>	30-120	30-360
<b>Feed moisture</b>	No moisture	Can accommodate high-moisture feedstock

#### 2.4.2 Activation

After the production of biochar through carbonisation, the procedure is followed by activation. The primary goal for activation procedures is to form pores and cracks, which result in more readily available adsorption sites. This can be achieved by heating the

biochar after being incorporated by an activating agent. Depending on the activating agent, the activation process can be categorised into two groups which are physical and chemical activation. The common medium for physical activation, which is also known as thermal activation, is steam and carbon dioxide, while chemical activation utilises a chemical reactant such as strong acids, KOH and ZnCl<sub>2</sub>. In chemical activation, the reagent is integrated into the precursor to activate the carbon inside the char.

#### **2.4.2.1 Physical activation**

During physical activation, the char produced through pyrolysis is activated by using hot gases. This is typically accomplished through a single or a combination of carbonisation procedures assisted with the presence of inert gas. As a result, the organic matter in the precursors can be converted to primary carbon, which is a mixture of crystalline and amorphous carbon, ash and tar. Next, activation/oxidation places at high temperatures to activate the carbon, with steam or carbon dioxide depending on the desired outcome.

According to Pallarés et al. (2018), activation of char through steam and CO<sub>2</sub> enhances microporous structures. Moreover, Zaini et al. (2021) found that the surface area of AC synthesis through steam activation is better than char treated with CO<sub>2</sub>. According to Ouyang et al. (2020), this happens due to the spontaneous moisture adsorption-desorption on the active site of biochar. This resulted in the creation of hydrogen and oxygen functional groups which assist in pore formation and increment of surface area. However, activation through steam resulted in lower yield compared to the CO<sub>2</sub> treatment. Similar findings were reported by Zaini et al. (2021) and Yek et al. (2020). It can be suggested that the steam resulted in material degradation at high temperature caused by the water molecule. In contrast, CO<sub>2</sub> assisted in reconstructing graphite structure due to the reverse Boudouard reaction.



Physical activation is favourable due to the simplicity of operation and low cost. However, this method led to a low yield of activated carbon as high carbonisation temperature resulted in the production of volatile matter and loss of decomposed organic molecules. Plus, the study by Yang et al. (2010) shows that holding time has the same influence factor as carbonisation temperature. As a result, a longer holding period increases the possibility of the organic compound decomposing, resulting in lower AC yield. Moreover, physical activation requires prior carbonisation leading to more production of tar. As a result, void space in porous carbon is highly subjected to deposition of these decomposed products resulting in the reduction of surface area. In short, the physical treatment uses steam or CO<sub>2</sub> to activate the carbon in the char. High energy is required, and two-step procedures resulted in less productivity of the method.

#### **2.4.2.2 Chemical activation**

The precursors are impregnated with chemicals during the chemical activation approach before carbonisation (Gao et al., 2018). After incorporating the activating agent such as acid, strong base and salt, the samples undergo carbonisation at a lower temperature than physical activation, which is around 500 °C to 800 °C compared to 800 °C to 1000 °C. As the chemical saturate the raw materials, the activation process takes place concurrently with carbonisation. Due to the impregnation of chemical agents, the formation of tar during carbonisation can be reduced significantly. This is crucial as build-up, and deposition of tar at the pore spaces lead to blockage and reduction of surface area. As a result, AC with well-developed pore spaces can be manufacture with the one-step operation. In addition, the incorporation of the activating agent before carbonisation/activation led to a homogenous mixture between precursor and chemical, specifically at the interior wall of raw materials particles. Consequently, the production



of volatile matter during pyrolysis is minimised due to the chemical reaction between carbon in the bio-adsorbent and activating agent. This mechanism prevents the shrinkage of particles and minimizes damage on the surface of the precursor during activation. As a result, a high yield of AC with high carbon content is being produced.

Table 2.6 highlighted some of the differences in operating physical and chemical activation methods. Chemical activation is favoured due to the shorter time and lower heat energy required to synthesise AC. As a result, chemical activation has been widely employed in different projects regarding the synthesis of AC from biomass. Research conducted by Açıkyıldız et al. (2014), Şahin et al. (2015) and Hidayu and Muda (2016) supported that chemical activation approach resulting in lower treatment temperatures, shorter treatment times and production of larger surface area. In placing more emphasis, Oginni et al. (2019) claimed that chemical treatment resulted in the production of AC with better-developed porosity than physical activation. Furthermore, in the study conducted by Yorgun and Yıldız (2015), the findings have shown that chemical activation enables control on porosity structured formed in AC.

**Table 2.6: Characteristics of physical and chemical activation**

<b>Properties</b>	<b>Chemical activation</b>	<b>Physical activation</b>
<b>Activating agent</b>	Chemicals such as H <sub>3</sub> PO <sub>4</sub> , ZnCl <sub>2</sub> , NaOH, KOH, Na <sub>2</sub> CO <sub>3</sub> , K <sub>2</sub> CO <sub>3</sub> , or their combinations	Steam, CO <sub>2</sub> , or their mixtures
<b>Thermal treatment steps</b>	Typically one or two steps	Two steps
<b>Activation temperature (°C)</b>	500-800	800-1000
<b>Activation time (min)</b>	30-120	30-300
<b>Typical yield (%)</b>	40-45	20-25
<b>Predominant pore size</b>	Large pores	Small pores

The study conducted by Asnawi et al. (2019) found that at a similar temperature, AC activated through chemical treatment has higher iodine and methylene blue numbers. A similar finding was reported by Sütçü (2019) in which biomass started by KOH has a higher surface area compared to AC produced through thermal activation. This indicates that chemical activation enhances the porosity formation better than physical activation. This can be due to the properties of the chemical agent which hold the carbon structure from collapsing due to the high temperature. In addition, the chemical agent also enhances the degeneration of lignocellulose structure in the waste materials.

It is reported that the production of AC through physical activation resulted in narrow pore distribution, concentrating at micropore formation compared to AC produced through  $ZnCl_2$  and  $H_3PO_4$  treatment. This feature is desirable for adsorption of gaseous such as  $CO_2$ . However, a study conducted by Prauchner and Rodríguez-Reinoso (2012) found that activation through a physical approach resulted in more control in the distribution of pores formed. Although scarce, a similar finding was reported by Sütçü (2019) and Kim et al. (2017). Moreover, research conducted by Kim et al. (2017) found that physical activation resulted in higher AC yield at a temperature below 800 °C. This is because, at higher temperatures, the porous carbon structure deteriorates, resulting in a sharp reduction of yield AC. This claim can be supported by findings from Hadi et al. (2016).

Both physical and chemical activation have respective advantages and disadvantages. The technique used to combine the activator and precursors during chemical activation can significantly affect the physicochemical properties of the resulting activated carbon. Essentially, wet impregnation and dry solid-solid mixing may be used to mix the starting materials or char substance with the chemical agent. In wet impregnation, precursors are introduced to a solution of activating agent and water. In the meantime, in solid-solid

mixing, raw material or char is mixed immediately with the activating agent before thermal treatment is carried out.

## **2.5 Operating parameters affecting the synthesis process of adsorbent**

### **2.5.1 Effect of activating agent**

The choice of chemical agent plays a significant control on the produced AC. This is because the reactivity, oxidizing properties and thermal stability of the activating agent will alter the surface area, porosity, and functional group of AC by reacting with existing minerals. During the physical activation process, utilising steam and air has improved the reaction time significantly compared to CO<sub>2</sub>. However, it can be challenging to control the activation process as the reaction between carbon and the atmosphere is speedy, resulting in the burnout of internal pore structures and the external carbon's surface. Therefore, despite the considerable potential of air, CO<sub>2</sub> shows more significant efficacy in physical activation as it results in higher yield and is more easily handled and cleaned.

In chemical activation, the effect of an activating agent towards AC is more complex. Different chemicals result from other products on the precursors. Nevertheless, specific trends can be portrayed when comparing other activating agents with the same raw materials. Compared to acidic-based activating agents, utilisation of alkaline-based chemicals can assist in the degradation of glucose, dissolution of ether linkages, lignin, and hydroxyl functional groups. As a result, the accessibility of pores increases due to the breakage of longer fibres. In addition, utilisation of the alkaline solution associated with potassium, such as KOH and K<sub>2</sub>CO<sub>3</sub> led to an increase in micropore generation due to potassium's ability to stretch the carbon layers. According to Li et al. (2016), the addition of KOH to pine cone-shell increases the surface area and the CO<sub>2</sub> adsorption performance. This finding is also being supported by Jawad et al. (2021) by incorporating KOH in dragon fruit peel during production. It was recorded that the AC's total volume improved

significantly to  $0.376 \text{ cm}^3/\text{g}$  from  $0.003 \text{ cm}^3/\text{g}$ . Furthermore, the investigation conducted by Li et al. (2017) found that the addition of a strong alkaline activating agent such as KOH onto wood promotes the pyrolysis process at lower activation temperature. AC precursor poplar wood saturated with KOH has a high specific surface area and a more uniform microporous distribution. These findings are on par with claims made by Elmouwahidi et al. (2017), in which samples activated with KOH consist of more pore spaces. Furthermore, the study also portrays that olive residues activated by KOH have higher  $\text{CO}_2$  adsorption than samples impregnated with  $\text{H}_3\text{PO}_4$ , which is  $0.54 \text{ mmol/g}$  and  $0.18 \text{ mmol/g}$ , correspondingly. This review also confirmed that KOH treatment led to micropores formation as the sample showed type I isotherms.

Albeit the use of KOH is advantageous in micropores formation, this chemical is subjected to high corrosion and environmental risk. Production of AC usually requires a high-temperature condition that can enhance KOH's corrosive properties towards the equipment. Therefore, some studies suggested using mild activators such as  $\text{K}_2\text{CO}_3$  as suited as not harmful to nature. Research conducted by Yue et al. (2018), Kim et al. (2020), and Guo et al. (2015) highlighted the potential of  $\text{K}_2\text{CO}_3$  as an activating agent and some relevant issues on the application. According to Guo et al. (2015), treatment of  $\text{K}_2\text{CO}_3$  on coconut activated carbon results in higher utilisation of active components and higher stability. The maximum  $\text{CO}_2$  adsorption capabilities were also found to reach  $1.015 \text{ mmol/g}$  with a carbonation conversion of 79%. The value obtained shows the potential of the produced AC by  $\text{K}_2\text{CO}_3$  activation when compared to the  $\text{CO}_2$  capacity of commercially activated carbon. Findings by Yue et al. (2018) also support this finding. It was reported that the urea-modified carbonised coconut shell (CN)  $\text{CO}_2$  adsorption capacity improved by more than 60%, from  $1.44 \text{ mmol/g}$  to  $3.71 \text{ mmol/g}$  through  $\text{K}_2\text{CO}_3$  treatment. In a recent study, Kim et al. (2020) emphasize that activation of spent coffee ground at a ratio of 1 between  $\text{K}_2\text{CO}_3$  and AC at  $700^\circ\text{C}$  resulting in a  $\text{CO}_2$  capacity of

4.54 mmol/g. This value is almost identical to Travis et al. (2015) where AC precursor waste coffee activated at 700°C with KOH has CO<sub>2</sub> adsorption capacity of 4.42 mmol/g. These findings prove that K<sub>2</sub>CO<sub>3</sub> has identical and/or superior potential in replacing KOH for the activation of carbon materials with a focus on high creation of micropores. The accessibility of pores increases when utilising K<sub>2</sub>CO<sub>3</sub> due to the occurrence of redox reactions which formed potassium metal and carbon monoxide during the activation of carbon-rich materials.

A study conducted by RAHMAN (2020) found that activation of rice husk by using NaOH produced AC with lower ash content and volatile matter. By incorporating NaOH, the values were reduced from 19.11% to 13.09% and 14.06% to 7.47%, respectively. The fixed carbon value, determined by proximate analysis, increased from 66.83% to 78.63% after activation, indicating a notable improvement in the carbon content. Conversely, the carbon content values, as determined by ultimate analysis, also increased from 55.08% to 69.02% after activation. The surface area increases due to the diffusion of Na particles into the carbon's surfaces at the temperature of boiling point resulting in the formation of new pores. This claim can be supported by findings from Rostamian et al. (2015), Zhang et al. (2019), and Liew, Azwar, et al. (2018).

A study conducted by Luo et al. (2016) compares the AC properties produced by chemically activated pinewood char using KOH and H<sub>2</sub>O<sub>2</sub>. A more significant improvement of pore properties was observed on AC treated with KOH compared to H<sub>2</sub>O<sub>2</sub>. The surface area increases from 363.0 m<sup>2</sup>/g to 1124.4 m<sup>2</sup>/g. Chowdhury et al. (2013) conduct research on the influence of two alkaline activating agents; NaOH and KOH, on AC precursor rice husk. It was concluded that both treatments resulted in activated carbon production subjected to high surface area properties, approximately 1000 m<sup>2</sup>/g and above. AC produced from NaOH treatment has a larger surface area than

KOH that is around 2952 m<sup>2</sup>/g compared to 2551 m<sup>2</sup>/g. The fast intercalation of potassium can explain this occurrence due to its low boiling point compared to NaOH.

Alkaline-based activating agent assisted in the activation of carbon through the breakdown of lignin structure. Among all the alkaline activating agents, KOH is most preferred due to the formation of metallic potassium, which enhances the formation of microporous structures. NaOH, H<sub>2</sub>O<sub>2</sub> and K<sub>2</sub>CO<sub>3</sub> are other alkaline treatments used to activate the biochar.

### **2.5.2 Effect of holding temperature**

Other essential factors that mainly decide the pore volume, distribution of pore size, development of microporosity, and surface area of the produced activated carbon are the temperature during the carbonisation and activation of carbon materials. In general, higher temperatures will eliminate moisture and volatile matter content in the precursor, leading to more pore creation which is preferable due to the creation site for adsorption. However, as the temperature increases, it is expected that the yield of AC will decrease significantly. Simultaneously, higher ash and fixed carbon content formed.

According to studies conducted by various researchers such as Zhang et al. (2010), Ceyhan et al. (2013), Esterlita and Herlina (2015), Kumar and Jena (2015), Mochizuki et al. (2016), Allwar et al. (2017), Li et al. (2017) and Van Tran et al. (2017), it can be deduced that the selection of chemical treatment plays a crucial role in determining the suitable activating temperature. This is due to each chemical reacting differently with the carbon component in the biomass. In addition, these activating agents have diverse chemical properties such as boiling and melting points as well as mobilization of metallic ions.

Esterlita and Herlina (2015) claimed that the best-activating temperature for KOH treatment is between 700°C to 800°C. Mochizuki et al. (2016) also discovered that an

increment of activation temperature from 700°C to 800°C improves the surface area and micropore volume significantly. It was recorded that the surface area increased by 33%, from 1955 m<sup>2</sup>/g to 2600 m<sup>2</sup>/g, which is significant compared to less than 10% improvement of surface area when the temperature shifted from 600°C to 700°C. This is in line with the findings by Li et al. (2017), Tiwari et al. (2018), and Han et al. (2019). According to Li et al. (2017), increment of activation temperature from 700-800 °C enhances the surface area of AC significantly, up to 3228 m<sup>2</sup>/g. However, a depreciation in carbon yield and surface area was recorded as the temperature rose to 850°C.

Moreover, Han et al. (2019) reported that the average pore width increases from 0.520 nm at 500°C to 0.573 nm at 800°C. This exponential improvement can be explained by the formation and mobilization of metallic potassium at a temperature of about 700 °C, which assists the formation of the pore. In addition, the reaction between potassium, carbon, and water produced potassium carbonate, which would minimize the burn-off of precursors.

### **2.5.3 Effect of impregnation ratio**

Another variable that manipulates the properties of AC produced is the impregnation ratio during the chemical activation procedures. The impregnation ratio is the ratio between the weight of the activating agent and the weight of the raw material impregnated. In theory, a greater impregnation ratio results in more swelling, and enables a stronger release of volatile matter contents, resulting in pore widening. Concurrently, a low concentration of activating agent assists in more stable elimination of volatile matter contents while inhibiting tar deposition, resulting in more micropores.

Studies conducted by Örkün et al. (2012), Ateş and Özcan (2018), and Misran et al. (2020) show the importance of impregnated ratio to the development of pore structures. The effect of the impregnation ratio is supported by Foo and Lee (2010). The experiment

discovered that AC prepared from *Parkia speciosa* pods with the mass ratio of 1 is better adsorbent than the product formed by incorporation of acid to precursor ratio of 0.5. In placing more emphasis, Al-Swaidan and Ahmad (2011) discovered that the surface area of AC precursor date tress frond waste can be maximized by impregnation of  $H_3PO_4$  with a concentration of 60%. By increasing the  $H_3PO_4$  concentration from 0% to 40%, the surface area and micropores volume increase. Nonetheless, the extension of  $H_3PO_4$  concentration to 80% led to an increase in surface area and shifted the porosity distribution to mesoporous structures. At 60%  $H_3PO_4$  concentration, the surface area reported was  $1139\text{m}^2/\text{g}$ . Further examination revealed that the optimum temperature for activation of the sample is  $400^\circ\text{C}$ . Furthermore, Örkün et al. (2012) discovered that by increasing the concentration of  $H_3PO_4$  from 35% to 65%, the pore distribution shifted from mainly micropores to dominantly mesoporous structures. It was also noted that the surface area increases from  $2120.7\text{ m}^2/\text{g}$  to  $2322.5\text{ m}^2/\text{g}$  when the concentration of  $H_3PO_4$  rise from 35% to 65% due to a high reaction between the chemical and raw materials.

According to Ateş and Özcan (2018), a higher impregnated ratio resulted in the formation of mesopores, whereas the production of microporous structure can be manifest by lowering the concentration of the activator. In the study, the ratio experimented on sawdust were 1:1, 2:1, 3:1, and 4:1. Each of the samples saturated with  $ZnCl_2$ , KOH and  $H_3PO_4$  were carbonised at  $500^\circ\text{C}$ ,  $700^\circ\text{C}$  and  $800^\circ\text{C}$ . It was recorded that increment of  $ZnCl_2$  and KOH concentration led to a lower yield of AC. Similar findings were demonstrated regardless of the carbonisation temperature employed. This might be due to an oversupply of  $ZnCl_2$  and KOH, resulting in widening pores. Thus, higher formation of meso and macropores were observed. Studies by Örkün et al. (2012), Fiuza-Jr et al. (2016) and Joshi and Bishnu (2020) reported a similar finding. However, a study conducted by J. Singh et al. (2019) shows that increment of KOH concentration led to the increment of micropore volume. Taking into account, BET surface area of AC was found



to have increment up to 1884.2 m<sup>2</sup>/g from 1152.46 m<sup>2</sup>/g when the KOH ratio has increment from 1:1 to 3:1. The amount of micropores also increased to 1.34 cm<sup>3</sup>/g from 0.33 cm<sup>3</sup>/g. A similar finding was also reported by (Shen et al., 2019) through synthesise of porous carbon using rice husk as precursor. This occurrence is due to the reaction of KOH during carbonisation/activation leads lead to the formation of K<sub>2</sub>CO<sub>3</sub>, K and H<sub>2</sub>. The existence of metallic K in the pore formation widened the graphitic layered structures and generated the pores, increasing the surface area.

## **2.6 Functionalisation of carbon materials**

As feed stream from flue gas contains water, SO<sub>x</sub>, NO<sub>x</sub> and CO in addition to CO<sub>2</sub>, it is crucial to develop adsorbent with high CO<sub>2</sub> selectivity. Considering both material composition and textural properties, it is essential to understand the surface functional group. Suitable functional group will enhance the CO<sub>2</sub> adsorption as well as selectivity compared to other components. Functional groups of AC can be formed through many methods such as inclusion of heteroatoms and metal oxides.

### **2.6.1 Heteroatoms**

It is well known that adsorption of CO<sub>2</sub> takes places at the smallest pore of the adsorbate. Thus, high density of microporous formation is crucial in synthesising AC. However, the readily available micropores also enhance the adsorption of other gases such as CH<sub>4</sub>, N<sub>2</sub> and CO, resulting in disturbance of adsorption process due to the competitiveness. As a result, the CO<sub>2</sub> adsorption capacity of AC decreases. In this regard, heteroatoms such as oxygen, sulphur and nitrogen play an essential role by exclusively interact with CO<sub>2</sub> leading to increase in CO<sub>2</sub> selectivity and assist in gas separation.

A heteroatom in an organic molecule is any atom that is not a carbon atom or a hydrogen atom. Generally, these are three types of heteroatoms can lead to creations of

many functional groups such as phenol, carbonyl, ethers, hydroxyl, amine amid, pyridine, sulphones and sulphoxides. However, not all functional group created has direct relationship with enhancement of CO<sub>2</sub> selectivity. Therefore, examining the suitable functionalities is crucial to determine the suitable heteroatoms impregnated with the AC precursor.

By treating AC with oxygen or utilising raw materials rich with oxygen as AC precursor, formation of hydroxyl, carboxylic and phenol functional groups can facilitate capture of carbon dioxide. According to Wang (2021) incorporation of hydroquinone with carbon matter resulted to increment of CO<sub>2</sub> adsorption capacity from 3.02 mmol/g to 3.46 mmol/g. This can be supported by Bai et al. (2015) in which the performance of AC precursor polyacrylonitrile enhanced through simple liquid-oxidization on CO<sub>2</sub> adsorption by up to 111% as compared to the raw AC. Vega et al. (2013) found that incorporating nitrogen and oxygen into the AC reduced the surface area from 927 m<sup>2</sup>/g to 861 m<sup>2</sup>/g and 858 m<sup>2</sup>/g. Similar findings were noted for micropore volume and total pore volume. The results also show that nitric acid treatment resulted in more formation of oxygen functional group such as -OH group. Creation of -OH group will enhance the carbon dioxide adsorption capacity.

Studies by Xia et al. (2011), Kronast et al. (2016), Boyjoo et al. (2017), Manmuanpom et al. (2018), Yue et al. (2018), and Wang et al. (2018) highlighted the improvement of CO<sub>2</sub> adsorption capacity through enhancing the adsorbent with nitrogen. Ma, Li, Chen, Wang, Li and Li (2018) observed that an increase in mesopore and macropore formation, resulting from higher activation temperatures, did not significantly affect carbon dioxide adsorption capacity. In their study, the highest CO<sub>2</sub> adsorption capacity was observed with a urea-enriched activated metal-organic framework, attaining a value of 3.70 mmol/g. Cong et al. (2015) reported that the functionalisation of nitrogen functional groups onto carbon materials led to an improvement in CO<sub>2</sub> selectivity over N<sub>2</sub>, increasing

from 28.4 to 48.7. J. Singh et al. (2019) demonstrated that activated carbons with elevated nitrogen content, even with reduced surface area and micropore volume, exhibited superior CO<sub>2</sub> adsorption capacity compared to adsorbent with larger pore volume and surface area.

Han et al. (2019) further highlighted the significance of both micropores and nitrogen functional groups, particularly pyridine, pyridone, and pyrrolic groups, in enhancing carbon dioxide adsorption capacity. Saha et al. (2019) further highlighted the significant influence of pyridine and pyridone functionalities on carbon dioxide adsorption. These functionalities, even in the absence of hydroxyl groups, are considered by some to be more effective surface modifications for CO<sub>2</sub> capture. This claim is supported by Bae et al. (2014), who observed improved CO<sub>2</sub> adsorption under humid conditions through reduced H<sub>2</sub>O adsorption upon modifying MOFs with pyridine. Surface property analysis conducted by Han et al. (2019) also confirms the presence of similar functional groups on nitrogen-doped activated carbon.

According to Yadavalli et al. (2017), modification of carbon using ammonium sulphate improve the performance of CO<sub>2</sub> capture. In addition, enhancement of AC resulted in better CO<sub>2</sub> selectivity compared to methane. This can be explained by the existence of sulphur functional group which allow interaction between polarisable d-orbitals and the sole pair of electrons of S atoms with oxygen in CO<sub>2</sub>. Similar finding can be obtained from Guo et al. (2018) in which sulphur saturated AC resulted in better removal of phenol. Kronast et al. (2016) also reported that CO<sub>2</sub> adsorption improve up to 2.4mmol/g due to addition of organic sulphide into MOF. Moreover, study by Seema et al. (2014) shows that sulphur-doped microporous carbon enhanced the selectivity of CO<sub>2</sub> compared to CH<sub>4</sub>, N<sub>2</sub> and H<sub>2</sub> exponentially.

According to the review, AC's oxygen, nitrogen, and sulphur heteroatoms resulted in higher CO<sub>2</sub> adsorption performances. This is due to introduction of new functional groups

such as hydroxyl, pyridine and sulphones which lead to more active site for CO<sub>2</sub> binding. There are two methods in incorporation of heteroatoms which are synthesis AC from rich heteroatoms materials and doping.

### 2.6.2 Metal oxides

Shahkarami et al. (2016), Hakim et al. (2015), and Hidayu and Muda (2016) study the effect of incorporation of metal oxides with adsorbent with CO<sub>2</sub> adsorption performance. According to Hakim et al. (2015), impregnating iron (III) oxide to AC enhances the CO<sub>2</sub> adsorption capacity even though the surface area decreases as the concentration of Fe<sub>2</sub>O<sub>3</sub> increases. Although increment of metal oxides leads to pore clogging, the existence of functional group due to acid base properties overcome the physisorption limitation. Similarly, Shahkarami et al. (2016) reported that impregnation of MgO into AC has improve the adsorption performance of CO<sub>2</sub> at higher temperature. It was noted that the performance of AC in adsorbing CO<sub>2</sub> at 100°C improve 65% due to impregnation of MgO. Moreover, by incorporating magnesium oxide (MgO), titanium oxide (TiO<sub>2</sub>) barium oxide (BaO), cerium oxide (CeO<sub>2</sub>) and copper oxide (CuO) separately into AC precursor palm kernel shell and coconut shell, Hidayu and Muda (2016) reported that the adsorption of CO<sub>2</sub> improved, especially with BaO-enhanced AC. BaO resulted in highest improvement due to its high difference in electronegativity compared to other metal oxides. As a result, BaO is more polar leading to increase of affinity of AC towards CO<sub>2</sub>.

According to Walton et al. (2006), basic oxides will enhance CO<sub>2</sub> adsorption more than acidic, amphoteric and neutral oxides. In general, adsorbent impregnated with metal like calcium and magnesium oxide produced 1 mol of oxide through chemical reaction between CO<sub>2</sub> and metal component. This indicated that higher concentration of metal oxides will result in better performance of CO<sub>2</sub> adsorption due to the availability of active site. Among the alkaline metal, MgO has high potential due to low heat required for

regeneration and can operate at lower temperature than CaO, BaO, and LiO. In addition, the study by Hanif et al. (2016) shows that MgO has a high surface area of up to 400 m<sup>2</sup>/g, higher than other potential metal oxides such as TiO<sub>2</sub>. The standard metal oxides incorporated are MgO, BaO, CeO, LiO and Fe<sub>2</sub>O<sub>3</sub>.

The addition of metal oxide enhances the adsorption and selectivity of CO<sub>2</sub> despite the reduction in surface area due to the increment in the basic sites which lead to acid-based interaction with CO<sub>2</sub>. In terms of CO<sub>2</sub> capacity and selectivity, BaO is more preferred due to its high alkalinity and electronegativity. However, MgO has more advantages due to low heat requirement for regeneration.

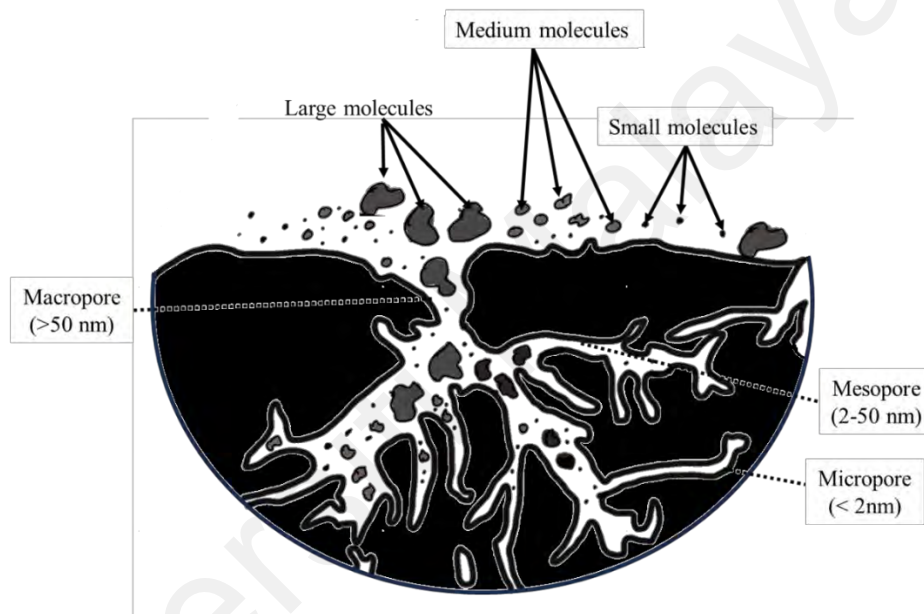
## **2.7 Significant physicochemical characteristics of adsorbent**

Both the physical and chemical qualities of adsorbent are essential in order to generate it for a particular application. This sub-chapter explains important characteristics such surface area, porosity, and surface chemistry as a consequence. Additionally, it is crucial to characterise the bio-adsorbents because each material has unique properties that rely on the types of starting materials and the conditions of the processing.

### **2.7.1 Porosity and surface area**

The textural properties of adsorbents, including porosity, pore geometry, and specific surface area, critically influence their adsorption performance. These parameters dictate the accessibility of adsorption sites, diffusion kinetics, and overall capacity. Porosity in adsorbents is classified by the International Union of Pure and Applied Chemistry (IUPAC) into three categories based on pore width. Pore geometry—whether slit-shaped (distance between opposing walls) or cylindrical (radius)—further influences adsorption behavior. Figure 2.4 illustrates the hierarchical pore structure typical of activated carbon, highlighting the coexistence of macro-, meso-, and micropores. Macropores is defined as

any pores with a width which exceeds 50 nm, mesopores are pores with a width range between 2 and 50 nm, enabling capillary condensation and multilayer adsorption, whereas micropores are pores with width less than 2 nm. Micropores are further classified into super-micropores (pore width < 0.7 nm) and ultra-micropores (pore width between 0.7 and 2.0 nm), which resulted in its dominate surface area contributions due to their high internal surface-to-volume ratios (Hidayat & Sutrisno, 2016).



**Figure 2.4: Pore structure of an activated carbon**

The Brunauer-Emmett-Teller (BET) method, utilizing  $N_2$  physisorption at 77 K, is the standard technique for quantifying specific surface area. Activated carbon-based bio-adsorbents typically exhibit BET surface areas of 500–1,500  $m^2/g$  (Onawumi et al., 2021).  $N_2$  is frequently employed as an adsorbate in the determination of surface area.  $N_2$  is ideal for materials with surface areas  $> 0.5 m^2/g$  due to its inertness and molecular cross-sectional area (0.162  $nm^2$ ). Adsorption data are plotted as isotherms, which correlate adsorbed gas volume with relative pressure ( $P/P_0$ ) and reflect pore structure

characteristics. Isotherm profiles provide insights into adsorbent-adsorbate interactions and pore morphology. The IUPAC classifies six isotherm types (Figure 2.5(a)), each associated with distinct adsorption mechanisms.

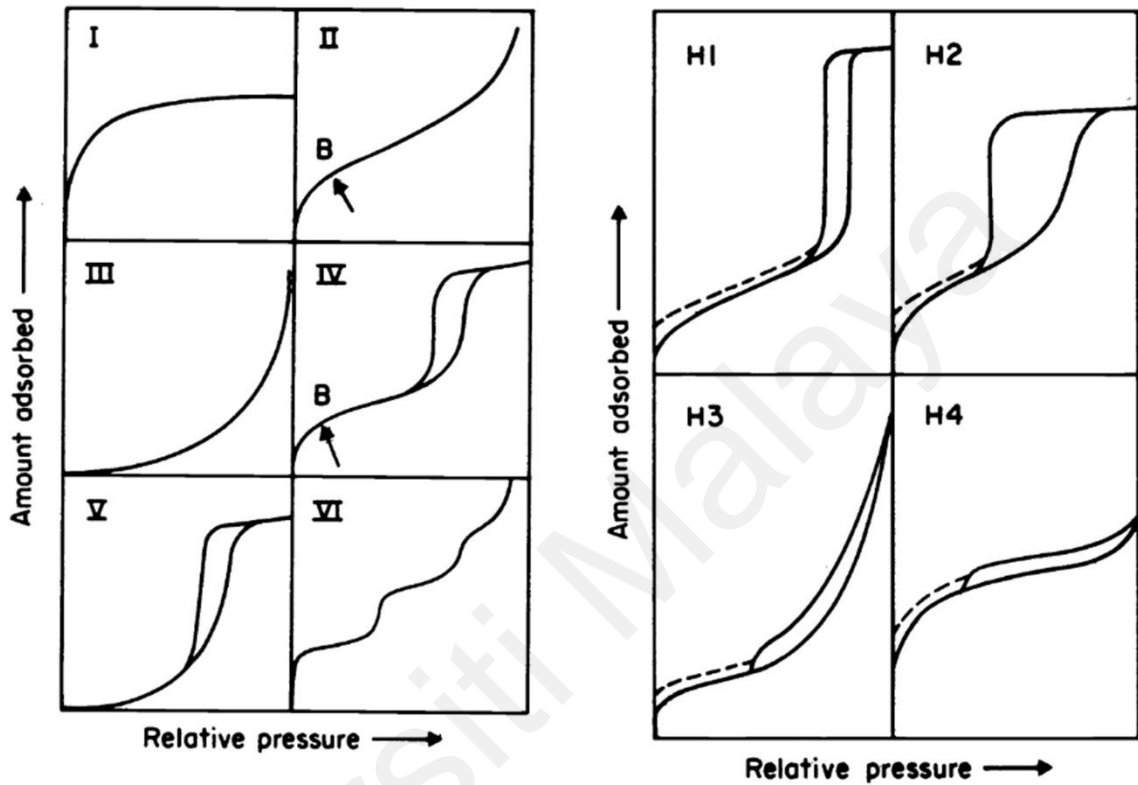


Figure 2.5: Classification of (a) isotherm based on  $N_2$  physisorption, and, (b) types of hysteresis (Sing, 1985)

Type I isotherms are characteristic of microporous materials, such as activated carbon, where adsorption occurs predominantly via monolayer formation at low relative pressures ( $P/P_0$ ). The rapid saturation observed at higher  $P/P_0$  signifies limited pore accessibility, as micropores ( $< 2$  nm) become filled without hysteresis, indicating a reversible process. Type II isotherms, typical of non-porous or macroporous ( $>50$  nm) adsorbents, exhibit unrestricted multilayer adsorption. The initial linear region (up to point B) corresponds to monolayer coverage, followed by a gradual rise due to multilayer formation. Unlike Type I, Type II lacks a saturation plateau, reflecting the absence of pore-filling constraints. Type III isotherms, marked by a convex upward curve, arise from weak, non-specific

interactions between the adsorbate and macroporous/non-porous surfaces, such as hydrophobic materials. Adsorption increases gradually with  $P/P_0$ , driven primarily by adsorbate-adsorbate interactions rather than surface affinity.

Type IV isotherms are associated with mesoporous (2–50 nm) materials, combining monolayer-multilayer adsorption at low  $P/P_0$  with capillary condensation at intermediate to high pressures. This results in a steep uptake followed by a plateau, signifying pore saturation. Hysteresis loops (H1–H4 in Figure 2.5 (b)) emerge during desorption due to delayed evaporation of condensed adsorbate, influenced by pore geometry and connectivity. Type V isotherms resemble Type IV but are distinguished by weaker adsorbent-adsorbate interactions, leading to minimal adsorption until capillary condensation dominates at elevated  $P/P_0$ . This behavior is common in materials with both weak surface affinity and mesoporosity. Finally, Type VI isotherms, observed in highly ordered non-porous surfaces like graphitized carbon, display stepwise multilayer adsorption. Each step corresponds to the completion of a molecular monolayer, with step height reflecting monolayer capacity. This isotherm underscores the role of surface homogeneity in dictating adsorption layering (Rahman et al., 2019).

### **2.7.2 Surface chemistry**

The surface chemistry of adsorbents plays an important role in influencing the adsorption capacity and behaviour of adsorbate onto the material, as it dictates the adsorption interaction. The chemical properties of bio-adsorbents are dependent by the presence of heteroatoms such as oxygen, nitrogen, sulphur, phosphorus, and halogens within the carbon matrix (Saha & Kienbaum, 2019). These heteroatoms disrupt the graphitic structure, creating active sites that enhance surface polarity, hydrophilicity, or catalytic activity. For instance, oxygen-containing groups (e.g., carboxyl, hydroxyl, carbonyl) improve hydrophilicity and ion-exchange capacity, while nitrogen functionalities (e.g.,



pyridinic, pyrrolic) can enhance  $\pi$ - $\pi$  interactions or redox activity. While elemental analysis is used widely to characterise the types and composition of elements present in the carbon structure, it cannot determine the specific functional groups formed on the surface of the adsorbent. Accordingly, the elemental analysis could not reflect the surface chemistry of porous carbon.

Fourier Transform Infrared (FTIR) spectroscopy offers a promising method for investigating the surface chemistry and functional groups of adsorbents. When molecules absorb infrared radiation, transitions in the molecule vibrational or rotational energy states generate characteristic absorption bands in the IR spectrum (Ranjan, 2023). By comparing these bands to reference spectra, specific functional groups—such as C=O stretching ( $1,650$ – $1,750$   $\text{cm}^{-1}$ ) or O-H bending ( $3,200$ – $3,600$   $\text{cm}^{-1}$ )—can be identified. For example, a broad peak near  $3,400$   $\text{cm}^{-1}$  typically indicates hydroxyl groups, while a sharp peak at  $1,700$   $\text{cm}^{-1}$  suggests carbonyl functionalities. FTIR thus bridges the gap left by elemental analysis, enabling precise mapping of surface chemistry and its role in adsorption mechanisms.

### **2.7.3 Thermal stability**

Thermal stability is a critical characteristic that defines the applicability of adsorbent materials in various high-temperature processes. Thermogravimetric Analysis (TGA) is a widely used technique to evaluate the sensitivity and thermal stability of adsorbents. TGA measures the amount and decomposition rate of materials through weight change as a function of temperature or time under a controlled atmosphere. This technique provides valuable insights into the thermal degradation behavior and composition of the adsorbent. The thermal stability of an adsorbent is determined by heating the sample at a constant rate while recording the weight loss. The resulting thermogram reveals important information about the thermal decomposition temperatures, thermal degradation

mechanisms, and the presence of various components within the adsorbent. For instance, weight loss at lower temperatures might indicate the loss of moisture or volatile compounds, whereas weight loss at higher temperatures typically signifies the breakdown of the adsorbent's matrix.

Using TGA, the thermal sensitivity of material can be identified at specific temperatures in which different phases of decomposition occur, which assist in understanding the overall stability of the material. This information is essential for determining the suitability of adsorbents in applications requiring thermal resilience. Furthermore, the analysis can be complemented with differential scanning calorimetry (DSC) to provide a more comprehensive understanding of the thermal transitions occurring within the adsorbent. The comparison of TGA data with standard thermograms of known materials can facilitate in identifying the presence of specific compounds or functional groups that contribute to the thermal behavior of the adsorbent.

## **2.8 Recent advances in adsorption prediction for practical application**

Usually, adsorption prediction is made based on isotherms, thermodynamics, and kinetics to model and predict adsorption behavior as well as the adsorption mechanism. Isotherms are crucial as the model used describe the amount of CO<sub>2</sub> adsorbent into the adsorbent, providing vital information about the capacity and affinity of the adsorbent. However, the drawback of isotherms is that the model is structured based on empirical or semi-empirical models, which may not fully capture the molecular-level interactions and complexities of the adsorption process. To overcome these limitations, recent approaches involving computational modelling and quantum chemistry have been developed to provide deeper insights into the CO<sub>2</sub> adsorption mechanisms.

Quantum chemistry focused on applying quantum mechanics to chemical systems, offers detailed insights into the electronic structure of molecules and materials. This

information is crucial for studying adsorption mechanisms at an atomic level, which is essential for designing efficient materials for CO<sub>2</sub> capture. Several key computational methods are used in this field. Density Functional Theory (DFT) is predominantly used in quantum chemistry for studying adsorption due to several key advantages that make it more practical and accessible compared to other methods such as Quantum Monte Carlo (QMC), Molecular Dynamics (MD), Ab Initio Molecular Dynamics (AIMD), Hartree-Fock (HF), Coupled Cluster Single and Double (CCSD), and Brueckner Doubles (BD). DFT optimise both the computational cost and accuracy, handling systems with a relatively large number of atoms (hundreds to thousands) efficiently, which is suitable for studying complex adsorbent-adsorbate interactions.

Similar to other model, DFT enable approximation of the electronic structure of systems with many electrons by using functionals of the electron density, predicting adsorption energies, optimising geometries, and providing insights into electronic properties of adsorbent-adsorbate interactions. In contrast, methods like QMC, CCSD, and BD are highly accurate but computationally expensive, scaling poorly with system size and making them impractical for large systems or routine calculations. DFT provides good accuracy for a wide range of chemical systems, including those involving adsorption processes, with functionals like PBE, B3LYP, and van der Waals-corrected functionals enhancing its ability to model dispersion interactions critical for adsorption. While Hartree-Fock can offer insights into the electronic structure, it neglects electron correlation, leading to less accurate predictions for adsorption energies compared to DFT.

Applications of these computational methods span various adsorbent materials. For example, Deng et al. (2024) analysed the interactions between CO<sub>2</sub> molecules and bio-adsorbents. Employing density functional theory and molecular dynamics, they revealed a shift from monolayer to bilayer adsorption of CO<sub>2</sub> when pore size surpasses 0.5 nm. The presence of oxygen and nitrogen functional groups was reported to enhance

adsorption capabilities by modifying hydrogen bonding interactions and electron transfer between carbon dioxide molecules and carbon-based adsorbent surface. This finding is further corroborated by the DFT analysis of corn cob-based bio-adsorbents conducted by Li et al. (2024), which demonstrated that heteroatom doping improves both adsorption energy and selectivity towards CO<sub>2</sub> compared to other gases.

Aside from bio-adsorbent, study by Lv et al. (2024) has successfully analysed the influence of different metal doped with MgO on the efficiency of CO<sub>2</sub> adsorption. Their study concluded that doping MgO (100) surface with transition metals increased CO<sub>2</sub> adsorption capacity, attributed to the formation of additional O-top sites during the doping process, facilitating stronger interactions between CO<sub>2</sub> and the surface through Mg-O bond formation. Recent work by Zhao et al. (2024) further revealed that CO<sub>2</sub> adsorption is more favorable on the MgO (110) plane compared to the (100) plane, due to higher adsorption energy. The optimisation of both the crystallographic orientation and the selection of dopant metal can significantly enhance interfacial charge transfer processes, resulting in efficient CO<sub>2</sub> capture on the surface of M/MgO (110) adsorbent.

Selection of models during DFT analysis is essential in achieving accurate and efficient simulations of molecular and material properties. The model should be selected in order to optimise the structure, predict reaction mechanisms, and understand the electronic properties of the system. In DFT and Gaussian simulations, several models and functionals are commonly used. B3LYP (Becke, 3-parameter, Lee-Yang-Parr) is a hybrid functional that combines the Hartree-Fock method with DFT, incorporating both exchange and correlation energies. It is widely used because it provides a good balance between accuracy and computational cost, particularly for organic molecules and systems with significant non-covalent interactions (Yanai et al., 2004). PBE (Perdew-Burke-Ernzerhof), a generalized gradient approximation (GGA) functional, is favoured for solid-state calculations and materials science due to its good accuracy for structural properties

and relatively low computational cost. Study by I. Singh et al. (2019) highlighted the role and importance of model selection in DFT calculation. It was concluded that the B3LYP functional, M06-2X, X3LYP, and CAM-B3LYP are widely used and reliable functionals for studying non-covalent interactions, van der Waals, and hydrogen bond interactions, respectively, and their hybrid qualities enhance their applicability.

Aside from bio-adsorbent and metal oxide, other adsorbent such as zeolites, crystalline aluminosilicates with high surface area and carbon dioxide adsorption capacity were previously modelled by using quantum chemical studies to predict and formulate the interaction between CO<sub>2</sub> and the framework's acidic or basic sites, using DFT calculations. MD simulations were used to study cation-exchange and CO<sub>2</sub> diffusion within zeolite pores. Carbon-based materials such as biochar, graphene, activated carbon, and carbon nanotubes also feature in quantum chemistry studies, focusing on the influence of surface functional groups in enhancing carbon dioxide adsorption. Investigations often explore nitrogen-doped graphene for improved CO<sub>2</sub> capture and the effect of defect sites on adsorption energy.

## **2.9 Summary**

This chapter has detailed and enlarged on the role of adsorption in the post-combustion process, specifically the use of bio-adsorbent-based activated carbon. The first section of this chapter provides a full explanation of the principle of adsorption process, which includes the mechanism and forms of adsorption. Investigation of industrial and agricultural waste as the precursor for the synthesis of bio-adsorbent derived from activated carbon has received a lot of attention. Synergistic effects may well be expected in the case of generating bio-adsorbent utilising these blend precursors due to changes in chemical/physical properties brought on by the relationship between the blend ingredients. Furthermore, studies on synthesise of hybrid bio-adsorbents consisting of

heteroatoms and metal oxides are limited. Physical mixing, also known as dry-dry mixing, is still not looked thoroughly by researchers. Hence based on this limitation, there is an urge to employ the solid-solid mixing technique. Compared to the conventional solvent-based protocols, this solid-solid mixing method prevents lengthy impregnation process. Thus, this method is simple, mild reaction conditions, more cost-effective and environmentally friendly. Moreover, there has been little work in regard to the details of understanding the CO<sub>2</sub> adsorption at the quantum level is crucial to predicts the behavior and performance under different operating conditions. Thus, this research focusses on producing optimum condition of bio-adsorbent derived from coconut shell and functionalised with microalgae, followed by impregnation of magnesium oxide and evaluating their isotherm model and thermodynamics characteristic. Additionally, to further understand the adsorption mechanism, integration of molecular modelling is crucial to evaluate the role and influence of functional groups in facilitating the adsorption process.

## CHAPTER 3: METHODOLOGY

### 3.1 Overall methodology

The materials, equipment and methods that have been used to develop and characterise the adsorbents from coconut shell and microalgae were elaborated in this chapter. Design of Experiment using Response Surface Methodology were used to analyse and optimise the synthesis process. The efficiency and performance of the adsorbent in carbon capture were investigated using two operational parameters: pressure and temperature of the operating system. Adsorption studies were conducted which include adsorption selectivity, adsorption isotherm, thermodynamics, and regeneration study. Gaussian 09W and GaussView were utilised to model and optimised adsorbent's structure based on the energy values. Figure 3.1 illustrated the overall flow chart of the methodology for this study, divided into four main objectives. Objective 1, the synthesis of the CS-based bio-adsorbent, focuses on the preparation and functionalization of the biomass, including the pretreatment of the CS biomass, carbonization, activation and functionalization to enhance surface area, functional groups, chemical affinity and improve adsorption properties. Objective 2 centres on the physicochemical characterization of the synthesized bio-adsorbent. This involves analysing the surface area, surface morphology, thermal stability, crystallographic structure, and functional groups to evaluate the physical, chemical, and structural properties of developed bio-adsorbents. Objective 3 focus on investigating the effect of operating temperature and pressure on CO<sub>2</sub> adsorption performance of the bio-adsorbent. Performance indicators assess desorption, regeneration, selectivity, and competitiveness with commercial adsorbents. Objective 4 examines adsorption mechanisms using isotherm models and thermodynamic analyses. Objective 5 examine synergistic effect of dual-functionalised through computational methods (e.g., DFT, electrostatic potential, and HOMO-LUMO) to evaluate energy dynamics and identify physisorption or chemisorption interactions.

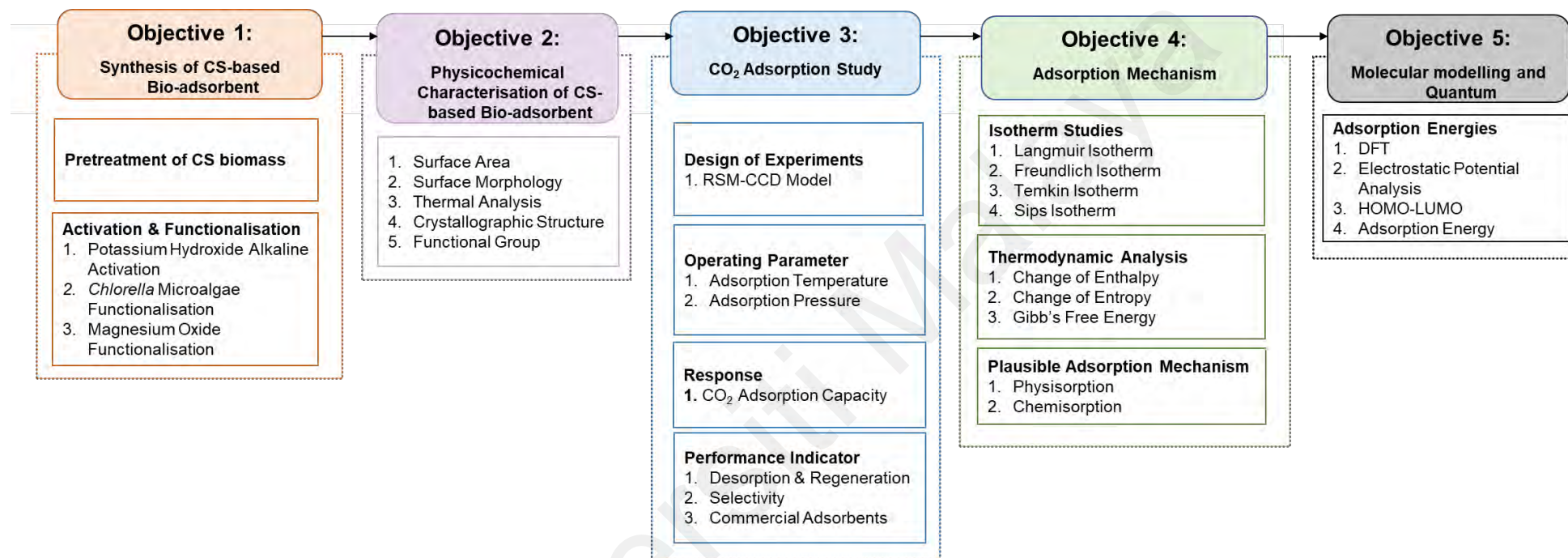


Figure 3.1: Flow diagram representing the overall methodological approach of the study

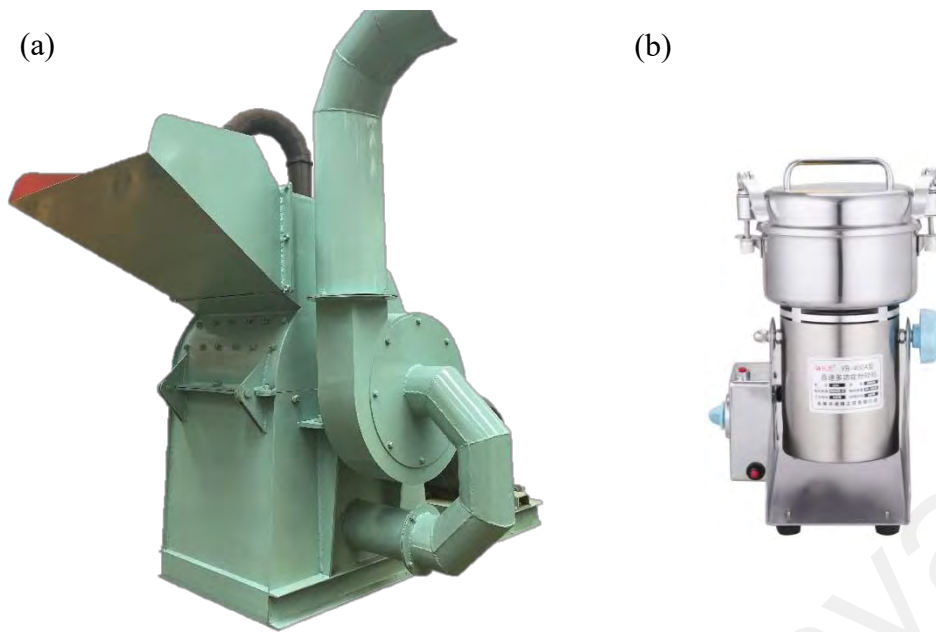


### 3.2 Materials and chemicals

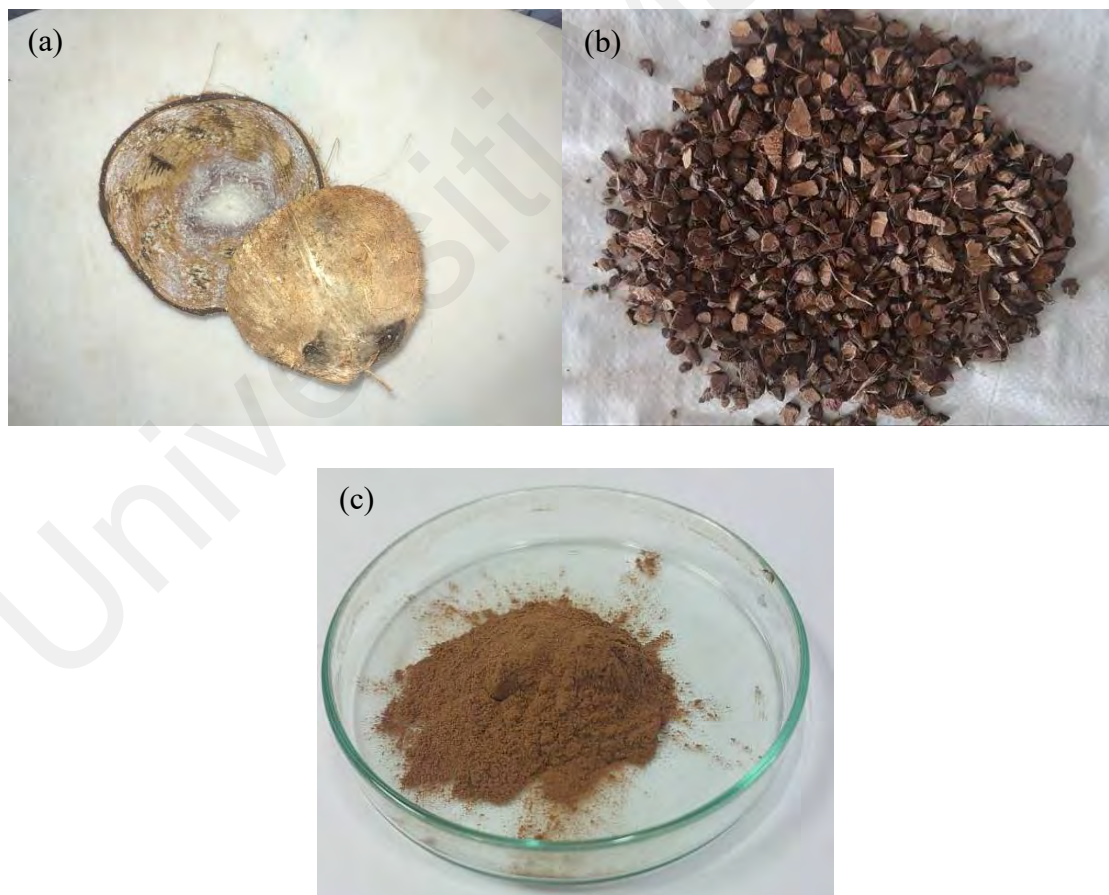
Coconut shells were obtained from local market in Selangor, Malaysia. Microalgae (*Chlorella s.p.*) were sourced from Matahari Sdn. Bhd. in Malaysia. Air (99.99% purity), CO<sub>2</sub> (99.8% purity), helium (99.99% purity), and compressed air were procured from Linde (Malaysia) Sdn. Bhd. Hydrochloric acid (HCl) and potassium hydroxide (KOH) were purchased from Merck. Sdn. Bhd., Selangor. Magnesium oxide nanopowder (MgO) (50-100nm) with a basic metal purity of 99.9% were obtained from Shanghai Aladdin Biochemical Technology Co., Ltd, China. Magnesium nitrate hexahydrate (Mg(NO<sub>3</sub>)<sub>2</sub>·6H<sub>2</sub>O) was purchased from Chemiz Malaysia. Deionized water was used for rinsing, synthesizing, and preparing the bio-adsorbent samples. All chemicals were used without additional purification.

### 3.3 Synthesis of adsorbent

The coconut shell was processed to remove pulp debris, fibre, and husk (Figure 3.3(a)). The remaining biomass was then thoroughly cleaned and rinsed with tap water to eliminate any contamination. Next, the CS was oven-dried for an entire night at 105 °C. Using a granulator (Figure 3.2 (a)) and a grinder (Figure 3.2 (b)), respectively, dried CS was subsequently ground into a granules (Figure 3.3 (b)) and fine powder (Figure 3.3 (c)). The dry materials were sieved into a fine powder with a size range of 0-150 µm and physically crushed before being kept in an airtight container.



**Figure 3.2: (a) Granulator and (b) table grinder**



**Figure 3.3: (a) Raw CS at the collection stage, (b) Raw CS after cleaning, washing and granulation, and (c) Raw powdered CS**

### 3.3.1 Carbonisation process

In this study, the bio-adsorbent was developed through two-step activation, in which the raw coconut shell was first carbonized hydrothermally, followed by chemical activation. Two-step activation was selected due to its ability to enhance the porosity and surface area of the resulting bio-adsorbent, ensuring improved adsorption capacity. The initial hydrothermal carbonization step facilitated the removal of volatile components and the formation of a stable carbon framework, while the subsequent chemical activation further developed the pore structure, optimizing it for enhanced pollutant removal. This approach allowed for better control over pore size distribution and structural integrity, making the bio-adsorbent more effective for adsorption applications. Additionally, the two-step activation process minimized excessive burn-off and material loss, leading to a higher yield and improved efficiency in the final product.

The hydrothermal carbonization was performed by filling 75% of the autoclave tube with sludge containing 5-35% raw precursor. The process involved mixing 3.75-26.25 g of the raw coconut shell with 48.75-71.25 g of distilled water. The autoclave system was placed inside a pre-heated oven at a varied temperature, ranging from 180 °C to 260 °C and heated for 1-5 hours to check the yield of the materials and their potential in dye removal. After the carbonisation time was achieved, the autoclave was removed immediately and quenched in water to stop the heating process immediately. The resulting carbonised material was washed repeatedly with distilled water, filtered thoroughly till the filtrate was clear in colour, and dried at 105 °C overnight. The hydrochar yield (%) and bio-adsorbent yield (%) were calculated by using Equation (3.1).

$$\text{Mass yield (\%)} = \frac{\text{mass}_{\text{hydrochar or bio-adsorbent}}}{\text{mass}_{\text{precursor}}} \times 100\% \quad (3.1)$$

To investigate the influence of the hydrothermal carbonisation process in synthesizing suitable activated carbon for CO<sub>2</sub> adsorption, different carbonisation temperatures (180-260°C), solid-to-sludge ratio (5-35%) and holding time (1-5 hours) were involved to find the optimum setting in producing high bio-adsorbent yield (Y<sub>2</sub>) and CO<sub>2</sub> adsorption capacity at an ambient condition (Y<sub>3</sub>). The range of these variables and the complete experimental design were tabulated in Table 3.1.

**Table 3.1: RSM-CCD design for the synthesis process of coconut shell bio-adsorbent through hydrothermal carbonisation and KOH activation**

Run	Independent variables		
	X <sub>1</sub> : Carbonisation Time (hours)	X <sub>2</sub> : Carbonisation Temperature (°C)	X <sub>3</sub> : Solid weight in sludge (%)
1	3	220	0.200
2	2	200	0.275
3	3	220	0.200
4	3	220	0.200
5	5	220	0.200
6	3	220	0.200
7	3	220	0.050
8	3	220	0.200
9	2	240	0.125
10	4	240	0.275
11	3	220	0.350
12	2	200	0.125
13	3	180	0.200
14	4	240	0.125
15	3	260	0.200
16	1	220	0.200
17	4	200	0.275
18	3	220	0.200
19	2	240	0.275
20	4	200	0.125

### **3.3.2 Chemical activation of the adsorbent**

The chemical activation was performed by using a 1:3 ratio of hydrochar to potassium hydroxide (KOH) through dry mixing. For dry-dry mixing, the measured weight of the KOH pellet was mixed with AC for a short time before being pyrolyzed in the muffle furnace. Next, the solid mixture was subjected to pyrolysis in a muffle furnace. This process involved heating the mixture to 700 °C at a gradual rate of 5 °C per minute and maintaining this temperature for 120 minutes. After that, the system was cooled down gradually to room temperature. The resultant material was purified with diluted HCl aqueous solution to remove the excess KOH and ash, followed by rinsing with distilled water until pH reached 6.5-7. Finally, the purified material was dried at 105 °C overnight and sieved one more time to ensure a uniform size before storing them in air-tight containers. The suitability of synthesis adsorbent was first investigated with carbon dioxide adsorption capacity at 25 °C and 1 bar, to determine the optimum approach of synthesis of bio-adsorbent.

The optimum synthesis condition was then tested using wet-dry mixing in which the measured weight of KOH was diluted in 60ml of distilled water, followed by the addition of hydrochar. The mixtures were left to stir for 1 hour before being heated at 105 °C before pyrolyzing at the condition of solid-solid activation mentioned above.

### **3.3.3 Functionalisation of bio-adsorbent with magnesium oxide**

The investigation of the effect of impregnation of metal oxide onto activated carbon towards carbon dioxide adsorption capacity can be divided into two sections; the effect of the functionalisation method and the effect of metal oxide concentration.

Firstly, the effect of the MgO functionalisation method using direct mixing, wet impregnation and hydrothermal treatment was investigated. For direct mixing, 1.5 g of MgO nanopowder was dispersed in 50 mL of distilled water and stirred for 30 minutes at

120°C. Next, 8.5 g of HCS was added to a magnesium oxyhydroxide (MgOH) solution. The mixture was sonicated for 1 hour before left to be stirred at 300 rpm at 105 °C for 1 hour until a slurry was produced. Lastly, the samples were dried at 105 °C for 12 hours. The impregnation of magnesium oxide onto activated carbon through wet impregnation was also investigated. Firstly, 1.5g of magnesium nitrate salt was added to 50 mL water, followed by 8.5 g of HCS. The mixture was stirred for 3 hours at 105°C and then dried in the oven for 12 hours. Next, the solid residue was calcinated in the furnace at 450°C for 1 hour. After the sample cool down, the solid residue was carefully collected and stored in a labelled airtight container.

Functionalisation of metal oxide through hydrothermal treatment was conducted by first, diluting 1.5 g of magnesium nitrate salt into distilled water. Next, 8.5 g of HCS was added to the solution and the mixture was left to stir for 1 hour. The mixture was then added to the HTC autoclave and was left to undergo HTC at 200 °C for 20 minutes. After the sample cooled down, the mixture was filtered and washed under distilled water to remove any residual impurities. The filter cake was collected and dried in the oven at 105 °C for 12 hours. Finally, the prepared samples were heat-treated at 450 °C for 1 hour. Dried samples were carefully collected and stored in labelled airtight containers.

Based on the optimum functionalisation method, the effect of MgO concentration was investigated by varying the MgO concentration between 5-50 wt.%. Dried samples were carefully collected and stored in labelled airtight containers (HCS\_5MgO, HCS\_10MgO, HCS\_15MgO, HCS\_30MgO and HCS\_50MgO).

### **3.3.4 Functionalisation of bio-adsorbent with microalgae**

The influence of the incorporation of microalgae onto activated carbon performance in carbon capture was also investigated. Four functionalisation methods were investigated, which were direct mixing, HTC, wet impregnation and co-carbonisation. Co-

carbonisation of microalgae and coconut shell was conducted by dispersing 4.5g of *Chlorella s.p.* powder with 10.5g of raw coconut shell in 60 g of distilled water for 5 minutes. The slurry was then carbonised through optimum hydrothermal carbonisation procedures and activated using solid-solid KOH activation. For direct mixing, 5 g of raw *Chlorella s.p.*, were dispersed with 10 g of HCS in 60 g of distilled water for 5 minutes. The slurry was then dried at 105 °C for 12 hours, before use for CO<sub>2</sub> adsorption performance analysis. Lastly, for wet impregnation, a similar process was followed as in direct mixing, with the additional step of subjecting the mixture to pyrolysis at 450 °C for 1 hour. Dried samples were carefully collected and stored in labelled airtight containers.

### **3.4 Adsorbent characterisations**

The pore size distribution and specific surface area of the developed bio-adsorbents were investigated using nitrogen adsorption-desorption isotherms and analysed via the Brunauer-Emmett-Teller (BET) and Barrett-Joyner-Halenda (BJH) methods with a TriStar II-Micromeritics instrument. Surface morphology and elemental composition of both pristine and functionalised bio-adsorbents were characterised using Field Emission Scanning Electron Microscopy (FESEM) coupled with Energy Dispersive X-Ray (EDX) spectroscopy, employing a PHENOM ProX instrument and Phenom Pro Suite software for analysis. The crystalline structure of the bio-adsorbents was examined through X-ray diffraction (XRD) using a powder diffractometer within a  $2\theta$  range of 10.0° to 80.0°, with specific settings (step size: 0.02; scan step time: 1s). Additionally, Fourier Transform Infrared (FTIR) spectra of the bio-adsorbents, before and after carbon dioxide adsorption, were obtained using a Perkin Elmer Frontier FTIR spectrometer in the wavenumber ranging between 500 cm<sup>-1</sup> and 4000 cm<sup>-1</sup> to characterise surface functional groups and chemical bonds. The thermal stability and carbonisation behaviour of the developed adsorbents were analysed by using Thermogravimetric Analysis (TGA) using a Perkin

Elmer TGA 4000 instrument. The analysis was performed under a continuous nitrogen flow, heating the samples from room temperature to 900 °C at a rate of 10 °C/min.

### 3.5 Design of experiment

The Response Surface Methodology (RSM) approach was utilised to design the experimental set for optimising the CO<sub>2</sub> adsorption capacity, and analyse the interrelationship between adsorption operational parameters and optimise the process condition for carbon dioxide adsorption capacity. RSM facilitates the reduction of experimental runs and the identification of optimal conditions from various influencing input variables for process performance (Pali et al., 2023; Prabhu et al., 2023). The central composite design (CCD), a well-established approach in RSM, is utilised due to its efficacy in interpreting the relationship between parameters (Karyab et al., 2023).

Table 3.2 tabulated the experimental conditions, detailing the range and levels of operating pressure (A) and operating temperature (B) variables at five levels represented by codes -2, -1, 0, +1, and +2. This investigation pertains to two distinct adsorbent types, namely HCS and HCS-N-Mg. The efficacy of the adsorbents in capturing CO<sub>2</sub> was evaluated by utilising the High-Pressure Volumetric Analysis (HPVA II) analyser from the Particulate System (Micromeritics®).

**Table 3.2: RSM-CCD design for adsorption condition of bio-adsorbents**

Factors	Name	Unit	Symbol	Coded level				
				-2	-1	0	+1	+2
Pressure	P	bar	A	-	0.1	2.55	5.00	6.01
Temperature	T	°C	B	-	25	75	125	146

### 3.6 Carbon dioxide adsorption study

The efficacy of the bio-adsorbents in capturing CO<sub>2</sub> was evaluated by utilising the High-Pressure Volumetric Analysis (HPVA II) analyser from the Particulate System (Micromeritics®) (Figure 3.4), at the University of Technology Petronas (UTP),

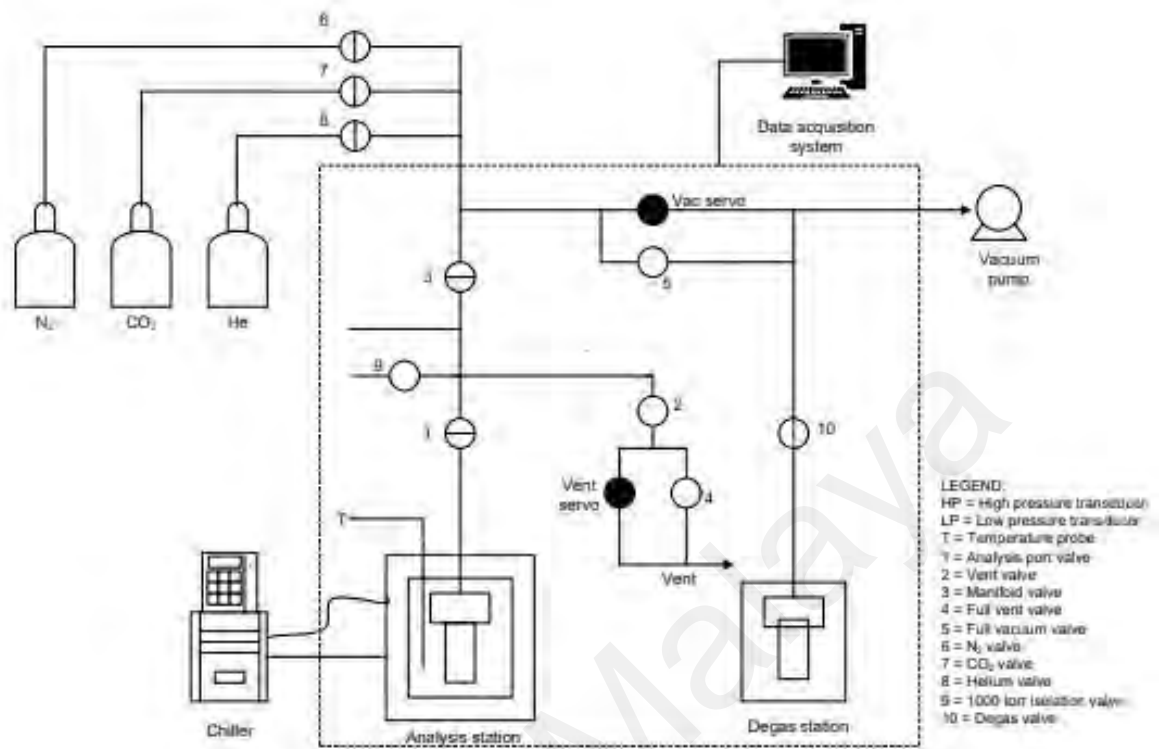


Malaysia. Figure 3.5 presents the schematic diagram of the HPVA II. This analyser employs a static volumetric approach to measure high-pressure adsorption and desorption isotherms of gases like carbon dioxide, methane and hydrogen (Chi et al., 2019).



**Figure 3.4: High Pressure Volumetric Analyser (HPVA II)**

The measurement of static volumetric gas adsorption involves adding a specific volume of gas adsorbate from a dosing manifold into a sample cell containing activated carbon. Before the adsorbent material stopped adsorbing the adsorbates, the activated carbon had adsorbed the desired adsorbate and a pressure drop was observed. When no further pressure changes were seen, the equilibrium condition was presumed. As a consequence, the gas adsorption capacity was calculated using the pressure variation in the dosing manifold. Whereas kinetic analysis employed the pressure's decrease with time, isotherm study used the gap between relative pressure differences. The following part outlined the steps involved in determining a gas adsorption capacity.



**Figure 3.5: Schematic diagram of HPVA II**

### 3.6.1 Sample preparation

The measuring cylinder was cleansed with an ultrasonic bath and heated in the oven before sample loading. First, the sample chamber (Figure 3.6 (a)) was weighed using a weighing balance and recorded. Then, the "zero" button was pressed. Followed by weighing the samples of activated carbon (between 0.20 to 0.25 g) and putting them into a sample chamber made of tared stainless steel. A 20-micron filter gasket (Figure 3.6 (c)) was put on top of the sample cell to prevent microscopic particles from entering the valve. Using wrenches and a clamp, the sample cell was then connected to a tube with a diaphragm valve (Figure 3.6 (b)). Ensure sure the connection is secure.

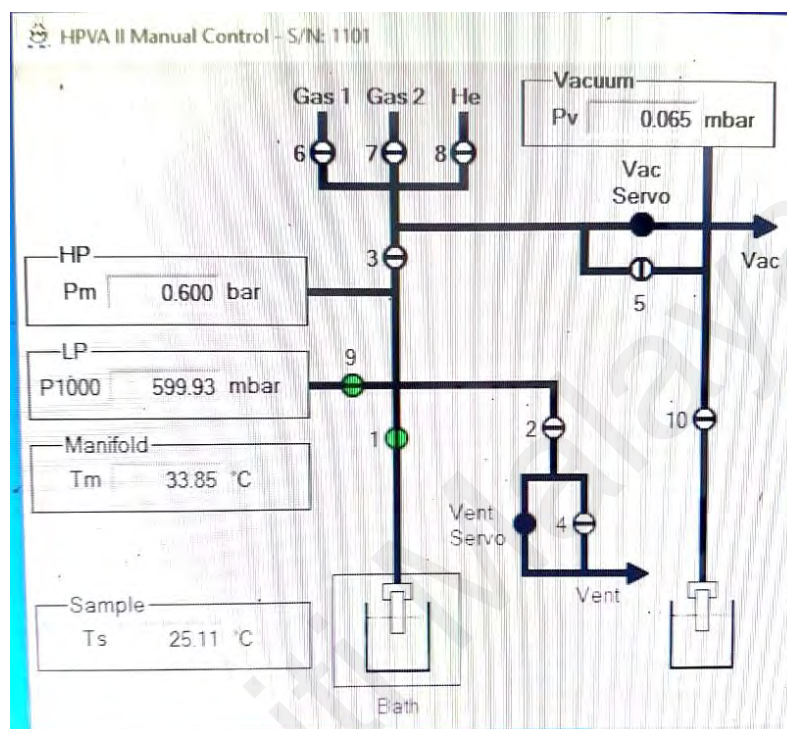


**Figure 3.6: (a) Sample chamber, (b) housing, and (c) filter gasket**

### 3.6.2 Sample Degassing

Once the sample had been loaded, the degassing port was joined to the sample tube. The isolation valve on the sample holder was slowly opened for degassing to start, and the Manual Control screen was clicked in the HPVA II Main Menu to open valve 10. A closed valve was indicated by yellow, and an open valve was indicated by green (Figure 3.7). The sample was allowed to degas for an appropriate amount of time. The vacuum gauge was monitored using the Manual Control screen to ensure that the vacuum was reached. Subsequently, the asterisk button was held down while the up arrows on the display were used to set the degassing temperature to 90 °C. After 1 hour, the temperature was increased to 150 °C in a vacuum condition before the CO<sub>2</sub> adsorption-desorption process was carried out. The degassing process was carried out for at least four hours. The asterisk button was held down while the down arrows on the display were used to cool down the temperature. The sample was allowed to cool to room temperature after the furnace was set at 0 °C. To finish the degas operation, the isolation valve and valve 10 were then closed. After the sample had cooled to room temperature, the connector nut was loosened, and the sample holder was removed from the degassing port. The O-ring was ensured to remain in place, then a cap was placed on the port. Lastly, the sample holder assembly was removed from the furnace by tilting it. Degassing

was conducted to remove moisture or adsorbed contaminants from the surface of activated carbon. Additionally, a two-temperature stage was conducted to maintain the integrity of the porous bio-adsorbent.



**Figure 3.7: Manual control screen of HPVA II**

### 3.6.3 HPVA II analysis

The instrument was connected to the recirculating bath first. Then, the chamber was installed to the analysis port to evacuate the sample and the connector nut was hand-tightened. The nut was tightened using the 3/4 –inch and 5/8-inch wrenches until snug after ensuring that the O-ring was in place. The purging process was initiated by clicking the Manual Control screen in the HPVA II Main Menu. Valves 1, 3, and 8 (He) were opened to pressurize the instrument until the High-Pressure Transducer (HP) reading reached 3 bar. Valve 8 was closed and valves 2 and 4 were opened. They were closed when the HP reading was approximately 1 bar. The purging step was repeated three times. Then, the vac servo valve was set to 0.5 bar. The set pressure was reached, and the

Vac Servo valve was turned off. Valve 5 was opened and left open until the internal Vacuum Gauge reached the minimum value specific for the vacuum pump. After the minimum value was reached, all valves were closed. The temperature probe cable was plugged into the connector on the instrument and the temperature probe was inserted into the temperature control vessel. The appropriate liquid was added to the vessel until full. The isolation valve was then opened. The HPVA II system was opened in the computer by double-clicking and the Main Menu was accessed. The experiment conditions were entered in the adsorption screen, including holding time, interval, pressure point, and evacuation time. The run experiment button was clicked, and the data/file was saved. Once the analysis was finished, the isolation valve was closed. The instrument was turned off and the HPVA II program was closed.

To study the selectivity of CO<sub>2</sub> and N<sub>2</sub> adsorption onto the developed bio-adsorbents, the HPVA II experiment was carried out using N<sub>2</sub> gas at the same condition as CO<sub>2</sub> adsorption executed. The compiled data then will be used to plot a graph implementing the best-fitted isotherm and the graph then will be observed. The selectivity of CO<sub>2</sub>/N<sub>2</sub> was calculated using the below equation.

$$S_{CO_2/N_2} = \frac{q_{CO_2}/q_{N_2}}{P_{CO_2}/P_{N_2}} \quad (3.2)$$

Referring to the above equation,  $q_e$  is the adsorbed amount of adsorbates while P is the partial pressure of adsorbates. The selectivity of bio-adsorbents towards CO<sub>2</sub> over N<sub>2</sub> was determined by calculating the ratio of their respective adsorption capacities at specific pressure and temperature conditions.

Regeneration of the optimised bio-adsorbents were carried out by applying the pressure swing adsorption using the volumetric adsorption analyser. CO<sub>2</sub> adsorption was measured within the pressure range of 0.1 bar to 1 bar at a fixed adsorption temperature

of 25 °C. Upon reaching equilibrium at 1 bar, the desorption (regeneration) process was applied by stepwise pressure reduction to 0.1 bar. The cyclic CO<sub>2</sub> adsorption-desorption process was performed up to ten times. The degree of regeneration (*D<sub>reg</sub>*) was calculated by Eq. (3.3).

$$D_{reg} = m_{reg}/m_1 \quad (3.3)$$

### 3.7 Adsorption mechanism

Adsorption mechanisms, including isotherm and thermodynamics, are vital in understanding and optimising the interaction between adsorbates and adsorbents for various applications. Isotherms describe how adsorbates partition between the liquid or gas phase and the solid surface at equilibrium, offering crucial insight into the capacity and affinity of adsorbents. Thermodynamic principles provide the underlying energetic perspectives of adsorption processes, enabling the prediction of spontaneity and feasibility under different temperature conditions.

#### 3.7.1 Adsorption isotherm

The adsorption isotherm modelling was conducted to describe the performance of CO<sub>2</sub> adsorption onto the bio-adsorbent. Understanding these isotherms is crucial as it helps predict and compare how CO<sub>2</sub> interacts with developed adsorbents, decipher the underlying mechanisms, and optimise the adsorption system (Al-Ghouti & Da'ana, 2020). The isotherm models that had been analysed in this research study include the Langmuir, Freundlich, Temkin and Sips, which are represented by Eq. (3.4) to (3.7). This study examines the capture of CO<sub>2</sub> across a temperature range of 25–125°C, taking into account that the range of flue gas temperature is within 50-120°C (Kaithwas et al., 2012).

Eq. (3.4) represents the Langmuir model, which characterises monolayer adsorption on uniform sites. It includes  $q_e$ , denoting the equilibrium amount of carbon dioxide adsorbed per 1 g of adsorbent (mmol/g),  $P_s$  representing the equilibrium pressure (bar), and  $k_L$ , the Langmuir constant ( $\text{bar}^{-1}$ ) related to adsorption rate and capacity.  $q_{\max}$  represents the maximum adsorption capacity of adsorbent onto  $\text{CO}_2$  (mmol/g), indicating a complete monolayer coverage (Tun & Chen, 2021).

$$q_e = \frac{q_{\max} k_L P_s}{1 + k_L P_s} \quad (3.4)$$

The Freundlich model, represented in Eq. (3.5), suggests multilayer adsorption on heterogeneous adsorbents. According to Ammendola et al. (2017), this heterogeneity stems from the physical and chemical nature of adsorption sites and the quantity of already adsorbed molecules, with increasing molecules leading to diminished binding probability due to exponentially increasing energy requirements. In this model,  $k_F$  represents the Freundlich constant (mmol/g.bar), while  $n_F$ , identified as the heterogeneity factor or Freundlich constant, indicates the adsorption nature ( $n_F < 1$  for chemical,  $> 1$  for physical adsorption) (Fatima et al., 2023).  $1/n_F$  is the intensity parameter, reflecting the driving force or surface heterogeneity.

$$q_e = k_F P_s^{\frac{1}{n_F}} \quad (3.5)$$

The Temkin isotherm model Eq. (3.6) includes the interaction of the adsorbate and adsorbent and the uniform distribution of binding energies among the molecules undergoing adsorption and the surface adsorbent. Additionally, the model assumes that the heat of adsorption changes linearly with coverage as a function of coverage and temperature, contrasting with a logarithmic relationship. (Al-Ghouti & Da'ana, 2020).

$$q_e = \frac{T_R}{b} \ln(k_T P_s) \quad (3.6)$$

Unlike the Langmuir, Freundlich, and Temkin models, the Sips model combines features from Langmuir and Freundlich, introducing a three-parameter framework. Eq. (3.7) outlines the non-linear expression for this model, where  $q_e$  represents the amount of adsorbed carbon dioxide per gram of adsorbent at equilibrium (in mmol/g),  $P_s$  represents the equilibrium pressure (in bars), and  $b_s$  and  $q_{max}$  are the Sips constants, indicating the Sips affinity constant (in  $\text{bar}^{-1}$ ) and the maximum adsorption capacity (in mmol/g) respectively. Additionally, the variable 'n' characterises the system's heterogeneity.

$$q_e = q_{max} \frac{(b_s P_s)^{\frac{1}{n}}}{1 + (b_s P_s)^{\frac{1}{n}}} \quad (3.7)$$

Adsorption isotherms of the purified  $\text{CO}_2$  and  $\text{N}_2$  adsorption onto HCS and HCS-N-Mg at ambient conditions were performed by fitting the experimental data that was obtained from the HPVA II system into four isotherm models.

### 3.7.2 Adsorption thermodynamics

Van Hoff equation (Eq. (3.8)) was used to calculate the thermodynamic parameters expressed in terms of  $\Delta H^\circ$  and  $\Delta S^\circ$ . The gradient and y-intercept values from the plotted graph of  $\ln K_L$  (Langmuir equilibrium constant) against the reciprocal of absolute temperature in Kelvin ( $1/T$ ) were utilised to determine the magnitudes of  $\Delta H^\circ$  and  $\Delta S^\circ$ . In addition, the value of  $\Delta G^\circ$  was calculated based on the difference of  $\Delta H^\circ$  and  $T\Delta S^\circ$ .

$$\ln k_F = \frac{\Delta S^\circ}{R} - \frac{\Delta H^\circ}{RT} \quad (3.8)$$



### 3.8 Quantum chemical calculation

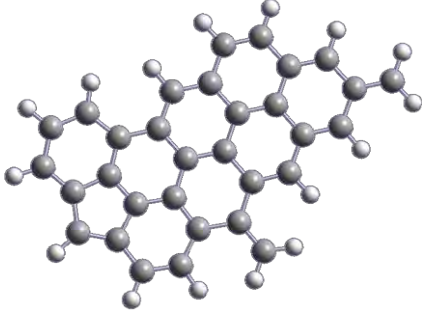
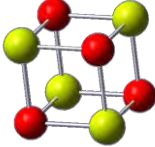

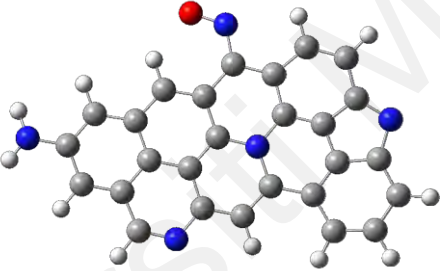
The molecular modelling and quantum chemical computations were conducted by utilising the Gaussian 09W software package, with initial molecular geometries generated using the GaussView 06 visualization tool. Structural attributes of the involved chemical species are detailed in Table 3.3. Due to the complexity and uncertainty of carbon-based bio-adsorbent structure, pristine bio-adsorbent was simulated as monolayer graphene slabs within 8x6 carbon ring unit cells (32 atoms for pure graphene) (Wu et al., 2014; Xing et al., 2012). The adsorption of a carbon dioxide molecule onto the (100) face of MgO, represented by a (MgO)<sub>4</sub> cluster, was modelled to investigate the adsorption process (Shayeganfar et al., 2017). Molecular structures were optimised using the B3LYP method with 6-31G (d, p) and LANL2DZ basis sets. The adsorption behaviour of carbon dioxide onto the respective substrates was simulated, and the CO<sub>2</sub> adsorption energy was computed using Equation (3.9).

$$E_{ad} = E_{surface+CO_2} - (E_{surface} + E_{CO_2}) \quad (3.9)$$

where  $E_{ad}$ ,  $E_{surface+CO_2}$ ,  $E_{surface}$  and  $E_{CO_2}$  represent the adsorption energy, total energy of the adsorbate-surface complex, the energy of the substrate surface, and the energy of isolated carbon dioxide, respectively. A negative  $E_{ad}$  value signifies an exothermic adsorption process, with a larger negative value corresponding to a more stable structure and stronger interaction.

Furthermore, the chemical properties of the molecule, including the highest occupied molecular orbital (HOMO) energy, lowest unoccupied molecular orbital (LUMO) energy, dipole moment and total electronic energy were evaluated. Determining these parameters is crucial as they provide a theoretical basis for predicting chemical reactivity, stability, and interaction patterns of the chemical species under investigation.

**Table 3.3: Structural and molecular properties of adsorbent and adsorbate**

Name	Structure	Molecular formula	Molecular weight
Carbon surface		C <sub>32</sub> H <sub>16</sub>	160.25
Magnesium oxide		(MgO) <sub>4</sub>	161.22
Carbon dioxide		CO <sub>2</sub>	44.01
N-doped carbon surface		C <sub>27</sub> H <sub>12</sub> O <sub>1</sub> N <sub>5</sub>	422.42

### 3.9 Safety precautions

While using chemicals and reagents, appropriate PPE such as safety masks, gloves, and lab coats was used throughout the experiments. Standard safety precautions and laboratory rules and regulations were followed while handling hazardous chemicals which included using the fume cupboard to prepare chemical solutions. Table 3.4 outlines the potential risks associated with the chemicals and procedures involved, along with recommended safety precautions to mitigate these hazards.

**Table 3.4: Safety precautions during the experiment**

<b>No.</b>	<b>Activities/ Components</b>	<b>Potential Hazards</b>	<b>Preventive measures</b>
1.	Handling/storage of chemicals (magnesium nitrate, magnesium oxide, potassium hydroxide (KOH), hydrochloric acid (HCl))	Eye/skin irritation upon direct contact, lung irritation upon inhalation, dizziness from high concentration exposure.	Use standard PPE (gloves, goggles, apron, mask). Move to fresh air if inhaled. Ensure good ventilation and store chemicals in dry, ventilated areas.
2.	Carbonisation using hydrothermal autoclave	Rapid steam release during cooldown, potential pressure explosion when retrieving samples.	Wear PPE (gloves, lab coat). Ensure complete cool down before opening the pressurized chamber.
3.	Pyrolysis of hydrochar	High-temperature activated hydrochar may cause burns from splashes.	Wear PPE (gloves, lab coat). Conduct carbonisation in a closed system.
4.	Adsorption study using HPVA (inert gas, high temperature & pressure)	The hot surface of the plate may burn the skins	Wear proper PPE such as protective gloves
5.	Mixing of adsorbent using a magnetic stirrer	Skin burns from contact with a hot surface.	Always wear heat-resistant gloves when handling hot plates or equipment

**Table 3.4, continued**

<b>No.</b>	<b>Activities/ Components</b>	<b>Potential Hazards</b>	<b>Preventive measures</b>
6.	Chemicals with Low Boiling Points	Inhalation of vapours can cause dizziness or other health issues.	Work in a well-ventilated area or fume hood when using volatile chemicals.
7.	Spills of Liquids	Wet floors create a slipping hazard.	Wear appropriate footwear and promptly clean up any spills.
8.	Scheduled Waste Disposal	Improper disposal can lead to water pollution and environmental damage.	Collect scheduled waste in designated containers and follow proper disposal procedures according to waste codes. Always wear appropriate personal protective equipment (PPE) when handling waste.

## CHAPTER 4: RESULTS AND DISCUSSION

### 4.1 Introduction

This chapter consists of three main sections. The first section discusses the results of the experimental design that has been adopted for the synthesis of coconut shell bio-adsorbent, via different operating conditions of hydrothermal carbonisation. The second section refers to the effect of incorporation of magnesium oxide onto bio-adsorbent towards the carbon dioxide adsorption capacity via three different methods. In addition, the effect of MgO loading onto pristine adsorbent was discussed. The influence of the incorporation of microalgae onto the synthesis bio-adsorbent was also discussed in this chapter. Finally, the last section deals with thorough CO<sub>2</sub> adsorption studies of the optimised activated carbon; including the effect of temperature and pressure towards CO<sub>2</sub> adsorption, cyclic CO<sub>2</sub> adsorption-desorption operation, CO<sub>2</sub>/N<sub>2</sub> selectivity, together with adsorption isotherm, and thermodynamic analysis

### 4.2 Optimisation of bio-adsorbent synthesis from coconut shell

The synthesis of coconut shell-based-activated carbon bio-adsorbent has been carried out through two-step chemical activation by utilising HTC to carbonise the biomass and KOH as an activating agent. In evaluating the quality of synthesised hydrochar as a precursor for activated carbon, RSM was utilised to investigate the interrelationship between hydrothermal carbonisation operation parameters (percentage of precursor in slurry, carbonisation temperature, and carbonisation time), towards the hydrochar yield ( $Y_1$ ), bio-adsorbent yield ( $Y_2$ ) and CO<sub>2</sub> adsorption capacity ( $Y_3$ ) was considered. The outcomes of fitting the experimental data through multiple regression analysis are presented with the results obtained from assessing the fitness of the model by using analysis of variance (ANOVA) and the Adj-R<sup>2</sup>. Additionally, the response surfaces for non-coded values of independent variables are depicted.

### 4.2.1 Coconut shell bio-adsorbent

This subchapter focuses on optimizing the hydrothermal carbonization (HTC) process for synthesizing pristine coconut shell bio-adsorbent. The primary objective is to enhance both the yield and the adsorption capacity of the bio-adsorbent, particularly for CO<sub>2</sub> capture. Various process parameters, such as reaction temperature, residence time, and precursor-to-water ratio, play a crucial role in determining the physicochemical properties of the final product.

#### 4.2.1.1 Statistical analysis

Table 4.1 provides a comprehensive overview of the experimental design matrices, including the actual and predicted values for hydrochar yield ( $Y_1$ ), bio-adsorbent yield ( $Y_2$ ), and CO<sub>2</sub> adsorption capacity ( $Y_3$ ). The hydrochar yield ( $Y_1$ ) ranges between 42.31% and 97.26% through alteration of feedstock ratio, temperature and residence time, whereas bio-adsorbent yield ( $Y_2$ ) obtained through further alkaline activation of corresponding hydrochar with KOH at ratio 3 for 2 hours at 700°C, is found to range from 22.65-31.21%. For CO<sub>2</sub> adsorption capacity ( $Y_3$ ), alteration of factors resulted in bio-adsorbent with adsorption performance of 1.31-1.78 mmol/g. Central points were included in the experimental design to assess experimental errors and data reproducibility (Khalili et al., 2015). The sequence of experiments was randomized to minimize the influence of uncontrolled variables (Essa et al., 2013). The process of selecting the most suitable model involved employing the sequential model sum of squares technique. This approach prioritized the highest-order polynomial where additional terms exhibited statistical significance while ensuring the model remained unaliased, aligning with the recommendations of Khalili et al. (2015) and Tan et al. (2008). Based on the suggestions from the Design-Expert® software, quadratic relationships were deemed appropriate for modelling both hydrochar yield ( $Y_1$ ) and CO<sub>2</sub>

adsorption capacity ( $Y_3$ ). Conversely, a linear equation was chosen for bio-adsorbent yield ( $Y_2$ ). Subsequent to this model selection phase, regression analysis was utilised to achieve a good fit between the chosen empirical model and the experimental data that had been gathered. The resulting empirical models, expressed in terms of coded factors ( $X_1, X_2, X_3$ ), are presented in Equations 4.1, 4.2, and 4.3 for hydrochar yield, bio-adsorbent yield from coconut shell precursor, and their corresponding  $\text{CO}_2$  adsorption capacities, respectively, whereas the parameters of coded equations for each parameter are tabulated in Table 4.2.

$$Y_1(\text{wt. \%}) = 77.43 - 6.77 X_1 - 14.02 X_2 + 4.05 X_3 - 1.54 X_1 X_2 - 0.54 X_1 X_3 - 0.29 X_2 X_3 - 0.79 X_1^2 - 1.94 X_2^2 - 0.86 X_3^2 \quad (4.1)$$

$$Y_2(\text{wt. \%}) = 27.30 - 0.46 X_1 - 2.11 X_2 + 0.42 X_3 \quad (4.2)$$

$$Y_3(\text{mmol/g}) = 1.76 + 0.0181 X_1 + 0.0110 X_2 + 0.0166 X_3 - 0.0844 X_1 X_2 + 0.0479 X_1 X_3 + 0.0687 X_2 X_3 - 0.0752 X_1^2 - 0.0613 X_2^2 - 0.0772 X_3^2 \quad (4.3)$$

Based on these equations, a positive coefficient indicates a synergistic effect where the term contributes to an increase in the response. Conversely, a negative coefficient implies an antagonistic effect, suggesting the term has a diminishing impact on the response (Khalili et al., 2015; Tan et al., 2008).

**Table 4.1: RSM-CCD design matrices with actual and predicted responses of synthesised bio-adsorbent precursor coconut shell**

Run	Independent variables			Responses					
				Y <sub>1</sub> (%)		Y <sub>2</sub> (%)		Y <sub>3</sub> (mmol/g)	
	X <sub>1</sub> (hours)	X <sub>2</sub> (°C)	X <sub>3</sub> (%)	Actual	Predicted	Actual	Predicted	Actual	Predicted
1	3	220	0.200	68.38	69.69	26.29	27.30	1.746	1.760
2	2	200	0.275	87.53	88.17	30.11	30.29	1.314	1.333
3	3	220	0.200	69.13	69.69	26.84	27.30	1.780	1.760
4	3	220	0.200	70.12	69.69	26.63	27.30	1.773	1.760
5	5	220	0.200	53.42	54.66	26.64	26.38	1.495	1.496
6	3	220	0.200	70.34	69.69	27.13	27.30	1.743	1.760
7	3	220	0.050	56.45	59.30	26.33	26.46	1.406	1.418
8	3	220	0.200	68.06	69.69	27.68	27.30	1.765	1.760
9	2	240	0.125	58.01	57.45	25.3	25.23	1.584	1.586
10	4	240	0.275	48.19	49.26	25.34	25.15	1.611	1.624
11	3	220	0.350	75.70	73.88	28.55	28.14	1.491	1.484
12	2	200	0.125	81.47	79.39	30.00	29.45	1.535	1.533
13	3	180	0.200	86.26	88.74	31.21	31.60	1.497	1.466
14	4	240	0.125	45.11	43.46	24.73	24.31	1.365	1.358
15	3	260	0.200	38.08	38.06	22.65	23.16	1.528	1.565
16	1	220	0.200	79.23	79.92	28.56	28.30	1.419	1.404
17	4	200	0.275	78.23	77.79	29.38	29.37	1.624	1.634
18	3	220	0.200	71.05	70.39	27.35	27.38	1.731	1.760
19	2	240	0.275	63.79	65.19	26.35	26.07	1.661	1.661
20	4	200	0.125	73.35	70.95	28.85	28.53	1.631	1.642



**Table 4.2: RSM-CCD design of coded equations for HTC process condition for synthesis of coconut shell bio-adsorbent**

Factor	Unit	Symbol	Coded Level				
			-2	-1	0	1	2
Carbonization time	hours	$X_1$	1	2	3	4	5
Carbonization temperature	°C	$X_2$	180	200	220	240	260
Solid weight percentage	wt.%	$X_3$	5.0	12.5	20.0	27.5	35.0

An analysis of variance (ANOVA) was conducted to analyse the effectiveness of the modelled equations, with results shown in Table 4.3. ANOVA assesses the statistical importance of variables using the p-value (at a 95% confidence level) and Fisher F-value. The p-value denotes the likelihood of observing results as extreme as those obtained, assuming the null hypothesis (no effect) is true. A small p-value ( $<0.05$ ) suggests a statistically significant variable, indicating its importance in the model (Yusup et al., 2014). The F-value, representing the ratio of variance between groups to variance within groups, indicates the overall variability explained by the model. A higher F-value implies a stronger model influence.

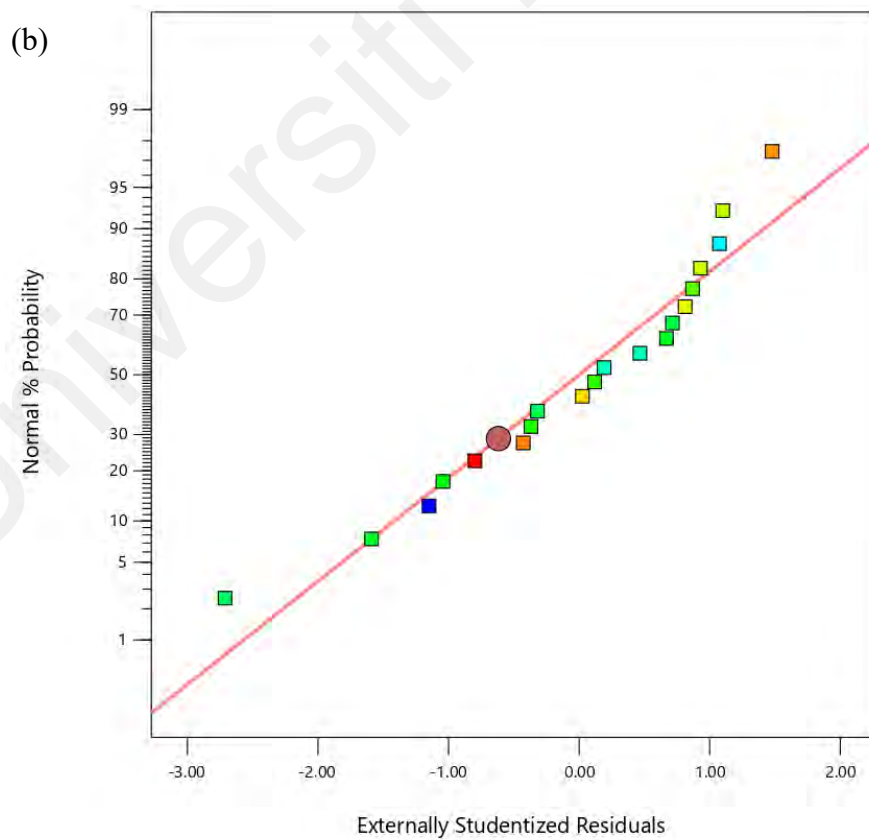
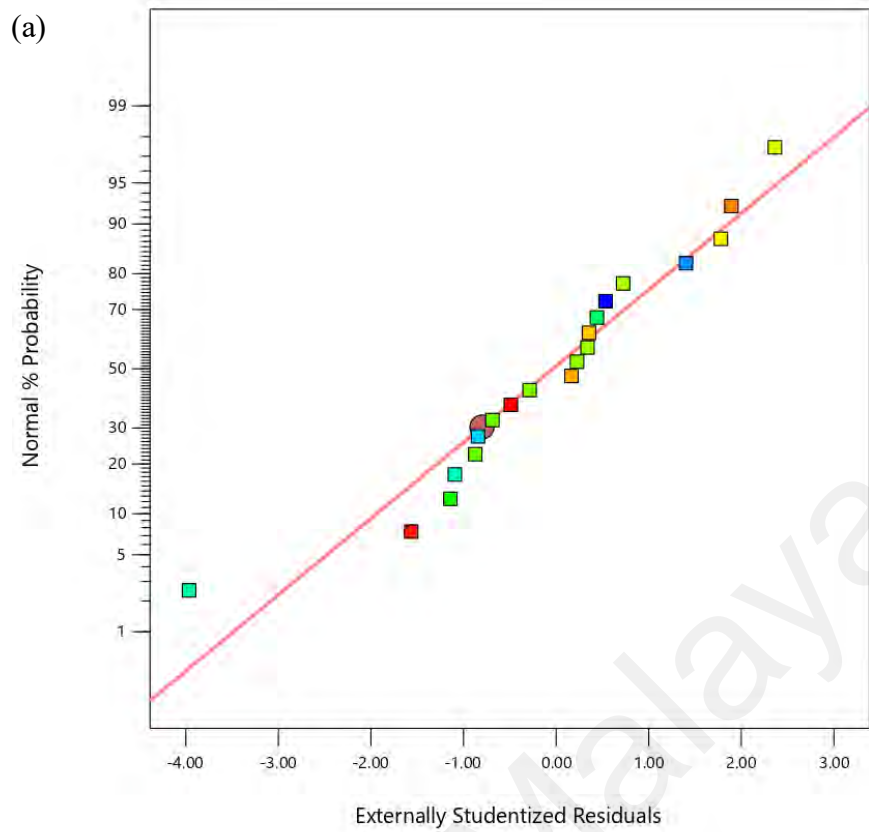
Considering the  $F$ -value and  $p$ -values, the most influential variables for the hydrochar yield ( $Y_1$ ) include all linear factors ( $X_1, X_2, X_3$ ) as well as the quadratic terms ( $X_2^2$ ). For bio-adsorbent yield ( $Y_2$ ), the significant model terms are  $X_1, X_2$ , and  $X_3$ . Whereas, all linear factors ( $X_1, X_2, X_3$ ) and quadratic terms ( $X_1^2, X_2^2, X_3^2$ ) play a prominent role in  $CO_2$  adsorption capacity ( $Y_3$ ). In addition, the interaction between the carbonisation time and carbonisation temperature ( $X_1X_2$ ), carbonisation time and solid percentage ( $X_1X_3$ ), and carbonisation temperature and solid percentage ( $X_2X_3$ ) are significant for response carbon dioxide adsorption capacity,  $Y_3$ .

Table 4.4 show the model fit summaries for bio-adsorbent precursor coconut shell. The model suitability is characterised by a large R-squared value and low prediction error sum of squares (PRESS) value (Garg & Prasad, 2016). The obtained squared that exceeds 0.9 suggests a good adequacy of this model. In addition, the model's predictive capability is

supported by the small difference (less than 0.2) between the predicted R-squared and adjusted R-squared values. This indicates a good fit between the model and the observed data. Additionally, the adequacy precision (AP), which quantifies the signal-to-noise ratio, exceeds 4. This suggests the model possesses sufficient accuracy to effectively explore and optimise the design space, as highlighted by Kundu et al. (2014). Furthermore, the suitability of this model can also be evaluated in terms of standard deviation (SD) and coefficient of variance (CV %). The CV%, calculated as the percentage ratio of the standard error of the estimate to the mean of observed responses, reflects the reproducibility of the model. As shown in Table 4.4, the CV% values for both responses fall below 10%, indicating that this model demonstrates good reproducibility (Mahmood et al., 2017). Apart from these analyses, model adequacy can also be validated by the diagnostic plots as presented in Figure 4.1. The residual plots and predicted vs actual plots in Figure 4.1 (a-c) and Figure 4.1 (d-f) provide evidence of a normal distribution of residuals and a good fit of the model to the data, respectively. The linear arrangement of data points in these plots indicates that the residuals are randomly scattered around the centre line. This is consistent with the expected behavior of residuals from a well-fitting model, where the residuals should be normally distributed with a mean of zero and a constant variance. The lack of any systematic deviations from the centre line in these plots suggests that the model is capturing the underlying relationships in the data effectively, and that the residuals are not influenced by any underlying patterns or biases.

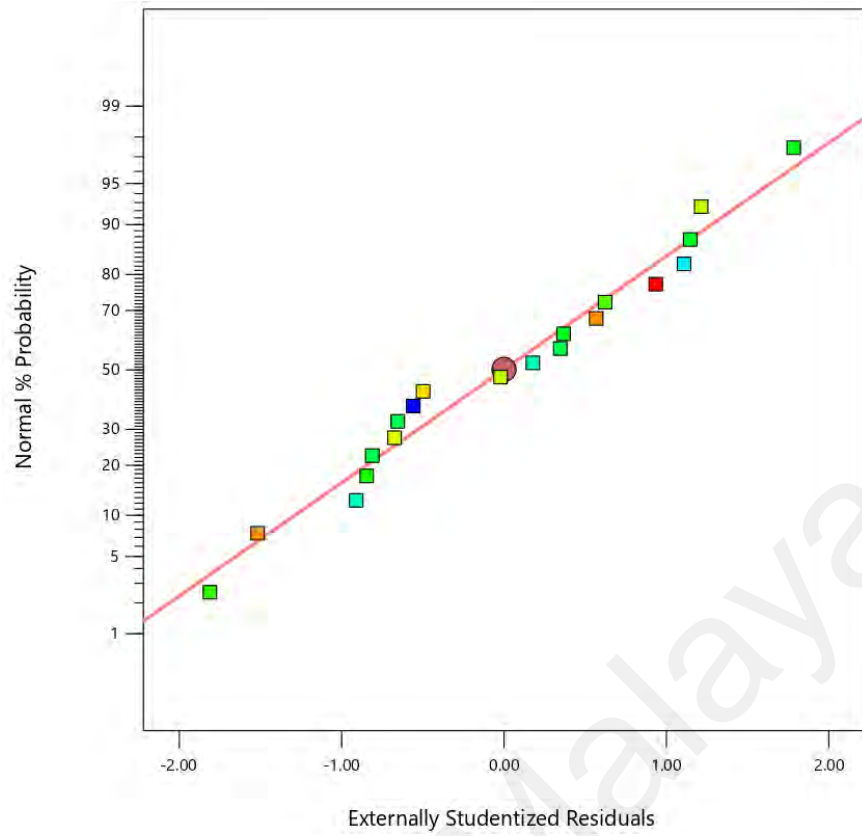
**Table 4.3: ANOVA analysis of hydrochar yield (Y<sub>1</sub>), bio-adsorbent yield (Y<sub>2</sub>), and CO<sub>2</sub> adsorption capacity (Y<sub>3</sub>)**

Source	Sum of square			Degree of freedom		Mean of square			F-value			Prob >F-value		
	Y <sub>1</sub>	Y <sub>2</sub>	Y <sub>3</sub>	Y <sub>1</sub> , Y <sub>3</sub>	Y <sub>2</sub>	Y <sub>1</sub>	Y <sub>2</sub>	Y <sub>3</sub>	Y <sub>1</sub>	Y <sub>2</sub>	Y <sub>3</sub>	Y <sub>1</sub>	Y <sub>2</sub>	Y <sub>3</sub>
Model	3454.34	77.32	0.3973	9		383.82	25.77	0.0441	95.53	127.34	166.35	< 0.0001	< 0.0001	< 0.0001
X <sub>1</sub>	594.87	3.33	0.0052	1		594.87	3.33	0.0052	148.06	16.46	19.73	< 0.0001	0.0009	0.0013
X <sub>2</sub>	2546.06	71.15	0.0019	1		2546.06	71.15	0.0019	633.68	351.55	7.31	< 0.0001	< 0.0001	0.0222
X <sub>3</sub>	212.45	2.84	0.0044	1		212.45	2.84	0.0044	52.87	14.03	16.65	< 0.0001	0.0018	0.0022
X <sub>1</sub> X <sub>2</sub>	15.37	-	0.057	1		15.37	-	0.057	3.82	-	214.78	0.079	-	< 0.0001
X <sub>1</sub> X <sub>3</sub>	1.89	-	0.0183	1		1.89	-	0.0183	0.4703	-	69.11	0.5084	-	< 0.0001
X <sub>2</sub> X <sub>3</sub>	0.545	-	0.0378	1		0.545	-	0.0378	0.1356	-	142.39	0.7203	-	< 0.0001
X <sub>1</sub> <sup>2</sup>	12.75	-	0.1423	1		12.75	-	0.1423	3.17	-	536.08	0.1052	-	< 0.0001
X <sub>2</sub> <sup>2</sup>	77.04	-	0.0944	1		77.04	-	0.0944	19.17	-	355.54	0.0014	-	< 0.0001
X <sub>3</sub> <sup>2</sup>	15.06	-	0.1497	1		15.06	-	0.1497	3.75	-	564.11	0.0816	-	< 0.0001
Residual	40.18	3.24	0.0027	10	16	4.02	0.202	0.0003						
Lack of fit	33.24	1.97	0.0008	5	11	6.65	0.179	0.0002	4.79	0.7069	0.458	0.0553	0.7073	0.7942
Pure error	6.94	1.27	0.0018	5		1.39	0.254	0.0004						
Corr. total	3494.52	80.56	0.4	19										



**Figure 4.1: Diagnostic plot of model adequacy: (a-c) normal probability plot of  $Y_1$ ,  $Y_2$  and  $Y_3$ ; (d-f) predicted vs. actual response of  $Y_1$ ,  $Y_2$  and  $Y_3$**

(c)



(d)

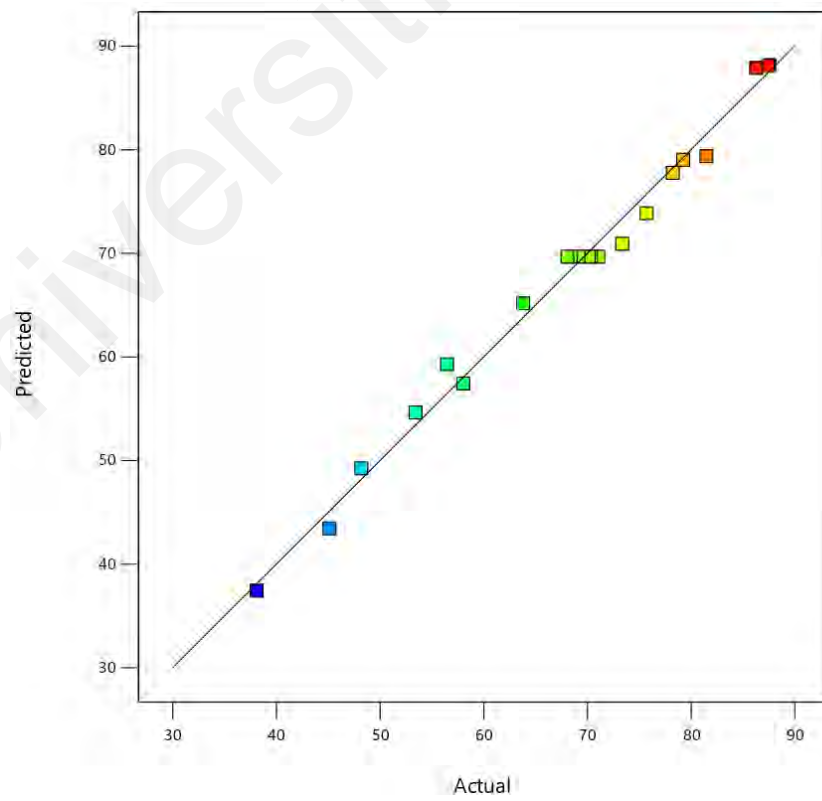


Figure 4.1, continued

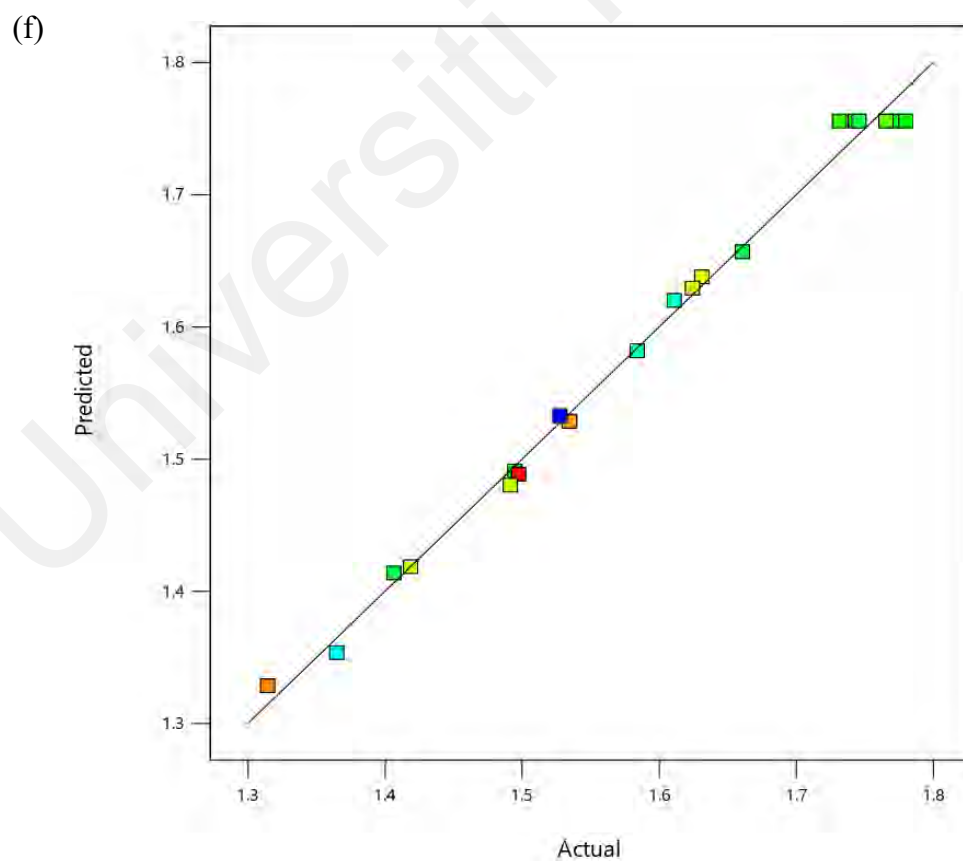
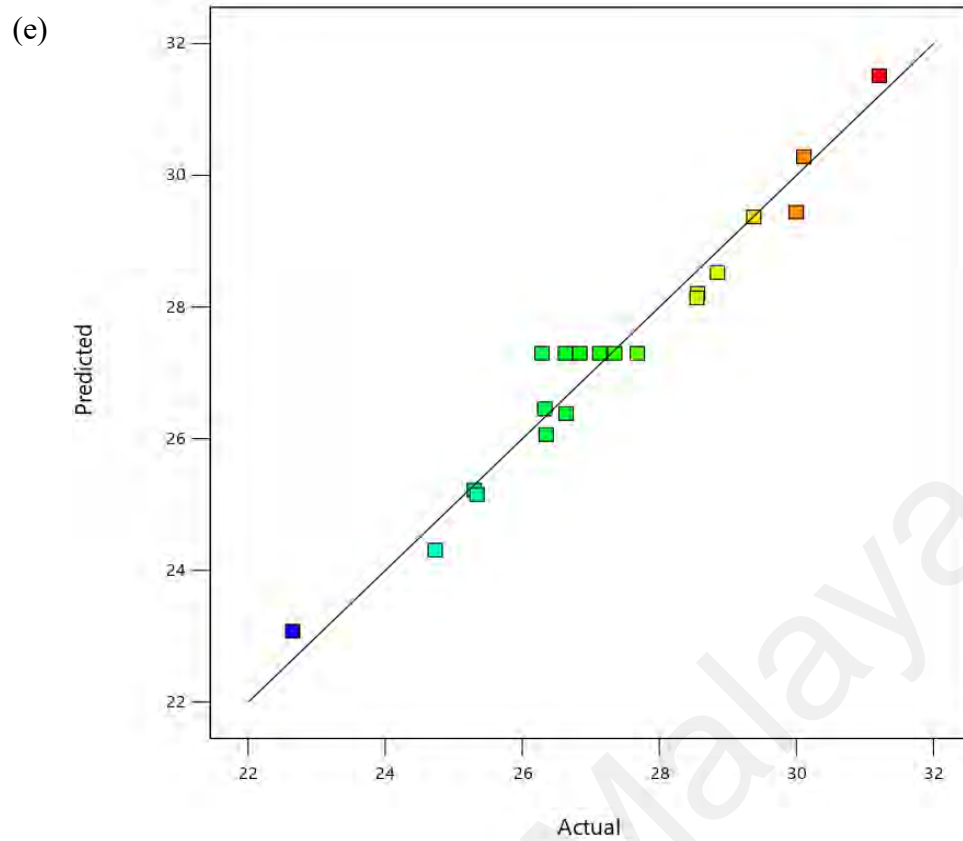


Figure 4.1, continued

**Table 4.4: Model fit summaries for bio-adsorbent precursor coconut shell**

	SD	Mean	CV	PRESS	$R^2$	Adj. $R^2$	Pred. $R^2$	AP
$Y_1$	2.0000	67.09	2.99	286.24	0.9885	0.9782	0.9181	35.7785
$Y_2$	0.4499	27.30	1.65	4.65	0.9598	0.9523	0.9423	41.9255
$Y_3$	0.0163	1.58	1.03	0.0092	0.9934	0.9874	0.9770	37.0816

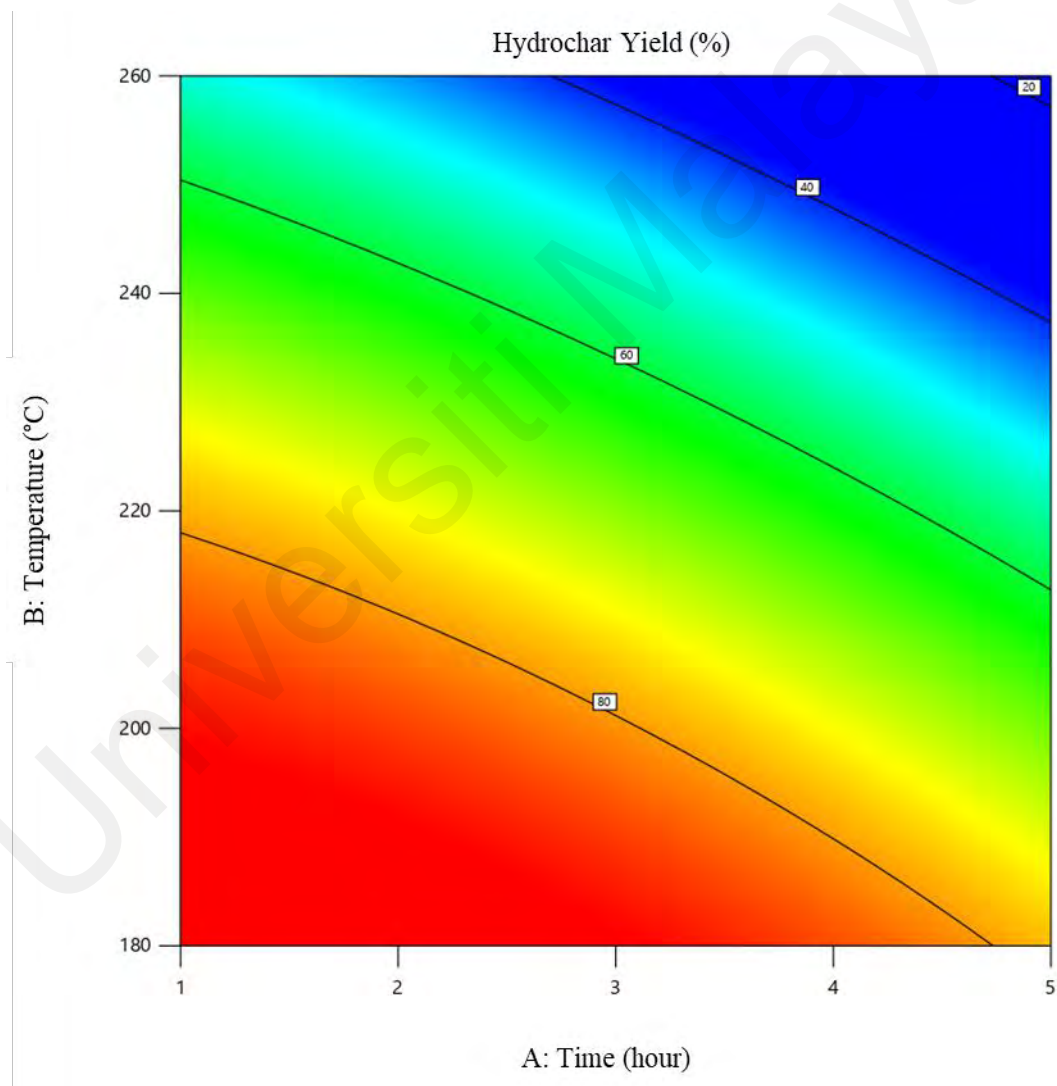
#### 4.2.1.2 Effect of operating condition on the hydrochar yield, bio-adsorbent yield and CO<sub>2</sub> adsorption capacity

Three-dimensional (3D) response surface plots were illustrated to visualize and analyse the effect of experimental variables (solid weight percentage, reaction temperature, and carbonisation time) on the responses (hydrochar yield, bio-adsorbent yield, and CO<sub>2</sub> adsorption capacity). Manzar et al. (2021) indeed reported that these response surface plots of the regression model analysis are recommended, since they provide information on the behavior of operating variables during the experimental runs. Moreover, the response surface curve assists in comprehending the interaction between the experimental variables and dependent variables. Understanding the effect of HTC condition on hydrochar yield ( $Y_1$ ) and corresponding hydrochar properties is important in ensuring successful carbon activation for the production of efficient bio-adsorbent. Understanding the bio-adsorbent yield ( $Y_2$ ) is crucial to ensure resource efficiency and economic viability in the bio-adsorbent synthesis process from biomass. Accurately determining the yield enables the optimisation of the conversion process, which maximizes the amount of bio-adsorbent produced per unit of biomass and minimizes waste. Meanwhile, CO<sub>2</sub> adsorption capacity ( $Y_3$ ), determines their technical efficiency.

##### (a) Carbonisation time

The relationship between carbonisation time ( $X_1$ ) and  $Y_1$ , and  $Y_2$  are inversely proportional, with hydrochar yield being affected the most. Figure 4.2 illustrates the

interaction between carbonisation time ( $X_1$ ) and carbonisation temperature ( $X_2$ ) on the yield of hydrochar ( $Y_1$ ), while solid weight % ( $X_3$ ) is fixed at 20%. The increment of carbonisation time from 1 to 5 hours resulted in a significant reduction of hydrochar yield. For instance, at a constant carbonisation temperature of 180 °C and 20% solid weight, hydrochar yield reduced from 91% to 78%. The rate of decrease in hydrochar yield reduced as carbonisation time increased, suggesting a rapid decomposition followed by a more gradual reduction in yield.



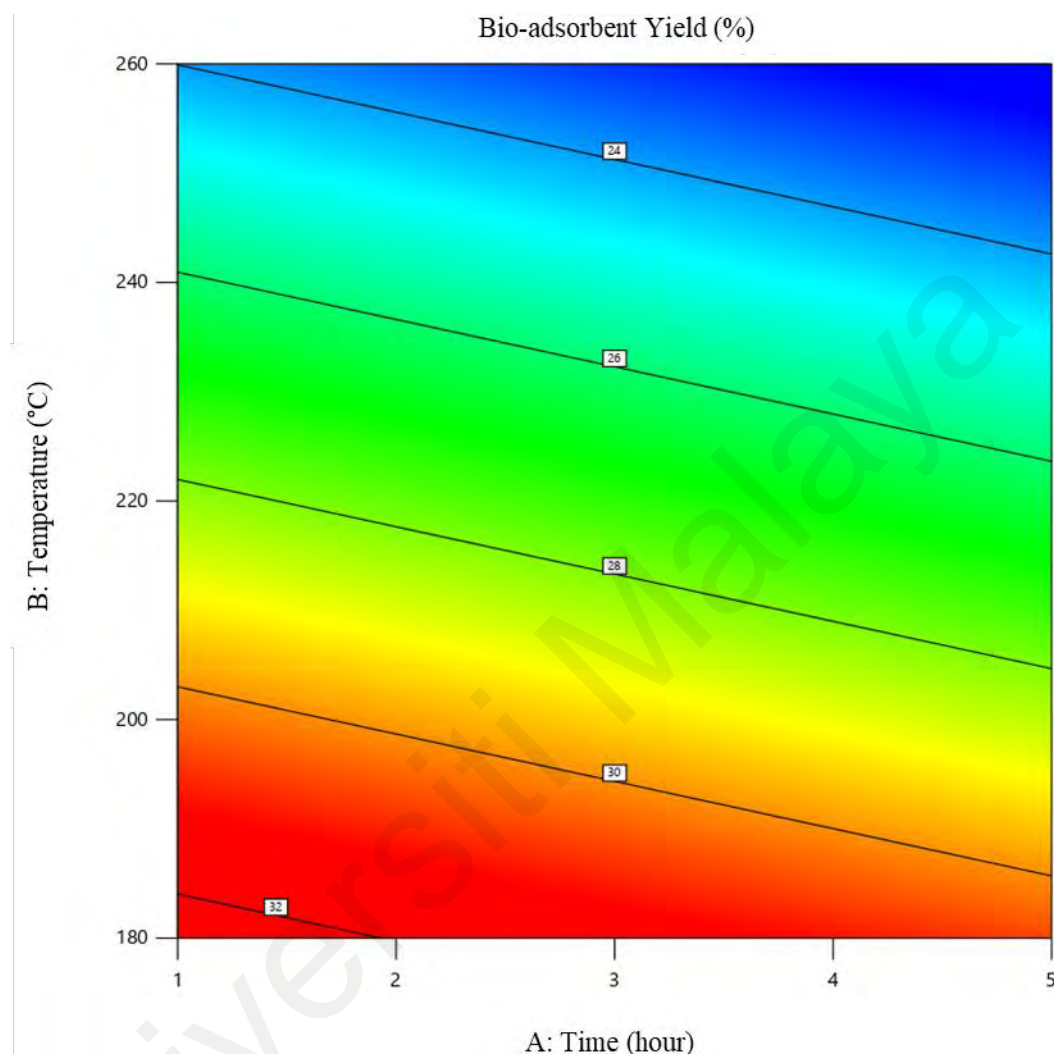
**Figure 4.2: Contour plot of carbonisation time ( $X_1$ ) and carbonisation temperature ( $X_2$ ) vs. response  $Y_1$ .**



The observed trends can be justified by considering the carbonisation process dynamics. Initially, the biomass undergoes mass loss due to the removal of moisture and light volatiles. Consequently, this causes a substantial decrease in hydrochar yield. Extended carbonisation times result in more intricate reactions, leading to the decomposition of the biomass structure and the generation of char. The remaining mass primarily constitutes stable carbon, resulting in a slower rate of yield reduction. For hydrochar yield ( $Y_1$ ), carbonisation time has a sum of squares of 594.87, indicating its substantial contribution to the variation in  $Y_1$ . The F-value of 148.06 is very high, demonstrating a significant effect, which is further confirmed by a p-value of less than 0.0001. This means that  $X_1$  has a strong and statistically significant effect on the hydrochar yield.

A similar relationship was also observed for the yield of bio-adsorbent. From Figure 4.3, the increment of carbonisation time from 1 hour to 5 hours, while maintaining the HTC temperature of 220 °C and % of solid weight to sludge at 20 wt.% resulted in a reduction of yield of bio-adsorbent by 2.4%, from 28% to 26%. Similar percentages of reductions of bio-adsorbent yield were recorded for carbonisation temperatures of 180, 200, 240 and 260 °C, as the carbonisation time increases from 1 to 5 hours. In comparison to hydrochar yield, the effect of carbonisation temperature on bio-adsorbent yield is less severe as portrayed in Figure 4.3. This is because the activation step with KOH involves additional chemical reactions that enhance the porosity and surface area of the carbon material. During activation, the hydrochar undergoes further mass loss, but this process also stabilizes the carbon structure and offsets some of the yield reductions observed during carbonisation (Diaz-Maroto et al., 2024). As a result, while hydrochar yield decreases significantly with increasing carbonisation time, the yield of bio-adsorbent remains relatively stable due to the compensatory effects of the activation process. The

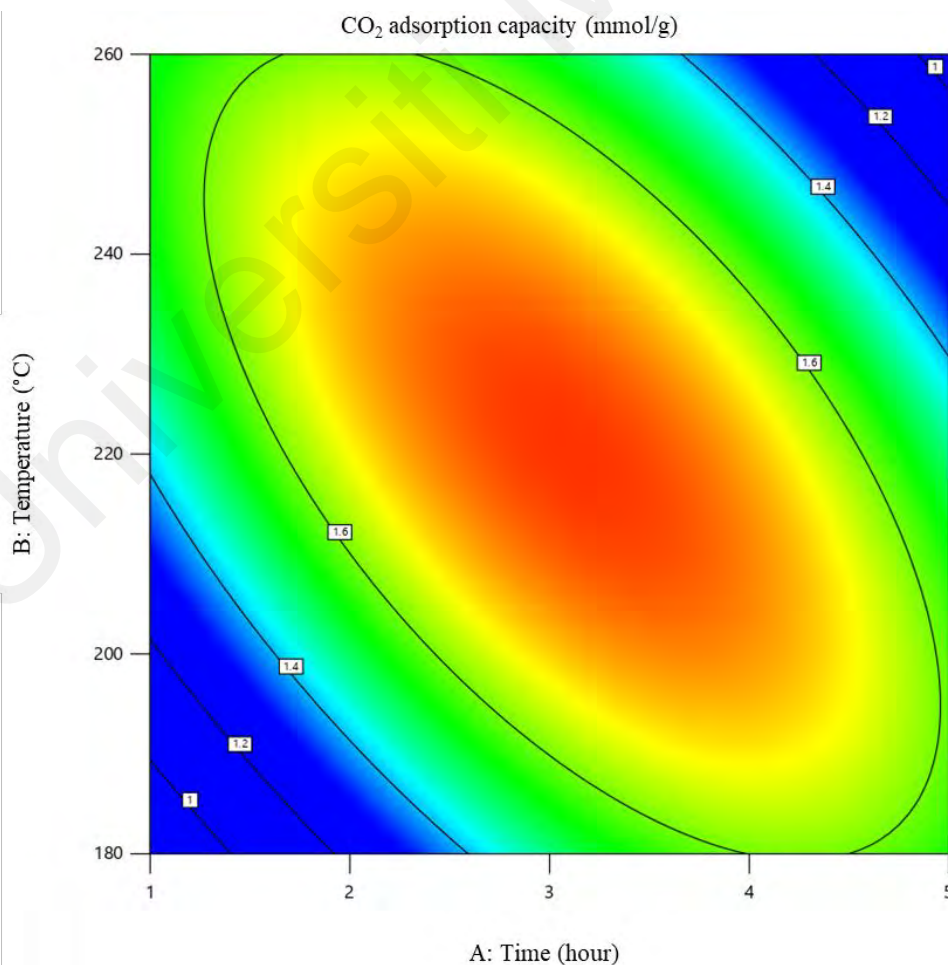
additional activation step thus mitigates the effect of prolonged carbonisation times, leading to a less severe reduction in activated carbon yield compared to hydrochar yield.



**Figure 4.3: Contour plot of carbonisation time ( $X_1$ ) and carbonisation temperature ( $X_2$ ) vs.  $Y_2$ .**

The ANOVA of carbonisation time on bio-adsorbent yield ( $Y_2$ ) is also in agreement with the trend. The sum of squares for  $Y_2$  is 3.33, and the F-value is 16.46, indicating a noticeable effect. The p-value of 0.0009 is well below the typical significance level of 0.05, confirming the statistical significance effect of  $X_1$  on  $Y_2$ . This suggests that while  $X_1$  is an important factor in determining the bio-adsorbent yield, its impact is not as pronounced as it is for the hydrochar yield.

Based on the ANOVA results in Table 4.3, carbonisation time ( $X_1$ ) is the most influential factor on  $\text{CO}_2$  adsorption ( $p$ -value = 0.0013), whereas carbonisation temperature ( $X_2$ ) and solid weight % ( $X_3$ ) exhibit less pronounced effects ( $p$ -values of 0.0222 and 0.0022, respectively). Figure 4.4 visualizes the interaction between carbonisation time ( $X_1$ ) and temperature ( $X_2$ ) on  $\text{CO}_2$  adsorption capacity ( $Y_3$ ). The plot demonstrates that carbon dioxide adsorption capacity initially increases with carbonisation time but then declines beyond a certain threshold. For instance, at 220 °C, increasing carbonisation time from 1 hour (1.42 mmol/g) to 3 hours leads to an optimised adsorption capacity of 1.78 mmol/g. However, extending the carbonisation time further to 4 and 5 hours results in a 5% and 16% decrease in adsorption capacity, respectively, as indicated by the lighter shades of red and orange in the figure.



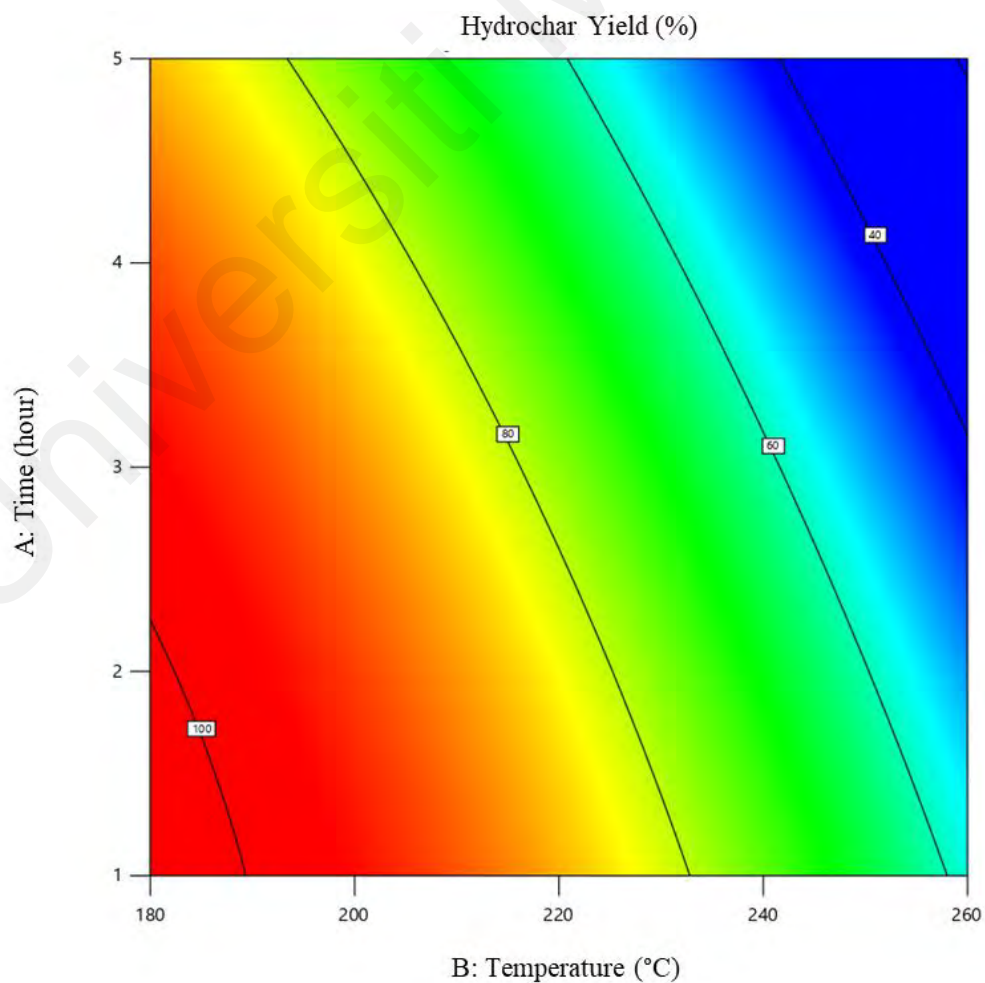
**Figure 4.4: Contour plot of carbonisation time ( $X_1$ ) and carbonisation temperature ( $X_2$ ) vs.  $Y_3$ .**

This trend suggests that while increasing carbonisation time initially enhances the development of porous structures and active sites beneficial for CO<sub>2</sub> adsorption, excessive carbonisation time leads to structural degradation and pore collapse, thereby reducing the adsorption efficiency. This result is consistent with existing literature, which suggests that the decrease in adsorption capacity is likely due to the formation of detrimental functional groups and the increased risk of pore wall collapse caused by excessive thermal treatment. This structural degradation can lead to a reduction in both pore volume and the overall effectiveness of the adsorbent. Ghanim et al. (2016) studied the effect of carbonisation time and temperature of the HTC process on poultry litter at 150-300 °C with 30-, 120- and 480-minute residence time. It was reported that temperature plays a significant role in determining the properties of hydrochar. An increment in residence time resulted in a reduction in hydrochar yield, an increment of ash, and fixed carbon.

In placing more emphasis, Karagöz et al. (2004) claimed that short heat exposure resulted in the formation of high-quality hydrochar. This can be supported by Inoue et al. (2008) and Inoue et al. (2002) through the carbonisation of cellulose and wood, which concludes that the synthesised hydrochar has better quality than lignite. However, study by Shen et al. (2024) have reported that prolonged retention times can lead to a decrease in the surface area. This reduction in surface area is attributed to extensive repolymerization occurring during prolonged HTC processing, which results in the formation of a denser, less porous structure. This structural compaction, while reducing porosity, may enhance the hydrochar's mechanical stability but could limit its effectiveness for applications requiring high surface areas, such as adsorption or catalysis.

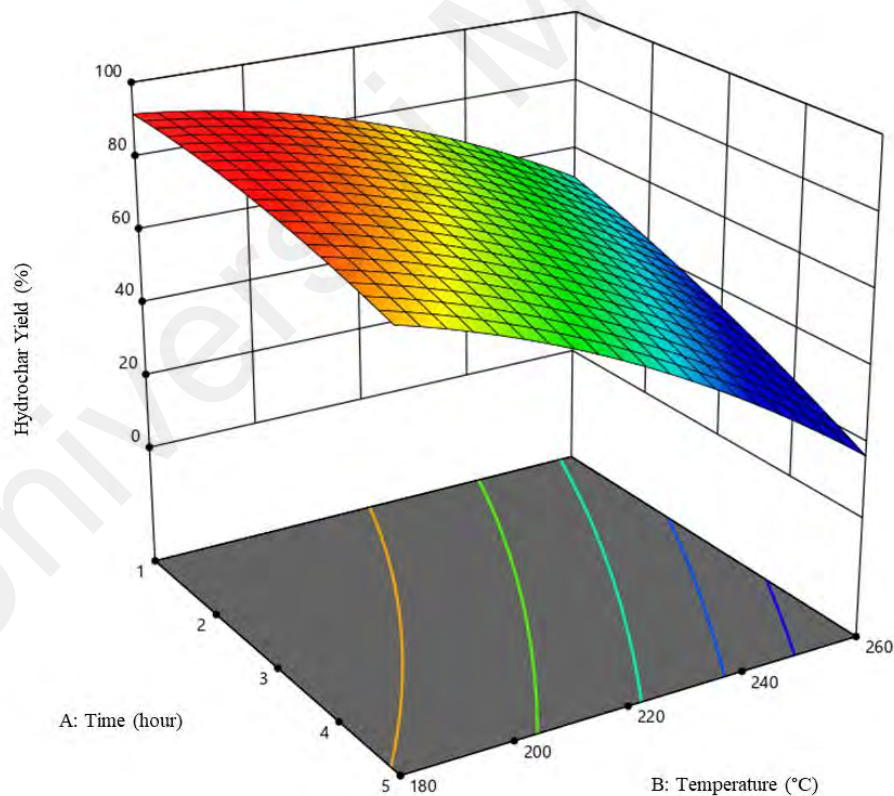
*(b) Carbonisation temperature*

The relationship between carbonisation temperature ( $X_2$ ) with  $Y_1$ , and  $Y_2$  are inversely proportional while quadratic with  $\text{CO}_2$  adsorption capacity of bio-adsorbent synthesised. Figure 4.5 illustrates the interaction between the carbonisation temperature ( $X_2$ ) and carbonisation time ( $X_1$ ) on hydrochar yield, while solid weight % was fixed at a central point. The figure demonstrates that the highest hydrochar yield is obtained when the parameters are set to their lowest factor. Specifically, at carbonisation time of 3 hours and solid weight % of 20%, the highest hydrochar yield of 86.26 wt.% was observed at carbonisation of 180 °C. Conversely, hydrochar synthesised at 260 °C, with the same carbonisation time and solid weight percentage, exhibited a considerably low yield of approximately 38.08%.

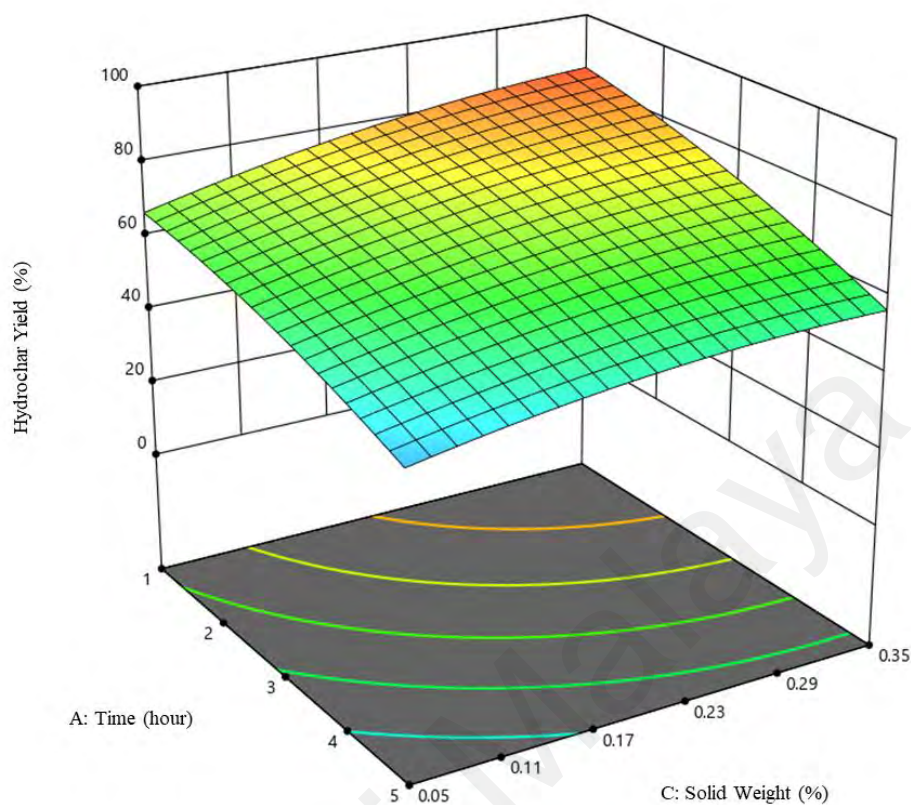


**Figure 4.5: Contour plot of carbonisation temperature ( $X_2$ ) and carbonisation time ( $X_1$ ) vs. hydrochar yield ( $Y_1$ )**

The 3D surface plot in Figure 4.6 and 4.7 reveals that carbonisation temperature has the most significant effect on hydrochar yield. This observation is supported by the F-value analysis in Table 4.2, where carbonisation temperature exhibits the highest F-value (633.68) compared to solid weight % (F-value = 52.87) and carbonisation time (F-value = 148.06). This finding aligns with previous research by Nizamuddin et al. (2016), which also demonstrated the dominant influence of carbonisation temperature (F-value = 1.86) on hydrochar yield, whereas variations in solid weight % (F-value =  $3.17 \times 10^{-3}$ ) and carbonisation time (F-value = 0.064) were not statistically significant. Basically, at high temperature, low product yield is due to intensified endothermic chemical reaction between carbon and water, leading to an extensive weight loss.



**Figure 4.6: 3D surface plots of Carbonisation time ( $X_1$ ) and carbonisation temperature ( $X_2$ ) vs. response  $Y_1$ .**



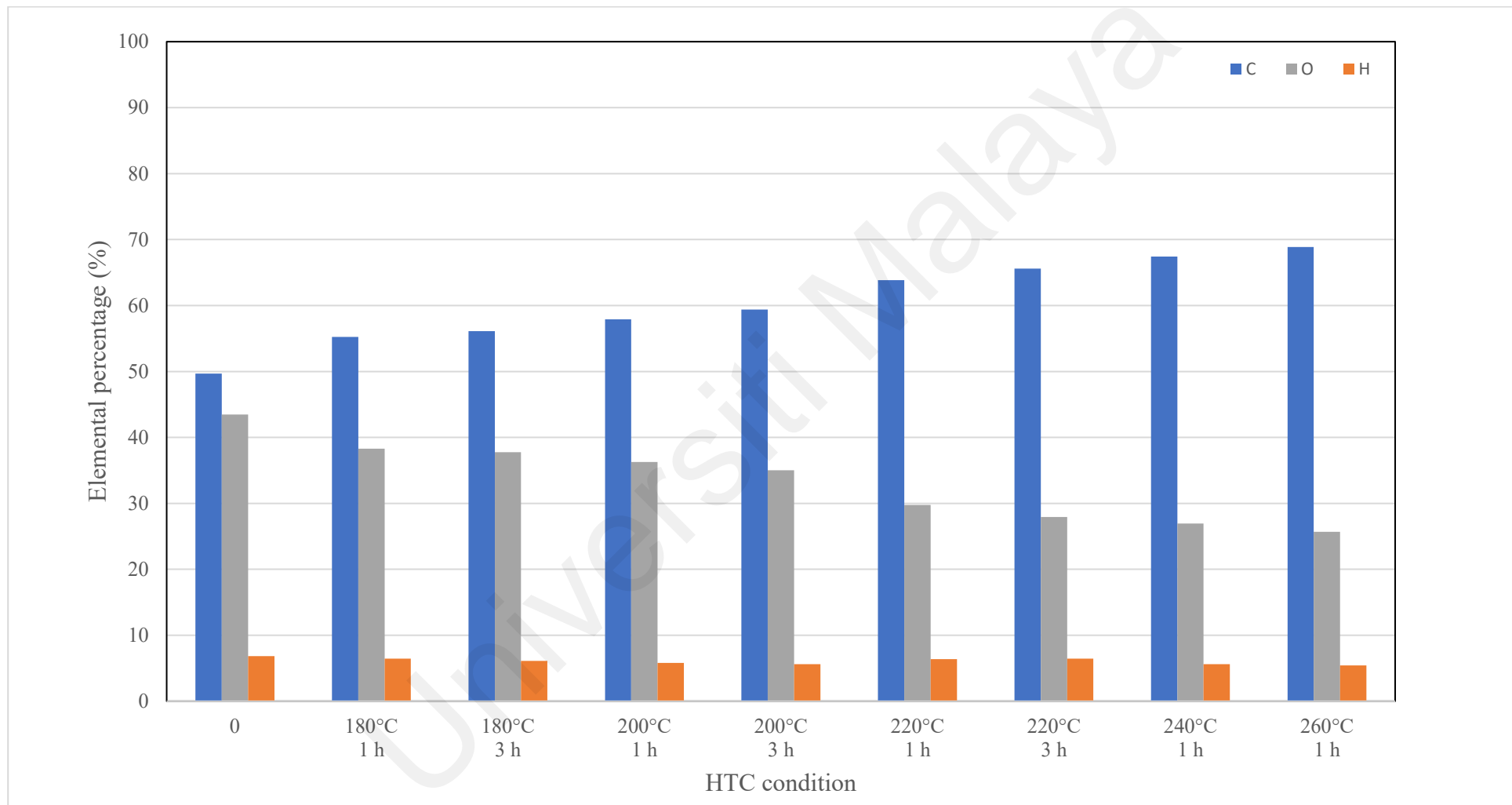
**Figure 4.7: 3D surface plots of Carbonisation time ( $X_1$ ) and solid weight % ( $X_3$ ) vs. response  $Y_1$ .**

According to Reza et al. (2015), temperature increment during hydrothermal carbonisation resulted in a lower hydrochar yield as more volatile matter and cellulose breakdown at higher temperatures. Higher temperatures also resulted in higher carbon and lower oxygen content, which is more suitable for adsorption of pollutant. However, in sustainable adsorbent production, achieving high yield and performance at lower synthesis temperatures is crucial. This approach reduces energy consumption while maximizing both production output and adsorption efficiency. Determining the optimum synthesis process is essential, as it ensures the balance between cost-effectiveness and the superior functional properties of the adsorbent, ultimately leading to more sustainable and efficient applications. In this study hydrochar yield can be maximized at Run 13.

However, EDX analysis (Figure 4.8) confirms that at 180 °C, the material did not undergo complete carbonisation, resulted in production of biomass-peat materials. In addition, visual inspection revealed that Run 13 produced a slightly darker brown material compared to raw material, instead of the expected black.

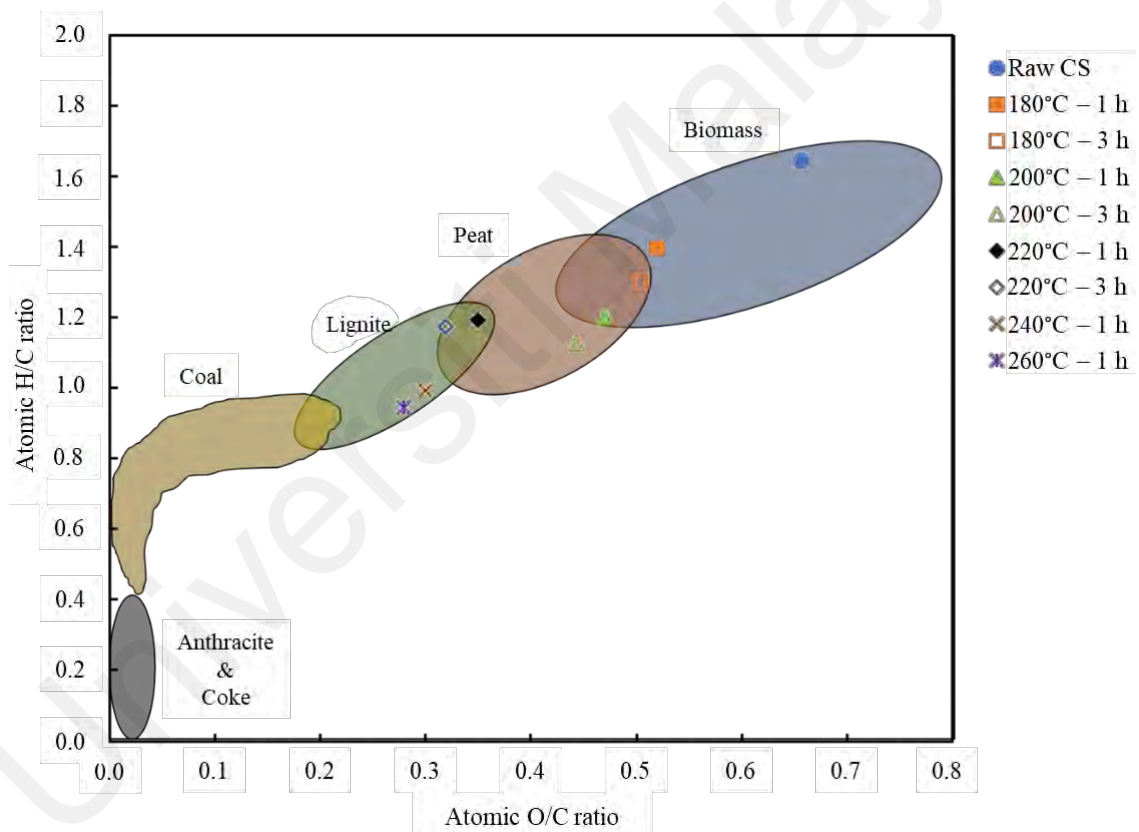
Universiti Malaya





**Figure 4.8: Energy dispersion x-ray spectroscopy of hydrochars**

Figure 4.9 illustrate the van Krevelen diagram in which the minimum temperature required for second stage carbonisation is 220 °C, allows complete reduction of volatile matter, and minimal amount of fibrous structure from original biomass retained. Consequently, this condition is essential for optimising bio-adsorbent synthesis. This finding is corroborated by Lee et al. (2018), who also reported that increasing the hydrothermal carbonisation temperature resulted in higher carbon content. Moreover, the study also concludes that only the solid product collected at 200 °C was classified as lignite, while other hydrochar samples fell under the peat category.



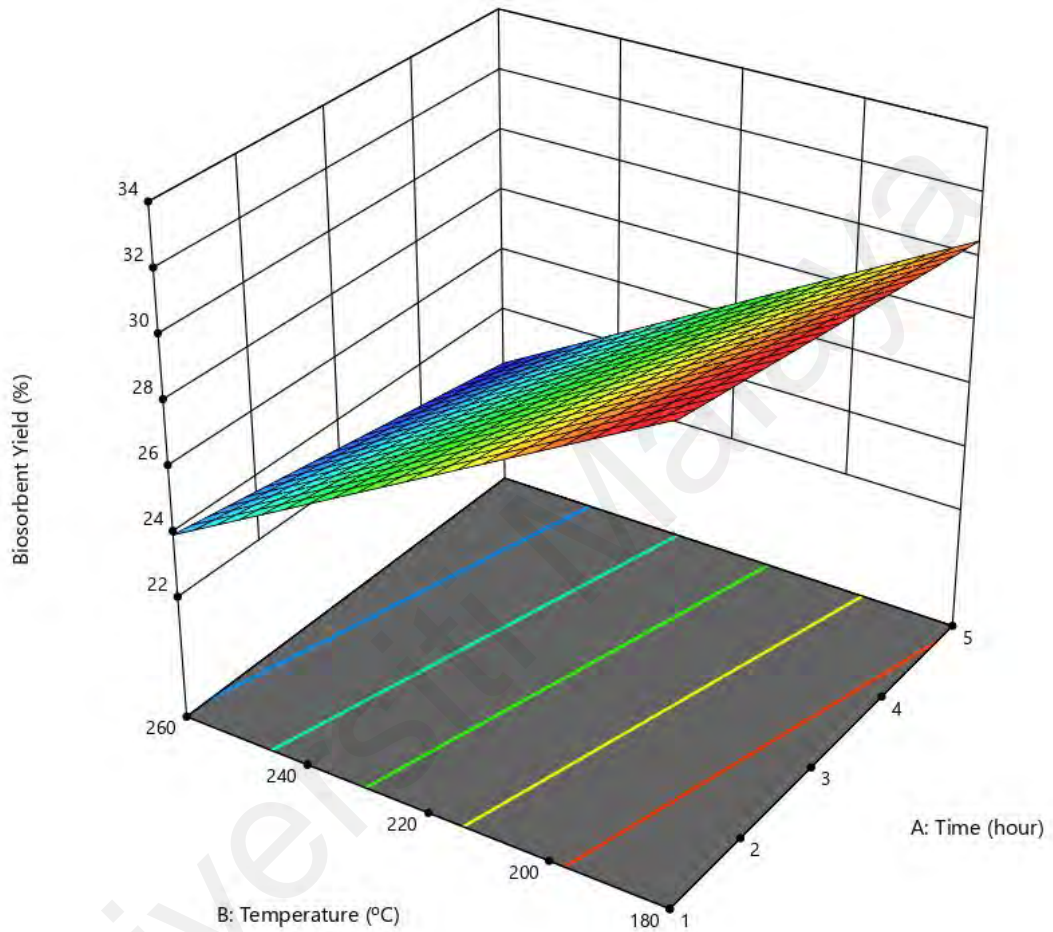
**Figure 4.9: Van Krevelen diagram of hydrochar at different HTC condition**

Based on contour plot in Figure 4.3, carbonisation temperature affected the bio-adsorbent (activated hydrochar) yield the most. This observation aligns with the F-value analysis presented in Table 4.3, wherein the carbonisation temperature exhibits the highest F-value (351.55) in comparison to solid weight % (F-value = 14.03) and carbonisation time

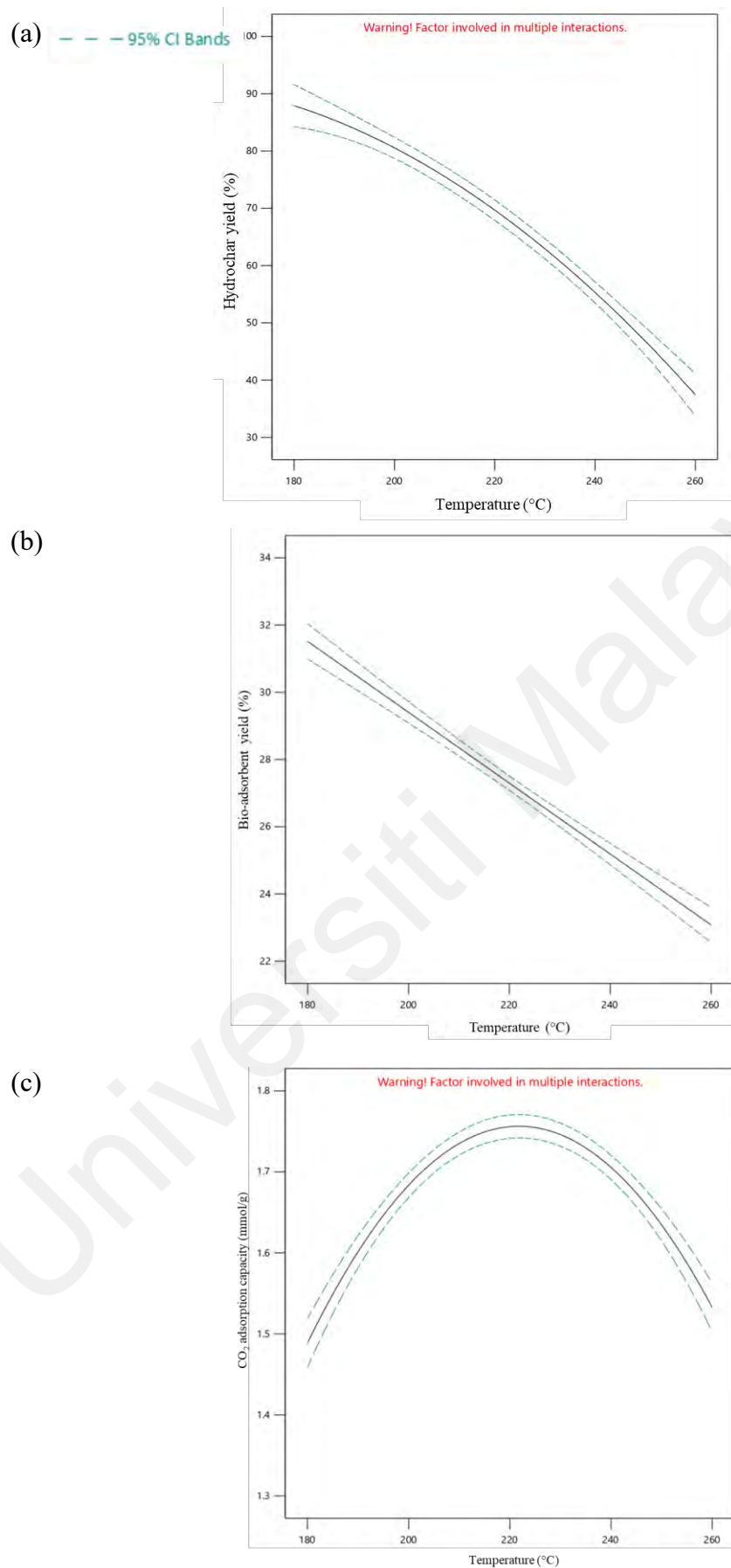
(F-value = 16.46). Similar to hydrochar yield, increment of HTC temperature resulted in higher degree of severe dehydration, decarboxylation, and depolymerization reactions on biomass. These reactions break down complex organic molecules into simpler, volatile compounds, leading to a significant mass loss. Elevated temperatures lead to increased carbonisation and volatilization of biomass, resulting in a reduced initial hydrochar yield and consequently a lower bio-adsorbent yield (Reza et al., 2015). Furthermore, hydrochar produced at higher temperatures undergoes changes in its chemical composition and structural integrity.

Figure 4.10 illustrates the interaction effect between carbonisation temperature ( $X_2$ ) and time ( $X_1$ ) on bio-adsorbent yield ( $Y_2$ ), while solid weight % ( $X_3$ ) is fixed at 20%. In addition to the 3D plot, the effect of carbonisation temperature on hydrochar yield, bio-adsorbent yield, and carbon dioxide adsorption capacity is visualized in the curvature plot (Figure 4.11). This plot reveals an initial increase in  $\text{CO}_2$  adsorption capacity with rising temperature, followed by a decline beyond an optimal point. This trend can be attributed to the increased energy available for endothermic reactions between carbon and water at elevated temperatures, leading to the formation of new pores that contribute to higher  $\text{CO}_2$  adsorption. However, excessive temperatures beyond the optimum negatively affect  $\text{CO}_2$  adsorption capacity. Moderate temperatures (200-220°C) favour the development of micropores and mesopores, enhancing surface area and adsorption sites (Bala Dhull et al., 2024). Further activation under optimal conditions promotes the development of microporous structures, which in turn improves the bio-adsorbent's capacity to adsorb  $\text{CO}_2$ . The synergy between the increased surface area and the presence of functional groups at these specific temperatures contributes to achieving optimal adsorption performance. However, at higher temperatures, above 220°C, the hydrochar undergoes further carbonisation, aromatization and repolymerization resulted in extensive structural changes (Sangare et al., 2022). While this increases the overall

carbon content and stability of the hydrochar, it also leads to the collapse of some porous structures and the reduction of surface functional groups, which is crucial in enhancing the chemical binding between CO<sub>2</sub> and bio-adsorbent.



**Figure 4.10: Response surface plot of carbonisation time (X<sub>1</sub>) and carbonisation temperature (X<sub>2</sub>) vs. response bio-adsorbent yield (Y<sub>2</sub>)**



**Figure 4.11: Effect of carbonisation temperature on (a) Y<sub>1</sub>, (b) Y<sub>2</sub>, and (c) Y<sub>3</sub>.**

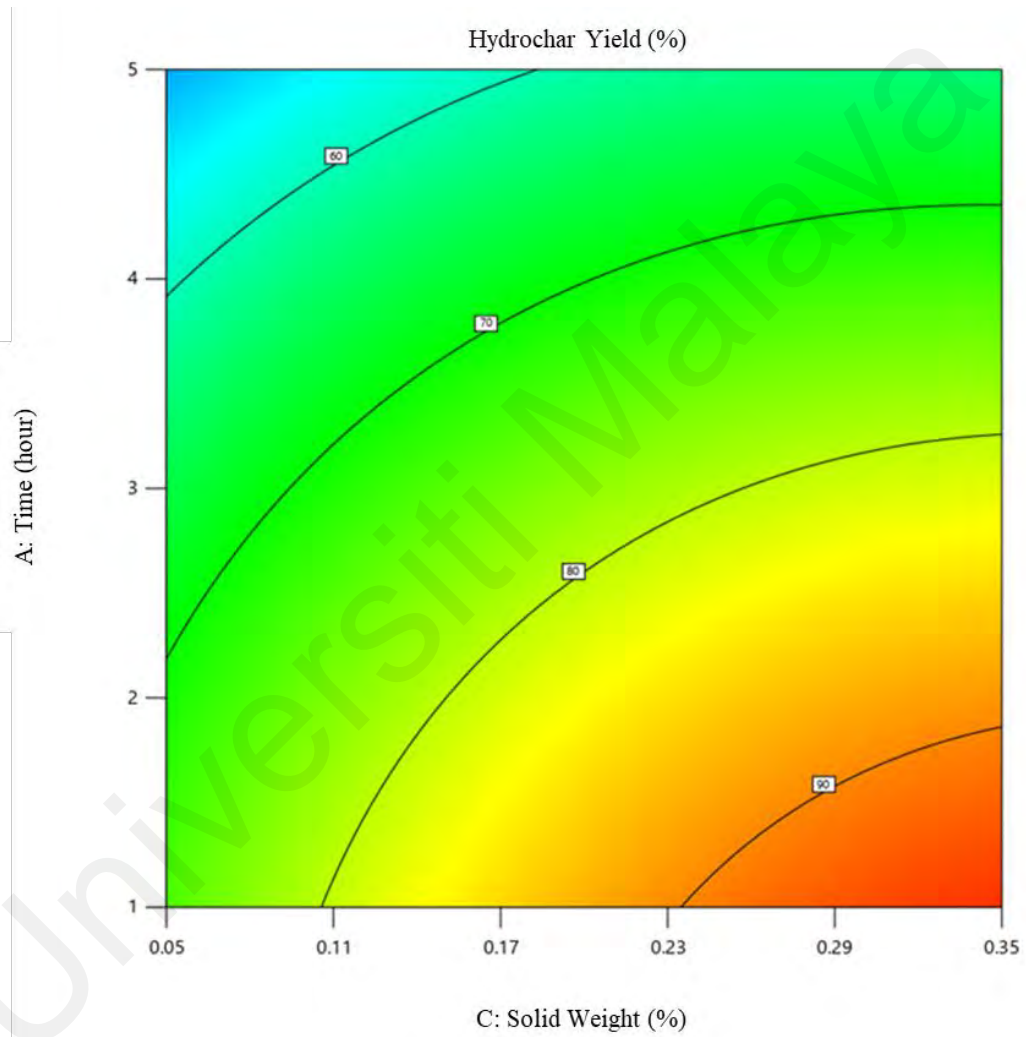
Several studies support the observation that reduced adsorption capacity is often associated with the degradation of functional groups and the collapse of pore walls due to excessive thermal annealing. This process disrupts pore structures and leads to a decrease in pore volume, negatively impacting adsorption capabilities. Reza (2022) observed that hydrochar produced at or below 220°C yielded microporous materials, whereas hydrothermal treatment above 220°C led to widening and coalescence of existing pores due to repolymerization, resulting in decreased microporous surface area.

*(c) Raw coconut shell to sludge percentage*

The yield of hydrochar is significantly affected by the percentage of raw coconut shell in the sludge. From Figure 4.12, it can be observed that an increment in solid weight percentage generally leads to an increase in hydrochar yield. Increment of percentage of raw coconut shell during HTC, from 5% to 35%, at carbonisation time and temperature of 1 hour and 220 °C, resulted in increment of hydrochar yield by 26%; from 74.98% to 94.51%. Similarly, at carbonisation time of 3 hours with similar carbonisation temperature, increment of solid weight percentage resulted in increment of hydrochar yield by 25%. This trend can be explained as the higher solid weight percentage indicating more biomass is available for conversion into hydrochar, thus increasing the overall yield. The solid weight percentage essentially represents the initial amount of material subjected to carbonisation; hence, a higher percentage results in a larger amount of solid residue after the volatile components have been driven off.

Additionally, previous study by Atallah et al. (2019) indicated that higher solid-to-liquid ratio in hydrothermal carbonisation process, hinder the efficient carbonisation to happen as the limited water availability reduces the hydrolysis and solubilization of organic components, resulting in a higher hydrochar yield. Nakason et al. (2018) have reasserted that the biomass liquid ratio and retention time of the HTC process

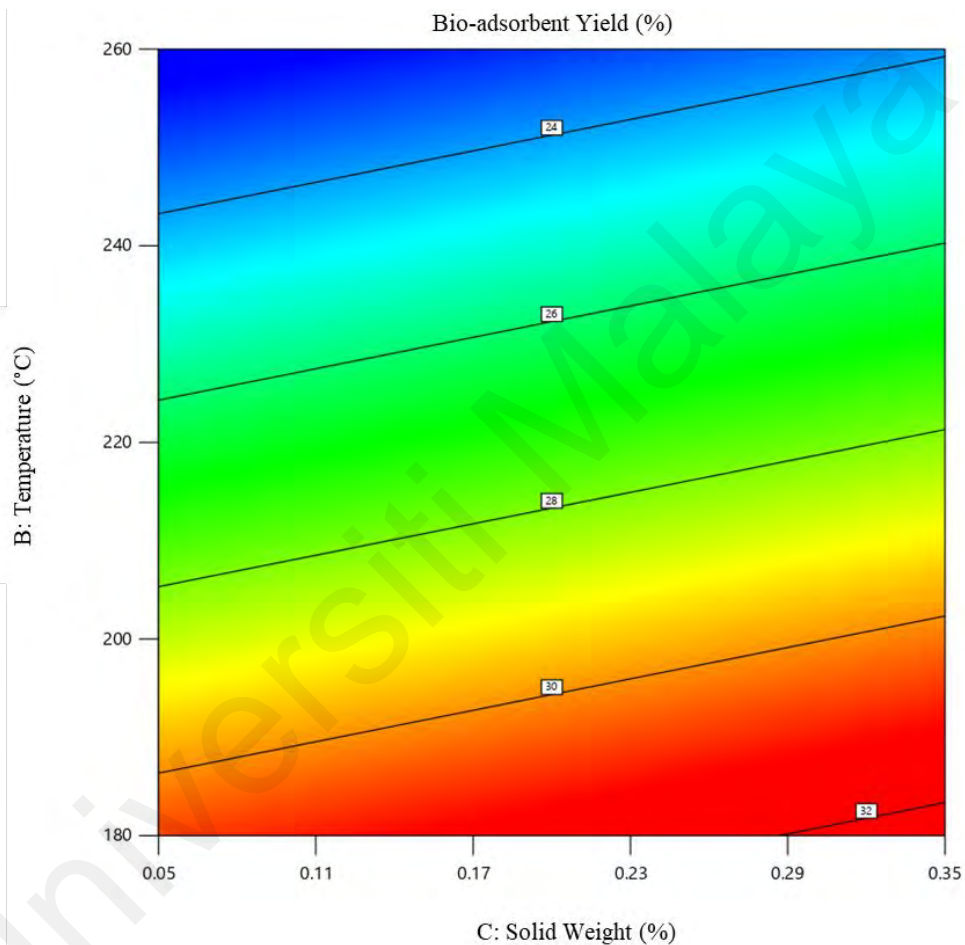
simultaneously influence the solid yield. An increment of solid-liquid ratio paired with a longer reaction time enhances the formation of secondary char, which masks the increment of hydrochar yield. Additionally, a higher liquid-solid ratio resulting in high availability of water promotes the kinetic reaction, which enhances the dissolution of lignocellulose structure, leading to low production of denser hydrochar.



**Figure 4.12: Contour plot of solid weight percentage ( $X_3$ ) and carbonisation time ( $X_1$ ) vs. response  $Y_1$ .**

The bio-adsorbent yield also shows a correlation with the solid weight percentage in the sludge (Figure 4.13). Higher solid weight percentages tend to result in higher bio-adsorbent yields, despite the higher activation temperature at 700 °C. Increment of solid weight % from 5% to 35% and carbonisation temperature from 180 °C to 260 °C resulted

in bio-adsorbent yield ranging between 22.65 % to 31.21%. This indicates that more starting material enhances the synthesis of bio-adsorbent. The bio-adsorbent yield is influenced by the availability of carbonaceous material that can be converted into adsorbent structures. Therefore, higher solid weights contribute more to the formation of these structures, increasing the yield.

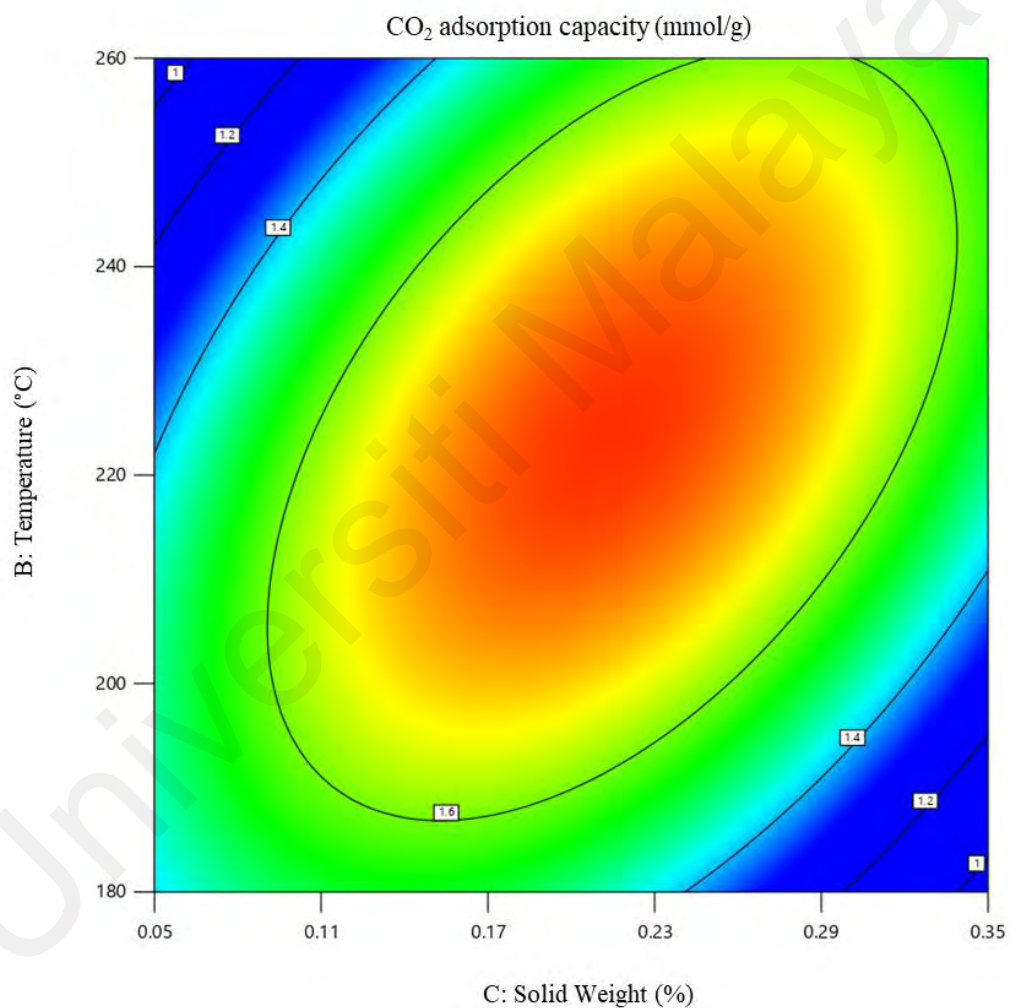


**Figure 4.13: Contour plot of solid weight percentage ( $X_3$ ) and carbonisation temperature ( $X_2$ ) vs. response  $Y_2$ .**

The  $\text{CO}_2$  adsorption capacity of the bio-adsorbent is also affected by the solid weight percentage in the sludge. Figure 4.14 shows the effect of solid weight percentage and temperature on  $\text{CO}_2$  adsorption capacity, with the temperature set to a constant carbonisation time of 3 hours. The  $\text{CO}_2$  adsorption capacity is represented by a gradient ranging from 1.31 to 1.78 mmol/g, indicating that the variations in solid weight



percentage and temperature influence the adsorption performance of the bio-adsorbent. Generally, a higher solid weight percentage results in improved CO<sub>2</sub> adsorption capacities. For example, increment of solid weight from 5% to 23% resulted in a noticeable increase in adsorption capacity, reaching its peak at around 1.78 mmol/g. This trend is due to the increased availability of carbonaceous material during the carbonisation process, resulting in efficient activation process.



**Figure 4.14: Contour plot of solid weight percentage (X<sub>3</sub>) and carbonisation temperature (X<sub>2</sub>) vs. response Y<sub>3</sub>.**

The contour plot reveals that beyond a certain point, the CO<sub>2</sub> adsorption capacity decreases despite further increases in solid weight percentage. This decline adsorption performance when the solid weight percentage exceeds approximately 23%, can be

attributed to several factors. One primary reason is pore blockage. As the solid weight percentage increases beyond the optimal level, the additional biomass can lead to the formation of larger aggregates or denser structures during the carbonisation process. These denser structures reduce the effective pore volume and surface area available for CO<sub>2</sub> adsorption, thereby diminishing the overall adsorption capacity. Another contributing factor is incomplete carbonisation. At higher solid weights, not all the biomass is effectively converted into porous carbon structures, resulting in biochar with fewer active sites for CO<sub>2</sub> adsorption. This incomplete conversion can lower the quality of the hydrochar and bio-adsorbent, making it less efficient in capturing CO<sub>2</sub> (Almahbashi et al., 2021).

The solid weight percentage plays a crucial role in determining the CO<sub>2</sub> adsorption capacity of bio-adsorbents. While increasing the solid weight initially enhances the adsorption capacity by providing more material for porous structure formation, excessive solid weight leads to performance degradation due to factors such as pore blockage and incomplete carbonisation. Optimising the solid weight percentage is essential to maximize the efficiency of CO<sub>2</sub> adsorption while maintaining the structural integrity and quality of the bio-adsorbent.

Besides response surface plots, a perturbation plot can also be used to evaluate the significance of variables. This is shown in Figure 4.15. This plot visualizes how changes in each parameter (A, B and C represent carbonization time, carbonisation temperature and solid weight percentage) affect the response value by individually moving each variable from a reference point (centre point) while keeping all others constant. This comparison allows analysis on the relative effect of each parameter on the response within the design space. A steep curvature or slope indicates high sensitivity of a variable towards the response, while a flat line signifies lower sensitivity. Figure 4.15 (c) reveals that carbonisation time (X<sub>1</sub>) and solid weight % (X<sub>3</sub>) strongly influence CO<sub>2</sub> adsorption

capacity ( $Y_3$ ) due to their steep curvatures, whereas carbonisation temperature ( $X_2$ ) exhibits less sensitivity with a moderate curvature.

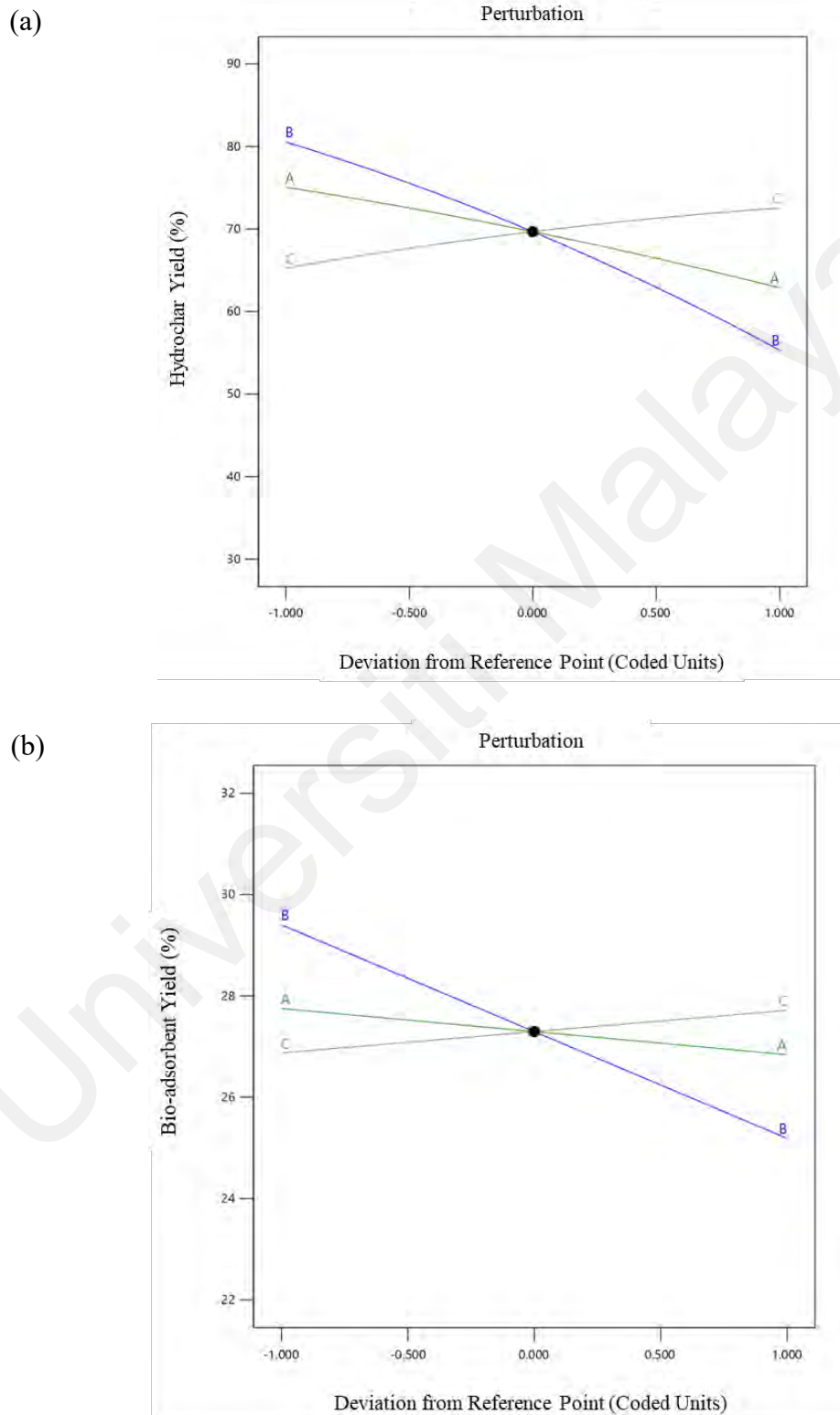
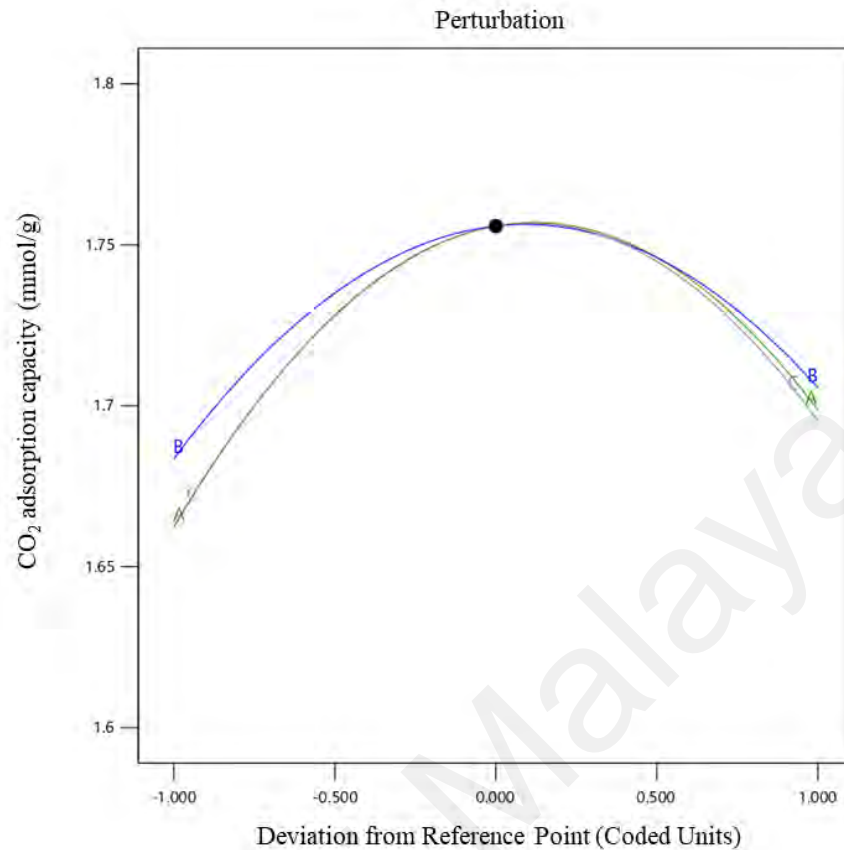


Figure 4.15: Perturbation plot for response (a) hydrochar yield ( $Y_1$ ), (b) bio-adsorbent yield ( $Y_2$ ), and (c)  $\text{CO}_2$  adsorption capacity ( $Y_3$ ).

(c)



**Figure 4.15, continued**

#### 4.2.1.3 Modelling optimisation of synthesis process

From a manufacturing perspective, achieving a high yield of bio-adsorbent is crucial for economic viability. However, the ultimate measure of an adsorbent's effectiveness lies in its adsorption capacity. Thus, it is essential to optimise the operating parameters to attain a bio-adsorbent that exhibits both high yield and superior adsorption performance (Kassahun et al., 2022). Accordingly, optimisation process has been carried out via Design Expert software and optimum conditions are selected at points where the desirability is the highest. Based on characterisation of hydrochar produced through RSM-CCD, it was concluded that the minimum carbonisation temperature to ensure production of carbon through HTC is 220 °C and above. This parameter has been included in optimisation parameter. The optimum parameters (at the highest desirability value of 0.856 that have been obtained from the software is summarized in Table 4.5.

**Table 4.5: Optimisation parameters and validation of hydrothermal carbonisation**

Variables	Factor			Response		
	X <sub>1</sub> : Time (hour)	X <sub>2</sub> : Temperature (°C)	X <sub>3</sub> : Solid weight (%)	Y <sub>1</sub> : Hydrochar yield (%)	Y <sub>2</sub> : Bio- adsorbent yield (%)	Y <sub>3</sub> : CO <sub>2</sub> adsorption capacity (mmol/g)
Set condition	In range	Minimize	In range	-	Maximize	Maximize
Optimum condition	3.00	220	0.200	-	-	-
Predicted	-	-	-	70.55	27.40	1.755
Actual	-	-	-	70.02	26.55	1.750
Error (%)	-	-	-	0.76	3.20	0.29

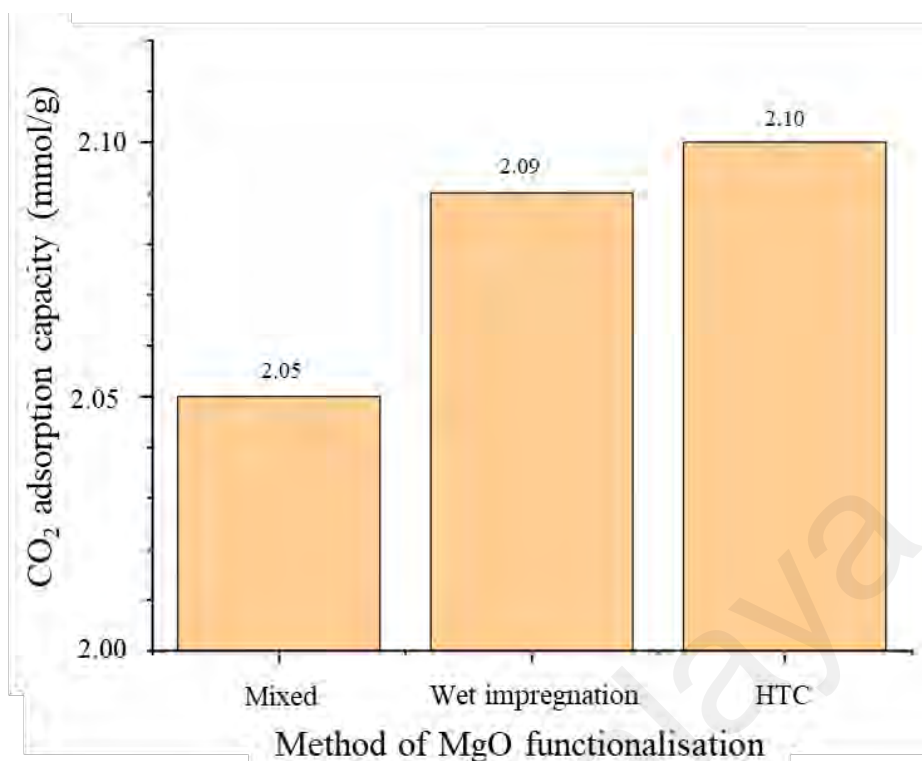
Referring to optimisation results in Table 4.5, it presents a small difference between the predicted and experimental value of response Y<sub>2</sub> and Y<sub>3</sub>, showing high reliability and adequacy of the model in predicting the bio-adsorbent yield and CO<sub>2</sub> adsorption capacity. To achieve the initial goal of maximizing both bio-adsorbent yield and CO<sub>2</sub> adsorption capacity, the optimal conditions were determined to be a 20% solid weight in slurry, a carbonisation temperature of 220°C, and a carbonisation time of 3 hours, followed by KOH activation at 700°C for 2 hours with a KOH to hydrochar ratio of 3. The estimated product yield of ~26 wt.% under these conditions exceeds the minimum industrial benchmark (Feng et al., 2020), with acceptable yields for bio-adsorbents typically ranging from 20-40 wt.%. In addition, the experimental yield obtained at this condition which is approximately 26.55 wt. % is considered attractive since based on the compilation on coconut shell-based bio-adsorbent from various chemical activation techniques de Mora et al. (2024), the range of activated carbon yield is in the range of 10-17 wt. %. The optimised bio-adsorbent derived from activated hydrochar precursor coconut shell is referred to as HCS.

#### **4.2.2 Coconut shell bio-adsorbent functionalised with magnesium oxide**

Coconut shell bio-adsorbent was successfully synthesised through hydrothermal carbonisation (HTC) at 220 °C for 3 hours with a solid weight percentage of 20%. This was followed by KOH activation at a ratio of 3, conducted at 700 °C for 2 hours. In addition to modifying and optimising the hydrothermal carbonisation and chemical activation techniques, another approach to enhance the CO<sub>2</sub> adsorption capacity at elevated temperatures is the functionalisation of the adsorbent with metal oxides. In this study, the performance of optimised coconut shell bio-adsorbent (HCS) in CO<sub>2</sub> adsorption capacity were further enhance through incorporation of magnesium oxide. The effect of MgO impregnation methods (direct blending, and wet impregnation through pyrolysis, and, hydrothermal carbonisation) on CO<sub>2</sub> adsorption capacity were investigated. After determination of optimum MgO impregnation method, the influence of weight percentage of MgO (5-50%) impregnated towards the mixture on performance of bio-adsorbents in CO<sub>2</sub> adsorption capacity were conducted. Following sub-section (4.2.2.1-4.2.2.2) discusses the influence of functionalisation of bio-adsorbent with MgO.

##### **4.2.2.1 Effect of impregnation method on CO<sub>2</sub> adsorption**

The performance of HCS that were incorporated with 15 wt.% magnesium oxide through wet impregnation, hydrothermally treated and direct mixing were compared to determine the effect of MgO impregnation method onto the CO<sub>2</sub> adsorption capacity of developed bio-adsorbent. Figure 4.16 shows the CO<sub>2</sub> adsorption capacity of all studied samples at standard condition.



**Figure 4.16: Effect of MgO functionalisation method onto CO<sub>2</sub> adsorption capacity of HCS**

Based on the figure, the highest carbon dioxide adsorption capacity was recorded through impregnation of magnesium oxide into activated carbon through hydrothermal treatment, followed by wet impregnation and direct mixing at 2.10, 2.09 and 2.05 mmol/g. Impregnation through hydrothermal approach resulted in higher adsorption capacity due to its ability to dispersed the metal oxide uniformly across the surface of activated carbon (Madzaki et al., 2018b). In addition, hydrothermal treatment facilitates the formation of oxygen functional groups which is crucial in ensuring stable binding between bio-adsorbent and carbon dioxide (Mamtani et al., 2021; G. Yang et al., 2022).

The effect of functionalisation method on CO<sub>2</sub> adsorption capacity can also be further validated by surface area analysis. From the analysis, functionalisation of MgO through wet impregnation resulted in higher BET surface area at 787.46 m<sup>2</sup>/g, followed by HTC method at 769.33 m<sup>2</sup>/g, and direct mixing. Direct mixing, which utilised industrial MgO, resulted in a fixed particle size based on its production process. In contrast, the functionalisation of magnesium nitrate through pyrolysis and hydrothermal methods

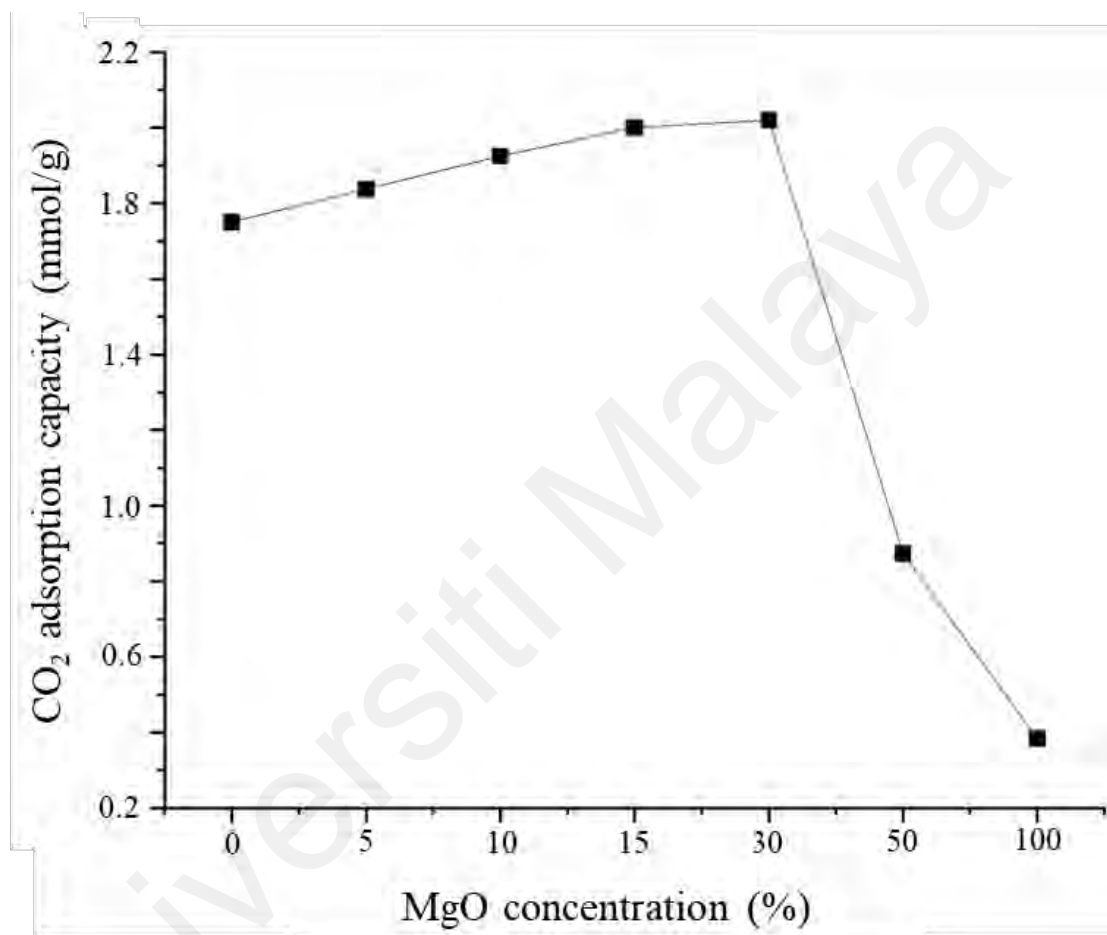
enabled the production of nanomaterials. However, the HTC method indirectly led to repolymerization, which subsequently reduced the total surface area of the MgO-functionalised bio-adsorbent. Despite the increment in adsorption capacity, the performance gains are minimal compared to the energy required for synthesis process. For instance, De Mena Pardo et al. (2016) highlighted that pyrolysis (wet impregnation) treatment is more detrimental compared to low-energy HTC. However, HTC required utilisation of water as carbonisation medium, which is less sustainable. In addition, the HTC need to be conducted in pressurized chamber, which might offset its environmental and energy benefits when evaluated economically. Therefore, the optimal method for MgO functionalisation into the bio-adsorbent is through direct blending (mixed).

#### **4.2.2.2 Optimisation of concentration of magnesium oxide**

Figure 4.17 shows the adsorption capacity of HCS when magnesium oxide was impregnated onto the adsorbent from concentration of 0% to 50%. The rationale behind the MgO loading is based on previous literature (Park et al., 2022; Zhou et al., 2018), whom investigated the effect of concentration of MgO loading onto activated carbon towards pollutant removal. The HCS were functionalised through direct blending of solid MgO and bio-adsorbent. Based on the figure, addition of 5% MgO resulted in increment of carbon dioxide adsorption capacity from 1.750 to 1.838 mmol/g, and incorporation of 10 wt.% and 15 wt.% of MgO onto HCS leads to increment of CO<sub>2</sub> adsorption capacity by 10%, and 17% respectively compared to pristine HCS. Addition of magnesium oxide increase the adsorption capacity due to introduction of basic sites on the surface of HCS. Since CO<sub>2</sub> is an acidic gas, which interacts strongly with these basic sites, leading to improved adsorption. In addition, the presence of metal oxide enhances the chemical affinity of HCS for CO<sub>2</sub> molecules, thus increasing the adsorption capacity. This can be supported by Madzaki et al. (2018a) through functionalisation of metal oxides on



commercial activated carbon. Addition of CeO<sub>2</sub> slightly improves adsorption by 31% due to favorable interactions between CeO<sub>2</sub> and CO<sub>2</sub>. Similar findings were reported by Ghaemi et al. (2022), indicating 8-11% increase in activated carbon performance through NiO and MgO functionalisation.



**Figure 4.17: Effect of MgO concentration onto CO<sub>2</sub> adsorption capacity of HCS**

However, incorporating 30 wt.% MgO resulted in smaller CO<sub>2</sub> adsorption capacity increment by 15%, compared to HCS. In addition, functionalisation of MgO onto HCS at a 1:1 ratio significantly reduced the CO<sub>2</sub> adsorption capacity to 0.873 mmol/g. This decrease in CO<sub>2</sub> adsorption capacity is attributed to the dominant blockage of pores, which limits the availability of active sites on HCS for CO<sub>2</sub> adsorption and offsets the benefits of the functional groups. A similar trend was reported by Madzaki et al. (2018a) in their study on the functionalisation of CuO onto commercial activated carbon (AC).

They noted that CuO functionalisation negatively effects CO<sub>2</sub> adsorption on commercial AC, reducing it by 11% due to the blockage of pores by metal, which lowers the surface area available for adsorption.

Reduction of surface area can be validated through surface area analysis in Table 4.6. The concentration of MgO onto HCS exhibits an inversely proportional relationship with the BET surface area. The surface area of the bio-adsorbent decreased from 976.30 m<sup>2</sup>/g to 405.95 m<sup>2</sup>/g with the incorporation of 50 wt.% MgO. In adsorption process, a higher surface area usually indicates higher adsorption performance, as it provides more active sites for CO<sub>2</sub> molecules to adsorb onto, enhancing the overall adsorption capacity (Sharma et al., 2021). Besides surface area, pore diameter also plays a critical role. Microporous structures (<2 nm) are highly effective for CO<sub>2</sub> adsorption because their size is comparable to that of CO<sub>2</sub> molecules, maximizing adsorption through pore filling. However, in this study, the functionalisation with MgO transformed the pore diameter from microporous to mesoporous. Despite the lower surface area and mesoporous structure HCS\_15MgO has highest CO<sub>2</sub> adsorption capacity, indicating the synergy of effective surface area and functional groups contributing to efficient CO<sub>2</sub> adsorption.

**Table 4.6: Structural properties of pristine HCS and functionalised with MgO**

Sample	S <sub>BET</sub> (m <sup>2</sup> /g)	S <sub>micro</sub>	V <sub>T</sub> (cm <sup>3</sup> /g)	V <sub>micro</sub> (cm <sup>3</sup> /g)	V <sub>non- micro</sub> (cm <sup>3</sup> /g)	V <sub>micro</sub> /V <sub>T</sub> (%)	D <sub>P</sub> (nm)	APS (nm)
HCS	976.30	789.38	0.4199	0.3144	0.1055	74.87	1.72	2.68
HCS_5MgO	920.51	740.27	0.4200	0.2916	0.1284	69.43	2.00	4.13
HCS_10MgO	874.68	700.97	0.4452	0.2792	0.1660	62.71	2.04	8.82
HCS_15MgO	721.05	581.88	0.3882	0.2319	0.1563	59.74	2.15	12.3
HCS_30MgO	527.12	411.15	0.3760	0.1643	0.2117	43.70	2.85	16.8
HCS_50MgO	405.91	295.92	0.3897	0.1186	0.2711	30.43	3.84	17.3
MgO	188.26	126.54	0.1044	0.0512	0.0532	49.04	2.22	8.75

In summary, the incorporation of MgO into HCS enhances CO<sub>2</sub> adsorption capacity on bio-adsorbent due to the basic nature of the metal oxide particles, which readily interact with the acidic CO<sub>2</sub> gas. The figure indicates that the optimal MgO impregnation concentration is 15% through direct blending. It is hypothesized that exceeding this concentration leads to reduction in the surface area of developed bio-adsorbent, potentially counteracting the benefits of the added functional groups.

#### **4.2.3 Bio-adsorbent functionalised with microalgae**

Apart from modification of hydrothermal carbonisation and chemical activation techniques, other approach that has been adopted for adsorbent with high CO<sub>2</sub> adsorption capacity is through functionalisation with nitrogen-rich materials. In this study, the performance of optimised HCS in CO<sub>2</sub> adsorption capacity were further enhance through incorporation of microalgae through co-carbonisation and blending. Following subsection (4.2.3.1-4.2.3.3) discusses the influence of microalgae functionalisation method towards performance of bio-adsorbents in CO<sub>2</sub> adsorption capacity.

##### **4.2.3.1 Effect of functionalisation method of microalgae on the CO<sub>2</sub> adsorption capacity**

The functionalisation of microalgae onto bio-adsorbents was achieved using four distinct methods: physical mixing, hydrothermal carbonisation (HTC), wet impregnation, and co-carbonisation. These methods were investigated to assess their effect on the CO<sub>2</sub> capture performance of the bio-adsorbents. The highest CO<sub>2</sub> adsorption capacity was observed by co-carbonise coconut shell and microalgae at 2.213 mmol/g. This superior performance is attributed to the porous structure formed due to the significant release of volatile matter, gas and heat during preparation of bio-adsorbent though co-carbonisation in HTC, followed by KOH activation. In comparison, other synthesis methods achieved

CO<sub>2</sub> adsorption capacity of 1.937 mmol/g and 1.850 mmol/g, for HCS functionalised with microalgae through wet impregnation of raw *Chlorella*, followed by HTC (HCS-HC) and HCS functionalised with microalgae through wet impregnation of raw *Chlorella*, followed with pyrolysis (HCS-PC) respectively. Even though the adsorption performance of functionalised HCS through pyrolysis and HTC methods increased compare to the pristine bio-adsorbent (HCS) and their corresponding individual alteration, these methods do not achieve the same level of porosity and functional group introduction as the combined co-carbonisation and KOH activation process.

According to surface area analysis, the BET surface area of the samples can be arranged in the following order: HCS-RC < HCS-HC < HCS-PC < HCS-N at value of 769.33, 779.51, 787.50 and 2038.80 m<sup>2</sup>/g. Despite higher surface area of HCS-N and HCS-PC compared to HCS-HC, HCS-HC has comparable performance with HCS-N. This is due to the presence of more oxygen-containing functional groups which enhance CO<sub>2</sub> adsorption through a combination of chemical interactions, increased surface polarity, enhanced surface reactivity, improved wettability, facilitation of pore formation, and stabilization of adsorbed CO<sub>2</sub>. However, despite the promising performance, additional treatments are required to achieve these microalgae-functionalisation, which is less sustainable due to additional requirement of energy and water resources.

For HCS-RC, the CO<sub>2</sub> adsorption performance was recorded at 1.788 mmol/g, which is the lowest compared to other approaches. Direct mechanical mixing, lacks the chemical transformation and enhancement of surface properties provided by thermal and chemical treatments, resulting in lower adsorption efficiency. Thus, the co-carbonisation method stands out as the optimal synthesis technique for functionalisation of microalgae onto bio-adsorbent.

#### 4.2.3.2 Effect of microalgae concentration on the CO<sub>2</sub> adsorption capacity

Microalgae functionalisation of bio-adsorbent through co-carbonisation shows high potential in enhancing CO<sub>2</sub> adsorption capacity compared to other approaches. Therefore, determining the optimum ratio of coconut shell to microalgae in co-carbonisation is important as it significantly affects the properties and performance of the resulting bio-adsorbents. Table 4.7 summarize the relationship between concentration of RC with yield of bio-adsorbent and carbon dioxide adsorption capacity. As the concentration of microalgae increases from 0-100 wt.% in co-carbonisation with coconut shell, the yield of bio-adsorbent decreased from 26.55 wt.% to 5.21 wt.%. The reduction in bio-adsorbent yield is due to the higher volatile content and lower fixed carbon content of microalgae compared to coconut shell. During carbonisation, microalgae release more volatiles, resulting in a lower solid residue yield. In contrast, coconut shell, with its higher lignin and fixed carbon content, contributes to a higher yield of carbon-based adsorbent. Therefore, increasing the proportion of microalgae in the mixture leads to a greater loss of material as volatiles, reducing the overall yield of the bio-adsorbent.

Correspondingly, the CO<sub>2</sub> adsorption capacity increase from 1.750 mmol/g to 2.31 mmol/g as the concentration of microalgae increases. The increment in CO<sub>2</sub> adsorption capacity is due to the enhanced surface area and porosity introduced by the microalgae component. Microalgae, due to their abundance in proteins and lipids, undergo substantial decomposition during carbonisation. This process generates a highly porous structure with increased surface area (Fu et al., 2019), providing more active sites for CO<sub>2</sub> adsorption. Moreover, the presence of nitrogen-containing functional groups, originating from microalgae proteins, further enhances CO<sub>2</sub> adsorption through chemical interactions (Shi & Liu, 2021). Thus, the higher proportion of microalgae contributes to

a bio-adsorbent with improved textural properties and functional groups, leading to increased CO<sub>2</sub> adsorption capacity despite the lower yield.

Based on the Table 4.7, the optimum microalgae concentration is 30 wt.%. At this concentration, the bio-adsorbent yield is 24.72 wt.% and the CO<sub>2</sub> adsorption performance is 2.213 mmol/g. This is considered optimal as it resulted in relatively high yield of bio-adsorbent with a significant high CO<sub>2</sub> adsorption capacity. Further increment of microalgae concentration, beyond 30%, increased the CO<sub>2</sub> adsorption capacity but drastically reduced yield of bio-adsorbent, which is not be practical or economical for large-scale applications. Therefore, a 30% microalgae concentration provides a good compromise between yield and adsorption performance.

**Table 4.7: Effect of various concentration of microalgae during co-carbonisation on bio-adsorbent yield and CO<sub>2</sub> adsorption performance.**

[Microalgae] (%)	Bio-adsorbent yield (%)	CO <sub>2</sub> adsorption capacity (mmol/g)
0	26.55	1.750
10	25.90	1.891
20	25.33	2.040
30	24.72	2.213
40	20.10	2.234
50	15.62	2.250
60	13.11	2.277
70	10.77	2.281
80	9.18	2.293
90	7.01	2.298
100	5.21	2.310

#### **4.2.3.3 Comparison CO<sub>2</sub> adsorption capacity of raw microalgae, hydrochar microalgae, pyrochar microalgae and coconut shell bio-adsorbent functionalised with microalgae**

The CO<sub>2</sub> adsorption performance of raw microalgae, hydrochar, pyrolyzed microalgae and bio-adsorbent (activated hydrochar) was analysed individually to understand the

basis of CO<sub>2</sub> capture by nitrogen-rich heteroatoms materials, in comparison to lignocellulosic bio-adsorbent. Based on the adsorption performance at room temperature and pressure, activated hydrochar precursor microalgae has the highest CO<sub>2</sub> adsorption capacity at 2.31, followed by pyrochar, hydrochar and raw microalgae at 0.921 mmol/g, 0.871 mmol/g, and 0.628 mmol/g respectively. This finding is coherent with the study by Karimi et al. (2022), which conclude that activated biomass has prominently higher adsorption capacity compared to biochar and raw biomass. Activated adsorbent has a significantly higher surface area resulting from the activation process, which can increase the BET surface area, creating more active site for adsorption of pollutant to occur.

The specific surface area of raw microalgae, microalgae-derived hydrochar (HC), microalgae-derived pyrochar (PC) and microalgae derived activated hydrochar (ACMA) is 12.64 m<sup>2</sup>/g, 5.82 m<sup>2</sup>/g, 64.22 m<sup>2</sup>/g and 2700.05 m<sup>2</sup>/g respectively. Despite the thermal degradation of raw microalgae through HTC, the surface area of hydrochar reduces, in comparison to pyrochar, due to the repolymerization occurrence during hydrothermal treatment (Yuan et al., 2009). The hydrochars' limited surface area and inverse relationship with CO<sub>2</sub> adsorption suggest a process other than physical adsorption, such as hydrogen bonding,  $\pi$ - $\pi$  interactions and/or electrostatic interactions.

Despite the large surface area and CO<sub>2</sub> high adsorption capacity of activated hydrochar derived from microalgae, the yield of this adsorbent is minimal, amounting to just 5.21 wt.%. In contrast, the yield of bio-adsorbent (HCS) is significantly higher at 26.55 wt.%. Similarly, the yield from hydrochar derived from microalgae is relatively low at 14.83 wt.%. Microalgae, although efficient at CO<sub>2</sub> adsorption, have high moisture content, volatile components (such as lipids, proteins, and carbohydrates), and a relatively lower carbon content compared to lignocellulosic materials like coconut shells. This composition results in a low adsorbent production yield, typically ranging between

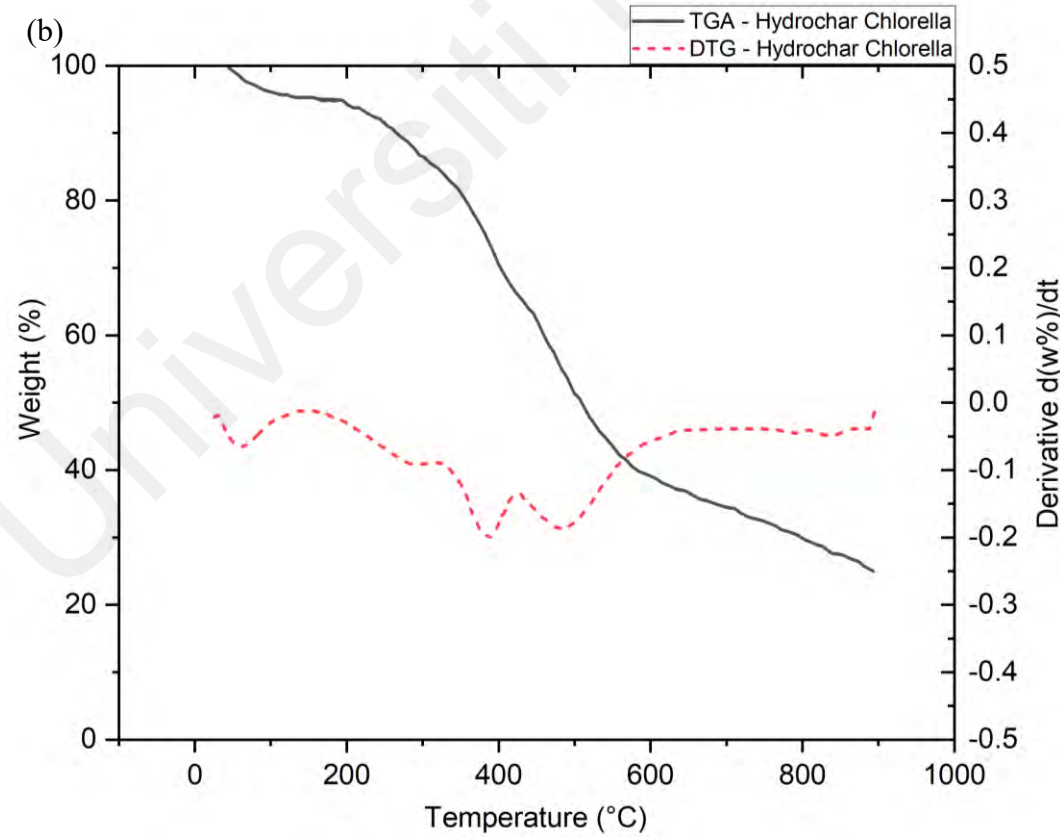
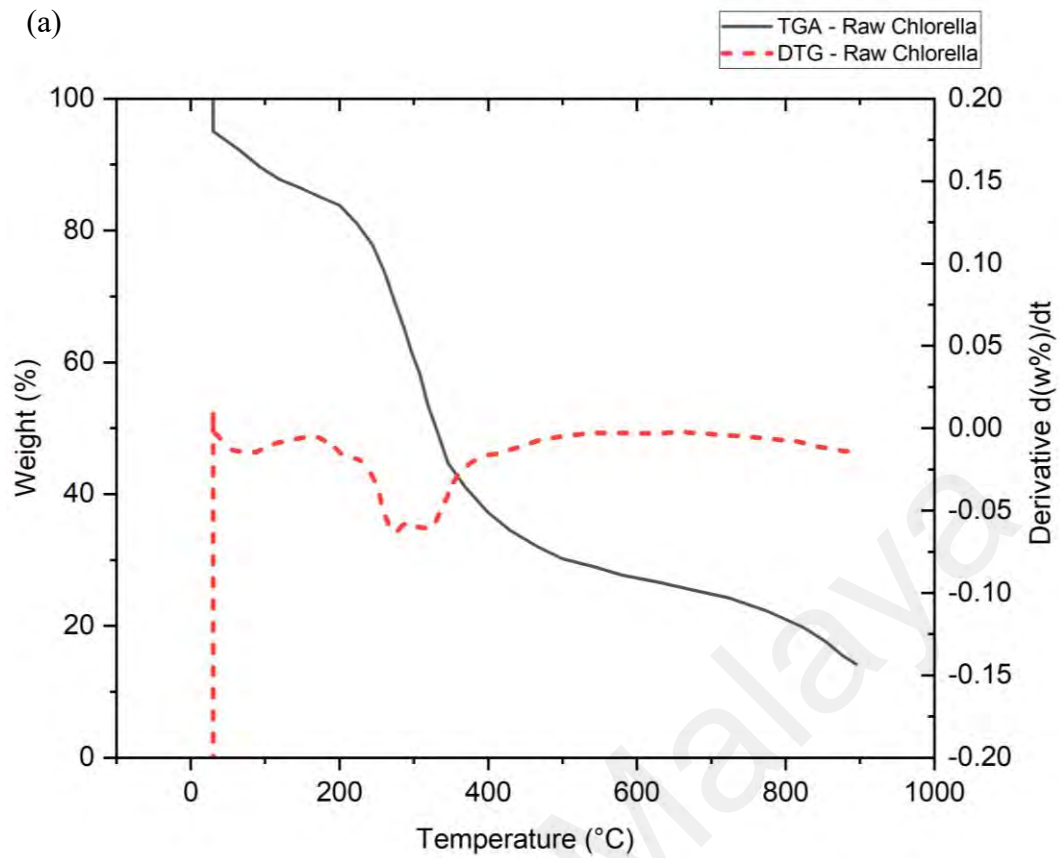
5-10 wt.%. This low yield is a significant factor impacting the sustainable production of adsorbents (Koçer et al., 2020; Masoumi & Dalai, 2020). Therefore, it is crucial to evaluate the optimal ratio of microalgae as a nitrogen-functional group onto the bio-adsorbent (with activated hydrochar precursor coconut shell as the substrate) to maximize both the CO<sub>2</sub> adsorption capacity and the bio-adsorbent yield.

The capability and stability of a specific material as an adsorbent is determined by detailed investigations of its physiochemical properties. In CO<sub>2</sub> adsorption, the thermal degradation of the materials plays an important role in synthesising optimum adsorbent as the adsorption process occur at higher temperature. Similar to this, it is crucial to conduct surface functional groups investigations of adsorbent in order to assess their potential in carbon capture. In addition, understanding the properties of materials resulted from different modification is crucial in determining suitable functionalisation method. As a result, raw microalgae, hydrochar and activated hydrochar derived from microalgae, under ideal conditions, have been characterised.

*(a) Thermal stability*

TGA studies are significant since the material stability and reactivity can be identified. The difference between microalgae, hydrochar and ACMA were observed as it decomposes over time. The thermal stability microalgae and derived adsorbents were investigated under N<sub>2</sub> atmosphere, and the findings are illustrated in Figure 4.18.(a) - (d).





**Figure 4.18: TGA Analysis (a) raw microalgae, (b) hydrochar-microalgae, (c) pyrochar-microalgae, and (d) activated hydrochar derived from microalgae**

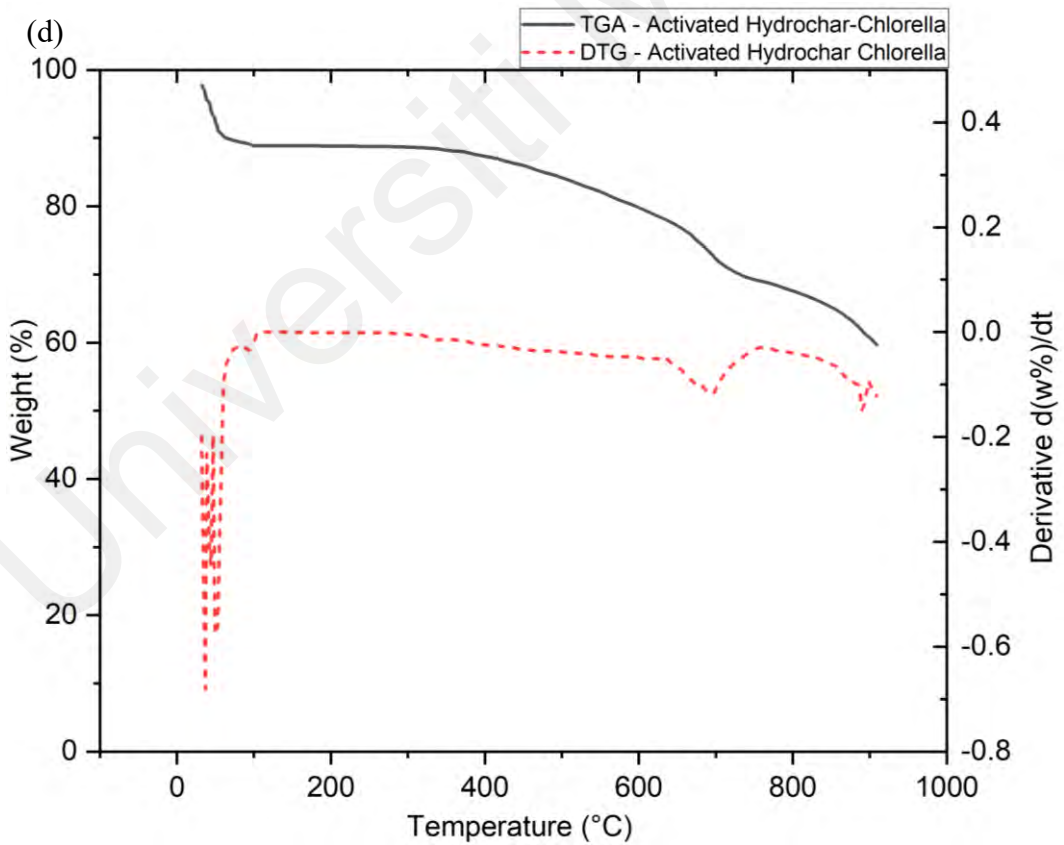
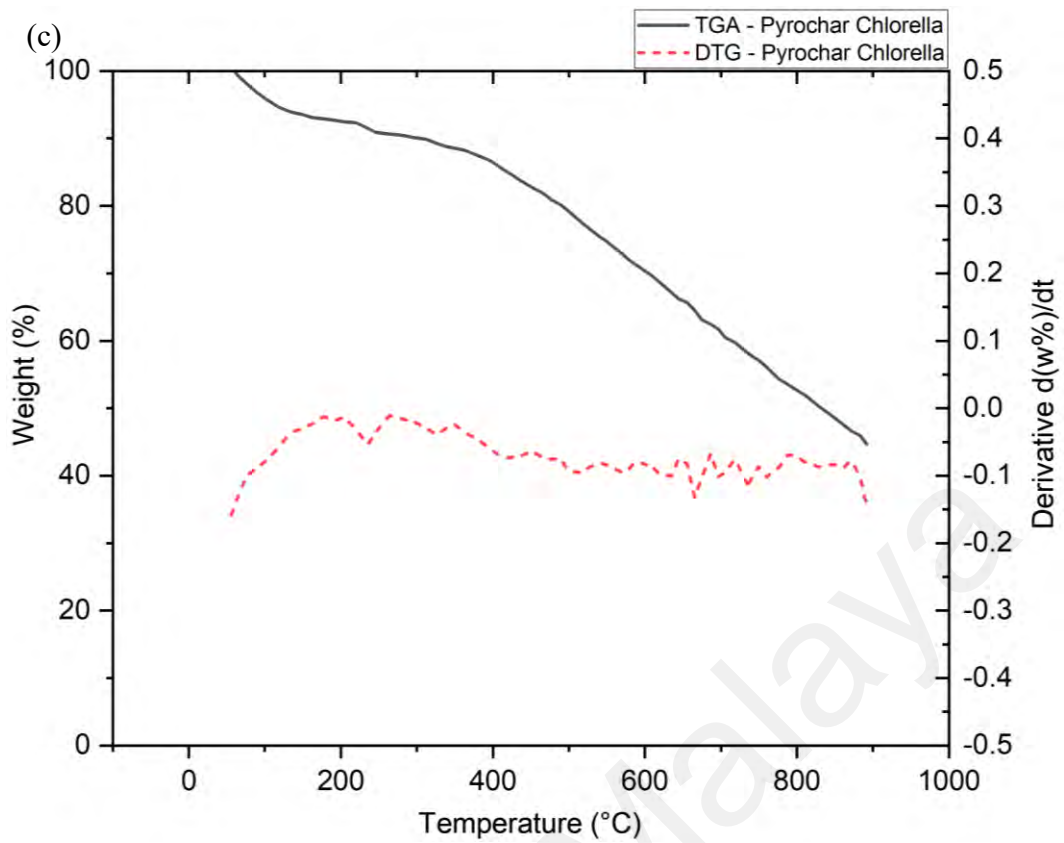


Figure 4.18, continued

From the graph, the HTC and pyrolysis of microalgae into hydrochar and pyrochar increase the material stability. Raw microalgae (RC) shows it can decompose at low temperature (450 °C) where only 21.32 wt.% left and further thermal treatment to 900 °C resulted in weight reduction of 85.81%. Individual thermal treatment through HTC and pyrolysis improves the stability of materials at high temperature in which the hydrochar and pyrochar weight at 25.02% and 44.70% left even at high temperature as high as 900 °C. Raw microalgae demonstrate the lowest stability with a near 90% total mass loss. The TGA profile of the raw material reveals multiple decomposition phases. Initial weight loss below 200 °C is associated with moisture and surface-adsorbed water release.

Between 200-400 °C, steep weight losses were recorded in raw, hydrochar, pyrochar at decreasing intensity. This observed weight loss can be attributed to the carbonisation process, where hemicellulose, cellulose, and low molecular weight compounds are converted into condensable products (like methanol, wood tar, and acetic acid) and non-condensable gases (such as CH<sub>4</sub>, H<sub>2</sub>O, CO, CO<sub>2</sub>, and H<sub>2</sub>) as described by Shoaib and Al-Swaidan (2015). In this stage, hydrochar recorded higher weight lost at 23.97%, compared to pyrochar at 5.70%. Hydrochar, produced via HTC, exhibits a higher weight loss (23.97%) in this stage compared to pyrochar (5.70%). HTC, involving biomass treatment with high-temperature and high-pressure water, yields a product that retains more of the original biomass structure, including elevated levels of hemicellulose, cellulose, and low molecular weight compounds. In contrast, pyrochar is produced through pyrolysis at higher temperatures (typically above 400 °C) in the absence of oxygen, resulting in a more thermally stable material with most volatile components already decomposed or volatilized. Consequently, hydrochar contains higher amounts of volatile matter, including hemicellulose and cellulose, which decompose significantly in the 200-400 °C range, leading to higher weight loss as they break down into condensable

and non-condensable gases (Al-Wabel et al., 2019; L. Chen et al., 2020; Liu et al., 2010; Sun et al., 2014).

The lignin degradation is then indicated by the third stage, which occurs at a reaction temperature of 350–913°C and a total weight loss of 30–35 wt.% for raw microalgae. The DTG curve has a comparable performance, with the greatest peaks appearing at temperatures corresponding to the breakdown of cellulose and hemicellulose, respectively, at 280°C and 320°C, respectively. The results are consistent with the literature, which states that lignin degrades at 150-900 °C, cellulose degrades at 300-400 °C, and hemicellulose degrades at 220-315 °C (Waters et al., 2017). Hemicellulose is simpler to break down than lignin, according to the temperature range at which the materials degrade. Lastly, a very little weight loss has been noticed at reaction temperatures higher than 900 °C. Specifically, for activated hydrochar precursor microalgae, the moisture content was removed at temperature 35-105°C. Then, ACMA start to decompose slowly starting at temperature of 200°C. Subsequently, the following stage at 200-620°C exhibits a mild weight loss of around 9%. Next, a rapid weight loss of 20% of body weight can be seen at temperatures between 620 and 914°C. The DTG curve has a comparable performance, with the greatest peaks appearing at 40°C and 690°C. Last but not least, a little weight loss has been noticed at reaction temperatures exceeding 900°C.

Also, it is possible to compare the thermal stability of raw microalgae and activated hydrochar derived from microalgae, based on the temperature at which weight loss started. According to Figure 4.18, the onset temperature of raw microalgae is 210°C, whereas the onset temperature of ACMA is 350°C. Therefore, ACMA more thermally stable than its precursors due to successful devolatilization of these volatile chemicals during the KOH activation process is the cause of a considerable change in the onset

temperature between raw microalgae and chemically synthesised microalgae activated hydrochar (Prakash et al., 2021).

*(b) FTIR analysis*

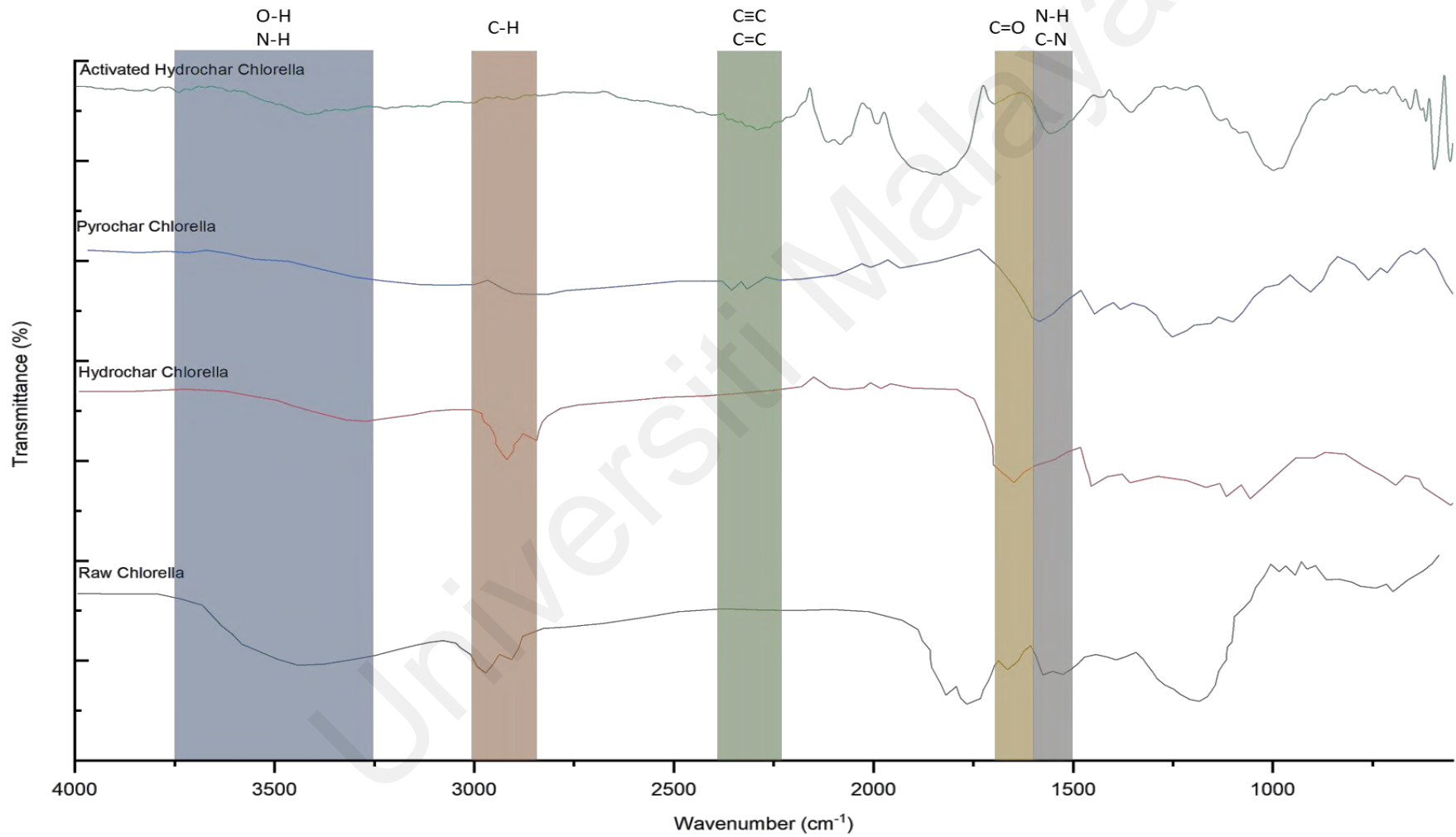
Aside from thermal stability, the alteration on functional groups of microalgae-based adsorbent plays significant role in CO<sub>2</sub> adsorption. Figure 4.19 illustrate the surface functional groups present in the raw microalgae, hydrochar and activated hydrochar precursor from microalgae. One of the primary features observed on the raw algae spectrum is a broad peak in the 3200-3600 cm<sup>-1</sup> region, indicative of hydroxyl (O-H) groups from carbohydrates and phenolic compounds, as well as amine (N-H) groups from proteins. This broad peak reflects the presence of extensive hydrogen bonding in the biomass. Similar peaks were also observed on hydrochar, pyrochar and activated hydrochar derived from microalgae with the peak intensity of RC > HC > ACMA > PC.

The less intense O-H stretching peak in pyrochar, compared to hydrochar, suggests a reduced presence of hydroxyl groups due to greater dehydration. Hydrochar, on the other hand, exhibits an abundance of hydroxyl groups resulting from the partial breakdown of cellulose and hemicellulose. This trend aligns with the findings reported by Gai et al. (2016) in their characterise of hydrochar and pyrochar derived from sewage sludge. Albeit high temperature of activation, ACMA exhibits a higher peak around 3200-3600 cm<sup>-1</sup> compared to PC, indicating the presence of more hydroxyl groups (O-H) and other oxygen-containing functional groups. This difference arises from the chemical activation process with KOH, which involves impregnating the hydrochar with potassium hydroxide followed by high-temperature treatment. KOH acts as a strong base and oxidizing agent, promoting the formation of oxygen-containing functional groups on the hydrochar surface. During activation, KOH facilitates the introduction of hydroxyl groups, resulting in a higher concentration of these groups compared to pyrochar, which

is produced through pyrolysis without chemical additives. This finding can be supported by W. Chen et al. (2020), whom highlighted that KOH activation promotes hydrolysis and oxidation reactions with carbon matrix, which introduce hydroxyl groups and other oxygen functionalities.

The peaks observed in the 2800-3000  $\text{cm}^{-1}$  region, signifying the presence of aliphatic hydrocarbons, are attributed to C-H stretching vibrations. Notably, a peak corresponding to aliphatic hydrocarbons, constituents of the lipid content in microalgae, was detected in the RC spectrum. These peaks serve as indicators of C-H stretching vibrations, a characteristic feature of lipid molecules. Similar pattern was also recorded on HC spectrum with higher intensity, indicating HTC promotes hydrolysis of the polymer. The peak in this region for ACMA is also less intense compared to RC and HC, suggesting that the activation process can partially degrade or remove aliphatic chains, resulting in a more aromatic structure. As for pyrochar, reduction of C-H stretching around 2850-2960  $\text{cm}^{-1}$  recorded in the region, indicating reduction/destruction of aliphatic hydrocarbons in the final pyrochar product due to thermal decomposition, dehydration, dehydrogenation, formation of aromatic compounds, and the evaporation of volatile matter. The high pyrolysis temperature resulted in degradation of complex organic molecules present in biomass, including aliphatic hydrocarbons, into simpler and more stable compounds (Leite et al., 2018).

Instead, peak was observed on PC spectrum at 2200-2300  $\text{cm}^{-1}$ , indicating the presence of carbon-carbon triple bonds ( $\text{C}\equiv\text{C}$ ) and double ( $\text{C}=\text{C}$ ), which associated with aromatic compounds or unsaturated hydrocarbons. Pyrolysis, the process of heating biomass without oxygen, triggers the breakdown and transformation of organic molecules.



**Figure 4.19: Fourier Transform Infrared Spectroscopy of microalgae and corresponding treatment**

This process favours the formation of aromatic structures and conjugated double bonds. Occurring at high temperatures, these reactions facilitate the conversion of aliphatic structures into aromatic compounds, which is reflected in the absorption peak observed in the 2200-2300  $\text{cm}^{-1}$  region. In contrast, hydrothermal carbonisation used to produce hydrochar involves lower temperatures and pressures, which favour the preservation of aliphatic structures and a lower degree of aromatization. Additionally, chemical activation of hydrochar does not typically lead to the formation of aromatic compounds to the extent seen in pyrolysis, as activation processes focus more on enhancing porosity and surface area (Leng et al., 2021).

Additionally, significant peaks of raw microalgae in the 1600-1700  $\text{cm}^{-1}$  and 1500-1600  $\text{cm}^{-1}$  regions are associated with the Amide I and Amide II bands, respectively. The Amide I band, centred around 1650  $\text{cm}^{-1}$ , is primarily attributed to C=O stretching vibrations within peptide bonds. Meanwhile, the Amide II band, located around 1540  $\text{cm}^{-1}$ , arises from a combination of N-H bending and C-N stretching vibrations, both of which are characteristic of proteins. In addition, the peaks in this region can also show the presence of aromatic compounds and alkenes, reflecting the complex mixture of organic compounds within the microalgae. Further valorisation of biomass resulted in negligible increment, indicating thermal treatment resulted in formation of various carbonyl-containing compounds, such as ketones, aldehydes, and carboxylic acids, as well as aromatic structures with carbonyl groups (Kumar et al., 2024). This suggests that thermal treatment, such as activation, altered the chemical composition of the biomass, increasing the abundance of carbonyl functional groups. This change could enhance the potential of biomass for various applications such as CO<sub>2</sub> adsorption. Notably, the presence of nitro-groups is crucial, as the study focuses on microalgae functionalisation, which can further enhance the CO<sub>2</sub> adsorption capacity.



The presence of aromatic compounds was confirmed by the observation of peaks in the 1400-1600  $\text{cm}^{-1}$  region, attributed to C=C stretching vibrations. Notably, ACMA displayed the most prominent peak in this region, suggesting that the activation process enhances aromaticity through the removal of volatile components and carbon structure condensation. This increased aromaticity enhances the stability and adsorption capacity of the activated hydrochar. Furthermore, all spectra displayed a peak within the 1402-1558  $\text{cm}^{-1}$  range, indicative of the formation of a C=C bond at approximately 1500  $\text{cm}^{-1}$ . This C=C group suggests an increment of carbon concentration in developed materials. Additionally, a spectral deflection observed around 1500-1830  $\text{cm}^{-1}$  indicative to the presence of a C=O group. C=O groups, commonly found in activated carbon, indicate successful conversion of biomass waste precursors into active carbon material (Mopoung et al., 2015). Compared to other spectrum, a peak was recorded in the 1100-1250  $\text{cm}^{-1}$  of RC spectrum, indicating the presence of phosphates, which are components of nucleic acids and phospholipids, essential for the structural and functional integrity of cells.

In summary, valorisation of raw microalgae removes the volatile matter such as phosphate, and enhance the formation of functional groups such as C≡C, C=O, C=C, and O-H, while maintaining the nitro group such as N-H and N=O. Hydrochar retains more oxygen-containing functional groups and aliphatic hydrocarbons, whereas pyrochar exhibits a higher degree of aromaticity and less oxygen functionality. While pyrochar exhibits significant peaks in the 2000-2500  $\text{cm}^{-1}$  region indicating the presence of aromatic structures, activated hydrochar also shows peaks in this region, albeit weaker. Compared to raw microalgae and hydrochar, activated hydrochar shows enhanced chemical properties that make it a more effective adsorbent. The activation process, enhances the presence of unsaturated bonds and aromatic structures on the hydrochar surface. These features provide more adsorption sites for various pollutants or

contaminants, making activated hydrochar a promising adsorbent for environmental remediation applications.

#### **4.2.4 Selection of adsorbents based on the bio-adsorbent yield and CO<sub>2</sub> adsorption capacity**

Considering the bio-adsorbent yield, carbon dioxide adsorption capacity, and characteristics of the different coconut shell bio-adsorbents (pristine, magnesium oxide-functionalised, and microalgae-functionalised), the optimal synthesis parameters were determined to be; hydrothermal carbonisation followed by KOH activation, with a carbonisation temperature of 220°C, a duration of 3 hours, and a solid weight percentage of 20%. Impregnation of MgO at 15% through HTC resulted in the highest CO<sub>2</sub> adsorption. However, the study found that the optimum method of MgO-functionalisation is through direct mixing, which reduces energy usage through additional thermal treatment. Co-carbonisation of microalgae resulted in the highest CO<sub>2</sub> adsorption with the highest formation of BET surface area.

Based on these findings, a dual-functionalised bio-adsorbent was synthesised by using the optimal conditions determined for single functionalisation; 15% MgO impregnation by direct mixing and nitrogen enrichment by co-carbonation with microalgae. This dual-functionalisation strategy was developed to take advantage of the beneficial properties of both MgO and microalgae functionality, thereby improving the overall performance of the adsorbent. MgO provides basic sites that are highly favourable for CO<sub>2</sub> adsorption, while the incorporation of nitrogen from microalgae increases surface polarity and creates additional active sites. The combined effect of these functionalities is expected to significantly enhance the CO<sub>2</sub> adsorption capacity by optimising the surface area, porosity and chemical reactivity of the bio-adsorbent.

### 4.3 Physicochemical characteristic of adsorbent

The physicochemical properties of adsorbents are critical determinants of their adsorption performance, influencing pore accessibility, surface reactivity, and interaction dynamics with target pollutants. Accordingly, coconut shell bio-adsorbent (HCS), MgO-functionalised coconut shell bio-adsorbent (HCS-Mg), microalgae-functionalised bio-adsorbent through co-carbonisation of *Chlorella* and coconut shell (HCS-N) and dual-functionalised bio-adsorbent with MgO and microalgae (HCS-N-Mg) at the optimum conditions have been characterised. Table 4.8 provides a systematic summary of the adsorbents, their synthesis procedures, and functionalization methods. This nomenclature ensures clarity in subsequent discussions of adsorption performance and characterization data.

**Table 4.8: Nomenclature for each optimised sample**

Sample	Process	Nomenclature
Coconut shell bio-adsorbent	Hydrothermal carbonisation at 220 °C for 3 hrs, followed by KOH activation at 700 °C, 2 hrs, KOH: sample ratio of 3	HCS
MgO-functionalised coconut shell bio-adsorbent	Similar preparation as HCS. Functionalised with MgO through direct blending of 15% MgO and dry in oven at 105 °C for 16 hrs	HCS-Mg
Microalgae-functionalised coconut shell bio-adsorbent	Hydrothermal carbonisation of coconut shell and microalgae at ratio of 7:3, at 220 °C for 3 hrs, followed by KOH activation at 700 °C, 2 hrs, KOH: sample ratio of 3	HCS-N
Dual-functionalised coconut shell bio-adsorbent with microalgae and MgO	Hydrothermal carbonisation of coconut shell and microalgae at ratio of 7:3, at 220 °C for 3 hrs, followed by KOH activation at 700 °C, 2 hrs, KOH: sample ratio of 3. Functionalised with MgO through direct blending of 15% MgO and dry in oven at 105 °C for 16 hrs	HCS-N-Mg
Norit® activated carbon	Steam activation of peat-based activated carbon	AC1

### 4.3.1 Surface area and porosity

Surface morphology was examined to analyse specific BET surface area and pore size, essential parameters for assessing the effectiveness of the synthesis process, and the effect of adsorbent functionalisation. HCS exhibits an exceptional specific surface area of 976 m<sup>2</sup>/g, as highlighted in Table 4.9. This exceptionally high surface area gives the adsorbent an enhanced ability to adsorb significant amounts of pollutants efficiently. In contrast to the raw activated carbon (AC) from coconut shells with a BET surface area of 3 m<sup>2</sup>/g, as reported by Yağmur and Kaya (2021), the raw coconut shell utilised in this study exhibited a slightly lower BET surface area of 2.824 m<sup>2</sup>/g. However, employing a chemical activating agent significantly improved micropore development and surface area (Yağmur & Kaya, 2021).

**Table 4.9: Surface area and pore properties of bio-adsorbents**

Sample	S <sub>BET</sub> (m <sup>2</sup> /g)	S <sub>micro</sub> (m <sup>2</sup> /g)	V <sub>micro</sub> cm <sup>3</sup> /g	D <sub>p</sub> (nm)	Pore Type
HCS	976.30	789.38	0.3144	1.72	Micropores
HCS-Mg	721.05	581.88	0.2319	2.15	Mesopores
HCS-N	2038.80	1648.76	0.5190	2.72	Mesopores
HCS-N-Mg	1045.21	843.48	0.2595	2.01	Mesopores

In comparison to other bio-adsorbent such as activated hydrochar derived from rambutan peel has a specific surface area of 499 m<sup>2</sup>/g (Zubbri et al., 2021), *Crocus sativus* petals-based AH recorded 862 m<sup>2</sup>/g (Rasam et al., 2021), and activated carbon precursor rice husk displayed 891 m<sup>2</sup>/g (He et al., 2021), HCS has a higher surface area. This trend is attributed to the material selection, specifically using coconut shell, which possesses high carbon content with uniform carbon particle shapes in both amorphous and crystalline structures. The balance between these two structures significantly contributes to the porosity, mechanical strength, and thermal stability of the coconut shell (Ahmad et al.,

2021), resulting in the formation of higher surface area on the developed adsorbent. A higher specific surface area of the adsorbent correlates to a higher affinity for pollutant adsorption due to many active sites on the adsorbent's defined surface (Sharma et al., 2021). The nature and surface area of the adsorbent material have a significant impact on the adsorption rate. Due to increased adsorbing sites, materials with a greater surface area augment the extent of adsorption. Additionally, porous materials contribute to a larger surface area, enhancing removal efficiency and adsorption capacity.

Functionalisation of bio-adsorbent with magnesium shows a lower BET surface area of 721.05 m<sup>2</sup>/g, a micropore surface area of 581.88 m<sup>2</sup>/g, and a micropore volume of 0.2319 cm<sup>3</sup>/g. Previous studies by Tolkou et al. (2023), Abriyani et al. (2022) and Yang et al. (2020) also reported similar findings in which functionalisation of MgO onto activated carbon from different resources, through different functionalisation method resulted in reduction of surface area by 63-94%. The reduction in surface area and micropore volume suggests that magnesium impregnation partially block some of the smaller pores or alter the structure, reducing the overall surface area available for adsorption. However, the percentages of the micropore surface area for HCS-Mg was almost identical to HCS, HCS-N and HCS-N-Mg, ranging at 80-81%. This consistency can be attributed to the selective blocking and creation of pores during magnesium impregnation. Furthermore, the proportion of micropores in the parent MgO was considerably high at 67.22%, despite its BET surface area and average pore width being only 188.26 m<sup>2</sup>/g and 8.7 nm respectively.

HCS-N exhibits the highest BET surface area at 2038.80 m<sup>2</sup>/g, with a micropore surface area of 1648.76 m<sup>2</sup>/g and a micropore volume of 0.5190 cm<sup>3</sup>/g. The substantial increase in surface area and pore volume due to microalgae functionalisation suggests the introduction of additional porosity and active sites, significantly would enhance the adsorption capacity of the bio-adsorbent. The higher surface area and larger pores make

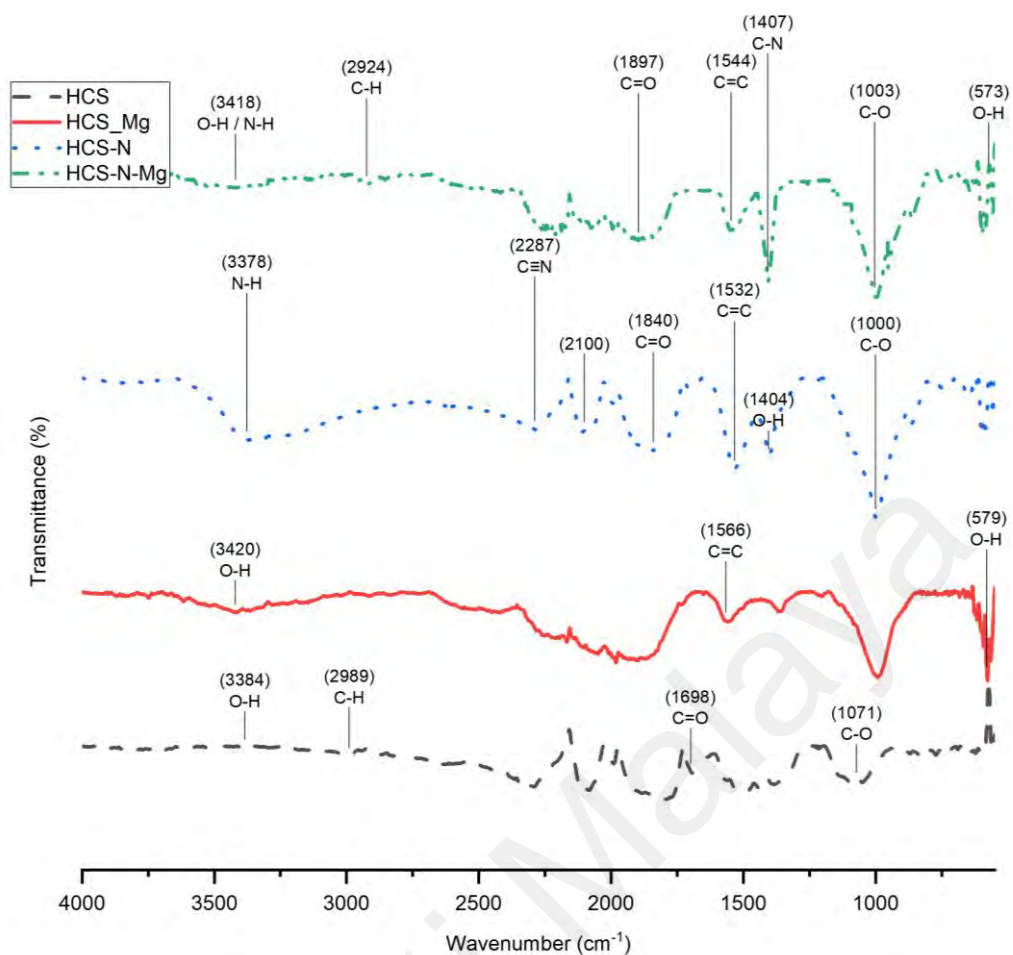
HCS-N suitable for adsorbing both small and large molecules effectively. HCS-N-Mg has a BET surface area of 1045.21 m<sup>2</sup>/g, a micropore surface area of 843.48 m<sup>2</sup>/g, and a micropore volume of 0.2595 cm<sup>3</sup>/g. This dual-functionalisation process resulted in a moderate increment of surface area and pore volume compared to individual MgO functionalisation despite not achieving the same level of enhancement as microalgae-functionalisation alone.

Aside from surface area, pore diameter also plays important role in determining efficient adsorption of pollutant. The critical pore diameter for efficient CO<sub>2</sub> adsorption is micropores, as this size range allows optimal interaction between CO<sub>2</sub> molecules and the pore walls, enhancing adsorption capacity (Gunawardene et al., 2022). The pore diameters of HCS, HCS-N, HCS-Mg, and HCS-N-Mg exhibit a clear trend influenced by the modifications applied to each bio-adsorbent. HCS has the smallest average pore diameter at 1.72 nm, indicating a predominantly microporous structure ideal for adsorbing small molecules - CO<sub>2</sub>. This also highlights the efficiency of the HTC process in synthesizing microporous bio-adsorbent. HCS-Mg and HCS-N exhibit mesoporosity shifts due to magnesium impregnation, while microalgae functionalisation introduces mesoporosity and additional micropores. HCS-N-Mg has an intermediate pore diameter of 2.01 nm, indicating dual functionalisation balanced the formation of both micro and mesopores. Despite the increment in pore diameter, mesoporous indirectly enhance the adsorption process by facilitating the diffusion of CO<sub>2</sub> molecules into the microporous regions, which improve overall adsorption kinetics. Therefore, while HCS, with its predominantly microporous structure, which would result in efficient CO<sub>2</sub> adsorption, the introduction of mesoporosity in HCS-Mg, HCS-N, and HCS-N-Mg as well as formation of additional functional groups, assist in balancing adsorption capacity and diffusion rates, potentially enhancing the efficiency of CO<sub>2</sub> capture in practical applications.

### 4.3.2 Surface chemistry

Figure 4.20 displays the FTIR profiles of HCS, HCS-Mg, HCS-N and HCS-N-Mg. Analysis of the spectra from the functionalised HCS sample revealed additional peaks attributed to interactions between porous support, nitrogen, and metal oxide functional groups. The FTIR results show that all the bio-adsorbents developed in this study contain hydroxyl, carboxyl, and carbonyl functional groups, indicating the success of the activation process in enhancing adsorption properties. Precisely, the hydroxyl and carboxyl groups form interaction with CO<sub>2</sub> through hydrogen bonding acid-base interactions, respectively (Song et al., 2020), enhancing the adsorption of CO<sub>2</sub> and showcasing the efficacy of chemical activation in tailoring the surface chemistry of activated hydrochar for carbon capture. Similarly, polar carbonyl groups, introduced through chemical activation, further contribute to the increased adsorption capacity by interacting with CO<sub>2</sub> through dipole-dipole forces (L. Wang et al., 2020).

The increasing intensity of carboxyl and carbonyl in the spectral band of functionalised bio-adsorbents compared to HCS, suggests the formation of aromatic compounds in the developed adsorbents. Moreover, the spectra reveal the emergence of a C=C bond within the range of 1530-1570 cm<sup>-1</sup>, indicating a higher carbon content. The spectral shift at 1500-1830 cm<sup>-1</sup> indicates the existence of C=O. The C=O group is a prevalent functional group identified in activated hydrochar, indicating the successful formation of an active carbon substance through the carbonisation and activation of adsorbent precursor from biomass wastes (Dabhane et al., 2021; Mopoung et al., 2015).



**Figure 4.20: Functional groups of pristine and functionalised HCS**

Additionally, a peak observed at  $3384\text{ cm}^{-1}$  for HCS is attributed to OH-stretching vibrations induced by the presence of surface hydroxyl groups. Similar peak is observed in HCS-Mg and HCS-N-Mg at  $3420$  and  $3418\text{ cm}^{-1}$  with increasing intensity. Because of the impregnation of MgO onto bio-adsorbents were conducted through dispersion of MgO in water, MgO is decorated into the samples in various state; MgO and  $\text{Mg}(\text{OH})_2$ , making the metal functionalised samples display a higher intensity of the hydroxyl group peak. In addition, the O-H peaks in MgO functionalised samples appear at higher wavenumbers compared to HCS due to the strong interaction between the magnesium cation and the hydroxide anion. Additional peak is also reflected on HCS-Mg and HCS-N-Mg at  $573$  and  $579\text{ cm}^{-1}$ . which is corresponding to success impregnation of MgO onto developed activated hydrochar. According to Kakade et al. (2021) the region under  $1000$



$\text{cm}^{-1}$  can be used to rapidly locate peaks in a MgO matrix. This can also be supported by recent study of Shkir et al. (2023), who emphasize that the transmittance band at  $861 \text{ cm}^{-1}$  and  $617 \text{ cm}^{-1}$  is associated to a series of transitions that involve Mg-O-Mg and Mg-O bond stretching metal oxygen bonding vibration respectively. The peak also is in line with previous study conducted by Tahir et al. (2023), where the existence of the Mg-O-Mg bond in the AC/MgO photocatalyst was identified by a broad peak ranging from  $501\text{-}777 \text{ cm}^{-1}$ .

Additional peak in HCS-N spectra compared to HCS indicate the presence of nitro functional group, presence of N-H stretching vibration near  $3200\text{-}3400 \text{ cm}^{-1}$ . The presence of basic nitrogen-containing groups, such as amines, can contribute to these features. In addition, the range also indicates the basicity in the bio-adsorbents due to the presence of C-H stretching vibrations. A fragile peak at  $800 \text{ cm}^{-1}$  were produced by N-H out-plane deformation vibration in HCS and HCS-N-Mg spectrum (Z. Wang et al., 2020). The presence of bands around  $1680\text{-}1890 \text{ cm}^{-1}$  indicative of carbonyl groups. The presence of C=O indicates the presence of oxygen-containing functional groups on the surface of bio-adsorbents. HCS-N and HCS-N-Mg peak at higher wavenumber indicating a carbonyl group in an amide ( $\text{CONH}_2$ ) can be more neutral or weakly basic. These groups can contribute to the adsorption of polar gases, including  $\text{CO}_2$ .

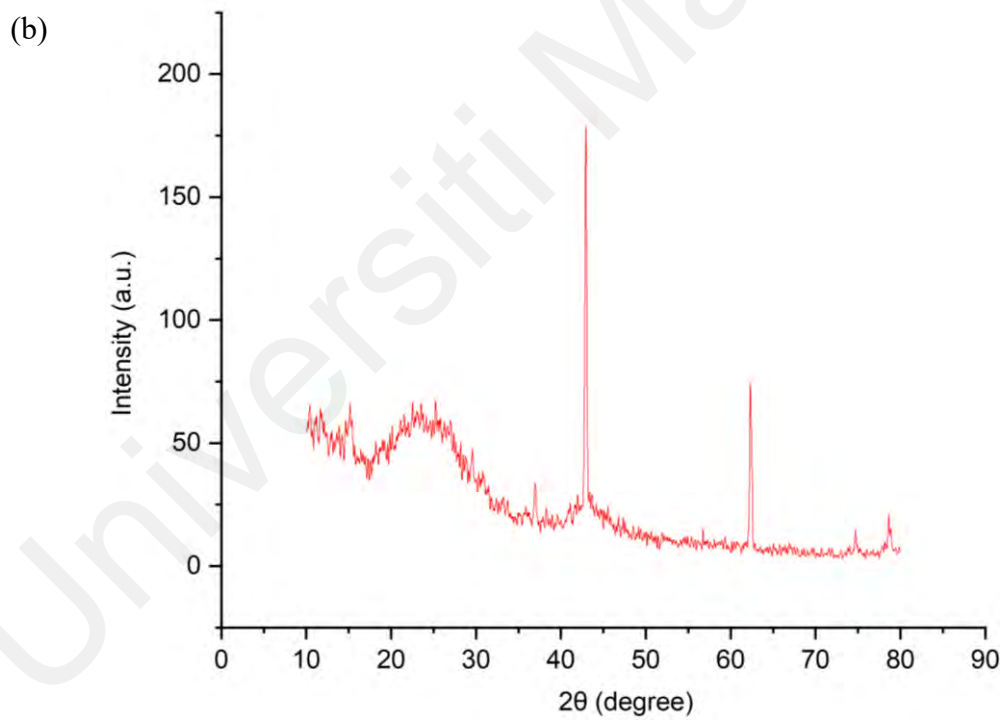
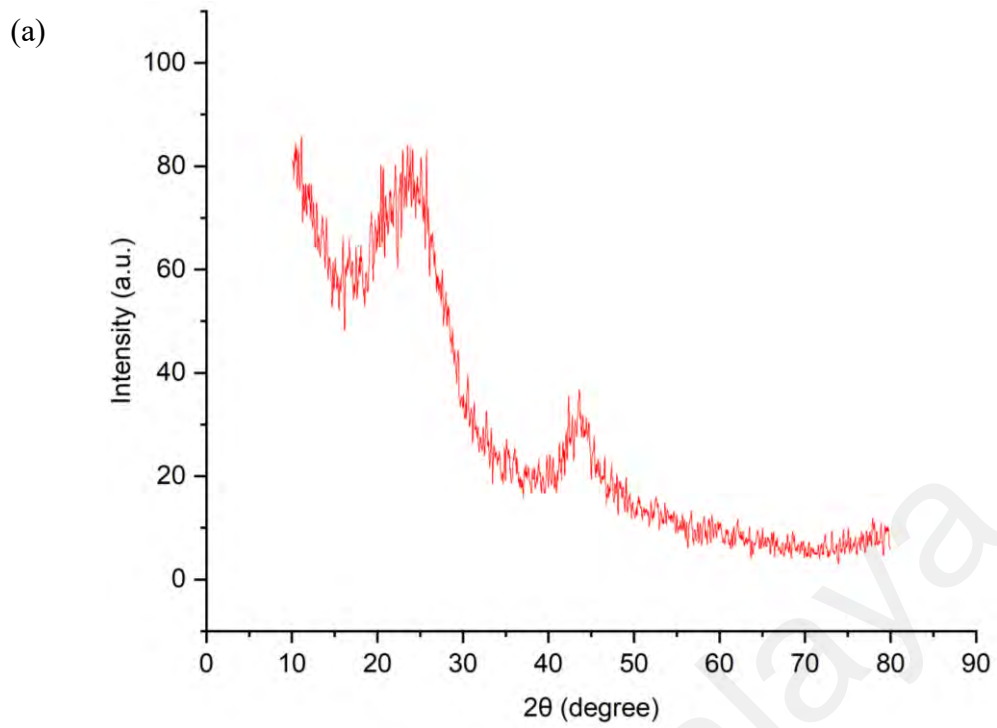
C=O, C-O, C=C, and O-H indicate the successful synthesis of bio-adsorbent from activation of hydrochar. Additional formation of functional groups such as -NH, -NH<sub>2</sub>, C≡N, Mg-O, and Mg-O-Mg suggests the success of single and dual-functionalisation on the developed adsorbent. The increased hydroxyl functional group also demonstrates the successful impregnation of metal oxide onto HCS. In contrast to HCS, HCS-N-Mg exhibits more prominent peaks, indicating a higher level of surface functionalisation in the adsorbent.

### 4.3.3 Crystallographic structure

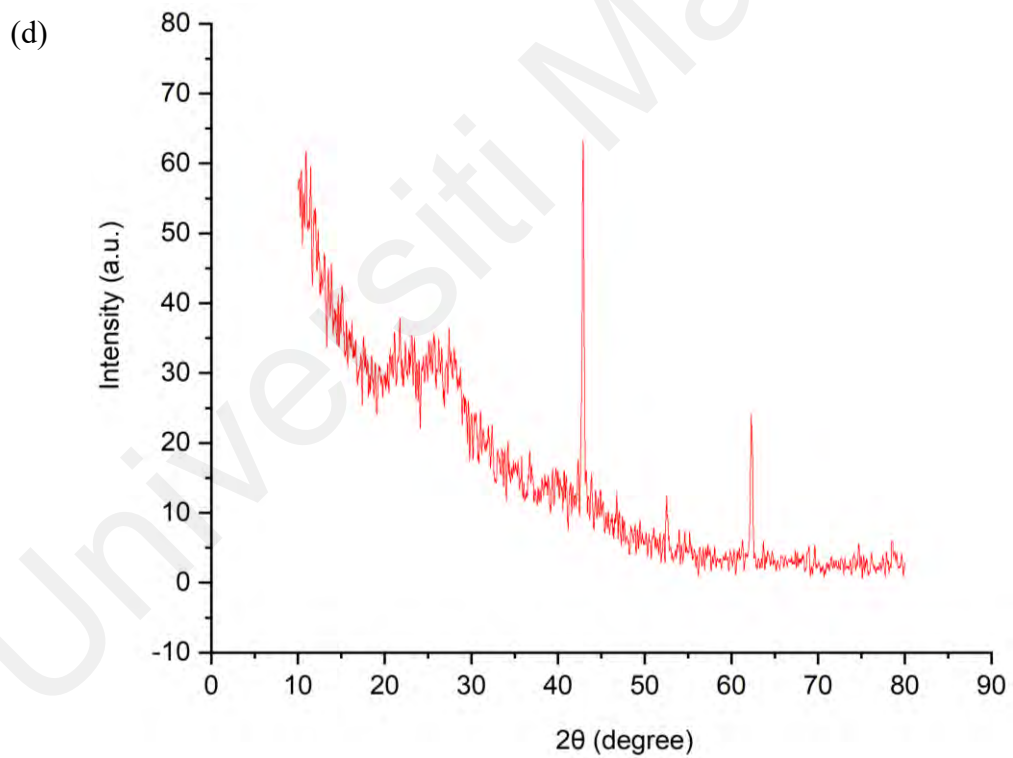
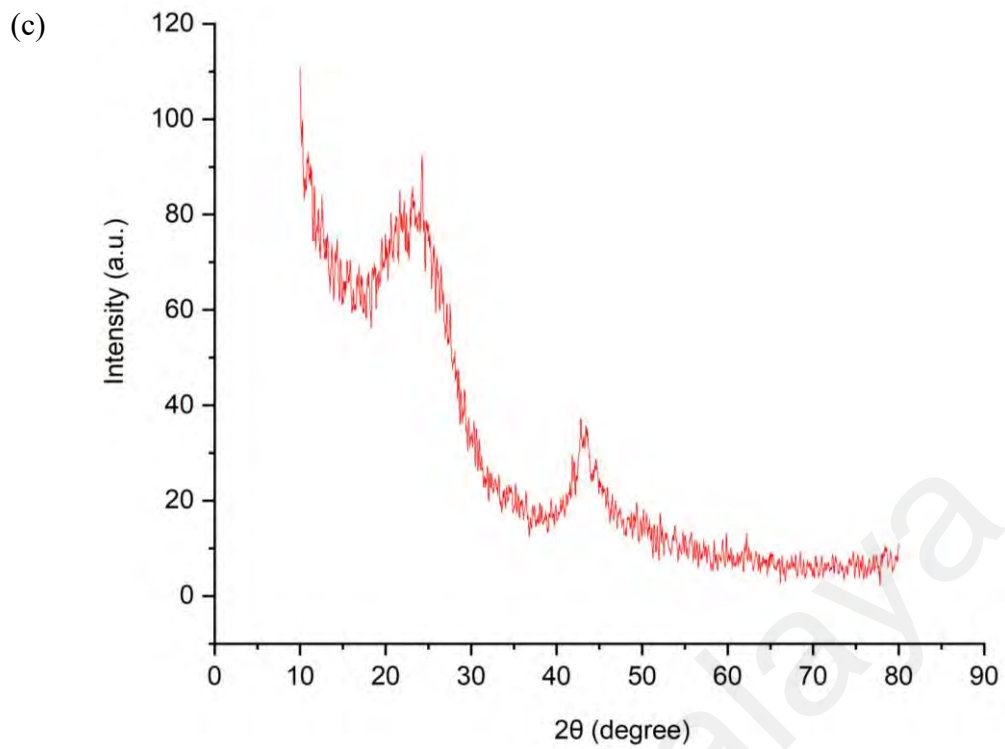
The XRD patterns of HCS, HCS-Mg, HCS-N, and HCS-N-Mg, shown in Figure 4.21, reveal structural changes in the bio-adsorbents following functionalisation. The diffractograms illustrate that HCS possesses four main diffraction peaks at  $2\theta$  angles of 23.9, 26.0, 43.6, and 77.9°. These characteristic peaks persist in the functionalised adsorbent, albeit with lower intensity, suggesting a predominantly amorphous structure.

The broad peak around 26° corresponds to the (002) plane, signifying an irregular arrangement of carbon atoms. Additionally, the peaks at 44° and 78°, attributed to the overlapping reflections from the (100), (101), and (110) planes, confirm the carbon-based nature of HCS, HCS-Mg, HCS-N, and HCS-N-Mg (Choi et al., 2005). The presence of the (100) and (110) planes further indicates a degree of crystallinity within these bio-adsorbents, consisting of small, ordered graphene sheet domains (Katta et al., 2023; Yang & Lua, 2006).

The XRD pattern for HCS-N shows a combination of broad peaks similar to HCS and additional features indicative of nitrogen incorporation. The peaks around 20-30° remain broad, suggesting that the microalgae functionalisation has not significantly altered the amorphous nature of the pristine bio-adsorbent. The increased peak intensity around 25° indicate improved graphitization or formation of nitrogen-containing functional groups within the carbon matrix (Katta et al., 2023). However, the presence of additional minor peaks or shoulder peaks indicates the introduction of nitrogen-containing functional groups, such as amines or nitriles. Higher scattering was recorded in the 10° to 20°  $2\theta$  range, in comparison to HCS, indicating larger structural features introduced by nitrogen functional groups. These functional groups enhance the basicity of bio-adsorbent and improve its adsorption capacity for acidic gases – CO<sub>2</sub>.



**Figure 4.21: Crystalline structure of (a) HCS, (b) HCS-Mg, (c) HCS-N, and (d) HCS-N-Mg**



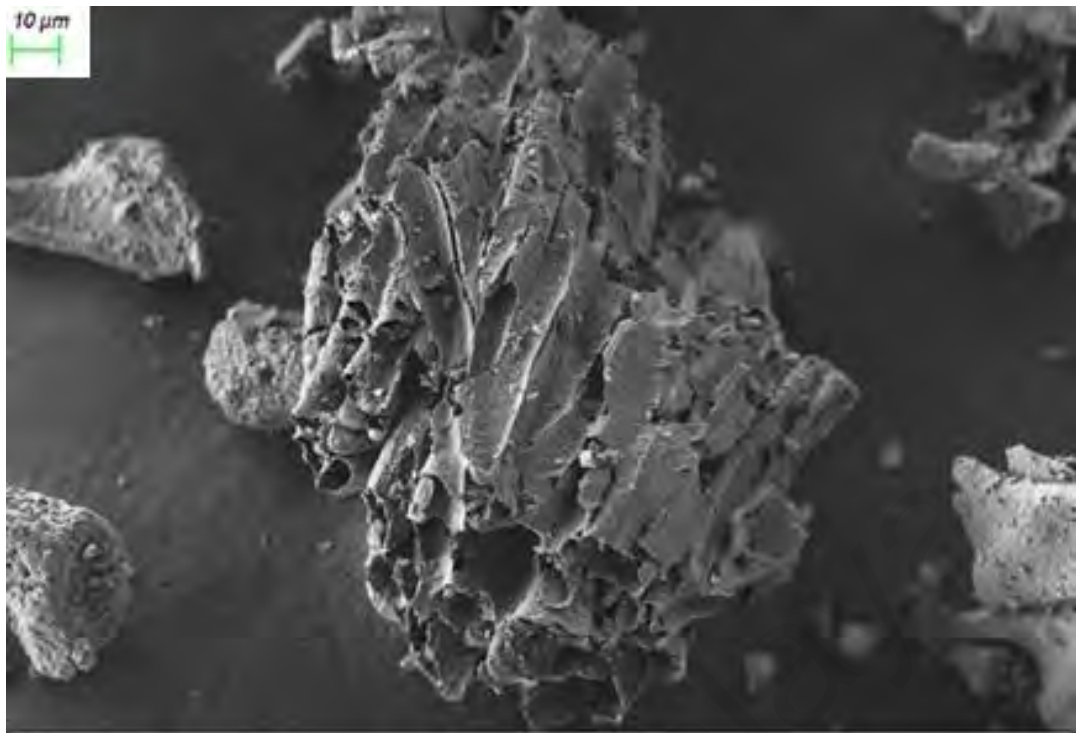
**Figure 4.21, continued**

For HCS-Mg and HCS-N-Mg, prominent sharp peaks at  $2\theta$  values of  $28.4^\circ$ ,  $36.8^\circ$ ,  $43.3^\circ$ ,  $63^\circ$ , and  $69.6^\circ$ , corresponding to the crystal planes (003), (312), (200), (222), and (023), were noted. This distinct peak sharpness is attributed to integrating magnesium oxide

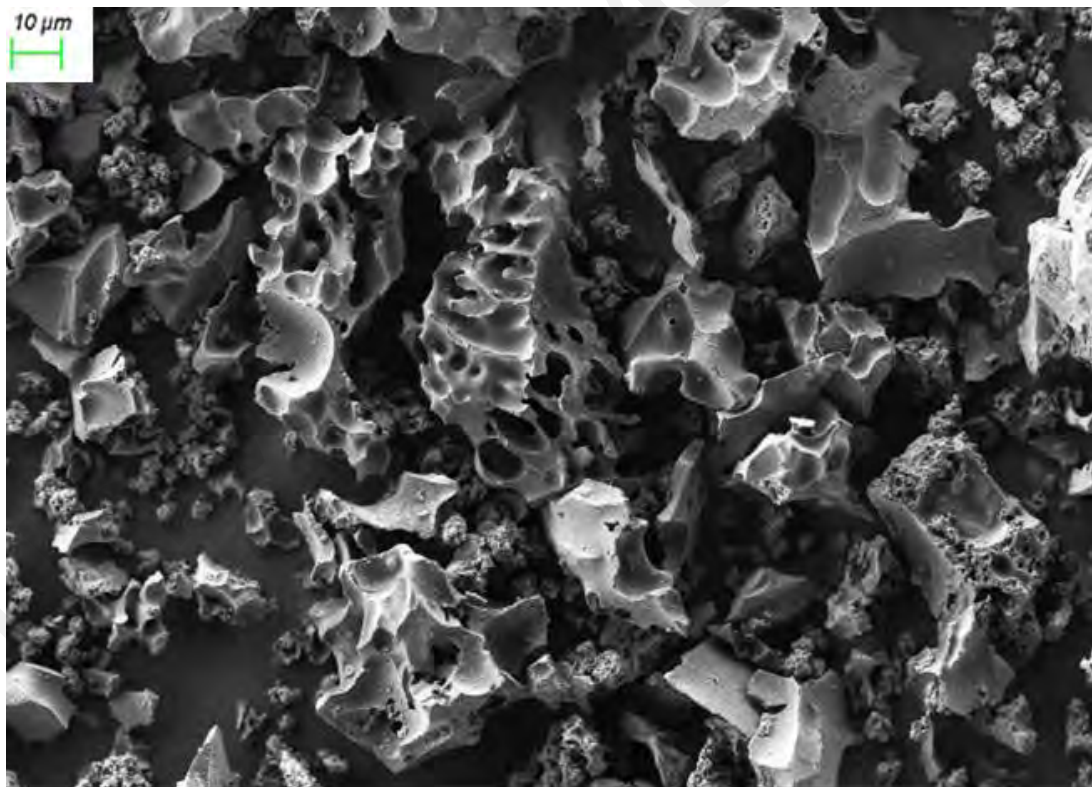
particles on the HCS surface. The inherent sharp-edged nature of these oxide particles contributes to the pronounced reflection of light, thereby resulting in these distinct peaks. This crystalline behavior aligns with the MgO standards per ICSD, as detailed in Vall et al. (2019). Furthermore, Gao et al. (2023) conclude that the interplanar spacing and diffraction patterns of material closely match the established standard diffraction patterns of MgO.

#### 4.3.4 Surface morphology

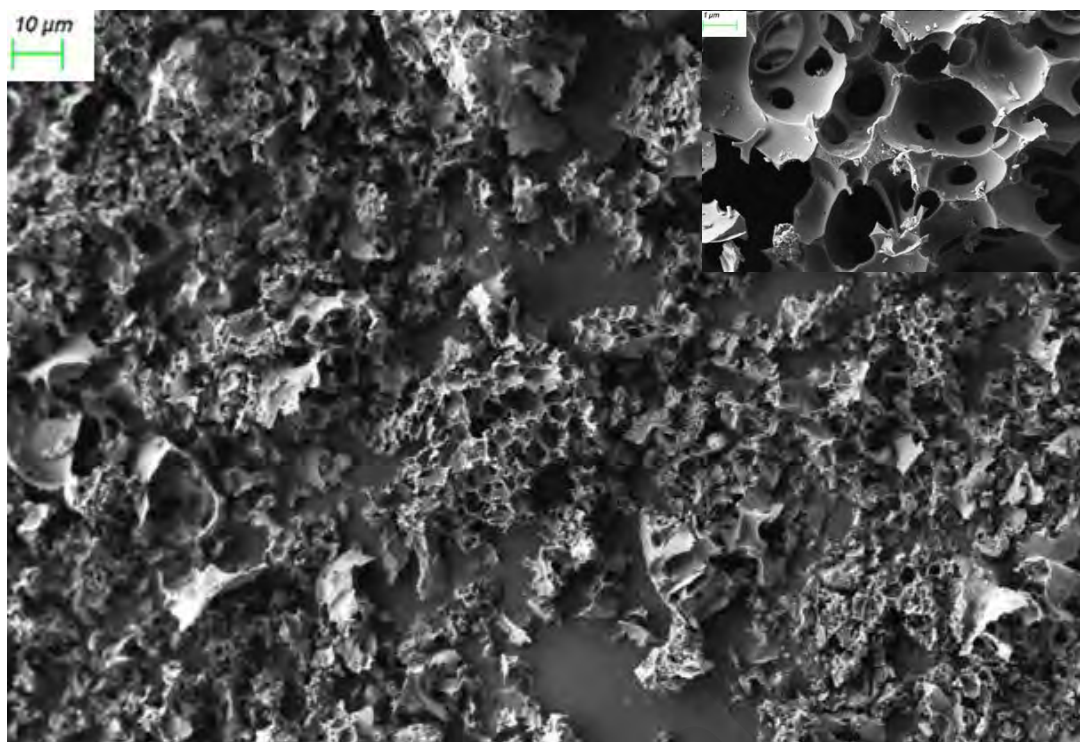
The FESEM analysis was conducted to evaluate the surface morphology of raw and modified coconut shell, and bio-adsorbent functionalised with microalgae through co-carbonisation with *Chlorella*, HCS functionalised with MgO and dual-functionalised bio-adsorbent. The analysis on surface morphology is significant in adsorbent development to analyse the change in exterior surface morphology before and after the thermal treatment and functionalisation. Figure 4.22-4.28 shows the surface morphology raw coconut shell, hydrochar, HCS, HCS-Mg, HCS-N and HCS-N-Mg. The images obtained revealed distinct differences in the surface structures of these materials. The surface of raw coconut shell sample does not appear to have any pores, as seen in Figure 4.22. The raw CS shows flat surfaces with some presence of rough surface. While hydrochar and HCS imaging show that thermal degradation and activation resulted in formation of pores on the surface of the materials.



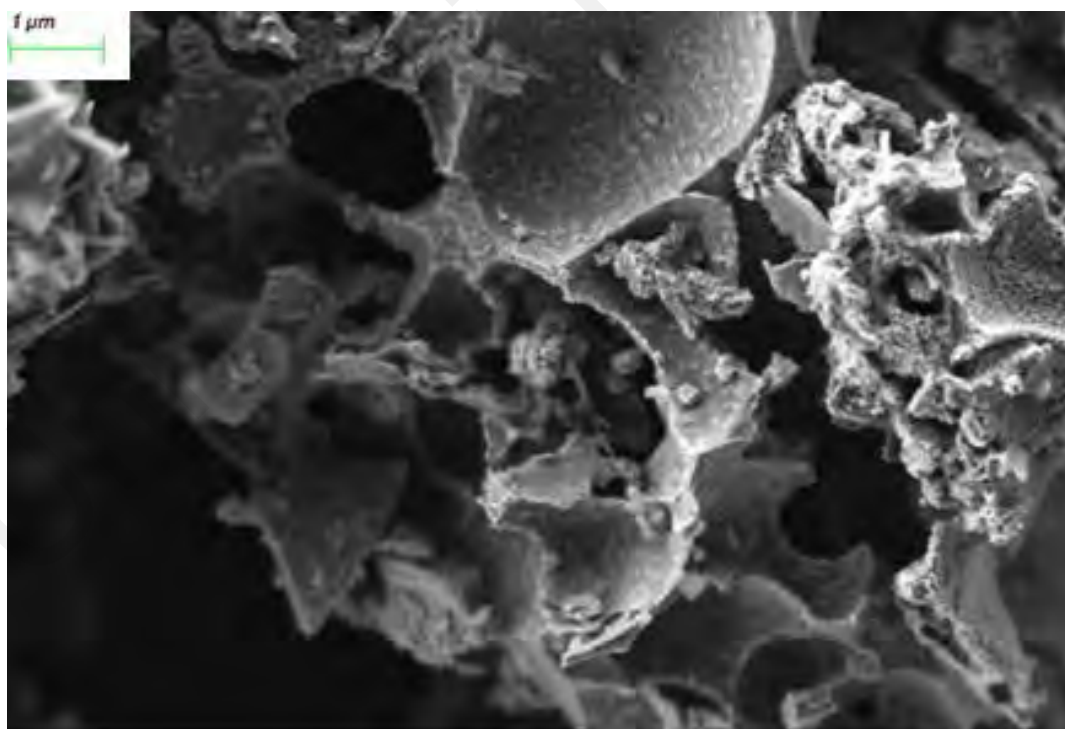
**Figure 4.22: Field Emission Scanning Electron Microscope image of raw coconut shell**



**Figure 4.23: Field Emission Scanning Electron Microscope image of coconut shell hydrochar**



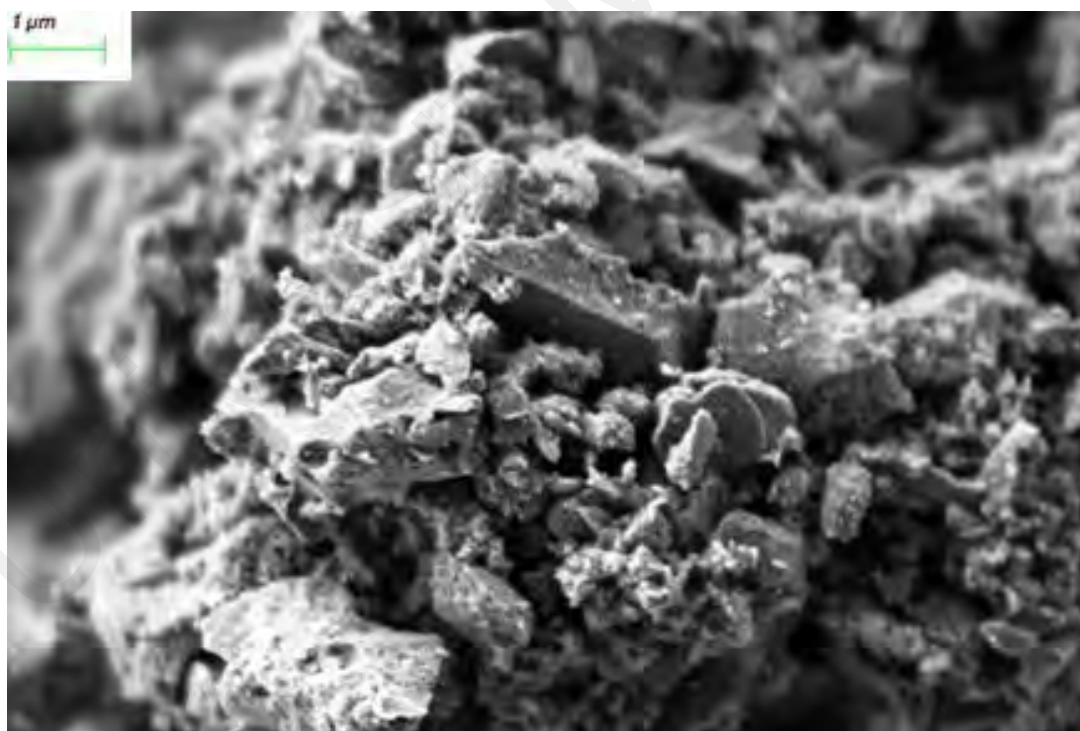
**Figure 4.24: Field Emission Scanning Electron Microscope image of pristine bio-adsorbent (HCS)**



**Figure 4.25: Field Emission Scanning Electron Microscope image of MgO functionalised bio-adsorbent (HCS-Mg)**

The pristine HCS exhibits a relatively smooth surface with well-defined porous structures, as shown in Figure 4.24. These pores are essential for adsorption applications,

as they provide the necessary surface area for interaction with adsorbates. However, the pristine HCS pores appear irregular and somewhat collapsed, indicating limited structural integrity. This morphology suggests that while the pristine HCS has inherent porosity, it may not be optimal for high-performance adsorption without further modification (Madzaki et al., 2018a). In contrast, the MgO-functionalised bio-adsorbent (HCS-Mg) displays a different surface morphology, as depicted in Figure 4.25. The FESEM images reveal significant white deposits on the surface of HCS-Mg, indicating the successful functionalisation with MgO. These MgO particles are well-dispersed across the carbon matrix, creating a heterogeneous surface, compared to raw MgO (Figure 4.26). However, it is also evident that some of the MgO particles block the pores of the HCS as some of the crystalline structure deposited in the HCS pores.

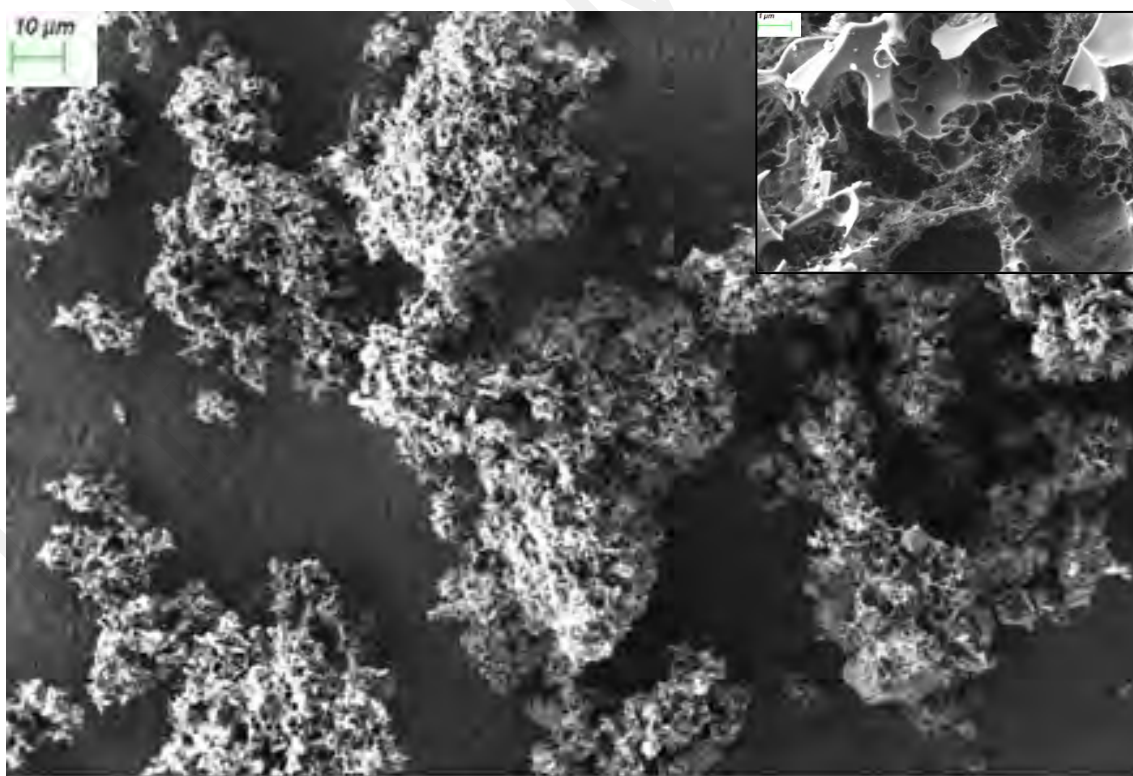


**Figure 4.26: Field Emission Scanning Electron Microscope image of raw magnesium oxide**

The microalgae-functionalised bio-adsorbent (HCS-N), shown in Figure 4.27, demonstrates a different morphological profile. The surface of HCS-N is characterised

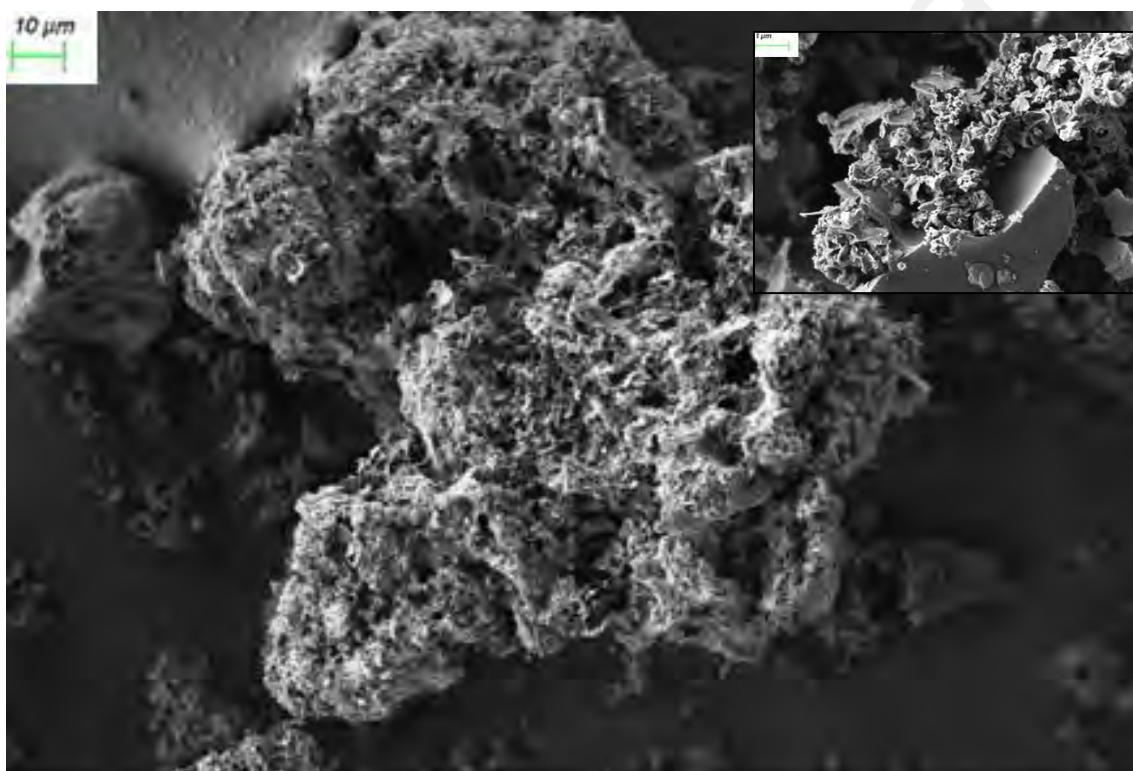


by uniformly distributed nitrogen-containing functional groups, appearing as small nodules on the carbon surface. These functional groups enhance the basicity of the material, improving its interaction with CO<sub>2</sub>. Additionally, the incorporation of microalgae during co-carbonisation plays a significant role in pore structure enhancement. The natural cell wall structure of microalgae, composed of robust and uniform cellular walls, contributes to the uniform creation of pores in the adsorbent (Weber et al., 2022). This results in a well-organized and consistent porous network, which is crucial for maximizing adsorption efficiency. The introduction of microalgae not only increases surface roughness but also contributes to the creation of additional active sites for adsorption. This modified morphology indicates that HCS-N could exhibit enhanced adsorption properties compared to pristine HCS.



**Figure 4.27: Field Emission Scanning Electron Microscope image of microalgae functionalised bio-adsorbent (HCS-N)**

The dual-functionalised bio-adsorbent (HCS-N-Mg), presented in Figure 4.28, shows the most complex morphology among the bio-adsorbent samples. The FESEM images reveal a highly roughened surface with a dense network of interconnected pores. This dual-functionalised sample combines the characteristics of both individual modifications: the dispersion of MgO particles and the nodular structures associated with microalgae functional groups.



**Figure 4.28: Field Emission Scanning Electron Microscope image of dual-functionalised bio-adsorbent (HCS-N-Mg)**

#### **4.3.5 Elemental analysis**

Elemental analysis is significant because bio-adsorbent (activated hydrochar/carbon) does not consist of carbon atom alone, but rather incorporation of other heteroatoms including hydrogen, nitrogen, halogen, and sulphur, which are bonded to the edge of carbon layers. Table 4.10 summarizes the EDX analysis results of starting materials and resulting bio-adsorbent, showing the elemental composition (in weight percentage) of carbon (C), nitrogen (N), oxygen (O), magnesium (Mg), and other inorganic elements.

The raw coconut shell exhibits a higher carbon content and oxygen content, at 53.0% and 45.3% respectively, with minimum amount of nitrogen and no presence of magnesium detected. In comparison, nitrogen-heteroatom precursor – raw microalgae, contains 39.3% carbon, 8.7% nitrogen, and 49.7% oxygen, with no magnesium detected and 2.3% other inorganic elements (mainly aluminium, potassium, and phosphorus). Presence of nitrogen in *Chlorella* microalgae, which is more than 800% compared to the lignocellulosic biomass (coconut shell), indicate the suitability of the material for nitrogen functionalisation.

**Table 4.10: EDX analysis (in wt.%) of bio-adsorbent materials**

Sample	Elemental composition (wt. %)				
	C	N	O	Mg	Other inorganic elements
Raw CS	53.0	0.2	45.3	-	1.5
Raw microalgae	39.3	8.7	49.7	-	2.3
HCS	88.4	-	9.0	-	2.6
HCS-N	75.3	4.7	18.1	-	1.9
HCS-Mg	74.5	-	18.1	6.8	0.6
HCS-N-Mg	73.6	5.3	12.6	6.5	2.0

The carbon content in HCS, HCS-N, HCS-Mg and HCS-N-Mg are significantly higher compared to the raw materials, indicating successful carbonisation and activation process. Among all the bio-adsorbent, HCS shows significantly higher carbon content (88.4%) with 9.0% oxygen, 2.6% other inorganic elements, and absent of nitrogen and magnesium element. Microalgae-functionalised bio-adsorbent has 75.3% carbon, 4.7% nitrogen, and 18.1% oxygen, with no magnesium detected and 1.9% other inorganic elements, while magnesium-functionalised bio-adsorbent contains 74.5% carbon, 18.1% oxygen, and 6.8% magnesium, with no nitrogen detected and only 0.6% other inorganic elements. Dual-functionalised bio-adsorbent (HCS-N-Mg) contains 73.6% carbon, 5.3%

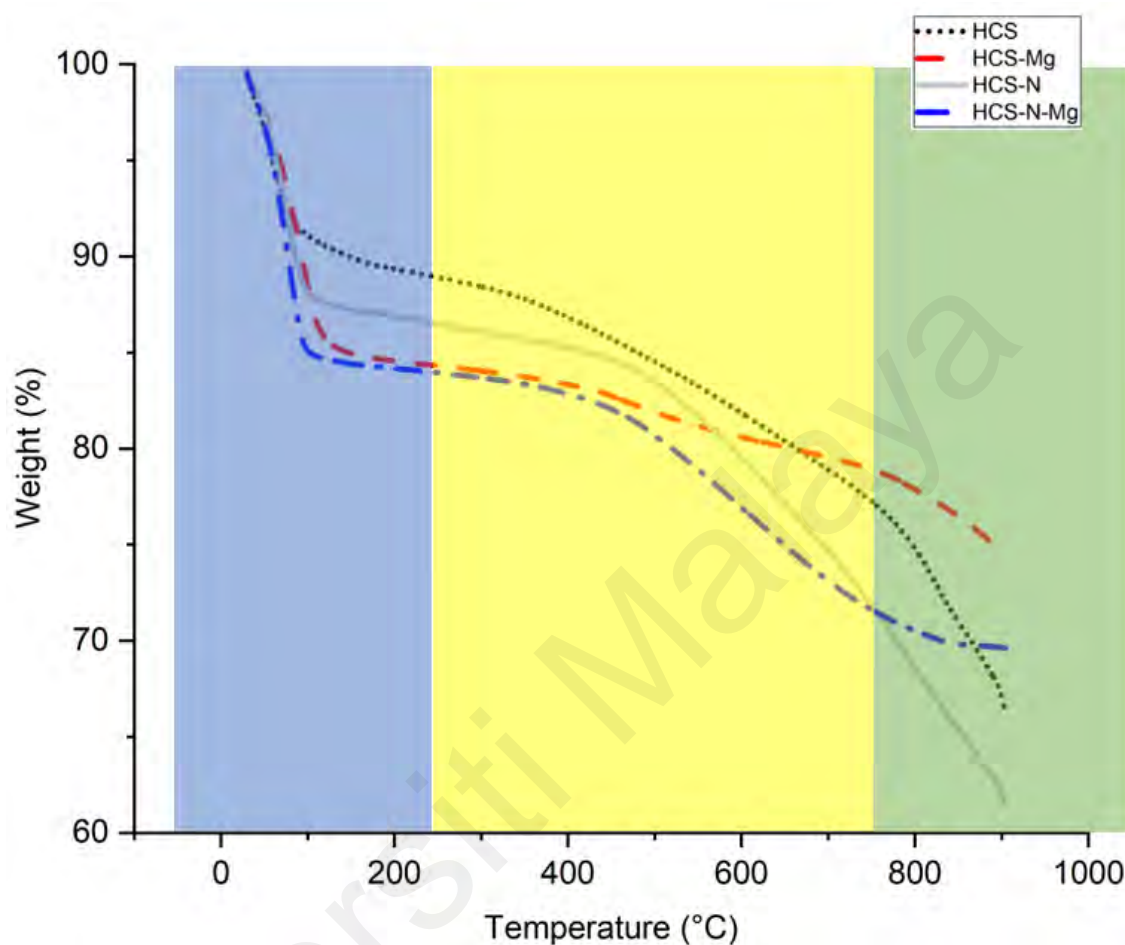
nitrogen, 12.6% oxygen, and 6.5% magnesium, with 2.0% other inorganic elements. Despite the functionalisation, the carbon content of bio-adsorbents remains high, suggesting that functionalisation with microalgae or magnesium oxide does not significantly reduce the carbon content.

The oxygen content, which is highest in raw CS and raw microalgae, decreases substantially in HCS, indicating a reduction in oxygen-containing functional groups during activation. Functionalisation with microalgae or magnesium slightly increases the oxygen content compared to HCS. Incorporation of microalgae, which are rich in nitrogen-containing compounds, through co-carbonisation introduces nitrogen into the carbon structure in various forms, such as amines, amides, pyridines, and pyrroles. During the co-carbonisation and activation of microalgae, nitrogen in the biomass react with available oxygen to form nitrogen-oxygen functional groups, such as nitro groups ( $-\text{NO}_2$ ), and nitrate ( $\text{NO}_3^-$ ) (D. Li et al., 2020). Additionally, functionalisation with MgO enhance the formation of hydroxyl ( $-\text{OH}$ ), carbonyl ( $\text{C}=\text{O}$ ), and carboxyl ( $-\text{COOH}$ ) groups on the carbon surface (Guo & Bulin, 2021). Nitrogen is present in raw microalgae but absent in raw CS and HCS. However, co-carbonisation of microalgae resulting in increment of nitrogen content in the bio-adsorbents, indicating successful functionalisation. Similarly, increment of Mg concentration in HCS-Mg and HCS-N-Mg, compared to HCS and HCS-N confirming successful metal oxide functionalisation.

#### **4.3.6 Thermogravimetric analysis**

Figure 4.29 displays the Thermogravimetric Analysis (TGA) profiles of both the pristine and hybrid bio-adsorbents. The weight losses were observed in three distinct regions. The initial stage, below  $200^\circ\text{C}$ , involves changes in adsorbent mass attributed to surface-bound moisture. The subsequent stage, spanning  $200^\circ\text{C}$  to  $700^\circ\text{C}$ , were characterised by

the predominant loss of mass resulting from the decomposition of attached functional groups. The final stage, occurring above 700 °C, represents another phase of mass loss.



**Figure 4.29: Thermal degradation of developed adsorbents**

At the first stage of temperature below 100°C, HCS undergo weight loss of 10.65 wt.% due to the moisture presence in the sample. The porous structure of HCS bio-adsorbent allows it to adsorb and retain moisture from the surrounding air. Similar patterns were also reported by Poomsawat and Poomsawat (2021); Salgado et al. (2018) and Nyamful et al. (2020) which reported 8-12% weight loss of activated carbon and hydrochar at a heating temperature of 100°C. However, functionalisation of HCS bio-adsorbent with microalgae resulted in increment of weight loss to 13.10 wt.% due to moisture entrapment in HCS-N. Presence of amines or amides, may have the capacity to form hydrogen bonds with water molecules, which can lead to increased moisture retention

(Tan et al., 2020). Similarly, addition of MgO into HCS and HCS-N resulted in higher decline of weight to 15.45 wt.% and 15.83 wt.% respectively. This is due to MgO functionalised onto bio-adsorbent as MgO and MgOH; increasing the moisture content in its vicinity (Huang et al., 2020).

In the temperature range between 200°C and 700°C, the bio-adsorbents exhibit a more gradual weight loss, primarily associated with the breakdown of stable carbonaceous structure and removal of adsorbed gasses and contaminants such as H<sub>2</sub>O, CO<sub>2</sub>, and CO, which are further reacted with surrounding air. The HCS bio-adsorbent shows a steady weight loss by 10.46%, indicative of consistent decomposition of carbon structures. In contrast, the HCS-N bio-adsorbent exhibits a more significant weight loss at 12.13%, indicating that nitrogen incorporation led to the formation of less thermally stable structures that decompose more readily. This could be due to the presence of nitrogen functionalities that destabilize the carbon matrix at elevated temperatures. Furthermore, the nitrogen functionalities introduced by algae functionalisation are prone to decomposition at elevated temperatures, releasing gases like nitrogen or ammonia (Bumajdad et al., 2023). However, the presence of MgO in HCS-N-Mg appears to mitigate this decomposition by reducing the weight loss to 10.99%. MgO is known for its catalytic properties, which alter the degradation pathways of nitrogenous compounds, leading to a more gradual weight loss. The MgO helps retain the nitrogen functionality within the structure, contributing to a slower and more controlled release of volatile degradation products. Similarly, addition of MgO onto HCS bio-adsorbent lower the weight loss to 4.99%, suggesting that the incorporation of magnesium oxide enhances the thermal stability of the sample.

Beyond 700°C, HCS, HCS-N, HCS-Mg and HCS-N-Mg undergo rapid mass reduction, which can be linked to the decomposition of the graphite structure of the bio-adsorbents. The decreased stability observed in the original adsorbent and HCS-N at

higher temperatures can be attributed to the numerous surface defects in their structure, expediting the combustion of the graphite network. In addition, porous structure from addition of microalgae resulted in more thermally sensitive materials than the carbon matrix itself. According to Ramalho et al. (2023), nitrogen functional group in adsorbent exhibit catalytic activity which catalysed the oxidation of the carbon matrix at lower temperatures. Comparing decomposition performance of these synthesised bio-adsorbents, it shows that HCS-Mg has high stability as at temperature of 900°C, the final weight of HCS-Mg is approximately 74.25% compared to HCS, HCS-N and HCS-N-Mg at 66.42%, 61.53% and 69.62% respectively. In general, the introduction of MgO enhanced the thermal stability of the AC. Comparable results were reported by Zhu et al. (2021) for biochar-based metal impregnated with magnesium citrate salt.

#### **4.3.7 Comparison of physicochemical properties of pristine and functionalised coconuts shell-based bio-adsorbents**

Table 4.11 displays the physicochemical properties of CS bio-adsorbent and functionalised CS bio-adsorbent. Despite having the highest surface area. HCS-N is the most thermally sensitive which is indicated by the reduced final mass of 61.53 wt.% retained after exposure to 900 °C.

For elemental composition, HCS-N and HCS-Mg have lower carbon percentages, 75.3% and 74.5%, respectively, with increased oxygen content, indicating more surface functional groups. The composition of HCS-N-Mg, with 73.6% carbon, 12.6% oxygen, 7.5% nitrogen, and 6.5% magnesium, indicates the effective functionalisation process and the introduction of basic sites that would enhance adsorption interactions. FTIR analysis further confirm the formation of additional functional groups in HCS-N, HCS-Mg and HCS-N-Mg through increment of nitro- and oxygen functional groups. These

groups contribute to creating more active sites for CO<sub>2</sub> binding on the adsorbents, enhancing their adsorption capabilities.

**Table 4.11: Comparison of physicochemical properties of developed bio-adsorbents**

Parameter	Unit	HCS	HCS-N	HCS-Mg	HCS-N-Mg
<b>Textural properties</b>					
BET surface area	m <sup>2</sup> /g	976	2038	721	1045
Average pore diameter	nm	1.72	2.72	2.15	2.01
Pore volume	cm <sup>3</sup> /g	0.314	0.519	0.232	0.260
<b>Elemental Composition</b>					
Carbon (C)	%	88.4	75.3	74.5	73.6
Oxygen (O)	%	9.0	18.1	18.6	12.6
Nitrogen (N)	%	-	4.7	-	5.3
Magnesium (Mg)	%	-	-	6.8	6.5
<b>Thermal Stability</b>					
Δ Mass at 200 °C	wt.%	-10.65	-13.10	-15.45	-15.83
Δ Mass at 700 °C	wt.%	-10.46	-12.13	-4.99	-10.99
Final Mass at 900 °C	wt.%	66.42	61.53	74.25	69.62
<b>Functional Groups</b>	-	O-H C-H C=O C-O C=C	O-H C-H C=O C-O C=C C≡N N-H	O-H C-H C=O C-O C=C	O-H C-H C=O C-O C=C C≡N N-H

Among the bio-adsorbents developed, HCS-N-Mg is the most promising CO<sub>2</sub> bio-adsorbent due to its high BET surface area, excellent thermal stability, and a variety of functional groups. Dual functionalisation with MgO and microalgae through single



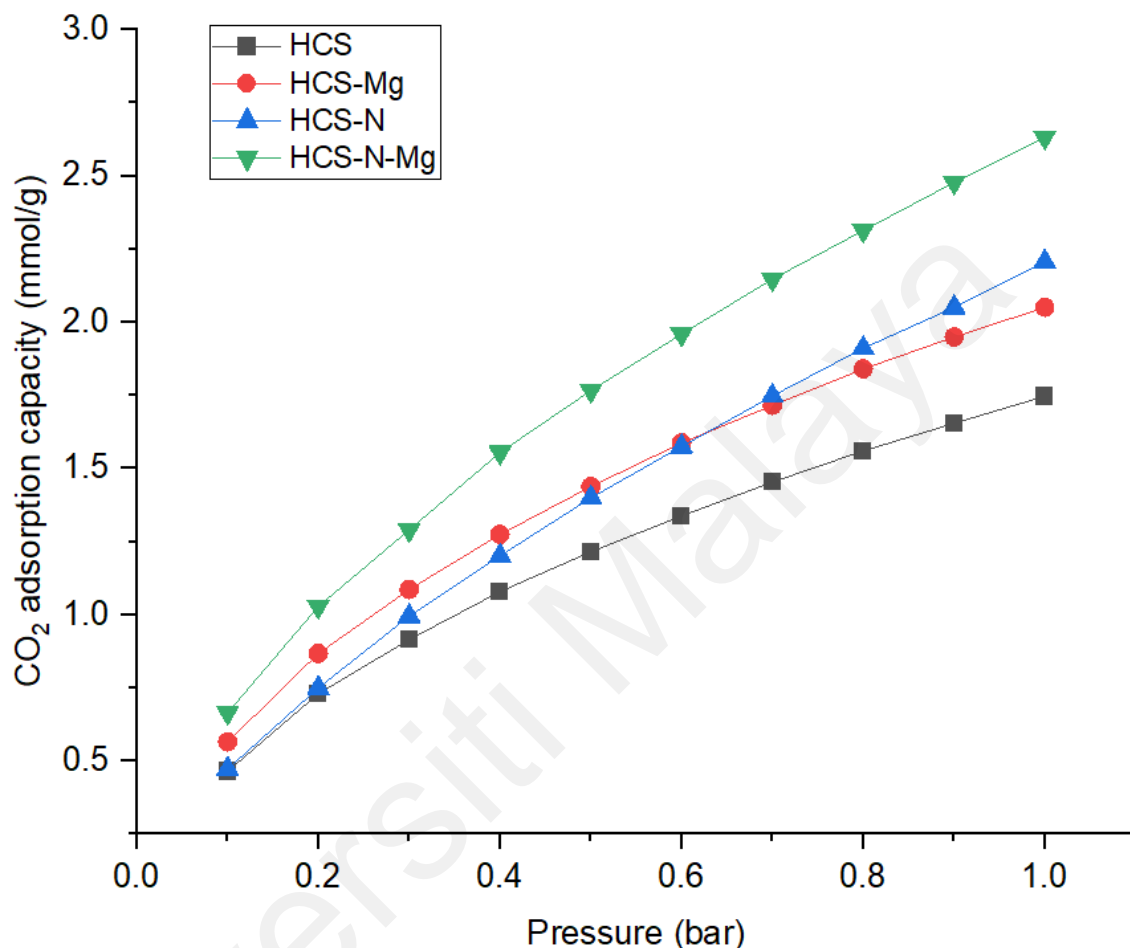
optimised MgO- and N- functionalisation of bio-adsorbent significantly increase the basicity HCS which is important in ensuring efficient CO<sub>2</sub> capture, making HCS-N-Mg the optimal choice.

#### **4.4 Carbon dioxide adsorption capacity evaluation**

The adsorption profile of carbon dioxide onto bio-adsorbent with and without magnesium oxide and microalgae functionalisation are shown in Figure 4.30. Based on the comparison of the adsorption profiles, a significant difference in the carbon dioxide adsorption capacity at 25°C can be seen between HCS, HCS-Mg, HCS-N and HCS-N-Mg. The adsorption capacity increases with pressure for all bio-adsorbents, but the extent and rate of increase vary, reflecting the effect of different modifications on the bio-adsorbents performance. At standard conditions, the CO<sub>2</sub> adsorption capacity of HCS, HCS-Mg, HCS-N and HCS-N-Mg are 1.75, 2.05, 2.21 and 2.63 mmol/g respectively.

HCS shows the lowest CO<sub>2</sub> adsorption capacity across all pressure, and individual functionalisation of HCS bio-adsorbent with microalgae and MgO, enhance the adsorption performance. Addition of 15% MgO onto the HCS bio-adsorbent resulted in 17% increment compared to pristine sample despite the reduction in  $S_{BET}$  and  $V_{micro}$  of developed adsorbent. In theory, materials with larger micropore volume and surface area exhibit superior CO<sub>2</sub> adsorption compared to those with smaller values. Although MgO incorporation obstruct some fine micropores, it also provides additional adsorption sites and enhances CO<sub>2</sub>-adsorbent interactions, leading to overall improvement. CO<sub>2</sub> adsorption is not solely governed by pore volume and surface area but is also influenced by chemical interactions between the adsorbent and CO<sub>2</sub> (Serafin et al., 2017). Similarly, HCS-N-Mg demonstrated higher CO<sub>2</sub> adsorption capacity than HCS-N. This improved catalytic activity of the inorganic functionalised bio-adsorbent is attributed to the presence of alkaline functionalities on its surface, absent in the parent material (Ghaemi

et al., 2022). The increase in carbon dioxide adsorption capacity is likely due to the acid-base reaction between MgO and CO<sub>2</sub>.



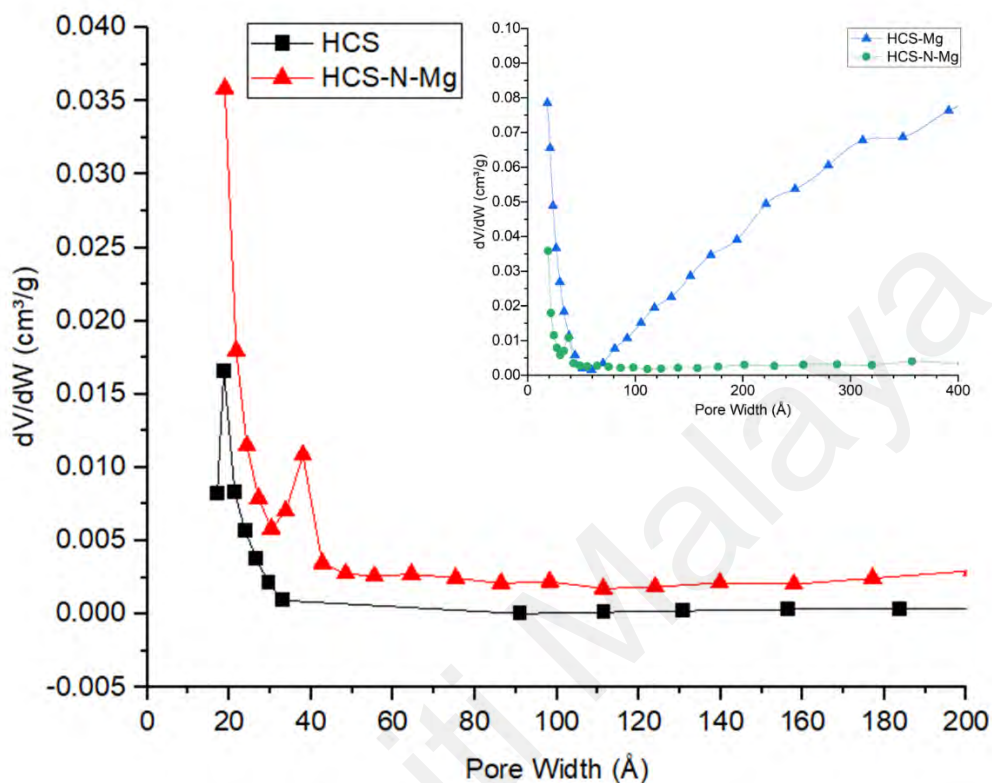
**Figure 4.30: Carbon dioxide adsorption capacity of pristine and functionalised HCS at standard temperature and pressure**

Surface modification through incorporation of microalgae into HCS and HCS-Mg resulted in increment of adsorption performance by 26% and 29% respectively. This phenomenon can be ascribed to the creation of a microporous structure during HTC carbonisation (Fu et al., 2019), leading to a greater surface area on HCS-N compared to HCS. Moreover, the introduction of new functional groups resulting from N-species doping on the HCS surface has contributed to higher CO<sub>2</sub> adsorption capacity, with this contribution exceeding that of pore filling (Yu et al., 2021). The HCS-N-Mg bio-

adsorbent exhibited the highest adsorption capacity, demonstrating a 50% increase compared to the pristine HCS. This enhanced capacity is attributed to the combined effects of physisorption and chemisorption, facilitated by the high surface area, microalgae functionalisation, and well-dispersed metal within the bio-adsorbent material.

Additionally, nitrogen-functionalised bio-adsorbent (HCS-N) facilitates better dispersion of MgO, as illustrated in Figure 4.31. The graph shows that the HCS-N-Mg has larger pore volume at smaller pore diameters, indicating a more homogeneous and efficient dispersion of MgO compared to HCS-Mg, which displays larger pore volume at larger pore diameters. This characteristic suggests that MgO particles are more uniformly distributed across the adsorbent surface, preventing aggregation and maximizing the available active sites for adsorption. The smaller pore diameters contribute to a higher surface area, enhancing the interaction between MgO and CO<sub>2</sub>. HCS and HCS-N-Mg indicate that the pore structures are microporous and mesoporous, respectively. This observation aligns with the research conducted Abriyani et al. (2022), which found that the impregnation of 5% MgO onto the substrate caused the pore diameter to shift from 1.87 to 2.23 nm. 17% reduction in micropore volume following impregnation suggests that MgO has indeed blocked the micropores in the porous carbon. Compared to HCS, HCS-N-Mg has a dual porosity (Figure 4.32), due to additional pore distribution between 3-5 nm. Similarly, a study conducted by F. Yang et al. (2022), found that incorporating MgO into a carbon-based adsorbent led to an additional pore distribution in the 2–4 nm range, as opposed to the sample without MgO, which primarily exhibited pores below 3 nm. Furthermore, this study indicated that the pristine sample predominantly featured microporous structures at 1.9 nm, whereas the MgO-modified samples contained smaller mesopores, with an average pore size of 1.99–2.3 nm and varying peak intensities based on the MgO dosage. This observation is

consistent with findings from Koo-Amornpattana et al. (2023), who noted that MgO-functionalized adsorbents displayed fewer pores compared to the original adsorbent.



**Figure 4.31: Pore width distribution of HCS, HCS-Mg and HCS-N-Mg.**

At the beginning of the adsorption, it is observed that the initial steep increase indicates that the amount of CO<sub>2</sub> adsorbed onto HCS-Mg and HCS-N-Mg is faster than the HCS-N and HCS. Steep initial region corresponds to a stronger binding force between CO<sub>2</sub> with metal oxides and CO<sub>2</sub> with micropores of HCS. From the figure, microalgae functionalisation improves the carbon dioxide adsorption better compared to MgO. In the whole pressure range, the carbon dioxide adsorption capacity of HCS-N was always higher than HCS-Mg. However, between 0.1-0.6 bar, carbon dioxide adsorbed concentration does not exceed 1.57 mmol/g for HCS-N which is actually lower than HCS-Mg at 1.59 mmol/g. This phenomenon can be attributed to the specific interactions occurring between the quadrupolar CO<sub>2</sub> molecules and the partial positive charges

present on the coordinatively unsaturated metal sites within HCS-Mg, particularly under conditions of reduced pressure.

#### 4.4.1 Statistical analysis

A systematic investigation utilising RSM was conducted to understand the interrelationship between operating temperature (A) and pressure (B) on CO<sub>2</sub> adsorption capacity of pristine and functionalised bio-adsorbents. The experimental design matrix, encompassing both actual and predicted adsorption capacities for pristine and functionalised HCS, is summarized in Table 4.12. This table also presents the results of multiple regression analysis applied to the experimental data, along with an evaluation of model adequacy using ANOVA and the Adjusted R-squared statistic.

**Table 4.12: Multiple regression analysis and ANOVA used to fit the quadratic model to the CO<sub>2</sub> adsorption capacity**

Model	Sum of squares	Mean squares	Coded coefficient	Standard error	df	p-value
<b>HCS</b>						
<b>Model</b>		1.57	1.38	0.0448	5	< 0.0001
A-Temperature	7.83	1.82	-0.6308	0.0469	1	< 0.0001
B-Pressure	1.82	5.17	1.06	0.0469	1	< 0.0001
<b>Model</b>	<b>Sum of squares</b>	<b>Mean squares</b>	<b>Coded coefficient</b>	<b>Standard error</b>	<b>df</b>	<b>p-value</b>
AB	5.17	0.7127	-0.4221	0.0501	1	0.0004
A <sup>2</sup>	0.7127	0.2132	0.2463	0.0534	1	0.0058
B <sup>2</sup>	0.2132	0.2999	-0.292	0.0534	1	0.0028
<b>Residual</b>	0.0502	0.01			5	
Lack of Fit	0.0033	0.0033			1	0.6217
Pure Error	0.0469	0.0117			4	

**Table 4.12, continued**

<b>Model</b>	<b>Sum of squares</b>	<b>Mean squares</b>	<b>Coded coefficient</b>	<b>Standard error</b>	<b>df</b>	<b>p-value</b>
<b>HCS-Mg</b>						
<b>Model</b>	14.71	2.94	2.16	0.0311	5	< 0.0001
A-Temperature	1.21	1.21	-0.5151	0.0326	1	< 0.0001
B-Pressure	8.98	8.98	1.40	0.0326	1	< 0.0001
AB	0.5837	0.5837	-0.3820	0.0348	1	0.0014
A <sup>2</sup>	0.2612	0.2612	-0.2726	0.0371	1	0.0166
B <sup>2</sup>	0.423	0.0423	-0.1097	0.0371	1	< 0.0001
<b>Residual</b>	0.0242	0.0048			5	
Lack of Fit	0.0214	0.0214			1	0.1676
Pure Error	0.0028	0.0007			4	
<b>HCS-N</b>						
<b>Model</b>	22.73	4.55	1.58	0.0922	5	< 0.0001
A-Temperature	8.14	8.14	-1.33	0.0964	1	< 0.0001
B-Pressure	10.02	10.02	1.48	0.0964	1	< 0.0001
AB	4.92	4.92	-1.11	0.1030	1	0.0001
A <sup>2</sup>	1.37	1.37	0.6235	0.1099	1	0.0024
B <sup>2</sup>	0.6457	0.6457	-0.4285	0.1099	1	0.0114
<b>Residual</b>	0.2124	0.0425			5	
Lack of Fit	0.2116	0.2116			1	< 0.0001
Pure Error	0.0008	0.0002			4	
<b>HCS-N-Mg</b>						
<b>Model</b>	30.39	6.08	2.97	0.0486	5	< 0.0001
A-Temperature	5.48	5.48	-1.10	0.0508	1	< 0.0001
B-Pressure	16.03	16.03	1.87	0.0508	1	< 0.0001
AB	2.77	2.77	-0.8320	0.0543	1	< 0.0001
A <sup>2</sup>	0.2899	0.2899	-0.2871	0.0579	1	0.0043
B <sup>2</sup>	0.6763	0.6763	-0.4385	0.0579	1	0.0006
<b>Residual</b>	0.0590	0.0118			5	
Lack of Fit	0.0189	0.0189			1	0.2414
Pure Error	0.0401	0.0100			4	

Quadratic model is suggested by Design Expert® and selected for all bio-adsorbents to understand the relationship between factors (temperature and pressure) and the response (CO<sub>2</sub> adsorption capacity). This model includes linear terms, interaction terms, and quadratic terms, providing a detailed insight into how each factor and their interactions

affect CO<sub>2</sub> adsorption of pristine and functionalised bio-adsorbents. Furthermore, regression analysis was utilised to fit the empirical model with experimental data. Additionally, the response surfaces of HCS, HCS-Mg, HCS-N and HCS-N-Mg for CO<sub>2</sub> adsorption capacity (Y<sub>1</sub>) in terms of coded values of independent variables (A, B) are presented in Equation 4.4, 4.5, 4.6 and 4.7 respectively.

$$q_{CO_2HCS}(mmol/g) = 1.38 - 0.6308A + 1.06B - 0.4221AB + 0.2463A^2 - 0.292B^2 \quad (4.4)$$

$$q_{CO_2HCS-Mg}(mmol/g) = 2.16 - 0.5151A + 1.40B - 0.3820AB - 0.2726A^2 - 0.1097B^2 \quad (4.5)$$

$$q_{CO_2HCS-N}(mmol/g) = 1.58 - 1.33A + 1.48B - 1.11AB + 0.6235A^2 - 0.4285B^2 \quad (4.6)$$

$$q_{CO_2HCS-N-Mg}(mmol/g) = 2.97 - 1.10A + 1.87B - 0.8320AB - 0.2871A^2 - 0.4385B^2 \quad (4.7)$$

For HCS, the adsorption capacity equation ( $q_{CO_2HCS}$ ) shows that both temperature and pressure significantly influence CO<sub>2</sub> adsorption. The negative coefficient for temperature ( $-0.6308A$ ) suggests that temperature increment resulted in reduction of CO<sub>2</sub> adsorption capacity, which is typical behavior for physical adsorption processes. The positive coefficient for pressure ( $+1.06B$ ) indicates that higher pressure favours increased adsorption, consistent with the principle that adsorption capacity generally increases with pressure due to enhanced CO<sub>2</sub> molecule interaction with the adsorbent surface.

For HCS-Mg, the regression model ( $q_{CO_2HCS-Mg}$ ), similar relationship was demonstrated in which higher pressure enhances adsorption ( $+1.40A$ ), but the negative  $T$  and  $P^2$  terms ( $-0.5151A$  and  $-0.197B^2$ ) imply a reduction in adsorption at elevated temperatures and a plateauing effect at high pressures. The smaller magnitude of the

temperature coefficient compared to HCS suggests a slightly lower sensitivity to temperature changes, potentially due to the stabilizing effect of Mg on the adsorbent structure. The model for HCS functionalised with microalgae ( $q_{CO_2_{HCS-N}}$ ) exhibits a higher sensitivity to both temperature and pressure changes. The negative temperature coefficient ( $-1.33A$ ) and positive pressure coefficient ( $+1.48B$ ) are more pronounced compared to HCS and HCS-Mg. This indicates a stronger dependency on these variables, possibly due to the increased surface functionality and improved interaction sites provided by nitro-functional groups. However, the larger negative  $TP$  and  $P^2$  coefficients ( $-1.11AB$  and  $-0.4285B^2$ ) also highlight a greater reduction in capacity at higher temperatures and pressures, suggesting a more complex adsorption mechanism involving multiple interaction sites.

HCS-N-Mg ( $q_{CO_2_{HCS-N-Mg}}$ ) shows a balanced behavior with moderate sensitivity to temperature and pressure changes. The negative temperature coefficient ( $-1.10A$ ) and positive pressure coefficient ( $+1.87B$ ) are less extreme compared to HCS-N, implying a more stable adsorption capacity over a range of conditions. The inclusion of both N and Mg seems to synergistically enhance the adsorbent's performance, making it less prone to the adverse effects of high temperature and pressure. The  $TP$  and  $P^2$  terms ( $-0.8320AB$  and  $-0.4385B^2$ ) are indicative of the complex interaction effects but are less dominant than in the HCS-N model.

ANOVA results showed the models for evaluating the adsorption capacity of carbon dioxide onto HCS, HCS-Mg, HCS-N and HCS-N-Mg to be statistically significant at a 95% confidence level ( $p\text{-value} < 0.05$ ). Additionally, the lack of fit for these models was statistically insignificant at the same confidence level ( $p\text{-value} > 0.05$ ). Table 4.13 shows the significant terms in the models ( $p\text{-value} < 0.05$ ), while non-significant terms ( $p\text{-value} > 0.05$ ) are excluded from the model.



The  $R^2$  values exceeding 0.8 for HCS, HCS-Mg, and HCS-N-Mg indicate a good fit of these models to the data. However, the negative predicted  $R^2$  for HCS-N suggests that the overall mean is a more accurate predictor of the response than the current model. This poor predictability maybe due to the missing interaction terms or higher-order terms within the model, as noted by Rajewski and Dobrzyńska-Inger (2021). Moreover, the significant lack of fit observed for  $CO_2$  adsorption capacity of HCS-N further contributes to its lower predicted  $R^2$  value, implying inadequate data representation by the model. In contrast, the CV% values for all models are below 10%, suggesting good reproducibility of the models.

**Table 4.13: Model fit summaries for adsorption conditions of bio-adsorbents**

<b>Bio-adsorbent</b>	<b>SD</b>	<b>Mean</b>	<b>CV</b>	<b>PRESS</b>	<b><math>R^2</math></b>	<b>Adj-<math>R^2</math></b>	<b>Pred <math>R^2</math></b>	<b>AP</b>
HCS	0.100	1.41	7.09	0.53	0.9936	0.9873	0.9331	45.78
HCS-Mg	0.070	2.07	3.37	2.92	0.9984	0.9967	0.8019	74.53
HCS-N	0.206	1.71	8.12	28.78	0.9907	0.9815	- 0.2544	36.99
HCS-N-Mg	0.109	2.67	4.06	2.64	0.9981	0.9961	0.9134	73.99

These findings from ANOVA highlight that the incorporation of Mg and N into coconut shell bio-adsorbent significantly alters its  $CO_2$  adsorption characteristics. HCS-N shows the highest sensitivity to temperature and pressure, indicating that nitro groups and porous structures are more susceptible to temperature and pressure change. Meanwhile, HCS-N-Mg combines the benefits of both modifications, resulting in a more stable adsorbent with balanced performance across a range of conditions. Therefore, as HCS-N-Mg demonstrated the highest  $CO_2$  adsorption capacity, with less sensitivity towards temperature increment, detailed analysis on the pristine and dual-functionalised bio-

adsorbent is crucial to understanding their performance and behavior in detail. In order to maximize the efficiency of these materials in capturing CO<sub>2</sub>, their interaction mechanisms, adsorption selectivity and long-term performance as well as adsorption behaviour should be further analysed to understand the efficacy of dual-functionalised bio-adsorbent.

#### **4.4.2 Effect of operating parameters on the CO<sub>2</sub> adsorption capacity**

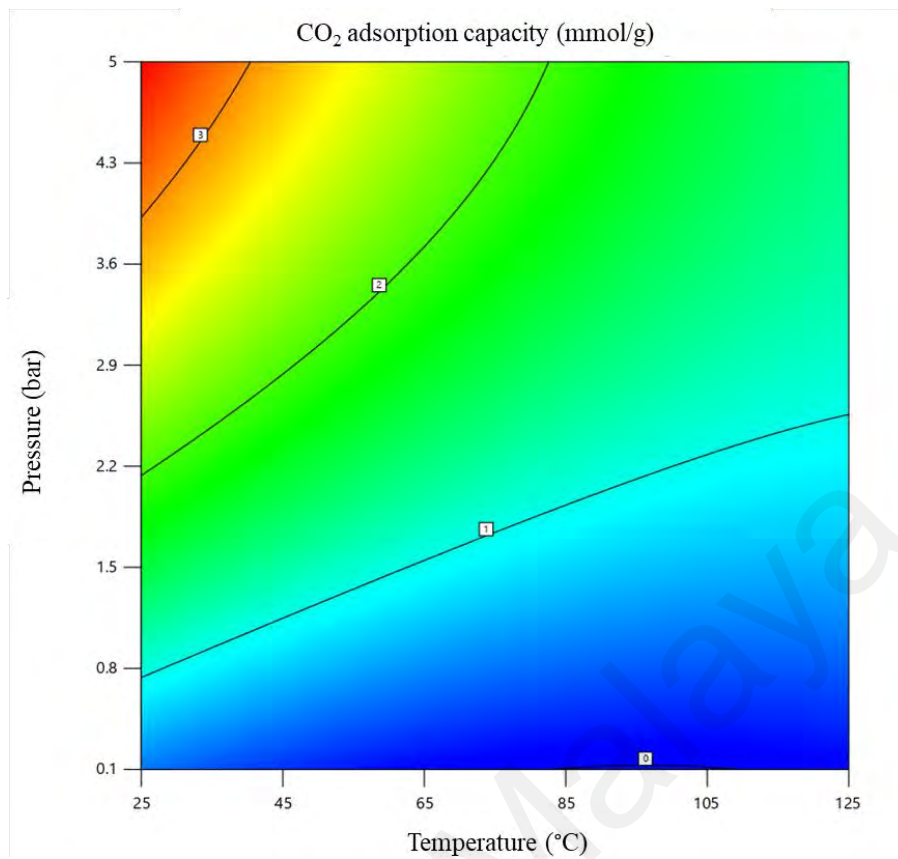
Understanding the effect of adsorption conditions on individual bio-adsorbents is crucial for optimising their performance in CO<sub>2</sub> capture applications. The performance of these materials is significantly influenced by various adsorption conditions, such as temperature and pressure. These conditions affect the interaction between CO<sub>2</sub> molecules and the surface of the bio-adsorbent, influencing the adsorption effectiveness. This subtopic discussed the effect of temperature and pressure on HCS, HCS-Mg, HCS-N and HCS-N-Mg towards CO<sub>2</sub> adsorption performance.

##### **4.4.2.1 Adsorption temperature**

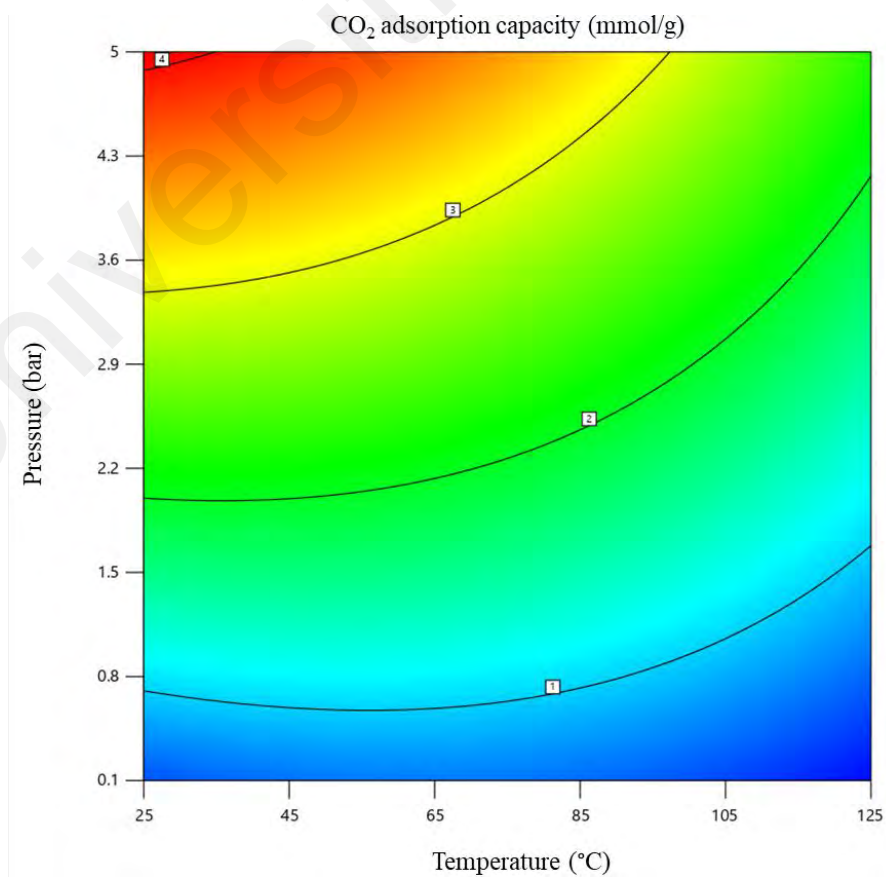
In the adsorption process, the effect of adsorption temperature towards adsorption capacity is significant, as the nature and type of that process can be determined. In this study, RSM-CCD was utilised to investigate the effect of temperature and pressure of operating condition on HCS, HCS-Mg, HCS-N and HCS-N-Mg adsorption performance. As per coded equations in Table 4.12, the negative values for temperature coefficients and positive values for pressure coefficients align with Le Chatelier's principle. This principle explains the decline in carbon dioxide adsorption capacity with temperature increments and the reduction of pressure in the adsorption process (Karimi et al., 2018). Additionally, these coefficients indicate that pressure dependency is the predominant factor in all devised approaches.

Figures 4.32, 4.33, 4.34, and 4.35 shows the effect of adsorption temperatures towards CO<sub>2</sub> adsorption capacity of HCS, HCS-Mg, HCS-N and HCS-N-Mg. Specifically, the carbon dioxide adsorption capacity of HCS at ambient temperature reduces from 3.45 mmol/g to approximately 1.35 mmol/g at 125°C (5 bar). HCS-N shows a similar trend but with a higher reduction in CO<sub>2</sub> adsorption capacity—53.8% and 85.8%, compared to HCS at 60.5% and 61.0% loss. At 25 °C, HCS-N exhibits higher CO<sub>2</sub> adsorption capacity compared to HCS, as the nitrogen functionality enhances the surface area and porous structure of the adsorbent, providing more active sites for CO<sub>2</sub> adsorption. However, HCS-N is more brittle and susceptible to degradation at higher temperatures, which affects its performance (Q. Li et al., 2020). This increased sensitivity can be attributed to the nitrogen functional groups, which enhance CO<sub>2</sub> adsorption at lower temperatures but diminish in effectiveness as temperature rises. Consequently, HCS-N is more sensitive to temperature changes than HCS.

The result reveals that HCS-Mg shows minimal sensitivity towards temperature change in comparison to other adsorbents. At 1 bar, increment of temperature from 25 °C to 75 °C and 125 °C resulted in reduction of CO<sub>2</sub> adsorption capacity from 1.234 mmol/g to 1.233 and 0.687 mmol/g respectively. Similarly, at 5 bar, increment of temperature from 25 °C to 75 °C and 125 °C resulted in reduction of CO<sub>2</sub> adsorption capacity by 15.3% and 44.0% respectively. This minimal sensitivity can be attributed to the stabilizing effect of magnesium doping, which enhances the structural integrity of the adsorbent, making it less susceptible to temperature-induced degradation. The slight decrease in adsorption capacity at higher temperatures indicates that HCS-Mg retains a significant portion of its CO<sub>2</sub> uptake capability, even under thermal stress, making it a robust option for applications requiring stable performance across a range of temperatures.

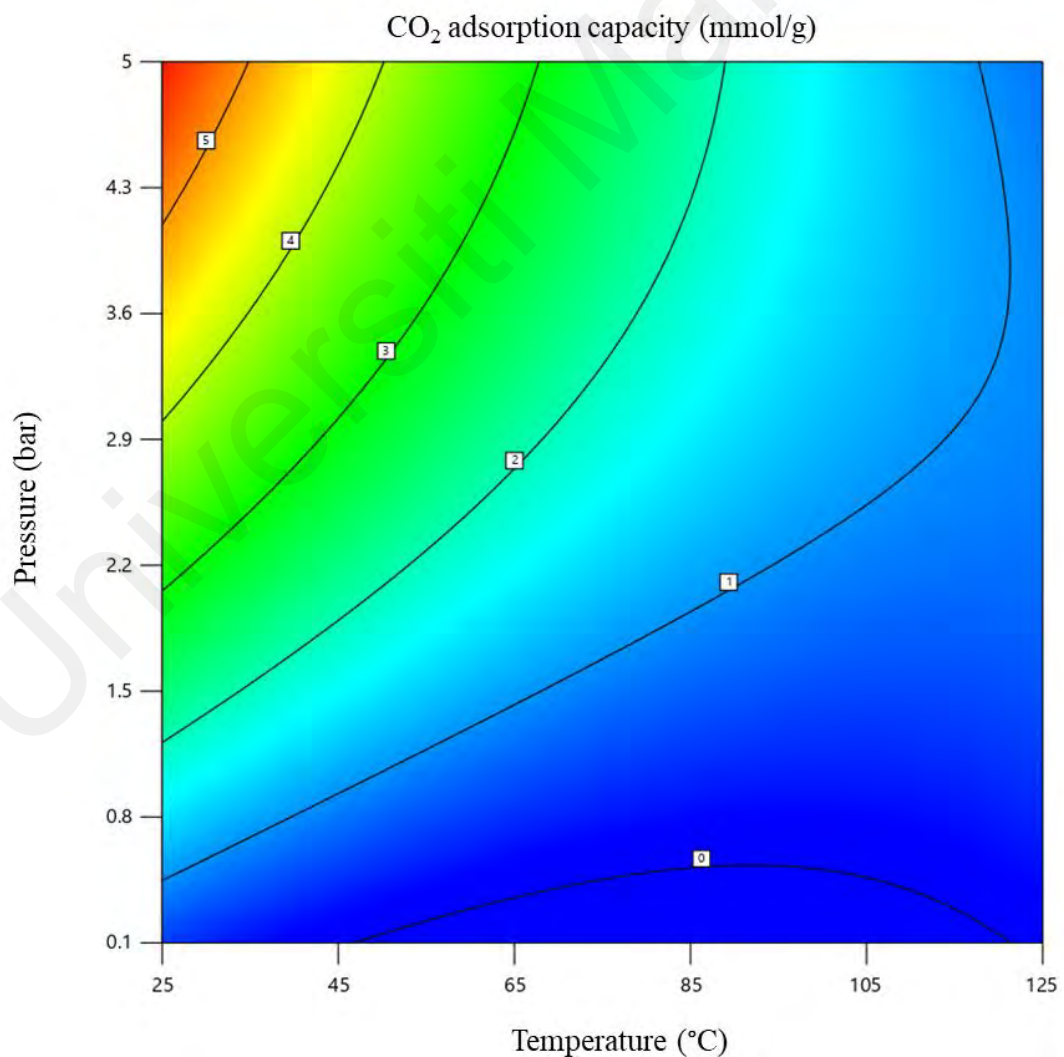


**Figure 4.32: 2D contour plot of CO<sub>2</sub> adsorption capacity of HCS for temperature and pressure interaction**

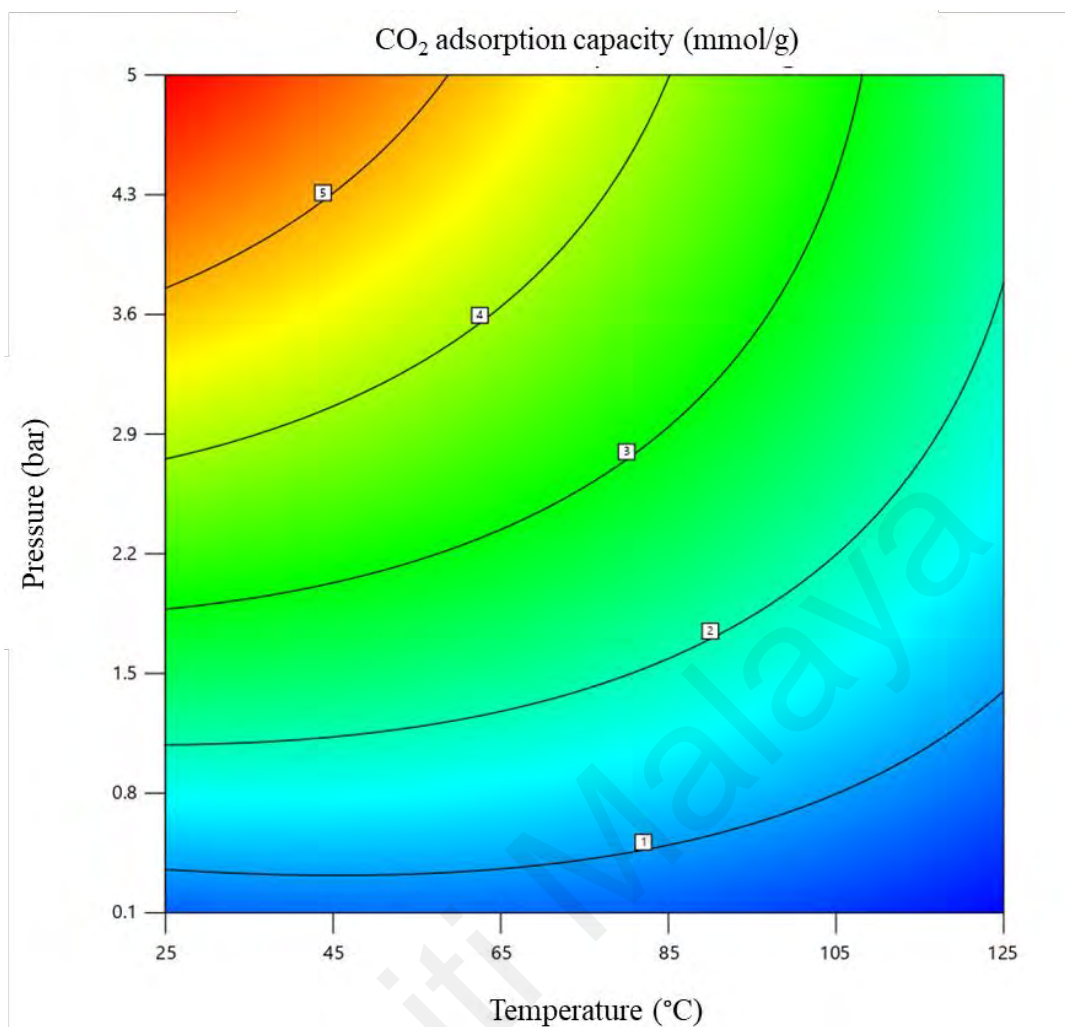


**Figure 4.33: 2D contour plot of CO<sub>2</sub> adsorption capacity of HCS-Mg for temperature and pressure interaction**

The dual-functionalised adsorbent (HCS-N-Mg) performance in CO<sub>2</sub> adsorption capacity reduce to 2.19 mmol/g from 6.04 mmol/g. Similarly, the carbon dioxide adsorption capacity of binary mixture of microalgae and coconut shell with MgO has less than one-third of its corresponding CO<sub>2</sub> adsorption capacity at room temperature when measured at 125°C. From the surface plot (Figure 4.32 and 4.34), HCS and HCS-N demonstrate high sensitivity toward the temperature change, as there is a reduction in CO<sub>2</sub> adsorption capacity when the temperature increases from room temperature to 125 °C. This trend can be attributed to the physical adsorption phenomenon (Gunawan et al., 2018).



**Figure 4.34: 2D contour plot of CO<sub>2</sub> adsorption capacity of HCS-N for temperature and pressure interaction**



**Figure 4.35: 2D contour plot of CO<sub>2</sub> adsorption capacity of HCS-N-Mg for temperature and pressure interaction**

At higher temperatures, the performance of HCS-N-Mg is better compared to HCS by 64%. This shows the tendencies of magnesium oxide to maintain a constant and minimal drop in CO<sub>2</sub> adsorption at elevated temperatures. Despite the reduction in pore volume, there is an increase in adsorption capacity. Within HCS, only physisorption occurs, leading to a sharp decrease in carbon dioxide adsorption capacity at elevated temperatures. Conversely, for HCS-N-Mg, carbon dioxide interacts with the nitrogen functional group from microalgae and the oxygen-functional group of magnesium oxide, facilitating both physisorption and chemisorption. As a result, the rise in temperature leads to a less significant decline in carbon dioxide adsorption capacity. The reduction of CO<sub>2</sub> adsorption capacity with temperature enhancement can be attributed to the

exothermic properties, where elevated temperatures lead to increased molecular diffusion and surface adsorption energy. Consequently, the adsorbate molecules become unstable, initiating desorption (Maroto-Valer et al., 2005).

Ammendola et al. (2017) observed that at higher temperatures, CO<sub>2</sub> molecules adsorbed on activated carbons gain enough energy to overcome van der Waals forces and return to the gas phase. In contrast, in the gaseous phase, they tend to remain. Tamilarasan and Ramaprabhu (2012) who have also obtained similar findings described that these findings are attributed to the kinetic energy of CO<sub>2</sub> molecules. Conversely, at lower temperatures, carbon dioxide molecules effectively interact with the surface of the adsorbent, leading to the formation of multilayers. However, when the reaction temperature is excessively high, these CO<sub>2</sub> molecules have much higher kinetic energy, and accordingly, have higher velocity to escape from active sites and pores.

#### **4.4.2.2 Adsorption pressure**

Based on the interaction coefficient value, it is evident that pressure dependency plays a predominant role in all devised approaches. The findings suggest a positive correlation between pressure and adsorption capacity, irrespective of the adsorbent type or the nature of adsorption (physical or chemical) (Taheri et al., 2019). At higher pressures, gas molecules undergo compression and tighter packing, enhancing the spontaneity of the adsorption process. This increased pressure promotes adsorption and augments the likelihood of molecules being adsorbed onto available sites, leading to more adsorbed molecules (Du et al., 2021). Despite the increase in temperature, which typically reduces the effectiveness of adsorption due to increased molecular motion, the data indicate that pressure continues to play a dominant role in enhancing the adsorption process.

For HCS, the enhancement in adsorption capacity with pressure is noteworthy. At 25°C and 75°C the adsorption capacity increases from 1.20 mmol/g and 0.59 mmol/g at

1 bar to 3.45 mmol/g and 2.154 mmol/g at 5 bars, an increment of 187% and 263%, respectively. Even at a higher temperature of 125°C, where kinetic energy is expected to counteract adsorption forces, the adsorption capacity increases from 0.48 mmol/g at 1 bar to 1.35 mmol/g at 5 bars, an increase of 183%. When HCS is functionalised with MgO (HCS-Mg), the pressure sensitivity of CO<sub>2</sub> adsorption capacity is notably higher. Increment of pressure from 1 bar to 5 bar at 25 °C, 75 °C and 125 °C resulted in increment of adsorption capacity by 231%, 180% and 233% respectively. The enhanced CO<sub>2</sub> adsorption is due to the inherent basicity of MgO. This characteristic provides additional active sites for binding of CO<sub>2</sub> molecules, thereby enhancing the interaction between the gas and the adsorbent's surface. The incorporation of microalgae (HCS-N) also improves CO<sub>2</sub> adsorption capacity, though to a lesser extent than MgO. Nitrogen groups introduce basic sites and increase the polarity of the adsorbent, which favours CO<sub>2</sub> adsorption due to stronger electrostatic interactions.

HCS-N-Mg shows a similar trend. At 25°C, the adsorption capacity increases from 1.89 mmol/g at 1 bar to 6.04 mmol/g at 5 bar, which corresponds to an increase of 220%. At 75°C and 125°C, an increment of pressure to 5 bar improved adsorption capacity by 174% and 192%, respectively. These results indicate that both HCS and HCS-N-Mg show a similar trend in which the changes in adsorption as pressure increases are linear and significant. This is because high pressure can cause the CO<sub>2</sub> molecules to be compressed, increasing their interaction with the surface of the adsorbent and making them more likely to be held onto the adsorbent (Fakher & Imqam, 2020). In addition, a higher increment of adsorption capacity was recorded by HCS-N-Mg due to the addition of functionalisation. A similar trend was also reported by Ramezanipour Penchah et al. (2021) through piperazine-functionalised activated carbon. Increment of pressure, allowing higher interaction between functionalised adsorbent and CO<sub>2</sub> molecules, enhancing the rate of adsorption, enabling multilayer adsorption of CO<sub>2</sub> gas molecules.



Despite the increment of temperature, the increases of pressure still dominantly increase the CO<sub>2</sub> adsorption due to the uniform mesopores into carbon structure via MgO functionalisation, which can also be supported by Thubsuang et al. (2023) through the incorporation of silica onto porous carbon. The introduction of mesoporous material enhances the mechanical stability of the adsorbent at high temperatures and high-pressure conditions, allowing stable adsorption performance.

This linear relationship highlights the predominant role of pressure in enhancing the CO<sub>2</sub> adsorption capacity of these materials, even at elevated temperatures. Including functional groups in HCS introduces specific chemical sites with increased affinity for CO<sub>2</sub> molecules. This enhanced chemical affinity can lead to stronger adsorption bonds, making the process more effective even at higher temperatures. For HCS-N-Mg, magnesium could facilitate adsorption through interactions with CO<sub>2</sub> conducive to higher adsorption capacities (Ghaemi et al., 2022).

#### **4.4.3 Optimisation and validation study of CO<sub>2</sub> adsorption performance**

RSM-CCD was used to investigate and optimise the effect of operational parameters on CO<sub>2</sub> adsorption performance. Table 4.14 summarizes the restriction to defined ranges, thus bounding the applicability of the regression models to these specified intervals. These parameters could be adjusted to the minimum, maximum, target value, or a specific range or even omitted (for responses) to achieve the most favorable results under certain conditions. The upper limits of temperature and CO<sub>2</sub> adsorption within the predetermined range were chosen to maximize the efficiency of adsorbent in flue gas treatment, in which the operating temperature is higher than 75°C. The operating pressure of the adsorption system was also kept within the range formulated for the newly developed adsorbent to maximize its response. Table 4.14 illustrates that the optimised adsorption capacity recorded for the HCS adsorbent was 1.62 mmol/g at operating

pressure and temperature of 4.5 bar and 100°C, respectively. Optimisation of CO<sub>2</sub> adsorption capacity of HCS-N was achieved at lower temperature of 83 °C with adsorption pressure of 5 bar, at 2.271 mmol/g, whereas HCS-Mg was optimised at higher temperature with higher adsorption capacity of 2.896 mmol/g at 101 °C. Similarly, the adsorption capacity of HCS-N-Mg was optimised at 4.6 bar and 101°C with CO<sub>2</sub> uptake of 3.27 mmol/g.

**Table 4.14: Optimised operating conditions of HCS and HCS-N-Mg**

Adsorbent		HCS	HCS-N	HCS-Mg	HCS-N-Mg
Parameter Condition	Temp.	Max			
	Pressure	In the range			
	CO <sub>2</sub> adsorption capacity	Max			
Optimum Condition	Temp. (°C)	100	83	101	101
	Pressure (bar)	4.5	5	5	4.6
CO <sub>2</sub> adsorption capacity (mmol/g)	Predicted	1.630	2.242	2.915	3.232
	Actual	1.622	2.271	2.896	3.272

The performance of these adsorbents highlights that HCS has the lowest CO<sub>2</sub> adsorption capacity, whereas HCS-N shows moderate improvement due to role of nitrogen in enhancing CO<sub>2</sub> capture. HCS-Mg further increases CO<sub>2</sub> adsorption capacity, suggesting that magnesium doping effectively enhances adsorption capacity. However, HCS-N-Mg stands out with the highest CO<sub>2</sub> adsorption capacity, indicating its superior performance among the adsorbents. This exceptional adsorption capacity is attributed to the synergistic effects of microalgae and magnesium oxide functionalisation, which create more active sites and improve CO<sub>2</sub> interaction.

#### 4.4.4 Adsorption performance evaluation of different types of functionalised bio-adsorbent based on published literature

Table 4.15 summarizes literature focusing on the single functionalisation of metal oxide and microalgae. Compared to commercial activated carbon, as Ghaemi et al. (2022), HCS exhibit a lower CO<sub>2</sub> adsorption capacity. This difference is attributed to the hydrothermal treatment, which yields a mesoporous surface area instead of the microporous surface area typically achieved through depolymerization (Rodríguez Correa et al., 2018). However, studies De Mena Pardo et al. (2016) indicate that the energy consumption, operating cost, and environmental risk of HTC are significantly lower than pyrolysis, suggesting a cleaner and more environmentally friendly synthesis process. Additionally, HCS demonstrates higher adsorption capacity than activated hydrochar, as reported by Huang et al. (2019), Isahak et al. (2018) and Han et al. (2019) underscoring the success in developing an effective CO<sub>2</sub> adsorbent. Notably, its performance surpasses that of activated carbon derived from *Nypha fruticans* and sugar bagasse at 1.36 and 1.66 mmol/g, respectively. This is due to the precursor's carbon-rich and high spherical fibre content, which can be converted into homogeneous porous biochar.

Dual functionalisation enhances performance by 50%, surpassing single functionalisation reported in previous studies. Madzaki et al. (2018a) noted that CuO functionalisation negatively effects CO<sub>2</sub> adsorption on commercial activated carbon, reducing it by 11% due to low surface area metal blockage of pores. However, the addition of CeO<sub>2</sub> slightly improves adsorption by 31% due to favorable interactions between CeO<sub>2</sub> and CO<sub>2</sub>. Similar findings were reported by Ghaemi et al. (2022), indicating 8-11% increase in activated carbon performance through NiO and MgO functionalisation. Microalgae functionalisation also enhances CO<sub>2</sub> adsorption. Han et al. (2019) found that incorporating urea increases adsorption performance by 17%, from

1.66 mmol/g to 1.94 mmol/g. Furthermore, Shi et al. (2022) achieved a higher CO<sub>2</sub> adsorption performance of 4.26 mmol/g by incorporating urea into an activated hydrochar precursor derived from glucose. The high CO<sub>2</sub> adsorption performance is mainly due to the ultrahigh surface area of the adsorbent at 3576 m<sup>2</sup>/g, attributed to glucose's influence in denser carbon formation mimicking graphene structure due to enhanced crystallinity effects.

**Table 4.15: Comparison of carbon dioxide adsorption capacity on adsorbent obtained from biomass at 25°C and 1 bar**

Biomass Precursor	Type of Functionalisation	CO <sub>2</sub> adsorption capacity (mmol/g)	Change of performance (%)	References
HCS	Raw	1.75	-	This work
	MgO	2.05	+17.1	
	Algae	2.21	+26.3	
	MgO + Algae	2.63	+50.3	
AH orange peel	Melamine	6.67	-	(Rehman et al., 2022)
Commercial activated carbon	-	0.65	-	(Madzaki et al., 2018a)
	CuO	0.58	-10.8	
	CeO <sub>2</sub>	0.85	+23.5	
AC Nypha fruticans	-	1.36	+5.1	(Isahak et al., 2018)
	CuO	1.43		
MOF-5	DMF	2.54	-	(Ma, Li, Chen, Wang, Li, & Wang, 2018)
AC sugar bagasse	-	1.66	-	(Han et al., 2019)
	Urea	1.94	+16.9	
AH Glucose	Urea	4.26	-	(Shi et al., 2022)
Commercial activated carbon	-	2.48	-	(Ghaemi et al., 2022)
	NiO	2.73	+10.1	
	MgO	2.68	+8.1	

These results demonstrate that dual functionalisation can significantly improve CO<sub>2</sub> adsorption performance, even from a base material with a lower initial capacity. HCS

shows lower adsorption capacity compared to commercial activated carbon, but the incorporation of multiple functional groups significantly enhances performance. This is especially significant considering the limitations of the pristine adsorbent. The findings suggest that even modest initial capacities can be substantially improved through dual functionalisation, leading to more effective CO<sub>2</sub> capture technologies.

#### **4.5 Isotherm analysis**

Based on the analysis on Chapter 4.4, the best performing adsorbent is HCS-N-Mg. Therefore, the following analysis covers the analysis of dual-functionalised adsorbent. For comparison purposes, pristine HCS properties were used to analyse the effect of dual-functionalisation. Based on the isotherm profile of CO<sub>2</sub> adsorption at temperature range of 25- 125 °C and set pressure range of 0-1.5 bar, isotherm analysis has been carried out. Four isotherm models including Langmuir, Freundlich, Temkin and Sips model have been applied. To select the appropriate model, nonlinear analysis has been carried out by using the Origin, and is selected based on the magnitude of regression coefficient ( $R^2$ ). Selection of the appropriate isotherm model is solely based on the estimated model parameters and regression coefficient ( $R^2$ ). This is in agreement with Raganati et al. (2018) who reported that consideration on the isotherm suitability is more clearly inferred from the analysis (i.e. model parameters and error function), rather than just from a mere observation of the adsorption isotherm plot. Nonlinear fitting was applied to determine each model and corresponding parameters and correlation coefficients ( $R^2$ ) for CO<sub>2</sub>, as detailed in Table 4.16 and Figures 4.36 and 4.37.

**Table 4.16: Adsorption isotherm constant and R-square values for carbon dioxide adsorption on bio-adsorbents**

Isotherm	Parameters	HCS			HCS-N-Mg		
		25°C	75°C	125°C	25°C	75°C	125°C
Langmuir	q <sub>m</sub> (mmol/g)	4.452	3.126	2.575	6.539	6.307	4.146
	K <sub>L</sub> (1/bar)	0.647	0.309	0.227	1.308	0.371	0.138
	R <sup>2</sup>	0.989	0.983	0.994	0.944	0.973	0.994
Freundlich	n	2.227	1.767	1.419	1.928	1.087	0.955
	K <sub>F</sub> (mmol/g.bar)	1.711	0.767	0.449	2.613	1.050	0.320
	R <sup>2</sup>	0.995	0.999	0.998	0.998	0.953	0.913
Sips	n	1.533	1.378	1.145	2.304	1.272	1.172
	q <sub>m</sub>	7.408	5.545	4.613	20.261	20.104	10.391
	b <sub>s</sub>	0.164	0.080	0.076	0.051	0.040	0.032
	R <sup>2</sup>	1.000	1.000	1.000	0.999	0.999	0.996
Temkin	b <sub>T</sub> (J/mol)	4817.6	8105.3	10213.3	2827.6	3359.9	8819.9
	K <sub>T</sub> (mmol/g.bar)	17.920	10.559	6.946	16.14	8.420	8.061
	R <sup>2</sup>	0.941	0.892	0.864	0.896	0.856	0.827

Figures 4.36 and 4.37 show the correlation between model data and isotherm data according to each isotherm. From the figure, Sips isotherm is the most compatible as the raw data (actual) and model data (predicted) are stacked between the model data and raw data line. All graph shows an exponentially increase pattern as the pressure increases. Sips isotherm accounts for surface heterogeneity, often observed in real-world adsorption systems (Sees et al., 2023). This makes it a more reliable model than the Langmuir isotherm, which assumes homogeneous surfaces, and the Freundlich isotherm, which assumes a logarithmic relationship between the adsorbate concentration and the adsorption capacity. Secondly, the Sips isotherm has a variable exponent, which allows it to fit a broader range of adsorption data than the Langmuir, Freundlich, and Temkin isotherms. This is particularly useful for carbon dioxide adsorption, which can exhibit non-ideal behavior at high pressures (Abunowara et al., 2023).

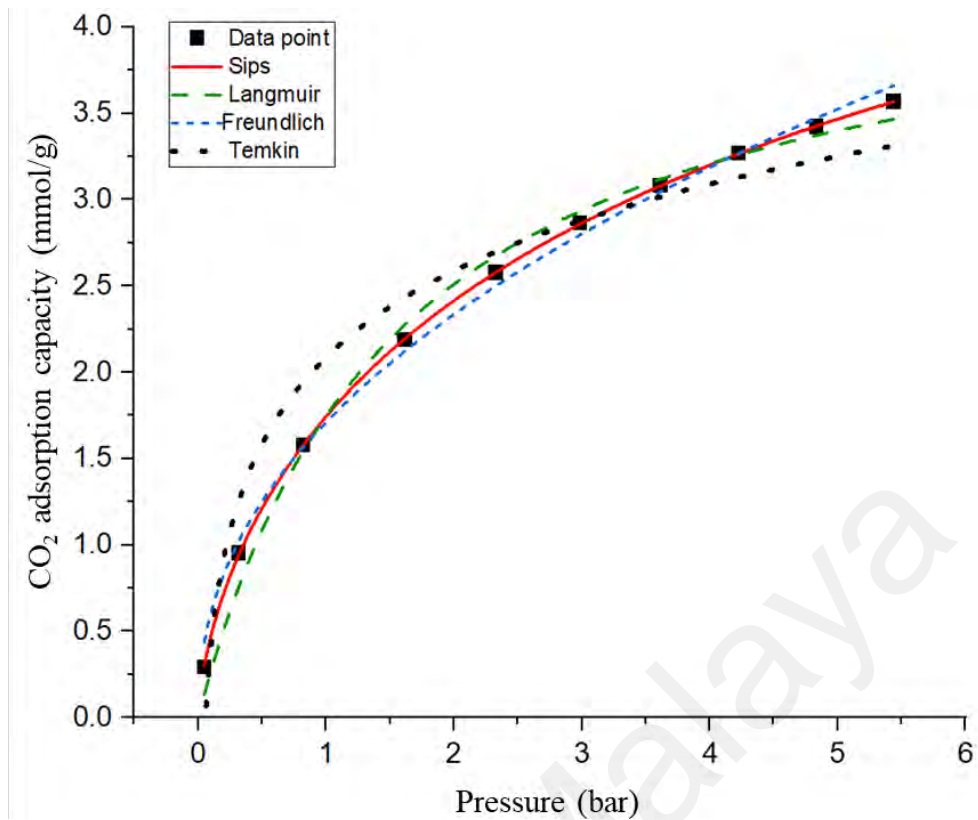


Figure 4.36: Nonlinear isotherm plots for HCS at 25 °C

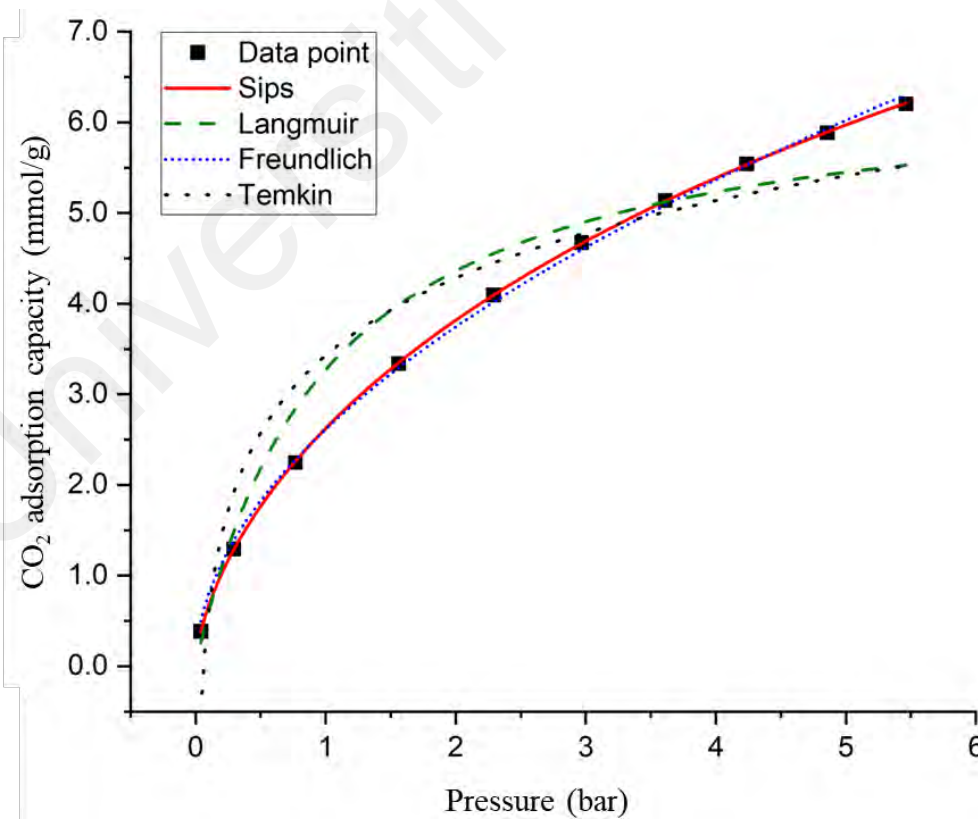


Figure 4.37: Nonlinear isotherm plots for HCS-N-Mg at 25 °C

HCS-N-Mg exhibits profound surface heterogeneity with an 'n' value of 2.3, while HCS demonstrates a moderate level of heterogeneity with 'n' equal to 1.5. This indicates a multilayer adsorption mechanism, which is more dominant in HCS-N-Mg, signifying higher accessibility of gas molecules deep into pores and a variety of adsorption sites for adsorbate binding (Fierascu et al., 2019; Maleki et al., 2023; Melouki et al., 2020).

Non-linear regression for Temkin isotherm is less suitable for analysing CO<sub>2</sub> adsorption as it does not consider the specific interactions between CO<sub>2</sub> and the adsorbent surface, which can lead to inaccuracies in the modelling of CO<sub>2</sub> adsorption (Mabuza et al., 2022). The Temkin isotherm assumes a linear relationship between the adsorption energy and the surface coverage, which is less accurate for CO<sub>2</sub> adsorption (Nandiyanto et al., 2020). CO<sub>2</sub> adsorption is a complex process that can exhibit non-linear behavior at high pressures, which is not accounted for in the Temkin isotherm (Mabuza et al., 2022). Furthermore, the Temkin isotherm implies that the heat of adsorption is inversely proportional to the coverage, which may not be accurate for CO<sub>2</sub> adsorption. CO<sub>2</sub> adsorption exhibits significant heat adsorption, especially at high pressures and low temperatures (Saleh, 2022). As tabulated in Table 4.16, the parameter n in the Sips isotherm model gradually decreases as the operating temperature increases from 25 °C to 125 °C. Precisely, a closer n value to unity at high adsorption temperature reduces the Sips model to the Langmuir model, implying the homogeneity of the CO<sub>2</sub>/bio-adsorbent system. In addition, Hamza et al. (2015) agreed that the Freundlich model describes CO<sub>2</sub> adsorption better at lower temperatures. However, the Langmuir isotherm model better represents the carbon dioxide adsorption capacity.



#### 4.6 Thermodynamic analysis

The fundamental thermodynamic parameters, including the change in enthalpy ( $\Delta H^\circ$ ), change in Gibbs free energy ( $\Delta G^\circ$ ), and change in entropy ( $\Delta S^\circ$ ) for HCS and HCS-N-Mg were tabulated in Table 4.17. The  $\Delta H^\circ$  values for carbon dioxide adsorption on the HCS and HCS-N-Mg are consistently negative across the 25–125°C. This implies that the adsorption of CO<sub>2</sub> onto developed adsorbents is exothermic, involving the release of energy. HCS-N-Mg adsorbents release higher energy than HCS during adsorption, as the  $\Delta H^\circ$  value of HCS increases from -13.238 kJ/mol to -20.452 kJ/mol. In addition, it corroborates the reduction in CO<sub>2</sub> adsorption capacity concerning adsorption temperature. Since the value of  $\Delta H$  is higher than 20 kJ/mole, it implies the dominance of physical adsorption, supported by weak chemisorption phenomena.

**Table 4.17: Thermodynamic Analysis Results**

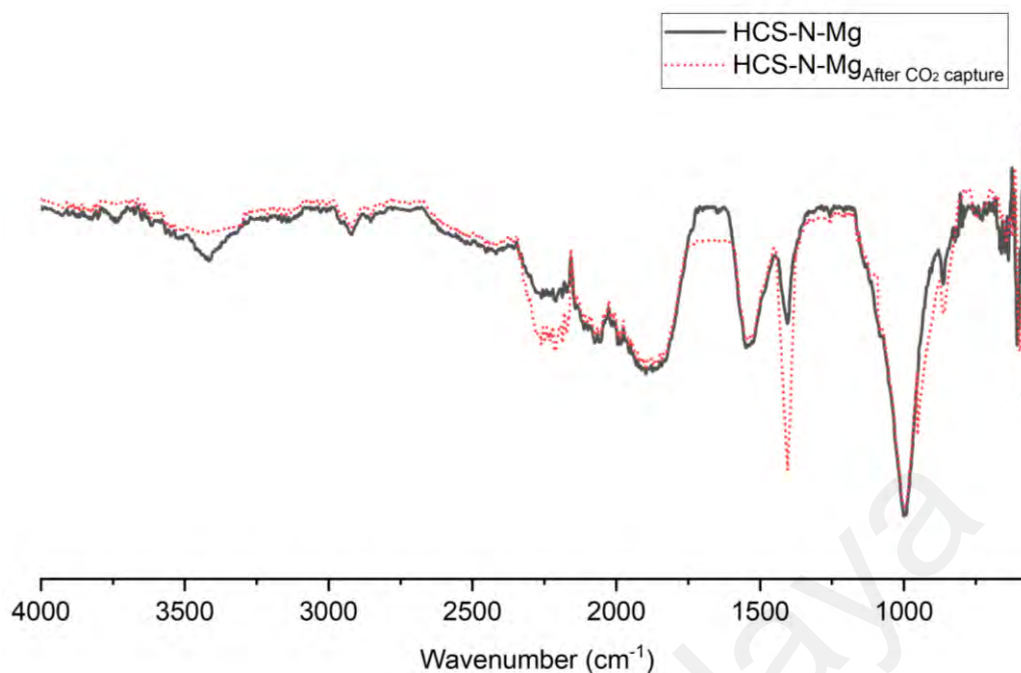
Sample	$\Delta H^\circ$ (kJ/mol)	$\Delta S^\circ$ (kJ/mol.K)	$\Delta G^\circ$ (kJ/mol)		
			298 K	348 K	398 K
HCS	-13.238	-0.0400	-1.3046	0.6964	2.6977
HCS-N-Mg	-20.452	-0.0599	-2.3810	-0.1412	3.7707

Additionally, the negative value of  $\Delta S^\circ$  implies the loss of entropy of CO<sub>2</sub> molecules during the adsorption process. CO<sub>2</sub> molecules exhibit random movement, especially in the gaseous state. However, when CO<sub>2</sub> are adsorbed by bio-adsorbent, CO<sub>2</sub> get arranged in an orderly manner on the carbon surface. This organized arrangement is responsible for the noticeable decrease in the  $\Delta S^\circ$  value. While negative  $\Delta G^\circ$  at 25°C and 75°C implies the feasibility and spontaneity of the CO<sub>2</sub> adsorption process at this adsorption condition (Pacze niak et al., 2018). At 298 and 348 K, HCS-N-Mg exhibits a negative  $\Delta G^\circ$ , indicating that the process can spontaneously occur and is thermodynamically favorable. However, the less negative  $\Delta G^\circ$  at elevated temperatures suggests a reduced

driving force for the adsorption process and a decreased tendency for the adsorption process to occur spontaneously at elevated temperatures. However, the value of  $\Delta G$  of HCS at elevated adsorption temperatures (75-125 °C) gradually increases and becomes positive, signifying a non-feasible process. Indeed, these findings are predictable because at high-temperature conditions, the desorption process is more dominant than the adsorption process. Raganati et al. (2018) reported in their studies that the  $\Delta G^\circ$  value of  $\text{CO}_2$  decreases with increasing temperature. These results were expected as the desorption process dominates over the adsorption process at higher temperatures (Head-Gordon et al., 1991). Negative values of  $\Delta H^\circ$ ,  $\Delta S^\circ$ , and  $\Delta G$  were observed at standard conditions, indicating that the adsorption of  $\text{CO}_2$  is spontaneous and is primarily driven by enthalpy. Dual-functionalisation of adsorbent increases the stability of  $\text{CO}_2$  adsorption at higher temperatures.

#### **4.7 Mechanism study**

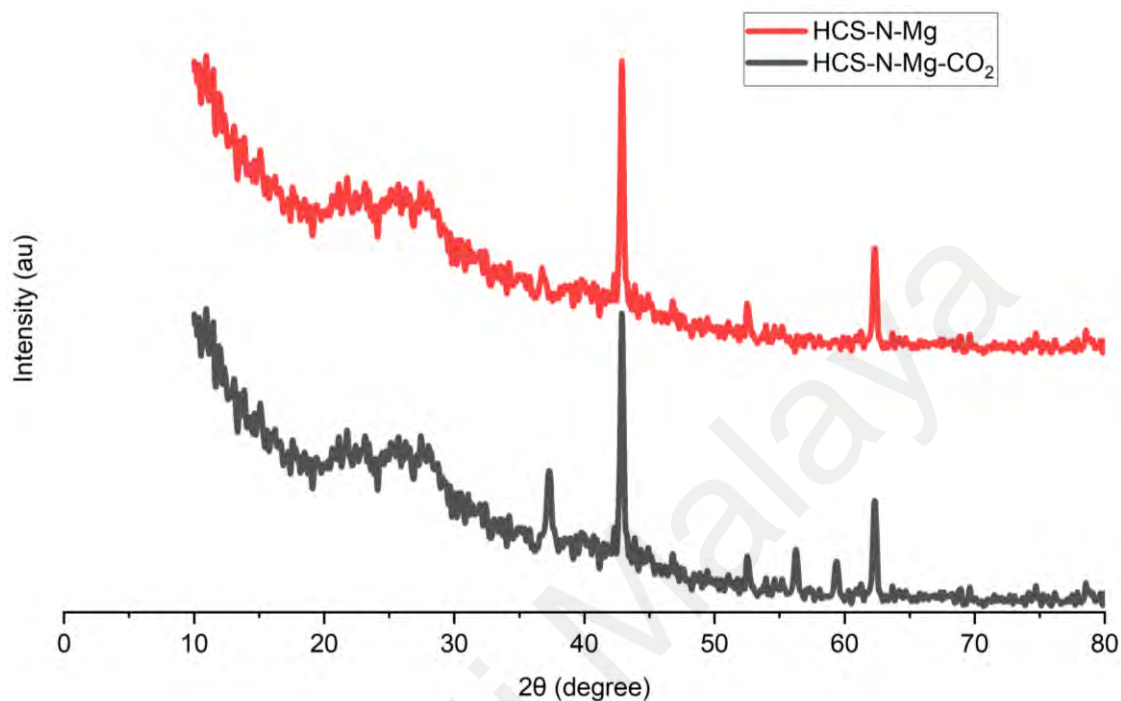
Characterise results of HCS-N-Mg before and after adsorption (Figure 4.38 and Figure 4.39) indicate that carbon dioxide involves a combination of physical and chemical interactions. Microalgae-functionalised groups act as Lewis bases, forming coordinate covalent bonds with  $\text{CO}_2$  molecules. This can be observed in the reduction of the N-H functional group at  $1630\text{ cm}^{-1}$  and N-O at  $1540\text{ cm}^{-1}$ . Concurrently, MgO contributes to Lewis acid sites, facilitating chemisorption and the formation of carbonate species on its surface. Hydrogen bonding, a dominant force in the interaction, plays a significant role, particularly between the oxygen atoms of  $\text{CO}_2$  and nitrogen functional groups



**Figure 4.38: FTIR of clean HCS-N-Mg and CO<sub>2</sub>-saturated HCS-N-Mg**

Additionally, the porous structure of bio-adsorbent facilitates physical adsorption through van der Waals forces. Electrostatic interactions, including diffuse adsorption, further contribute to the overall adsorption process. The positively charged sites on MgO and the partial charges on CO<sub>2</sub> lead to electrostatic attractions, enhancing adsorption efficiency. As a result, an increment of -OH bond was recorded in the infrared spectrum at 3400 cm<sup>-1</sup> after CO<sub>2</sub> adsorption. The monodentate and bidentate interaction between magnesium oxide and carbon dioxide was visible from the IR spectrum, in line with Wan Isahak et al. (2013) at wavenumber 1250 cm<sup>-1</sup> and 900 cm<sup>-1</sup>, respectively. The highest shift on the FTIR spectrum was recorded at 1500 cm<sup>-1</sup>, indicating a higher presence of non-coordinated CO<sub>3</sub>. Crystalline structure analysis on HCS-N-Mg before and after CO<sub>2</sub> adsorption further confirms the proposed adsorption mechanism. Addition peaks were recorded at 37.3°, 56.2°, and 59.3°, indicating the additional presence of MgCO<sub>3</sub> and MgOH. The synergistic effects of microalgae functional groups, MgO, and the activated hydrochar structure create a multifaceted adsorption system. These diverse interactions underscore the complexity of CO<sub>2</sub> adsorption onto this composite material, with

hydrogen bonding and electrostatic/diffuse adsorption playing essential roles in the comprehensive adsorption mechanism.



**Figure 4.39: Crystalline structure of HCS-N-Mg before and after adsorption**

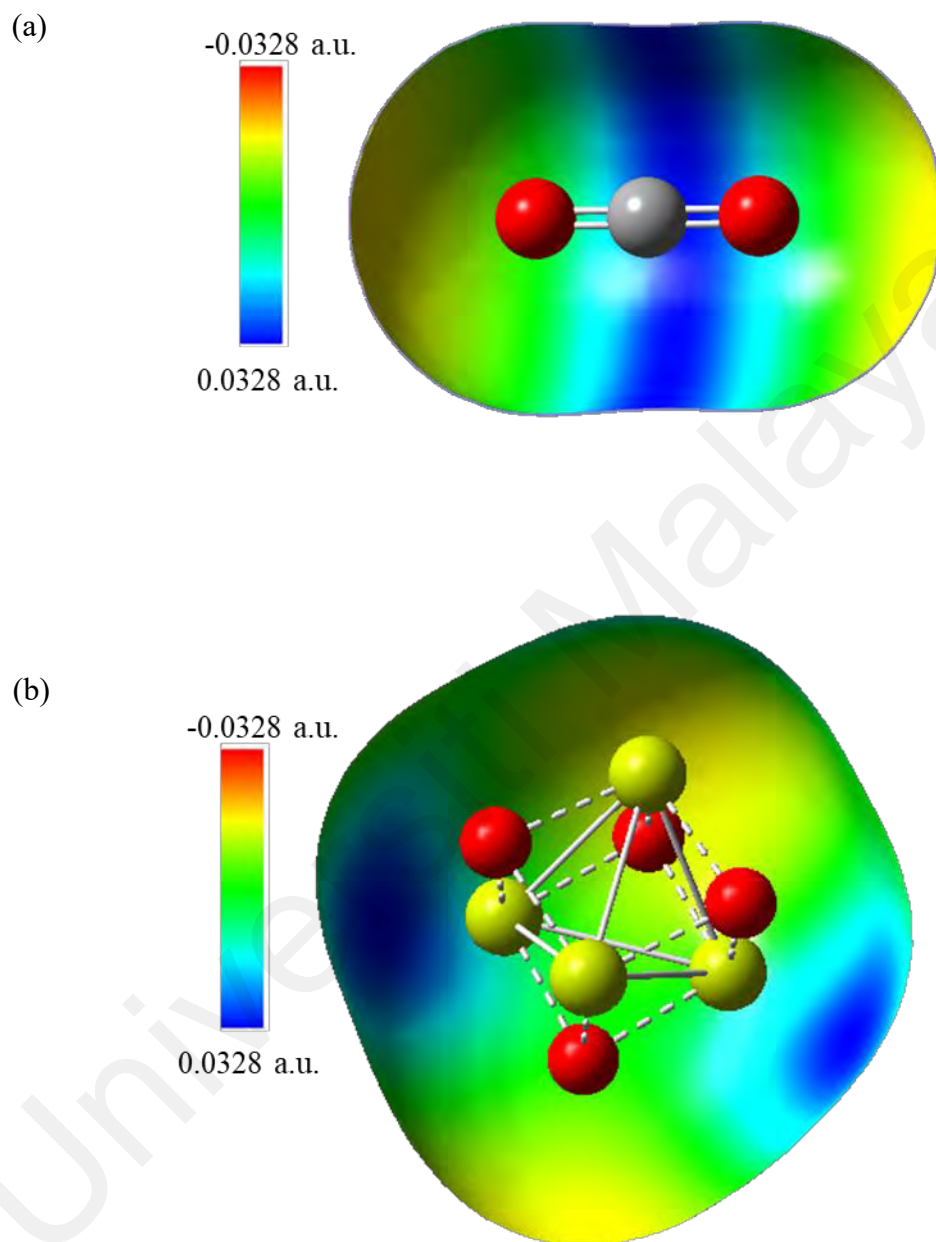
#### **4.8 Molecular modelling and simulation**

To investigate the presence of both physical and chemical adsorption mechanisms in CO<sub>2</sub> capture by dual-functionalised bio-adsorbents, density functional theory (DFT) simulations were employed to model the interaction of CO<sub>2</sub> molecules with the surfaces of HCS, HCS-N, MgO, and HCS-N-MgO composites. Analysis of highest occupied molecular orbital (HOMO), lowest unoccupied molecular orbital (LUMO) energies, electrostatic potential (ESP), binding distance, and adsorption energy were conducted to understand the interaction mechanisms and the efficiency of adsorption.

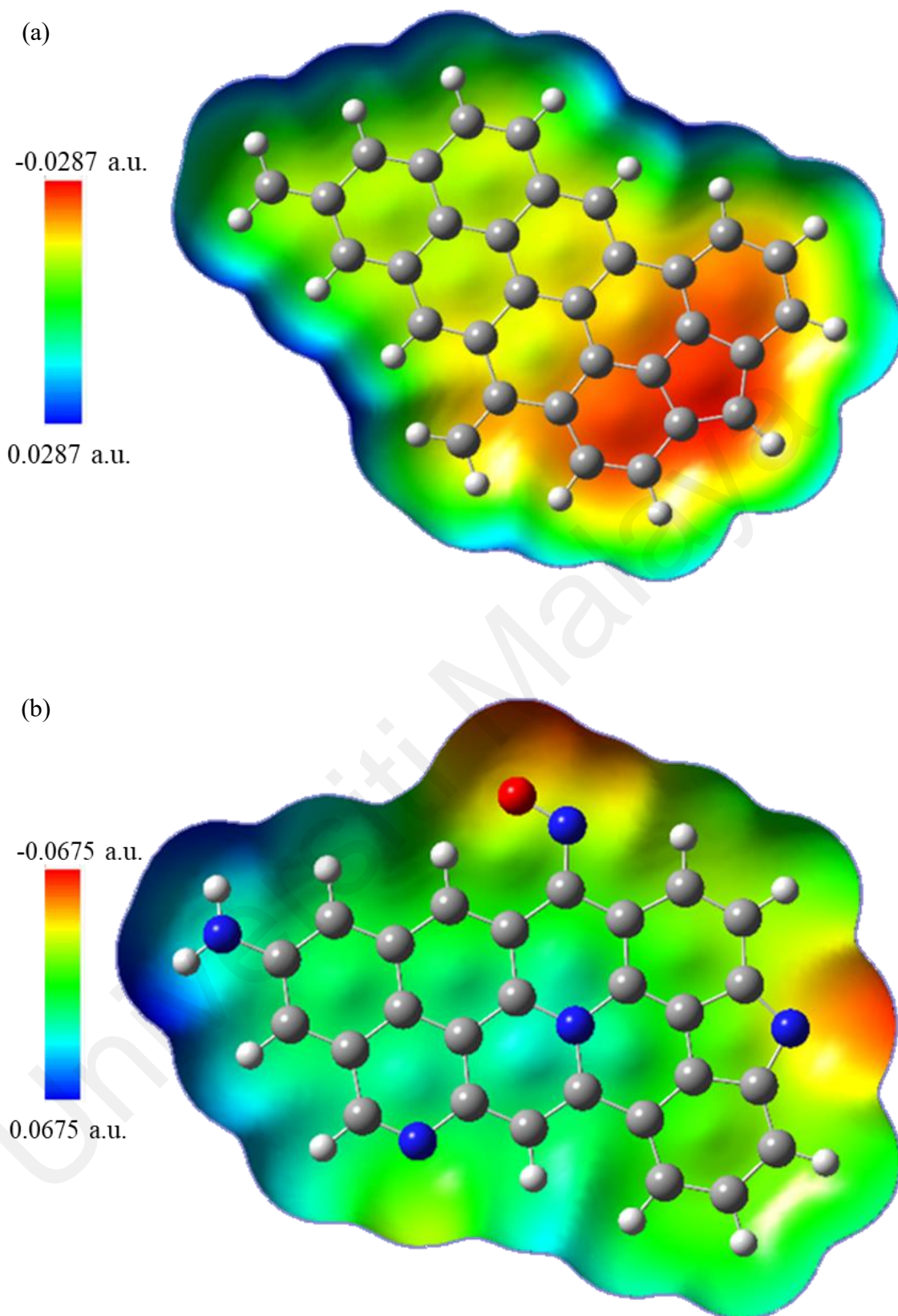
##### **4.8.1 Electrostatic potential analysis**

Electrostatic potential analysis was utilised to assess the influence of functionalisation on the electronic properties of the original CS bio-adsorbent model. Figures 4.40 (a)-(b)

and 4.41 (a)-(b) illustrate the ESP distributions of CO<sub>2</sub>, MgO, pristine HCS, and microalgae-functionalised HCS model respectively.



**Figure 4.40: Electrostatic potential of (a) CO<sub>2</sub>, and, (b) (MgO)<sub>4</sub> models**



**Figure 4.41: Electrostatic potential (a) HCS, and, (b) HCS-N-Mg models**

The figure visually represents electrostatic potential through the use of colour. Red areas signify regions of negative electrostatic potential, while blue areas indicate regions of

positive electrostatic potential. The intensity or depth of the colour, whether red or blue, directly corresponds to the magnitude of the electrostatic potential. A deeper colour signifies a higher value of potential, regardless of whether it's positive or negative. The ESP profile of the MgO molecule indicates a significant ionic character, which is evident from the distinct separation of charge within the molecule. The oxygen atoms exhibit regions of high negative potential, confirming their role as electron acceptors. This is consistent with the high electronegativity of oxygen, which draws electron density towards itself. Conversely, the magnesium atoms display regions of positive potential, aligning with their electron-donating nature due to their lower electronegativity (Jana et al., 2018).

Analysis shows that the pristine bio-adsorbent model demonstrates uniform electrostatic potential on its surface. Maximum value of electrostatic potential is detected at five-carbon ring region, indicating a variation in electron density or potential compared to the surrounding hexagonal carbon rings. In graphene, the  $\pi$ -electrons are typically delocalized over the entire structure (Jhaa et al., 2023). However, the introduction of a non-hexagonal ring can disrupt this delocalization, leading to localized regions of lower electron density. Similar finding was also reported by Bartashevich et al. (2023) in which modelling of defect-containing graphene resulted in electron delocalization that affects the electron density at critical bonding sites, with the density decreasing as one moves further away from the defect. Additionally, there is an observed variation of ESP at the boundary or end point of where the hydrogen atom is located in the molecular structure.

The electrostatic potential distribution of HCS shifted by the functionalisation with nitrogen functional groups. Introduction of pyrrole ( $\text{NH}_2$ ) onto the molecular structure, resulted in positive electrostatic potential. This suggests that the hydrogen atom acted as an electron acceptor, increasing the likelihood of an oxygen atom from a  $\text{CO}_2$  molecule

being attracted to and forming a bond with the pyrrole molecule through hydrogen binding. Formation of nitroso group (-N=O), resulted in partial positive charge on the nitrogen and a partial negative charge on the oxygen. This polarity can lead to dipole-quadrupole interactions between the nitroso group and CO<sub>2</sub>, in which the positive end of the CO<sub>2</sub> quadrupole (carbon) is attracted to the negative oxygen of the nitroso group, facilitating CO<sub>2</sub> adsorption. Consequently, this creates the potential for a Lewis acid-base interaction between the nitrogen of the nitroso group and the oxygen of a CO<sub>2</sub> molecule (Calcara & Caricaterra, 2023). Additionally, the positively charged magnesium ion (Mg<sup>2+</sup>) will be electrostatically attracted to this electron-rich oxygen atom, facilitating the formation of a bond.

The introduction of nitrogen atom within the ring also alters the electron distribution in the ring. As nitrogen has higher electronegativity compared to carbon, the ESP around nitrogen atom is slightly positive compared to the adjacent carbons due to the attraction of electron density towards the N-atoms. Additionally, the nitrogen atom disrupts the symmetry of the ring, further influencing the ESP distribution. These changes are particularly pronounced in the 5-membered ring due to its inherent ring strain, which enhances the effect of electronegativity of nitrogen atom. Consequently, the 5-membered ring likely exhibits the most significant ESP variations compared to the other two rings. The ESP results indicate that the functionalisation of N atoms caused a shift in the electron distribution within the bio-adsorbent model. This led to a non-uniform electrostatic potential and a subsequent change in surface polarity (J. Liu et al., 2022). Additionally, the scale range of ESP in HCS-N is wider compared to HSC, indicating more pronounced differences in electron density across the molecule.



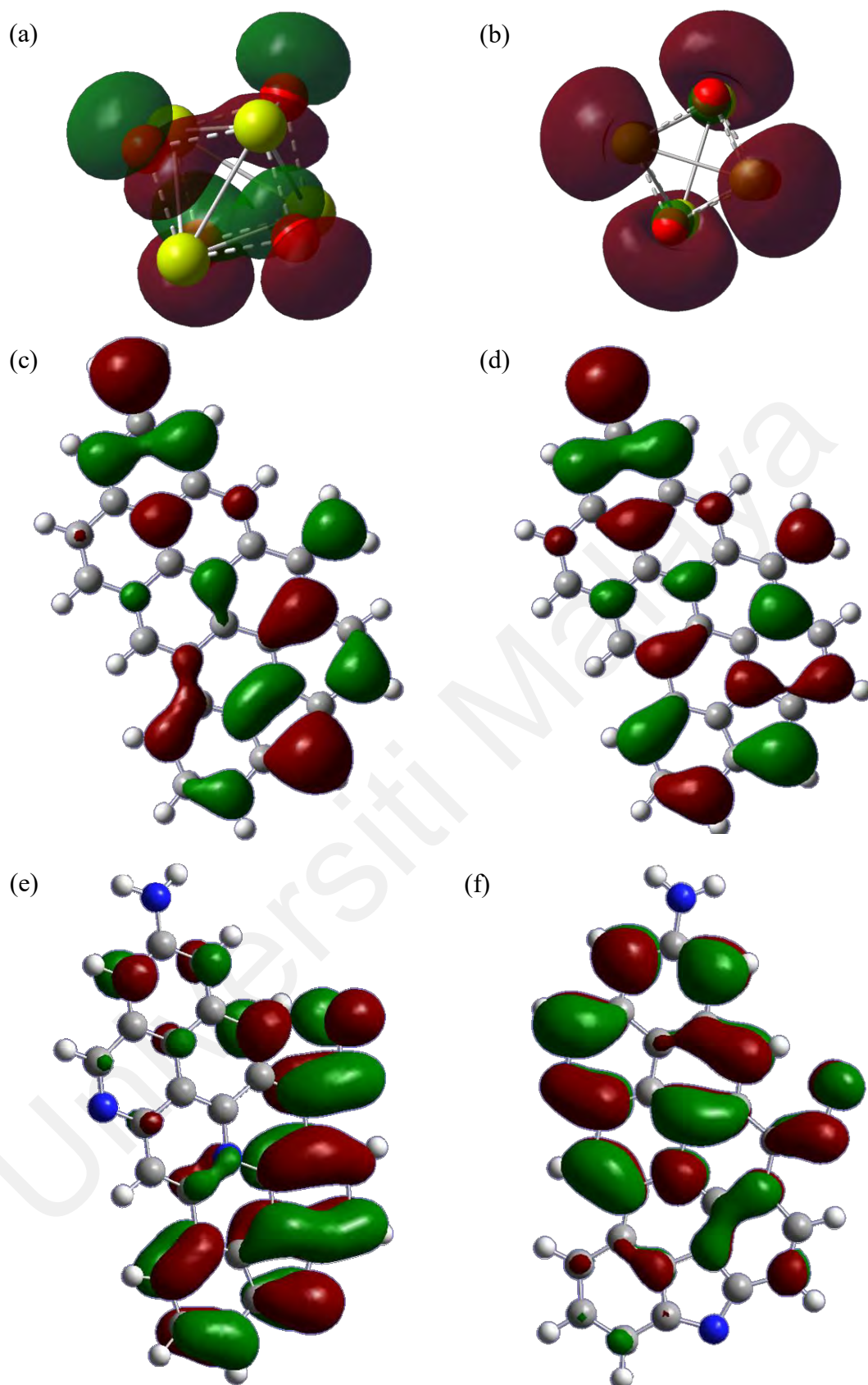
#### 4.8.2 Highest occupied and lowest unoccupied molecular orbital

In order to understand the chemical stability of the functionalised bio-adsorbent, HOMO and LUMO were conducted. The HOMO-LUMO gap will provide some insight on the chemical stability. Figure 4.42 illustrate the HOMO and LUMO of HCS, HCS-N and MgO. Based on Table 4.18, it was observed that for adsorbent, HCS-N has the smallest HOMO-LUMO gap of 2.496 eV, indicating that it is the most reactive. This small gap suggests that HCS-N can easily participate in electronic transitions, making it a good electron donor (Miar et al., 2021). This is consistent with its relatively high HOMO energy of -4.591 eV, which implies that the electrons in the HOMO are not tightly bound and can be donated easily. The energy gap between HOMO of bio-adsorbent (HCS and HCS-N) and LUMO of CO<sub>2</sub> is 4.880 eV and 4.591 eV respectively, whereas the energy gap between HOMO of CO<sub>2</sub> and LUMO of HCS and HCS-N is 7.612 eV and 8.376 eV respectively, suggesting that HCS and HCS-N donates electrons to CO<sub>2</sub> (Casares et al., 2022).

**Table 4.18: Highest occupied and lowest unoccupied molecular orbital of HCS, HCS-N, MgO and carbon dioxide**

Molecules	HOMO energy (eV)	LUMO energy (eV)	HOMO-LUMO energy gap (eV)
HCS	- 5.418	- 2.859	2.559
HCS-N	-4.591	-2.095	2.496
MgO	-6.039	-2.253	3.786
CO <sub>2</sub>	-10.471	-0.538	9.933

CO<sub>2</sub> has the largest HOMO-LUMO gap of 9.933 eV, indicating it is the most stable and least reactive among the listed molecules. This large gap suggests that CO<sub>2</sub> is a poor electron donor as it requires a significant amount of energy to excite an electron from the HOMO to the LUMO. The low HOMO energy of -0.538 eV further supports this, indicating that CO<sub>2</sub> holds onto its electrons tightly.

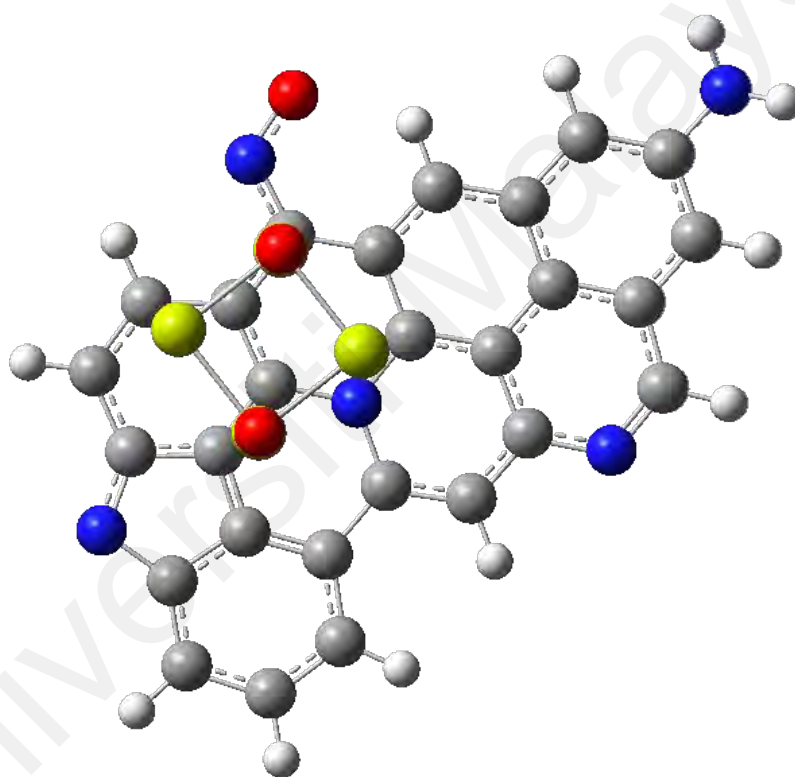


**Figure 4.42: (a) HOMO of MgO, (b) LUMO of MgO, (c) HOMO of HCS, (d) LUMO of HCS, (e) HOMO of HCS-N, and (f) LUMO of HCS-N**

Similarly, MgO has a high HOMO-LUMO gap of 3.786 eV, is relatively stable and less reactive than HCS and its microalgae-functionalised HCS. MgO is an ionic compound with a rock salt (NaCl) crystal structure, comprising  $Mg^{2+}$  and  $O^{2-}$  ions. The electronic structure of MgO is characterised by a distinct separation between the HOMO and LUMO, with the valence band primarily consisting of O 2p orbitals and the conduction band formed largely by Mg 3s orbitals. This significant band gap places the HOMO (valence band maximum) at a much lower energy level than the LUMO (conduction band minimum) (S. Hussain et al., 2021). Generally, MgO is not reactive in terms of electron donation or acceptance. However, the modelled  $(MgO)_4$  has a HOMO energy of -6.039 eV suggests it has a moderate tendency to donate electrons, though not as readily as HCS and HCS-N-Mg. In interactions with carbon matrix, MgO may accept electrons, particularly as carbon matrix tends to donate electrons due to its conductive properties and more favorable electronic structure.

Functionalisation of MgO onto HCS-N to synthesis dual-functionalised adsorbent (HCS-N-Mg), alter the electronic structure of the resulting composite material, leading to a modification of the HOMO-LUMO gap. The metal functionalisation process introduces new electronic states due to the interaction between the delocalized  $\pi$ -electrons of carbon matrix and the ionic nature of MgO. Li et al. (2021) also reported similar findings in which functionalisation of copper onto graphene resulted in delocalized conjugated  $\pi$  system in the graphene/metal interface, resulting in superior reactivity and thermal conductivity. The developed dual-functionalised bio-adsorbent emerge within the original band gap of MgO, resulting from the hybridization of the electronic states at the interface. Figure 4.43 illustrate the optimised structure of HCS-N-Mg. The  $(MgO)_4$  was overlaying on top of carbon matrix instead of embedded within it due to the distinct differences in their material properties and the nature of their interaction. Amorphous carbon matrix (HCS-N), differs fundamentally from crystalline

MgO resulting in challenging to embed graphene directly within the MgO matrix without extensive heating/calcination. Numerous studies corroborate the functionalisation of metal oxide onto graphene structure through overlaying. Studies by Al-Bagawi et al. (2020) and Husein et al. (2021) modelled iron, nickel and cadmium oxide functionalisation on graphene through overlying method and discovered that this modification results from the hybridization of electronic states, leading to the emergence of new states within the original band gap of the metal oxide.



**Figure 4.43: Top-view of optimised structure of HCS-N-Mg**

Functionalisation of MgO onto HCS-N resulted in elevation of HOMO level of the bio-adsorbent compared to the pure MgO, due to the contributions from carbon matrix. Similarly, the value of LUMO reduced significantly as carbon matrix introduce states within the band gap of MgO. This effect reduces the overall HOMO-LUMO gap of the composite material, making it smaller compared to pure MgO and bio-adsorbent. The narrowing of this gap enhances the charge transfer characteristic, resulted in higher

adsorption potential (R. Hussain et al., 2021). This phenomenon can be attributed to increased reactivity and the facilitated movement of electrons between the two energy levels, thereby influencing CO<sub>2</sub> adsorption.

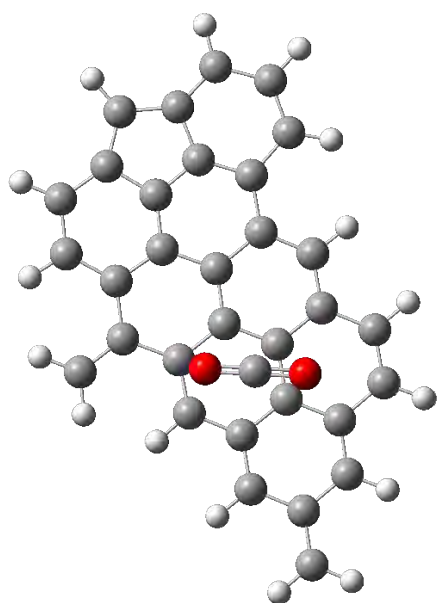
### 4.8.3 Adsorption energy and binding distance analysis

Prior to investigating the CO<sub>2</sub> adsorption on the HCS-N-Mg bio-adsorbent, the interaction of CO<sub>2</sub> with pristine HCS was computationally examined. Results illustrated in Figure 4.44 indicate a weak interaction between CO<sub>2</sub> and HCS, regardless of adsorption orientation. In contrast, Figure 4.45 illustrates that CO<sub>2</sub> readily interacts with the MgO surface, particularly at edge sites where its oxygen and hydrogen atoms interact with Mg and O atoms, respectively. This suggests that MgO surface reactivity is site-dependent, with edges and corners exhibiting stronger adsorption compared to defect-free faces, as supported by Añez et al. (2017). Similar behavior was observed in the CO<sub>2</sub>-HCS-N-Mg system (Figure 4.46). Adsorption energies for CO<sub>2</sub> complexes with various surface models were computed after geometry optimisation of the functionalised carbon surface and are presented in Table 4.19.

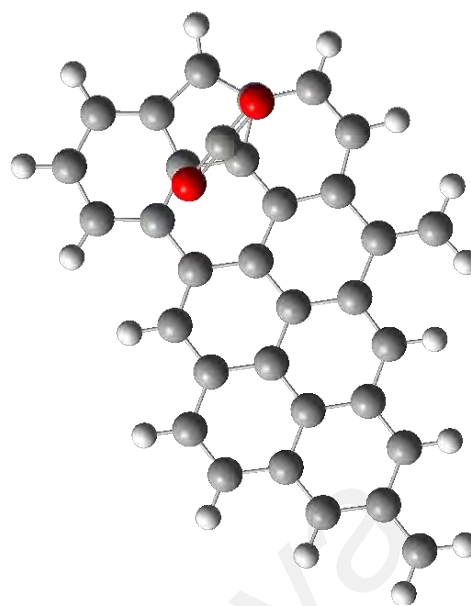
**Table 4.19: The binding distance and adsorption energy of CO<sub>2</sub> for pristine and dual-functionalised bio-adsorbent**

System	Binding Distance (Å)	Adsorption energy (kJ/mol)
CO <sub>2</sub> -HCS	3.721	-8.52
CO <sub>2</sub> -Mg	2.244	-38.92
CO <sub>2</sub> -HCS-N-Mg	2.243	-41.86

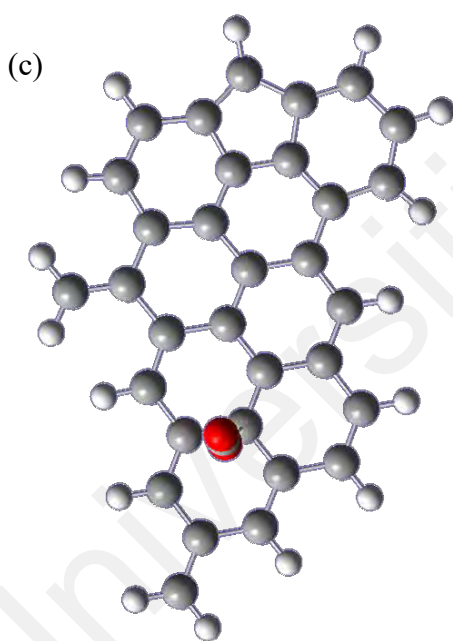
A higher degree of negative adsorption energy signifies a stronger adsorption capacity (Luhadiya et al., 2021). The data demonstrates that CO<sub>2</sub> interacts most strongly with (a) MgO, with an adsorption energy of -38.92 kcal mol<sup>-1</sup>, indicative of chemisorption. (b)



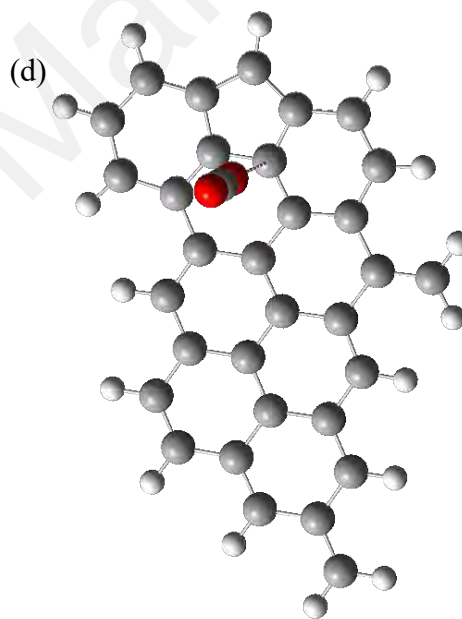
$$E_{ad} = -1.62 \text{ kcal/mol}$$



$$E_{ad} = -3.74 \text{ kcal/mol}$$

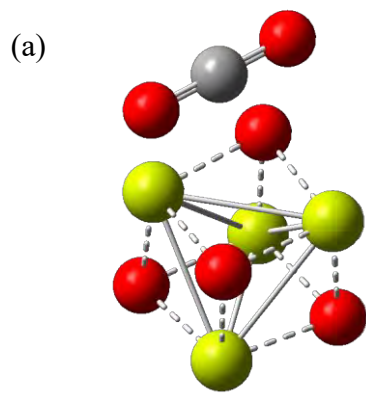


$$E_{ad} = -7.58 \text{ kcal/mol}$$

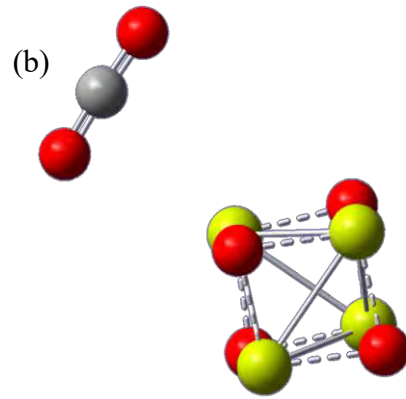


$$E_{ad} = -8.52 \text{ kcal/mol}$$

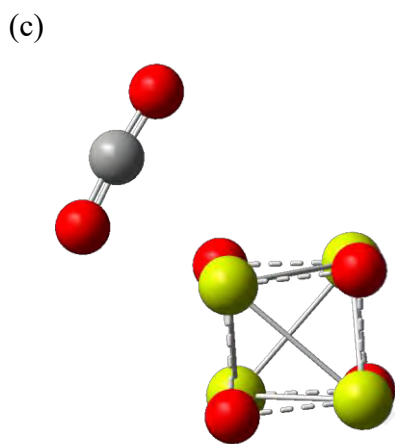
**Figure 4.44: Molecular interactions of HCS surface with CO<sub>2</sub>**



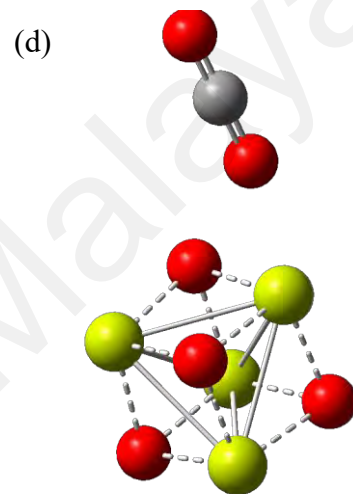
$$E_{ad} = -38.92 \text{ kJ/mol}$$



$$E_{ad} = -27.32 \text{ kJ/mol}$$



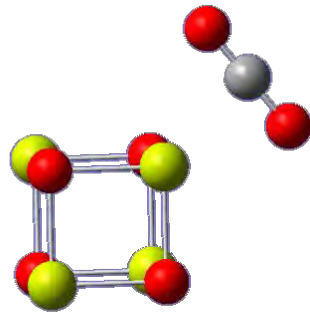
$$E_{ad} = -25.81 \text{ kJ/mol}$$



$$E_{ad} = -16.84 \text{ kJ/mol}$$

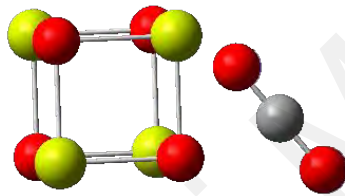
**Figure 4.45: Molecular interactions of MgO surface with CO<sub>2</sub>**

(a)



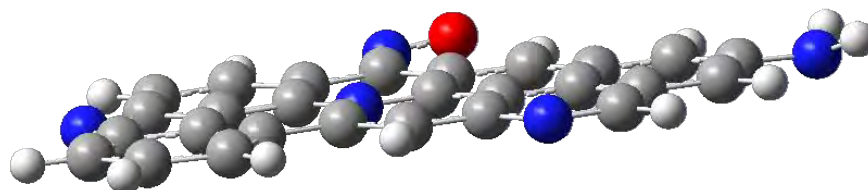
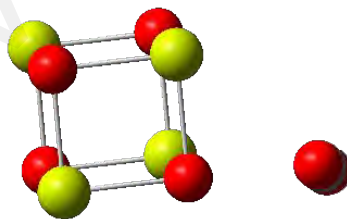
$$E_{ad} = -39.13 \text{ kJ/mol}$$

(b)



$$E_{ad} = -35.81 \text{ kJ/mol}$$

(c)

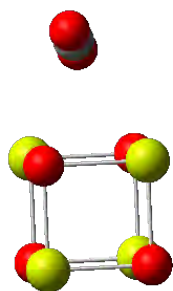


$$E_{ad} = -23.58 \text{ kJ/mol}$$

**Figure 4.46: Molecular interactions of HCS-N-Mg surface with CO<sub>2</sub>**

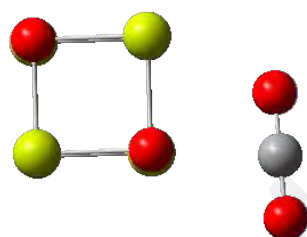


(d)



$$E_{ad} = -41.86 \text{ kJ/mol}$$

(e)



$$E_{ad} = -13.84 \text{ kJ/mol}$$

(f)

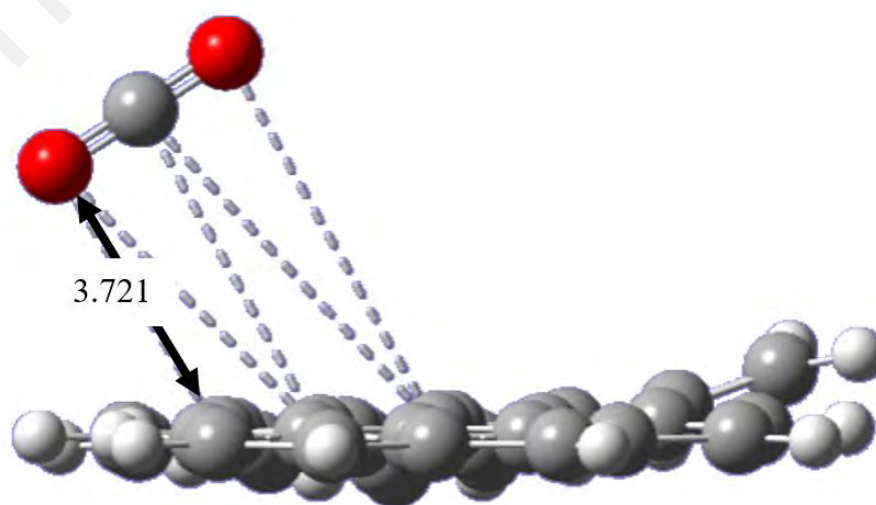


$$E_{ad} = -37.43 \text{ kJ/mol}$$

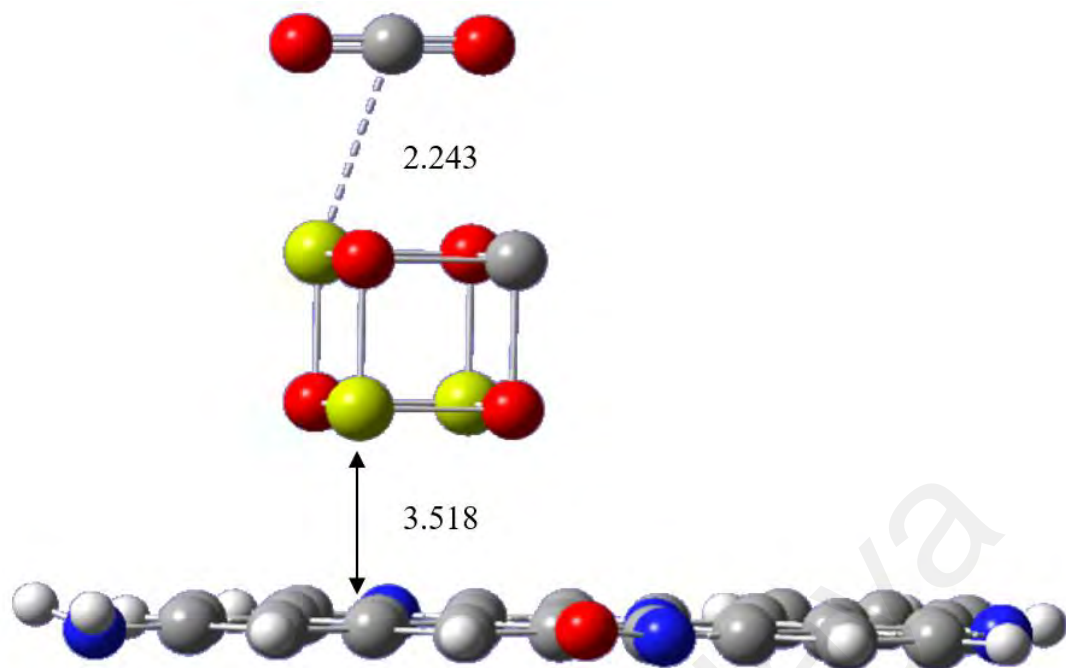
**Figure 4.46, continued**

In contrast, the adsorption energy for CO<sub>2</sub> on HCS is -8.52 kJ/mol, suggesting physisorption (Wei et al., 2022). This enhanced interaction with MgO can be attributed to the Lewis base sites provided by the pure MgO nanoparticles, which facilitate adsorption of the acidic CO<sub>2</sub> gas (Wang et al., 2023). Notably, the CO<sub>2</sub>-HCS-N-Mg system exhibits the highest binding energy at -41.86 kJ/mol, surpassing the sum of the individual energies for CO<sub>2</sub>-HCS and CO<sub>2</sub>-MgO. This result suggests a synergistic effect between MgO and N-functionalised HCS, promoting CO<sub>2</sub> adsorption.

The adsorbate-adsorbent equilibrium distance serves as a crucial indicator of adsorption strength. In this study, a shorter binding distance was observed between CO<sub>2</sub> and HCS-N-Mg (2.243 Å) compared to CO<sub>2</sub> and HCS (3.721 Å) as illustrated in Figure 4.47 and 4.48 respectively. A shorter distance typically implies a stronger interaction (Añez et al., 2017), highlighting the superior CO<sub>2</sub> adsorption capability of the dual-functionalised bio-adsorbent over pristine HCS. This suggests a strong affinity of CO<sub>2</sub> molecules towards the MgO component within the HCS. DFT calculations further corroborate these findings, revealing that dual functionalisation of HCS enhances charge transfer and substantiates the improved performance of HCS-N-Mg compared to HCS, thereby confirming the experimental observations.



**Figure 4.47: Side-view of interaction between CO<sub>2</sub> and HCS**



**Figure 4.48: Side-view of interaction between CO<sub>2</sub> and HCS-N-Mg**

#### 4.9 CO<sub>2</sub>/N<sub>2</sub> selectivity of bio-adsorbent

In post-combustion carbon capture, flue gas is often simplified to a CO<sub>2</sub>/N<sub>2</sub> binary mixture due to the negligible presence of other components besides water vapour. Acidic gases and particulate matter are typically removed in pre-treatment, leaving primarily CO<sub>2</sub> and N<sub>2</sub>. Given the prevalence of research on post-combustion CO<sub>2</sub> capture from N<sub>2</sub>, this study evaluates the effectiveness of bio-adsorbents in treating such pre-treated flue gas streams, aligning with the focus of many publications in this area (Rashidi & Yusup, 2017).

Selectivity modelling was executed to determine the suitability of HCS and HCS-N-Mg to be used as an adsorbent at standard pressure and temperature. To do so, isotherm analysis of purified N<sub>2</sub> for HCS and HCS-N-Mg were conducted and the findings were tabulated in Table 4.20. The adsorption isotherm of N<sub>2</sub> is best described by Langmuir, Freundlich, and Sips isotherm model with R<sup>2</sup> of 0.998-0.999. The result obtained suggests that the adsorption process exhibits characteristics of both monolayer

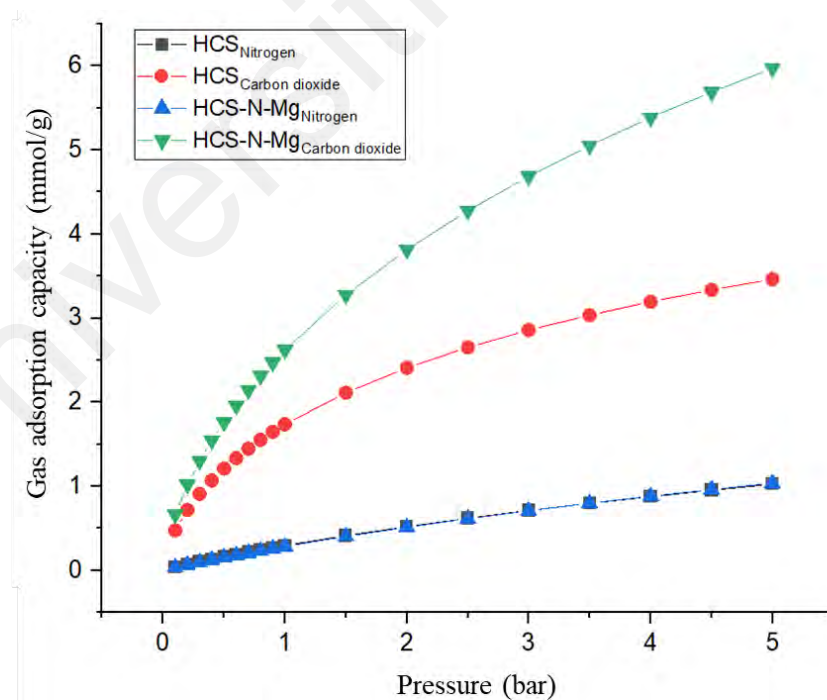
adsorption (Langmuir model) and heterogeneous or multilayer adsorption (Freundlich and Sips models).

**Table 4.20: Isotherm analysis of N<sub>2</sub> adsorption on HCS and HCS-N-Mg**

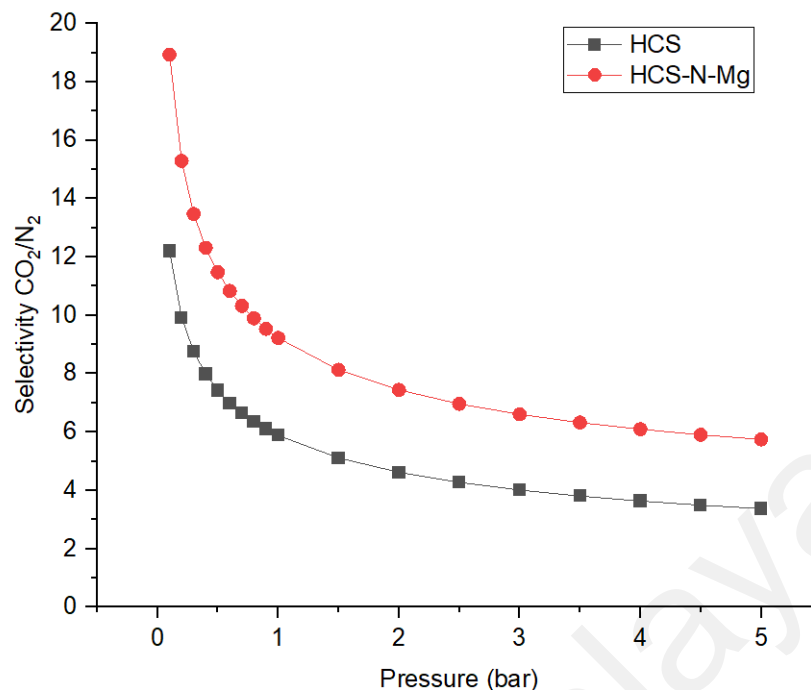
Isotherm	Parameters	HCS	HCS-N-Mg
		25°C	25°C
Langmuir	q <sub>m</sub> (mmol/g)	2.825	2.793
	K <sub>L</sub> (1/bar)	0.113	0.115
	R <sup>2</sup>	0.999	0.999
Freundlich	n	1.315	1.312
	K <sub>F</sub> (mmol/g.bar)	0.304	0.304
	R <sup>2</sup>	0.998	0.998
Sips	n	1.099	1.070
	q <sub>m</sub>	4.008	4.288
	b <sub>s</sub>	0.062	0.059
	R <sup>2</sup>	0.999	0.999
Temkin	b <sub>T</sub> (J/mol)	13682	10739
	K <sub>T</sub> (mmol/g.bar)	6.391	3.287
	R <sup>2</sup>	0.845	0.899

The adsorption capacity of HCS and HCS-N-Mg onto CO<sub>2</sub> and N<sub>2</sub> are illustrated in Figure 4.49. The results indicated that, at any given pressure, the adsorption capacity of HCS and HCS-N-Mg for N<sub>2</sub> was significantly lower than the adsorption capacity of CO<sub>2</sub>. Additionally, the CO<sub>2</sub> adsorption curves for HCS and HCS-N-Mg are more towards curve-shaped plots while N<sub>2</sub> adsorption curves exhibit linear-shaped isotherm. According to Rashidi and Yusup (2017), a curve-shaped isotherm represents favourable adsorption and equilibrium isotherm, while a linear-shaped isotherm implies weaker adsorption. Figure 4.50 demonstrates that the 'ideal selectivity' of CO<sub>2</sub>/N<sub>2</sub> decreases as pressure increases, eventually reaching a constant value. The declining selectivity at high pressure can be ascribed to the limited adsorption sites of the developed adsorbent (Liang et al., 2018). The initial slopes of nitrogen and carbon dioxide gas adsorption isotherms were analysed using the IAST equation to calculate the CO<sub>2</sub>/N<sub>2</sub> (50:50) selectivity, which was 18.93. This selectivity rate is higher than the averages reported

in previous studies by Hamyali et al. (2022) and Khalili and Jahanshahi (2021) at 9.55 and 12.08, respectively. These results indicate that both HCS and HCS-N-Mg are potential candidates for the adsorption and separation of carbon dioxide, with HCS-N-Mg demonstrating superior selectivity for CO<sub>2</sub> adsorption - showing an improvement of 41-57% across a pressure range of 0.1-5 bar. The increased CO<sub>2</sub> selectivity is attributed to the enhanced acid-base interactions resulting from the incorporation of algae and MgO into the structure. Principe and Fletcher (2020) and He et al. (2021) also reported a 25-33% improvement in selectivity using melamine and nitrogen-doped rice husk-derived adsorbents. Overall, in the context of post-combustion CO<sub>2</sub> adsorption, high CO<sub>2</sub>/N<sub>2</sub> selectivity refers to the high purity of CO<sub>2</sub> adsorbed by the activated carbons, as no other gas molecules (i.e. N<sub>2</sub> molecules) should be adsorbed during the adsorption process.



**Figure 4.49: CO<sub>2</sub> and N<sub>2</sub> adsorption isotherm onto HCS and HCS-N-Mg at 25°C**



**Figure 4.50: Selectivity of CO<sub>2</sub>/N<sub>2</sub> on HCS and HCS-N-Mg at 25°C**

#### 4.10 Reusability study

Long-term stability, durability, and regeneration of carbon dioxide adsorbents are critical for practical industrial applications. In this work, the reusability of hybrid adsorbent was also explored and benchmarked with the pristine bio-adsorbent. Figure 4.51 illustrates the cyclic carbon dioxide adsorption capacity of HCS and HCS-N-Mg over ten consecutive runs. This process encompasses the utilisation of the adsorbent in its initial, unsaturated form after the outgassing phase, ensuring it is devoid of contaminants. The findings suggest that both HCS and HCS-N-Mg exhibit minimal fluctuations in CO<sub>2</sub> adsorption capacity, identical to the adsorption capacity during the initial cycle, with a performance of 0.23% and 0.05%, respectively, in line with findings reported by Ravi et al. (2022), through CO<sub>2</sub> cyclic adsorption onto MgO- porous nitrogen-doped carbon. Notably, the observed reduction might be negligible, considering the machine accuracy of  $\pm 0.04\%$ . Despite the reduction in adsorption capacity of HCS and HCS-N-Mg over multiple cycles suggests partial irreversibility in the adsorption-desorption process.

However, the minimal variation in adsorption capability indicates that these bio-adsorbents possess remarkable reusability properties. Such a characteristic is due to the moderate intensity of adsorption or the significant surface compatibility these substances exhibit towards CO<sub>2</sub> molecules.

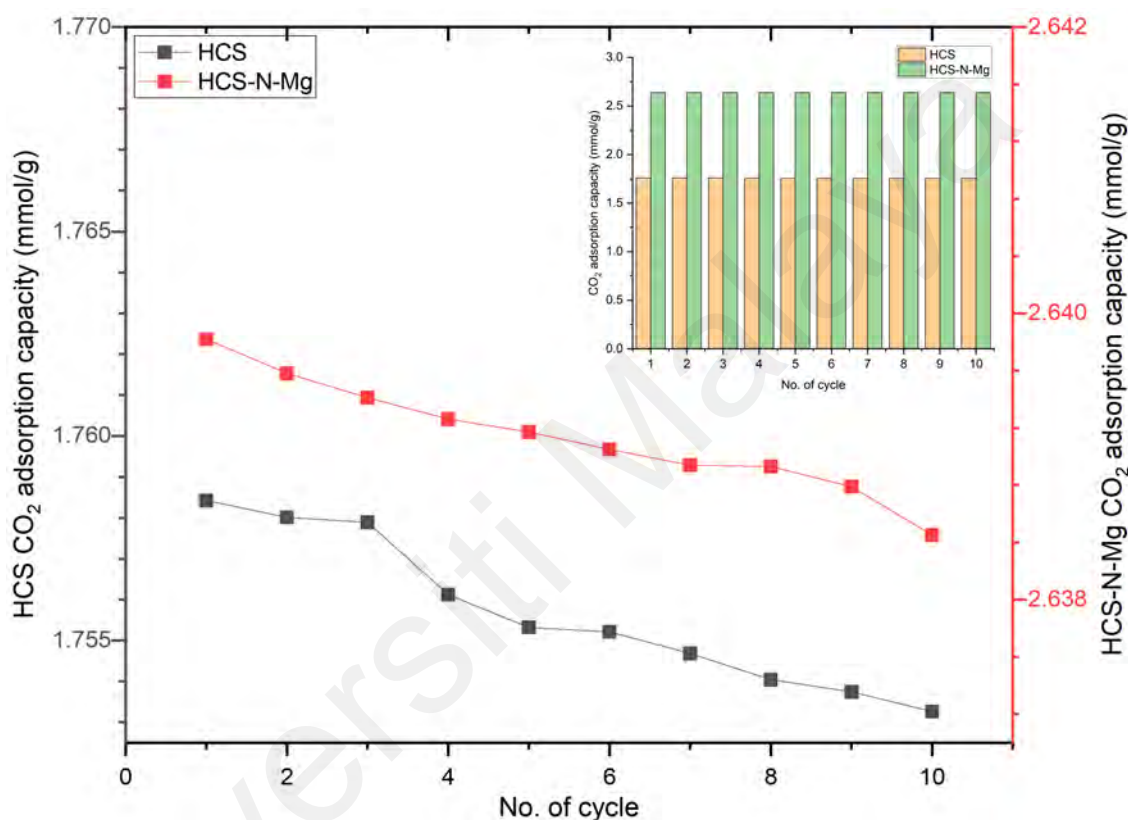


Figure 4.51: Cyclic CO<sub>2</sub> adsorption at 25°C and 1 bar.

#### 4.11 Comparison of adsorption performance of hybrid CS-bio-adsorbents with various activated carbon

The performance of HCS-N-Mg and its appropriateness to be regarded as a good adsorbent with high CO<sub>2</sub> adsorption were assessed by comparing it to the results of other adsorbents. Typically, the values for CO<sub>2</sub> adsorption with different adsorbents are as listed in Table 4.21. Comparing the CO<sub>2</sub> adsorption capability of commercial activated carbon with HCS-N-Mg can help assess the effectiveness of the production process and

the potential for dual-functionalised bio-adsorbents to be used in carbon capture and storage applications (Yang et al., 2019).

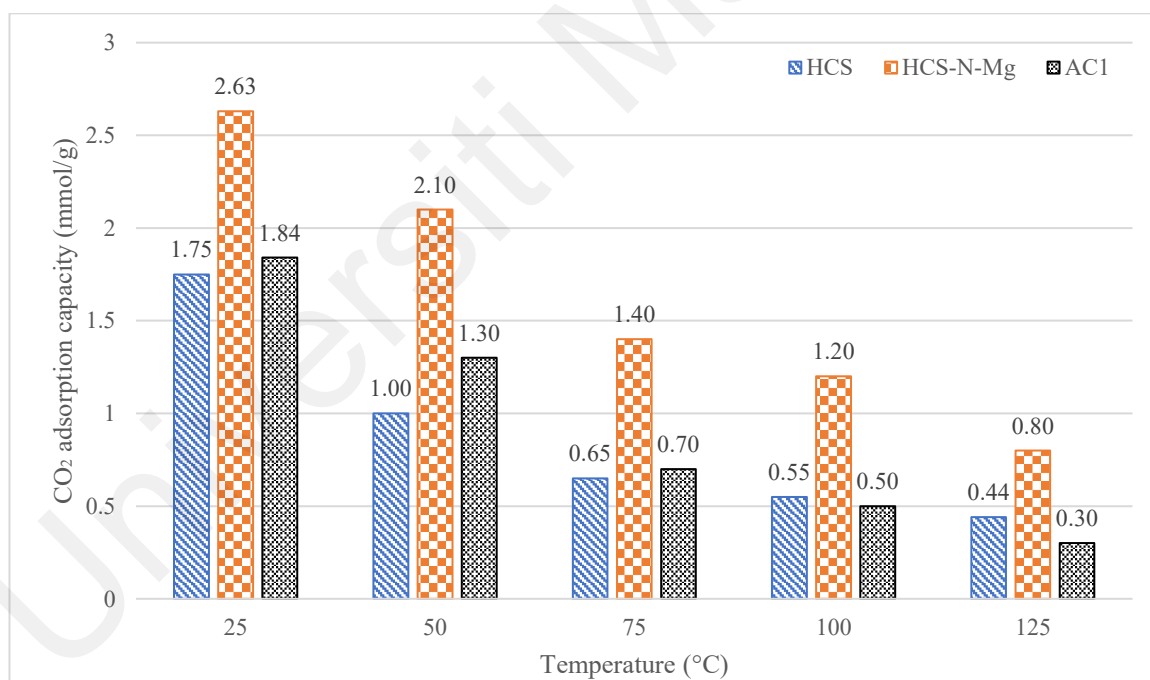
**Table 4.21: A comparison study of maximum CO<sub>2</sub> adsorption capacity (mmol/g) on various adsorbents (activated carbon)**

Adsorbent	Modification	Porosity	Adsorption capacity (mmol/g)	References
HCS	-	Microporous	1.75	This work
HCS-N-Mg	MgO + Algae	Micro & mesoporous	2.63	
Tea waste AC	KOH	Microporous	2.32	(Tahmasebpour et al., 2023)
Commercial AC	-	Mesoporous	1.37	
Bamboo	H <sub>3</sub> PO <sub>4</sub>	Microporous	1.45	(Ismail et al., 2022)
Garlic peel AC	KOH	Microporous	1.65	(Huang et al., 2019)
Chitosan AC	KOH	Microporous	2.97	(J. Wang et al., 2021)
Rubber seed shell AC	KOH	Microporous	1.23	(Fatima et al., 2022)
Rubber seed shell AC	K <sub>2</sub> C <sub>2</sub> O <sub>4</sub>	Microporous	2.16	

Table 4.21 demonstrates that both HCS and HCS-N-Mg exhibit strong CO<sub>2</sub> adsorption capabilities compared to other adsorbents such as garlic peel and rubber seed shell (RSS) AC with KOH activation chemical agent. Even though it is slightly lower than commercial AC with a difference of 0.09 mmol/g, it still has higher CO<sub>2</sub> adsorption capability than commercial PKSAC (Fatima et al., 2022). This underscores the potential of HCS and HCS-N-Mg as effective adsorbents. However, it is essential to conduct further analysis comparing these materials with commercial adsorbents at various operating temperatures to fully understand the benefits of dual functionalisation with microalgae and magnesium oxide.



Further comparison between HCS, HCS-N-Mg and commercial AC; AC1 (Figure 4.52) found that there is no significant difference between the CO<sub>2</sub> adsorption performance of HCS and AC1, as it shows that commercial AC only has slightly higher CO<sub>2</sub> adsorption than HCS (in this study). Even though commercial AC possess higher CO<sub>2</sub> adsorption, HCS still can be considered a good adsorbent, especially in our country as Malaysia is one of the world's largest producers of coconut, which means that coconut shell is readily available as a byproduct of this industry. Instead of burning or disposing of coconut shells that could bring harm to the environment, it is better to use them as CCS. As long as coconut is produced sustainably, coconut shell can be considered as renewable sources (Kumar & Saha, 2022).



**Figure 4.52: Comparison of commercial AC, HCS and HCS-N-Mg at different temperatures (1 bar)**

Nevertheless, this is cost-effective since there is no need to export or buy raw coconut shells from other countries as Malaysia possesses a lot of coconut plantations per year (Nor et al., 2020). Bio-adsorbent-based CS is less expensive than commercial AC (Gan,

2021). The lower CO<sub>2</sub> adsorption of HCS than commercial AC might be attributed to synthesis methods, chemical properties and surface area (Nille et al., 2021). Studies by Nowrouzi et al. (2018); Yang et al. (2017); Yue et al. (2018) have shown that certain activating methods, such as physical activation using CO<sub>2</sub>, chemical activation using phosphoric acid (H<sub>3</sub>PO<sub>4</sub>) and potassium carbonate (K<sub>2</sub>CO<sub>3</sub>), and dry-wet activation process, can produce activated carbon with high CO<sub>2</sub> adsorption capacity from lignocellulosic biomass. For chemical properties, activated carbon with a high density of oxygen-containing functional groups (such as carboxyl, hydroxyl, and carbonyl groups) has been shown to have higher CO<sub>2</sub> adsorption capacity (Wu et al., 2021).

#### **4.12 Commercialization prospects of dual-functionalised bio-adsorbent relative to pristine bio-adsorbent and with commercial activated carbon**

This section evaluates the commercialization prospects of dual-functionalized bio-adsorbents by benchmarking their performance, cost, and sustainability against pristine bio-adsorbents and commercial activated carbon. Tables 4.22 and 4.23 present the findings of the economic and environmental assessments.

##### **4.12.1 Economic analysis**

The economic feasibility of upscaling the dual-functionalized coconut shell bio-adsorbent for industrial-scale CO<sub>2</sub> capture was evaluated based on raw material costs, production scalability, and comparative performance with existing adsorbents. The primary raw materials—coconut shells, *Chlorella* microalgae, and magnesium oxide—are abundantly available and low-cost. Coconut shells, an agricultural waste product, typically discarded or incinerated, incur no procurement costs while mitigating environmental pollution (Gupta et al., 2024) Meanwhile, *Chlorella* microalgae, sourced as post-biofuel production waste eliminate cultivation expenses, whereas fresh

microalgae require processing costs of 5.90–14.16 USD/kg (Bhatt et al., 2022). Magnesium oxide, the third component in the system, is a cost-effective and widely utilized industrial chemical. Current market estimates from Chinese suppliers—including Hebei Suyou New Technology Co., Ltd. and Liaoning Metals and Minerals Enterprise Co., Ltd.—place its price at USD 0.30–0.50 per kilogram, reflecting its accessibility and affordability for industrial applications.

The production process involves simple functionalization steps, including pyrolysis, chemical activation, and impregnation, which are scalable and compatible with existing industrial infrastructure. Production costs are estimated at 3.52 USD/kg using waste microalgae and 10.49 USD/kg with fresh microalgae, markedly lower than conventional adsorbents such as Norit®SX2 activated carbon (343 USD/kg) and metal-organic frameworks (25 USD/kg) (Peng et al., 2022). Comparative cost analysis shows that the pristine and dual-functionalised bio-adsorbent synthesis cost (3.56 and 3.52 USD/kg respectively) undercuts commercial coconut shell-derived activated carbon (5.52 USD/kg) and chemically pure variants (28.06 USD/kg). Its adsorption capacity (115 mg/g) surpasses raw bio-adsorbents (77 mg/g), commercial coconut shell-activated carbon (70 mg/g), and chemically pure alternatives (81 mg/g). This demonstrates that the dual-functionalised bio-adsorbent not only reduces costs but also provides superior performance compared to widely used commercial alternatives.

**Table 4.22: Comparison of economic analysis of dual functionalised bio-adsorbent**

Adsorbent	Process	Unit cost (USD)	Net cost (USD)	Total cost - 15% overhead (USD)	Yield (%)	Total cost (USD/kg adsorbent)
Pristine Bio-adsorbent	Raw CS	0/kg (10 kg)	= 0.07 x (4.5+8.8+0.3+18.0) + 6 = 8.21	9.44	26.55	3.56
	HTC	0.07/kWh (1.5 kW, 220 °C, 3 h)				
	Pyrolysis	(4.4 kW, 700 °C, 2 h)				
	Grinding process	0.07/kWh (0.5 kW, 0.5 h)				
	Drying process	0.07/kWh (1.5 kW, 12 h)				
	KOH pellet	0.20/kg (30 kg)				
Functionalised Bio-adsorbent	Raw CS	0/kg (7 kg)	=0.22 + 0.07 x (4.5+8.8+0.3+7.1+18.0) + 6 =8.93	10.27	29.18	3.52
	MgO	0.50/kg (0.44 kg)				
	Algae	0/kg - (3 kg) spent or *5.9/kg – (3 kg) fresh				
	HTC	0.07/kWh (1.5 kW, 220 °C, 3 h)	Or	26.63*	30.61*	10.49*
	Pyrolysis	(4.4 kW, 700 °C, 2 h)				
	Grinding process	0.07/kWh (0.5 kW, 0.5 h)				
	Drying process	0.07/kWh (1.5 kW, 12 h)				
	KOH pellet	0.20/kg (30 kg)				
CAC - CS	-	5.52 / kg	-	-	-	5.52
Chemically pure AC	-	28.06 / kg	-	-	-	28.06

#### 4.12.2 Environmental analysis

The environmental sustainability of the dual-functionalized coconut shell bio-adsorbent was assessed through carbon footprint through life cycle analysis (LCA). The use of coconut shells, an agricultural waste product, mitigates the environmental burden associated with waste disposal and promotes circular economy principles. Similarly, the utilization of waste microalgae after lipid extraction reduces the environmental impact of biofuel production by repurposing a byproduct that would otherwise require disposal. *Chlorella* microalgae, whether in fresh or waste form, contribute to carbon neutrality due to their high photosynthetic efficiency, which sequesters CO<sub>2</sub> during their growth phase (You et al., 2022). Magnesium oxide, while energy-intensive to produce, is offset by its long-term stability and recyclability within the adsorption process.

Table 4.23 summarize the environmental impact of synthesis of bio-adsorbent as well as different scenario on waste valorisation and management. This analysis assumes a fossil-heavy energy grid, no methane recovery in landfills, and coconut shells as a waste feedstock, thereby avoiding the environmental burden of agricultural allocation. Process optimization, renewable energy integration, and methane capture could significantly alter these outcomes. The LCA results indicate that producing 1 ton of dual-functionalised bio-adsorbent via proposed methodology (HTC followed by pyrolysis), requires 2,500–3,500 kWh of energy. The majority of this consumption is attributed to heating during HTC (220°C) and pyrolysis (700°C), resulting in global warming potential (GWP) of 4,000–8,000 kg CO<sub>2</sub>eq and generating 10–16 m<sup>3</sup> of wastewater (Picone et al., 2024). In comparison, two-step pyrolysis (carbonization at 300°C followed by activation at 700°C) requires 30–40% more energy (approximately 4,000 kWh/ton) due to prolonged high-temperature processing. This leads to higher emissions (7,000–9,000 kg CO<sub>2</sub>eq) and the release of 5–10 kg of volatile organic compounds (VOCs) per ton (Gu et al., 2018). Meanwhile, production of industrial activated carbon, which

involves chemical activation (700°C) and steam activation (800–1,000°C), has the highest environmental impact, requiring 15,000–18,000 kg CO<sub>2</sub>eq emissions, and generating 200–300 kg of chemical-laden wastewater per ton due to the use of activation chemicals (Alhashimi & Aktas, 2017)

**Table 4.23: Environmental impact of synthesis of bio-adsorbent, waste valorisation and treatment**

Scenario	GWP (kg CO <sub>2</sub> eq)	Energy Use (kWh)	Chemical Use (kg)
HTC + Pyro	4,500–6,000	2,500–3,500	0–50
Two-Step Pyrolysis	7,000–9000	4,000–4,500	0–20
Activated Carbon	15,000–18,000	6,000–7,000	200–300 (H <sub>3</sub> PO <sub>4</sub> )
Incineration*	0 (biogenic)	-1,500 (offset)	0
Landfill**	20,000–34,000	0	0

\*Assumes energy recovery offsets fossil fuel use. \*\*Without methane capture.

For disposal, incinerating 4 tons of coconut shells releases 14,000 kg biogenic CO<sub>2</sub>, which is considered climate-neutral under ISO 14044 standards. However, it also generates 20–30 kg of nitrogen oxides (NO<sub>x</sub>) and 5–10 kg of particulate matter. Potential energy recovery from incineration can offset approximately 1,500 kWh of fossil fuel-based energy (Esfilar et al., 2021; Yong et al., 2019). Conversely, landfilling 4 tons of biomass resulted in emission of 800–1,200 kg of methane, equivalent to 20,000–34,000 kg CO<sub>2</sub>eq due to methane’s global warming potential, which is 25–34 times higher than CO<sub>2</sub> over a 100-year period. Additionally, landfilling produces 50–100 litres of organic leachate, posing environmental risks (Viegas et al., 2021)

In summary, valorisation of coconut shell into bio-adsorbent through hydrothermal carbonisation and pyrolysis emerges as the most sustainable approach. Coconut shells repurpose agricultural waste, circumventing methane emissions from decomposition,

while microalgae (particularly post-biofuel residues) avoid the water and fertilizer demands of virgin cultivation. The avoidance of additional step for functionalisation reduces cumulative energy demand by compared to nitrogen and MgO functionalized adsorbents produced via traditional routes. With lower emissions, reduced energy consumption, and minimal wastewater generation, this approach of bio-adsorbent synthesis offers a viable alternative compared to other valorisation technology.

#### **4.12.3 Feasibility of industrial upscaling of dual-functionalised bio-adsorbent**

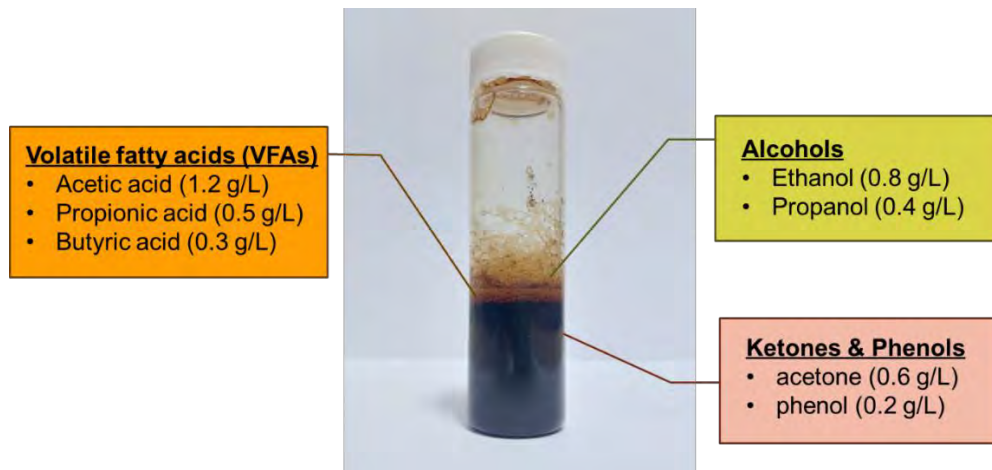
The feasibility of scaling up the production and application of the dual-functionalized coconut shell bio-adsorbent was evaluated based on technical, logistical, and regulatory considerations. The adsorbent's synthesis process is compatible with existing industrial equipment, such as rotary kilns and fluidized bed reactors, minimizing the need for capital-intensive infrastructure modifications (Darmey et al., 2022; Soni & Karmee, 2020; S. Wang et al., 2021; Zaccariello et al., 2022). The global availability of coconut shells and the scalability of *Chlorella* cultivation ensure a reliable supply chain for large-scale production.

Scaling up the production of the dual-functionalized bio-adsorbent, specifically activated hydrochar derived from coconut shell and functionalized with nitrogen using microalgae and MgO, presents several challenges. The large-scale production of dual-functionalised bio-adsorbent requires a substantial amount of coconut shell biomass, which may compete with food and animal feed markets (Archana et al., 2020). However, alternative lignocellulosic waste materials, such as palm kernel shell, have been identified as viable substitutes due to their similar chemical composition and properties. The functionalization process using microalgae and MgO may also necessitate specialized equipment and expertise, increasing production costs and potentially leading to inconsistencies in product properties that could affect CO<sub>2</sub> capture performance.

Additionally, HTC, a key process in dual-functionalised bio-adsorbent production, has limitations in large-scale implementation due to water usage concerns. However, recent advancements demonstrate that HTC can be scaled up, as seen in industrial facilities in Europe, China and the United States and worldwide, with capacities of 24-200 tons per day (Farru et al., 2024).

Moreover, water consumption in HTC can be minimised by recycling process water, which contains valuable compounds that can be upcycled into biofuels (Mathimani & Mallick, 2019). Figure 4.53 summarises the properties of process water obtained from the synthesis of dual-functionalised bio-adsorbent through the HTC stage of coconut shells and microalgae. It was found that the HTC process generates an acidic process water rich in organic compounds, offering further valorisation opportunities. GC-MS analysis revealed the presence of volatile fatty acids (VFAs) such as acetic acid (1.2 g/L), propionic acid (0.5 g/L), and butyric acid (0.3 g/L), alongside alcohols like ethanol (0.8 g/L) and propanol (0.4 g/L). These compounds can serve as substrates for biofuel production through anaerobic digestion, microbial electrosynthesis, or fermentation (Raj et al., 2022; Sharma et al., 2020; Stemann et al., 2013). Additionally, the detection of ketones like acetone (0.6 g/L) and phenols like phenol (0.2 g/L) shows potential applications in the synthesis of bio-based chemicals and resins (Basafa & Hawboldt, 2023). The estimated biofuel yield from the process water, based on VFA and alcohol content, is approximately 2.4 g/L, further emphasizing the potential of HTC for integrated biorefinery approaches.





**Figure 4.53: Process water from HTC consists of coconut shells and microalgae as precursors**

Despite these challenges, the feasibility of scaling up production remains promising. Dual functionalised bio-adsorbent has been successfully produced on a large scale with high yields and surface areas, and nitrogen functionalization using microalgae offers a renewable nitrogen source. MgO functionalization further enhances CO<sub>2</sub> capture capacity, and real-world applications have demonstrated high adsorption capacities and selectivity in flue gas CO<sub>2</sub> capture. Additionally, its CO<sub>2</sub> capture performance is comparable to commercial activated carbon and exhibits greater stability at higher temperatures, making it a suitable candidate for commercialization in industrial CO<sub>2</sub> capture applications.

## CHAPTER 5: CONCLUSION AND RECOMMENDATIONS

### 5.1 Conclusion

This study successfully achieved the first objective by employing a greener two-step activation technique to synthesize a coconut shell-based bio-adsorbent through hydrothermal carbonisation. The optimal process involved carbonisation at 220°C for 3 hours, followed by KOH activation at 700°C for 2 hours, achieving a yield of 25.5% and a CO<sub>2</sub> adsorption capacity of 1.75 mmol/g - HCS. Magnesium oxide-functionalised (HCS-Mg), microalgae-functionalised (HCS-N) and dual-functionalised bio-adsorbents (HCS-N-Mg) were successfully developed from coconut shell, *Chlorella* microalgae and MgO. Inclusion of 5-30% of MgO into CS bio-adsorbent through direct mixing improves the CO<sub>2</sub> adsorption capacity of activated carbon by 5%, 10%, 17% and 15% respectively. The optimal functionalisation of microalgae onto the CS bio-adsorbent was achieved through co-carbonisation, with microalgae comprising 30 wt.% of the total biomass weight. Co-carbonisation of coconut shell and microalgae impregnated with MgO further improved the adsorbent performance by 50% compared to pristine CS bio-adsorbent, 19% compared to co-carbonise adsorbent, and 28% compared to hybrid HCS-Mg. The study successfully achieved Objective 2 by demonstrating the improved physicochemical properties of functionalised bio-adsorbents. The result reveals that the dual functionalized adsorbent formed a mesoporous structure with a high specific surface area of 1044 m<sup>2</sup>/g. Analysis of functional groups shows the presence of hydroxyl (-OH), carbonyl (-CO-), and amine functional groups, contributing to efficient CO<sub>2</sub> adsorption. Sharp peaks were noted on MgO functionalised adsorbent indicating success functionalisation and presence of MgO crystalline structure.

Objective 3 was successfully achieved in which statistical analyses suggest that the adsorption capacity of HCS, HCS-Mg, HCS-N and HCS-N-Mg is influenced by pressure, temperature, and their interaction. Sensitivity analysis indicated that HCS-N

exhibited the highest sensitivity to adsorption temperature, suggesting instability at higher temperatures. HCS-N-Mg demonstrated optimal adsorption at 101°C and 4.6 bar, with a capacity of 3.27 mmol/g, suitable for post-combustion CO<sub>2</sub> capture. HCS and HCS-N-Mg maintained effective regeneration and stability across ten adsorption-desorption cycles, with HCS-N-Mg showing a lower performance loss of 0.05% compared to HCS (0.23%). The CO<sub>2</sub>/N<sub>2</sub> selectivity values of 12.20 for pristine bio-adsorbent and 18.93 for dual-functionalised adsorbent highlight their potential for flue gas applications. Objective 4 was successfully achieved with the pristine and dual-functionalised bio-adsorbents best fitted with a non-linear Sips isotherm model, suggesting multilayer adsorption. HCS-N-Mg exhibited a 53% higher heterogeneity index than HCS, indicating a more significant potential for various adsorption sites for CO<sub>2</sub> binding. The  $\Delta H^\circ$ ,  $\Delta S^\circ$ , and  $\Delta G^\circ$  of HCS-N-Mg indicate that adsorption is stable at 25-75°C.

Objective 5 was accomplished through Density Functional Theory simulations showed that functionalising the bio-adsorbents with nitrogen (HCS-N) and MgO significantly enhances their electronic properties and adsorption capabilities. The Electrostatic Potential analysis revealed increased polarity and more active sites for CO<sub>2</sub> adsorption due to these functional groups. Additionally, HOMO-LUMO gap analysis indicated that HCS-N is highly reactive, facilitating better electron donation. The adsorption energy studies confirmed that HCS-N-Mg exhibits the strongest CO<sub>2</sub> interaction, with an adsorption energy of -41.86 kJ/mol and a shorter binding distance of 2.246 Å, highlighting a substantial chemisorption process. In contrast, the pristine HCS showed a lower binding energy of -48.92 kJ/mol and a longer binding distance of 3.721 Å, demonstrating its comparatively weaker adsorption capability. This is attributed to the synergistic effect of MgO and nitrogen groups, which enhance the charge transfer capabilities of HCS-N-Mg.

The successful synthesis of a high-performance, dual-functionalised bio-adsorbent (HCS-N-Mg) from waste coconut shells, *Chlorella* microalgae and magnesium oxide represents a significant advancement in sustainable carbon capture technology. The remarkable 50% increase in CO<sub>2</sub> adsorption capacity compared to the pristine material, reaching 3.27 mmol/g under optimised conditions, highlighted the efficacy of the functionalisation strategy. The utilisation of waste biomass as a precursor not only aligns with the principles of a circular economy but also offers a cost-effective and environmentally friendly alternative to conventional adsorbents derived from coal and peat. The exceptional regeneration and stability of HCS-N-Mg over multiple adsorption-desorption cycles, coupled with its significantly enhanced adsorption capacity, establishes it as a highly promising candidate for post-combustion CO<sub>2</sub> capture applications. The findings of this research contribute to the development of innovative and sustainable solutions for mitigating climate change by effectively transforming waste into valuable resources for carbon capture and sequestration.

## **5.2 Significance of the study**

The knowledge gained from this study will contribute to synthesis of efficient CO<sub>2</sub> adsorbents using sustainable materials. When applied in industrial processes at post-combustion system, this bio-adsorbent can capture CO<sub>2</sub> emissions more effectively, thus reducing the environmental impact of such activities. The successful development of these dual-functionalised adsorbent from waste materials presents a promising approach to mitigate climate change by transforming solid waste into valuable carbon capture solutions. This directly supports Malaysia's goal of reducing CO<sub>2</sub> emissions by 45% by 2030, offering a practical and efficient solution for industrial carbon sequestration. Furthermore, utilising readily available biomass waste as a precursor for adsorbent synthesis not only promotes sustainable waste management practices but also addresses

the issue of greenhouse gas emissions associated with conventional waste disposal methods. In contrast to commercially used carbon-based adsorbents derived from expensive and non-renewable resources like coal or peat, this approach leverages low-cost waste materials, significantly enhancing economic viability and promoting wider adoption of carbon capture technologies. Ultimately, this research contributes to a circular economy model by transforming waste into valuable resources, while also taking a significant step towards mitigating climate change through effective carbon capture.

### 5.3 Knowledge contributions and novelty

This research makes significant contributions to the field of bio-adsorbent development through the innovative application of hydrothermal carbonization (HTC) processes for synthesizing CO<sub>2</sub> adsorbents from coconut shell.

1. The research introduces an efficient approach for microalgae functionalisation onto bio-adsorbent through co-hydrothermal carbonisation with coconut shell. This method offers a sustainable and efficient pathway to enhance the adsorbent's CO<sub>2</sub> capture capabilities
2. The study successfully synthesised a dual-functionalised bio-adsorbent, demonstrating a significant increase in surface area and the incorporation of targeted functional groups that facilitate efficient CO<sub>2</sub> adsorption.
3. The use of molecular modelling to gain insights into the interaction mechanisms between the bio-adsorbent, functionalised materials, and CO<sub>2</sub> gas molecules. This understanding aids in the design and development of more efficient adsorbents for carbon capture applications.

The novelty of this work lies in the dual functionalization strategy that combines magnesium oxide (MgO) and *Chlorella* microalgae, both of which are derived from sustainable sources. The introduction of MgO contributes basic sites, while *Chlorella*

microalgae introduce nitrogen functional groups that enhance the chemical affinity of the adsorbent for CO<sub>2</sub>. Additionally, the use of coconut shells as a precursor highlights the utilization of a green material, while *Chlorella* microalgae further emphasize the focus on eco-friendly resources. The study employs HTC, a green process, in conjunction with tailored activation techniques, leading to the production of high-surface-area bio-adsorbents with well-defined porosity, specifically optimized for CO<sub>2</sub> adsorption. This unique combination of materials and methods presents a novel pathway for developing highly efficient, sustainable bio-adsorbents tailored for carbon capture applications, promoting the use of environmentally friendly materials and processes in addressing the global carbon challenge.

#### **5.4 Potential Application**

The bio-adsorbent materials are effective in gas adsorption and purification processes. In CCUS technologies, bio-adsorbents can capture CO<sub>2</sub> emissions from power plants and industrial processes, aiding in climate change mitigation. The high surface area and porosity of bio-adsorbents allow for the trapping of CO<sub>2</sub>, preventing its release into the atmosphere. Additionally, these materials are applicable in water treatment to remove contaminants such as pesticides, herbicides, and organic pollutants, thus protecting aquatic life and human health. The developed bio-adsorbent can also function as catalysts in biodiesel production by facilitating the transesterification of vegetable oils. Due to their high surface area and reactivity, dual functionalised bio-adsorbent by using *Chlorella* microalgae and MgO are suitable for electrochemical capacitors, where they serve as electrode materials for energy storage and power delivery.

## 5.5 Recommendation for future work

While dual-functionalised adsorbent using *Chlorella* microalgae and magnesium oxide shows promise as a potential low-cost CO<sub>2</sub> adsorbent, the understanding of applicability in a more extensive scope is still lacking. Given the moisture content in flue gases, assessing the effect of humidity on adsorption performance is also essential. Moreover, the effect of initial CO<sub>2</sub> concentration on the adsorption capacity and efficiency of bio-adsorbents should be investigated. Since CO<sub>2</sub> concentration plays a crucial role in adsorption kinetics and equilibrium behavior, a more comprehensive understanding of its influence would enhance the development of efficient carbon capture materials. To achieve this, future research should consider using adsorption systems with adjustable CO<sub>2</sub> concentration control, allowing precise regulation of initial CO<sub>2</sub> levels. Employing dynamic breakthrough experiments or mixed-gas adsorption studies could provide deeper insights into how varying CO<sub>2</sub> concentrations affect adsorption performance. Additionally, it is essential to investigate how the presence of other gases—such as O<sub>2</sub>, CO, H<sub>2</sub>S, and methane—influences the selectivity and performance of the dual-functionalized bio-adsorbent for CO<sub>2</sub> capture. Industrial flue gases often contain multiple gas species, which may compete with CO<sub>2</sub> for adsorption sites or alter adsorption dynamics. Understanding these interactions would improve the practical applicability of bio-adsorbents in real-world scenarios. In this study, binary CO<sub>2</sub>-N<sub>2</sub> was investigated because post-combustion flue gas from power plants primarily consists of CO<sub>2</sub> (≈10–15%) and N<sub>2</sub> (≈75–80%), with smaller amounts of other gases. This approach ensures relevance to post-combustion CO<sub>2</sub> capture applications, where selective CO<sub>2</sub> separation from N<sub>2</sub> is the primary challenge. However, expanding future studies to include multi-component gas systems would provide a more comprehensive understanding of the bio-adsorbent's performance in complex gas environments.

In addition, exploring the effects of different microalgae species or metal oxides could potentially discover more effective combinations for adsorption. Long-term stability tests extending beyond ten cycles are crucial for assessing the reusability of adsorbent. Scaling up the research to pilot or industrial scales would provide insights into the practical applicability of the technology. For future research, it is recommended to pre-treat the biomass by soaking it in  $\text{Mg}(\text{OH})_2$  and  $\text{KOH}$  before subjecting it to the carbonization process at a temperature range of  $300\text{--}500^\circ\text{C}$ . This approach may enhance the structural stability and porosity of the resulting bio-adsorbent, leading to improved adsorption performance. In contrast to previous studies, HCS-N-Mg is classified as an intermediate-performing adsorbent. Many of the adsorbents developed in earlier research rely on energy-intensive processes such as pyrolysis and physical activation with  $\text{CO}_2$ , as well as the use of synthetic chemicals for functionalisation. Therefore, it is crucial to analyse the adsorption-to-energy ratio to gain deeper insights into the efficiency of the synthesised adsorbent. Comparative studies with other emerging materials, such as metal-organic frameworks, could position this technology within the broader  $\text{CO}_2$  capture landscape. Additionally, to facilitate CCU approaches, it is recommended to explore the potential of Mg-rich activated carbon for hydrogen adsorption, as it may serve as an effective hydride material. This approach might result in simultaneous advancement in both  $\text{CO}_2$  capture and hydrocarbon synthesis. These areas will help design efficient systems and reduce the technology's carbon footprint. Further research in this direction holds the key to unlocking the full potential of this eco-friendly and renewable resource in addressing carbon capture challenges.



## REFERENCES

- Abbas, M. (2021). Modeling of adsorption isotherms of heavy metals onto Apricot stone activated carbon: two-parameter models and equations allowing determination of thermodynamic parameters. *Materials Today: Proceedings*, 43, 3359-3364.
- Abd, A. A., Othman, M. R., Shamsudin, I. K., Helwani, Z., & Idris, I. (2023). Biogas upgrading to natural gas pipeline quality using pressure swing adsorption for CO<sub>2</sub> separation over UiO-66: Experimental and dynamic modelling assessment. *Chemical engineering journal*, 453, 139774.
- Abd, A. A., Shabbani, H. J. K., Helwani, Z., & Othman, M. R. (2022). Novel design of pressure swing adsorption using compact plates for adsorption heat recuperation of CO<sub>2</sub> capture in biomethane upgrading process. *Energy conversion and management*, 268, 115999.
- Abriyani, D., Ariyanto, T., & Prasetyo, I. (2022). Preparation of magnesium oxide confined in activated carbon synthesized from palm kernel shell and its application for hydrogen sulfide removal. IOP Conference Series: Earth and Environmental Science,
- Abunowara, M., Bustam, M. A., Sufian, S., Babar, M., Eldemerdash, U., Mukhtar, A., Ullah, S., Assiri, M. A., Al-Sehemi, A. G., & Lam, S. S. (2023). High pressure CO<sub>2</sub> adsorption onto Malaysian Mukah-Balingian coals: Adsorption isotherms, thermodynamic and kinetic investigations. *Environmental Research*, 218, 114905.
- Açıkyıldız, M., Gürses, A., & Karaca, S. (2014). Preparation and characterization of activated carbon from plant wastes with chemical activation. *Microporous and Mesoporous Materials*, 198, 45-49.
- Ahmad, R., Sulaiman, S., Suzana, Y., Dol, S. S., Inayat, M., & Umar, H. (2021, 06/01). Exploring the potential of coconut shell biomass for charcoal production. *Ain Shams Engineering Journal*, 13. <https://doi.org/10.1016/j.asej.2021.05.013>
- Al-Bagawi, A. H., Bayoumy, A. M., & Ibrahim, M. A. (2020). Molecular modeling analyses for graphene functionalized with Fe<sub>3</sub>O<sub>4</sub> and NiO. *Heliyon*, 6(7).
- Al-Ghouti, M. A., & Da'ana, D. A. (2020). Guidelines for the use and interpretation of adsorption isotherm models: A review. *Journal of hazardous materials*, 393, 122383.
- Al-Swaidan, H. M., & Ahmad, A. (2011). Synthesis and characterization of activated carbon from Saudi Arabian dates tree's fronds wastes. 3rd International conference on chemical, biological and environmental engineering,

- Al-Wabel, M. I., Rafique, M. I., Ahmad, M., Ahmad, M., Hussain, A., & Usman, A. R. (2019). Pyrolytic and hydrothermal carbonization of date palm leaflets: Characteristics and ecotoxicological effects on seed germination of lettuce. *Saudi journal of biological sciences*, 26(4), 665-672.
- Alhashimi, H. A., & Aktas, C. B. (2017). Life cycle environmental and economic performance of biochar compared with activated carbon: a meta-analysis. *Resources, Conservation and Recycling*, 118, 13-26.
- Alkadhem, A. M., Elgzoly, M. A., & Onaizi, S. A. (2020). Novel amine-functionalized magnesium oxide adsorbents for CO<sub>2</sub> capture at ambient conditions. *Journal of Environmental Chemical Engineering*, 8(4), 103968.
- Allwar, A., Hartati, R., & Fatimah, I. (2017). Effect of nitric acid treatment on activated carbon derived from oil palm shell. AIP Conference Proceedings,
- Almahbashi, N., Kutty, S., Ayoub, M., Noor, A., Salihi, I., Al-Nini, A., Jagaba, A., Aldhawi, B., & Ghaleb, A. (2021). Optimization of preparation conditions of sewage sludge based activated carbon. *Ain Shams Engineering Journal*, 12(2), 1175-1182.
- Ammendola, P., Raganati, F., & Chirone, R. (2017). CO<sub>2</sub> adsorption on a fine activated carbon in a sound assisted fluidized bed: Thermodynamics and kinetics. *Chemical engineering journal*, 322, 302-313.
- Añez, R., Sierraalta, A., & Soto, L. J. D. (2017). NO and NO<sub>2</sub> adsorption on subsurface doped MgO (100) and BaO (100) surfaces. A density functional study. *Applied Surface Science*, 404, 216-229.
- Archana, A., Vijay Pradhap Singh, M., Chozhavendhan, S., Gnanavel, G., Jeevitha, S., & Muthu Kumara Pandian, A. (2020). Coconut shell as a promising resource for future biofuel production. *Biomass valorization to bioenergy*, 31-43.
- Asnawi, T., Husin, H., Adisalamun, A., Rinaldi, W., Zaki, M., & Hasfita, F. (2019). Activated carbons from palm kernels shells prepared by physical and chemical activation for copper removal from aqueous solution. IOP Conference Series: Materials Science and Engineering,
- Atallah, E., Kwapinski, W., Ahmad, M. N., Leahy, J., & Zeaiter, J. (2019). Effect of water-sludge ratio and reaction time on the hydrothermal carbonization of olive oil mill wastewater treatment: Hydrochar characterization. *Journal of Water Process Engineering*, 31, 100813.
- Ateş, F., & Özcan, Ö. (2018). Preparation and characterization of activated carbon from poplar sawdust by chemical activation: Comparison of different activating agents

and carbonization temperature. *European Journal of Engineering and Technology Research*, 3(11), 6-11.

- Atif, M., Haider, H. Z., Bongiovanni, R., Fayyaz, M., Razzaq, T., & Gul, S. (2022). Physisorption and chemisorption trends in surface modification of carbon black. *Surfaces and Interfaces*, 31, 102080.
- Azevedo, V. G., Sartori, S., & Campos, L. M. (2018). CO<sub>2</sub> emissions: A quantitative analysis among the BRICS nations. *Renewable and Sustainable Energy Reviews*, 81, 107-115.
- Bae, Y.-S., Liu, J., Wilmer, C. E., Sun, H., Dickey, A. N., Kim, M. B., Benin, A. I., Willis, R. R., Barpaga, D., & LeVan, M. D. (2014). The effect of pyridine modification of Ni-DOBDC on CO<sub>2</sub> capture under humid conditions. *Chemical Communications*, 50(25), 3296-3298.
- Bai, B. C., Kim, E. A., Lee, C. W., Lee, Y.-S., & Im, J. S. (2015). Effects of surface chemical properties of activated carbon fibers modified by liquid oxidation for CO<sub>2</sub> adsorption. *Applied Surface Science*, 353, 158-164.
- Bala Dhull, S., Kumar Rose, P., Rani, J., Goksen, G., & Bains, A. (2024). Food waste to hydrochar: A potential approach towards the sustainable development goals, carbon neutrality, and circular economy. *Chemical Engineering Journal*. <https://doi.org/10.1016/j.cej.2024.151609>
- Bartashevich, E. V., Levina, E. O., Yushina, I. D., Sozykin, S. A., & Tsirelson, V. G. (2023). Electron delocalization in defect-containing graphene and its influence on tetrel bond formation. *Physical Chemistry Chemical Physics*, 25(36), 24342-24354.
- Basafa, M., & Hawboldt, K. (2023). A review on sources and extraction of phenolic compounds as precursors for bio-based phenolic resins. *Biomass Conversion and Biorefinery*, 13(6), 4463-4475.
- Bello, S. (2016, 07/01). PHYSICAL PROPERTIES OF COCONUT SHELL NANOPARTICLES. *KATHMANDU UNIVERSITY JOURNAL OF SCIENCE, ENGINEERING AND TECHNOLOGY*, 12, 63-79.
- Bhatt, A., Khanchandani, M., Rana, M. S., & Prajapati, S. K. (2022). Techno-economic analysis of microalgae cultivation for commercial sustainability: A state-of-the-art review. *Journal of Cleaner Production*, 370, 133456.
- Binti Mohd, N. A. (2017). *Conventional and microwave pyrolysis of empty fruit bunch and rice husk pellets* University of Sheffield].

- Boonpoke, A., Chiarakorn, S., Laosiripojana, N., Towprayoon, S., & Chidthaisong, A. (2011). Synthesis of activated carbon and MCM-41 from bagasse and rice husk and their carbon dioxide adsorption capacity. *Journal of Sustainable Energy & Environment*, 2(2), 77-81.
- Boonyoung, P., Treeweranuwat, P., Leewattanakarn, P., & Nueangnoraj, K. (2017). Hetero-atom Decoration of Activated Carbon without Post-Treatment. *Chemical Engineering Transactions*, 56, 1687-1692.
- Boyjoo, Y., Cheng, Y., Zhong, H., Tian, H., Pan, J., Pareek, V. K., Lamonier, J.-F., Jaroniec, M., & Liu, J. (2017). From waste Coca Cola® to activated carbons with impressive capabilities for CO<sub>2</sub> adsorption and supercapacitors. *Carbon*, 116, 490-499.
- Bumajdad, A., Khan, M. J. H., & Lukaszewicz, J. P. (2023). Nitrogen-enriched activated carbon derived from plant biomasses: a review on reaction mechanism and applications in wastewater treatment. *Frontiers in Materials*, 10, 1218028.
- Calcara, M., & Caricaterra, M. (2023). CO<sub>2</sub> dipole moment: a simple model and its implications for CO<sub>2</sub>-rock interactions. *Minerals*, 13(1), 87.
- Casares, R., Martínez-Pinel, Á., Rodríguez-González, S., Márquez, I. R., Lezama, L., González, M. T., Leary, E., Blanco, V., Fallaque, J. G., & Díaz, C. (2022). Engineering the HOMO–LUMO gap of indeno [1, 2-b] fluorene. *Journal of Materials Chemistry C*, 10(32), 11775-11782.
- Cecilia, J., Vilarrasa-García, E., García-Sancho, C., Saboya, R., Azevedo, D., Cavalcante Jr, C., & Rodríguez-Castellón, E. (2016). Functionalization of hollow silica microspheres by impregnation or grafted of amine groups for the CO<sub>2</sub> capture. *International Journal of Greenhouse Gas Control*, 52, 344-356.
- Ceyhan, A. A., Şahin, Ö., Baytar, O., & Saka, C. (2013). Surface and porous characterization of activated carbon prepared from pyrolysis of biomass by two-stage procedure at low activation temperature and its adsorption of iodine. *Journal of Analytical and Applied Pyrolysis*, 104, 378-383.
- Chen, C., & Ahn, W.-S. (2011). CO<sub>2</sub> capture using mesoporous alumina prepared by a sol-gel process. *Chemical Engineering Journal*, 166(2), 646-651.
- Chen, C., Yu, Y., He, C., Wang, L., Huang, H., Albilali, R., Cheng, J., & Hao, Z. (2018). Efficient capture of CO<sub>2</sub> over ordered micro-mesoporous hybrid carbon nanosphere. *Applied Surface Science*, 439, 113-121.
- Chen, L., Wen, C., Wang, W., Liu, T., Liu, E., Liu, H., & Li, Z. (2020). Combustion behaviour of biochars thermally pretreated via torrefaction, slow pyrolysis, or hydrothermal carbonisation and co-fired with pulverised coal. *Renewable Energy*, 161, 867-877.

- Chen, T., Deng, S., Wang, B., Huang, J., Wang, Y., & Yu, G. (2015). CO<sub>2</sub> adsorption on crab shell derived activated carbons: contribution of micropores and nitrogen-containing groups. *Rsc Advances*, 5(60), 48323-48330.
- Chen, W., Gong, M., Li, K., Xia, M., Chen, Z., Xiao, H., Fang, Y., Chen, Y., Yang, H., & Chen, H. (2020). Insight into KOH activation mechanism during biomass pyrolysis: Chemical reactions between O-containing groups and KOH. *Applied Energy*, 278, 115730.
- Cheng, K., Zhou, X., Wang, Y., Li, J., Shangguan, Y., Liu, H., Jiang, J., & Yi, P. (2023). Analysis of emission characteristics and driving forces of air pollutants and GHG from coal-fired industrial boilers in China. *Journal of Cleaner Production*, 430, 139768.
- Chi, Y., Zhang, Y., Li, G., Zhang, Q., Zhao, C., Liu, S., Yuan, L., Liu, S., & Song, Y. (2019). CO<sub>2</sub>/CH<sub>4</sub> adsorption property on shale from China for ESGR operation. *Energy Procedia*, 158, 5396-5401.
- Choi, J.-S., Kim, T.-H., Choo, K.-Y., Sung, J.-S., Saidutta, M., Ryu, S.-O., Song, S.-D., Ramachandra, B., & Rhee, Y.-W. (2005). Direct synthesis of phenol from benzene on iron-impregnated activated carbon catalysts. *Applied Catalysis A: General*, 290(1-2), 1-8.
- Chowdhury, Z. Z., Abd Hamid, S. B., Das, R., Hasan, M. R., Zain, S. M., Khalid, K., & Uddin, M. N. (2013). Preparation of carbonaceous adsorbents from lignocellulosic biomass and their use in removal of contaminants from aqueous solution. *BioResources*, 8(4), 6523-6555.
- Cong, H., Zhang, M., Chen, Y., Chen, K., Hao, Y., Zhao, Y., & Feng, L. (2015). Highly selective CO<sub>2</sub> capture by nitrogen enriched porous carbons. *Carbon*, 92, 297-304.
- Crippa, M., Oreggioni, G., Guizzardi, D., Muntean, M., Schaaf, E., Lo Vullo, E., Solazzo, E., Monforti-Ferrario, F., Olivier, J. G., & Vignati, E. (2019). Fossil CO<sub>2</sub> and GHG emissions of all world countries. *Publication Office of the European Union: Luxemburg*.
- Cruz, G., Rodrigues, A. d. L. P., da Silva, D. F., & Gomes, W. C. (2021). Physical-chemical characterization and thermal behavior of cassava harvest waste for application in thermochemical processes. *Journal of Thermal Analysis and Calorimetry*, 143(5), 3611-3622.
- Dabhane, H., Ghotekar, S., Tambade, P., Pansambal, S., Oza, R., & Medhane, V. (2021). MgO nanoparticles: Synthesis, characterization, and applications as a catalyst for organic transformations. *European Journal of Chemistry*, 12(1), 86-108.

- Darmey, J., Mensah, M., Adjah-Tetteh, C., Ntoni, G., Saaka, S. J., & Annor, L. P. (2022). Production of Activated Carbon in a Multi-Functional Platform Pilot Plant. *Ghana Mining Journal*, 22(2), 8-14.
- Das, D., & Meikap, B. (2021). Removal of CO<sub>2</sub> in a multi stage fluidised bed reactor by monoethanolamine impregnated activated carbon. *Mineral Processing and Extractive Metallurgy*, 130(2), 98-104.
- Das, S. (2014). *Characterization of activated carbon of coconut shell, rice husk and Karanja oil cake*
- De Mena Pardo, B., Doyle, L., Renz, M., & Salimbeni, A. (2016). Industrial scale hydrothermal carbonization: new applications for wet biomass waste. *Bremerhaven, Germany: ttz Bremerhaven*.
- de Mora, A., Diaz de Tuesta, J. L., Pariente, M. I., Segura, Y., Puyol, D., Castillo, E., Lissitsyna, K., Melero, J. A., & Martínez, F. (2024). Chemically activated hydrochars as catalysts for the treatment of HTC liquor by catalytic wet air oxidation. *Catalysis Today*, 429. <https://doi.org/10.1016/j.cattod.2023.114462>
- Deng, L., Shi, J., Zhao, Y., Feng, D., Zhang, W., Yu, Y., & Sun, S. (2024). Straw-based biochar prepared from multi-step KOH activation and its structure-effect relationship of CO<sub>2</sub> capture under atmospheric/pressurized conditions via experimental analysis and MD/DFT calculations. *Chemical Engineering Journal*, 153403.
- Diaz-Maroto, C. G., Verdugo, F., Feroso, J., Pizarro, P., Serrano, D. P., Moreno, I., & Feroso, J. (2024, Oct 1). Hydrochars derived from real organic wastes as carbonaceous precursors of activated carbons for the removal of NO from contaminated gas streams. *Sci Total Environ*, 945, 173897. <https://doi.org/10.1016/j.scitotenv.2024.173897>
- Dongardive, S. N., Mohod, A. G., & Khandetod, Y. P. (2019). Slow Pyrolysis Of Coconut Shell To Produce Crude Oil. *International Journal of Innovation in Engineering and Technology*, 12(3), 94-97. <https://doi.org/10.21172/ijiet.123.13>
- Du, X., Cheng, Y., Liu, Z., Yin, H., Wu, T., Huo, L., & Shu, C. (2021). CO<sub>2</sub> and CH<sub>4</sub> adsorption on different rank coals: A thermodynamics study of surface potential, Gibbs free energy change and entropy loss. *Fuel*, 283, 118886.
- Duan, Y., & Sorescu, D. C. (2010). CO<sub>2</sub> capture properties of alkaline earth metal oxides and hydroxides: A combined density functional theory and lattice phonon dynamics study. *The Journal of chemical physics*, 133(7), 074508.
- Duran-Jimenez, G., Monti, T., Titman, J. J., Hernandez-Montoya, V., Kingman, S., & Binner, E. (2017). New insights into microwave pyrolysis of biomass: Preparation of carbon-based products from pecan nutshells and their application

in wastewater treatment. *Journal of Analytical and Applied Pyrolysis*, 124, 113-121.

Elhenawy, S. E. M., Khraisheh, M., AlMomani, F., & Walker, G. (2020). Metal-organic frameworks as a platform for CO<sub>2</sub> capture and chemical processes: Adsorption, membrane separation, catalytic-conversion, and electrochemical reduction of CO<sub>2</sub>. *Catalysts*, 10(11), 1293.

Elmouwahidi, A., Bailón-García, E., Pérez-Cadenas, A. F., Maldonado-Hódar, F. J., & Carrasco-Marín, F. (2017). Activated carbons from KOH and H<sub>3</sub>PO<sub>4</sub>-activation of olive residues and its application as supercapacitor electrodes. *Electrochimica Acta*, 229, 219-228.

Emahi, I., Sakyi, P. O., Bruce-Vanderpuije, P., & Issifu, A. R. (2019). Effectiveness of Raw versus Activated Coconut Shells for Removing Arsenic and Mercury from Water. *Environment and Natural Resources Research*, 9(3). <https://doi.org/10.5539/enrr.v9n3p127>

Esfilar, R., Bagheri, M., & Golestani, B. (2021). Technoeconomic feasibility review of hybrid waste to energy system in the campus: A case study for the University of Victoria. *Renewable and Sustainable Energy Reviews*, 146, 111190.

Essa, M. H., Al-Zahrani, M. A., & Nesaratnam, S. (2013). Optimisation of activated carbon production from date pits. *International Journal of Environmental Engineering*, 5(3), 325-338.

Esterlita, M. O., & Herlina, N. (2015). Pengaruh penambahan aktivator ZnCl<sub>2</sub>, KOH, dan H<sub>3</sub>PO<sub>4</sub> dalam pembuatan karbon aktif dari pelepah aren (Arenga Pinnata). *Jurnal Teknik Kimia USU*, 4(1), 47-52.

Fadhil, A. B., & Kareem, B. A. (2021). Co-pyrolysis of mixed date pits and olive stones: Identification of bio-oil and the production of activated carbon from bio-char. *Journal of Analytical and Applied Pyrolysis*, 105249.

Fakher, S., & Imqam, A. (2020). High pressure-high temperature carbon dioxide adsorption to shale rocks using a volumetric method. *International Journal of Greenhouse Gas Control*, 95, 102998.

Farru, G., Scheufele, F. B., Moloeznik Paniagua, D., Keller, F., Jeong, C., & Basso, D. (2024). Business and market analysis of hydrothermal carbonization process: roadmap toward implementation. *Agronomy*, 14(3), 541.

Fatima, S. S., Borhan, A., Ayoub, M., & Ghani, N. A. (2022). CO<sub>2</sub> adsorption performance on surface-functionalized activated carbon impregnated with pyrrolidinium-based ionic liquid. *Processes*, 10(11), 2372.

- Fatima, S. S., Borhan, A., Ayoub, M., & Ghani, N. A. (2023). Modeling of CO<sub>2</sub> Adsorption on Surface-Functionalized Rubber-Seed Shell Activated Carbon: Isotherm and Kinetic Analysis. *Processes*, *11*(10), 2833.
- Feng, P., Li, J., Wang, H., & Xu, Z. (2020). Biomass-based activated carbon and activators: preparation of activated carbon from corncob by chemical activation with biomass pyrolysis liquids. *ACS omega*, *5*(37), 24064-24072.
- Ferrer, D. I. (2016). *Supported layered double hydroxides as CO<sub>2</sub> adsorbents for sorption-enhanced H<sub>2</sub> production*. Springer.
- Fierascu, I., DIMA, S. O., AVRAMESCU, S. M., CALOIAN, F., & Fierascu, R. C. (2019). Facile removal of pesticides from aqueous solutions using magnetic nanocomposites. *Rev. Chem*, *70*, 3931-3934.
- Fiuza-Jr, R. A., Andrade, R. C., & Andrade, H. M. C. (2016). CO<sub>2</sub> capture on KOH-activated carbons derived from yellow mombin fruit stones. *Journal of Environmental Chemical Engineering*, *4*(4), 4229-4236.
- Fonseca, J., Albis, A., & Montenegro, A. R. (2018). Evaluation of zinc adsorption using cassava peels (*Manihot esculenta*) modified with citric acid. *Contemp Eng Sci*, *11*, 3575-3585.
- Foo, P., & Lee, L. (2010). Preparation of activated carbon from parkia speciosa pod by chemical activation. *Proceedings of the World Congress on engineering and computer science*,
- Fu, M.-M., Mo, C.-H., Li, H., Zhang, Y.-N., Huang, W.-X., & Wong, M. H. (2019). Comparison of physicochemical properties of biochars and hydrochars produced from food wastes. *Journal of cleaner production*, *236*, 117637.
- Gai, C., Chen, M., Liu, T., Peng, N., & Liu, Z. (2016). Gasification characteristics of hydrochar and pyrochar derived from sewage sludge. *Energy*, *113*, 957-965.
- Gan, Y. X. (2021). Activated carbon from biomass sustainable sources. *C*, *7*(2), 39.
- Gao, M., Li, Z., Su, X., Zhang, X., Chang, J., Geng, D., Lu, Y., Zhang, H., Wei, T., & Feng, J. (2023). 2D/2D MgO/g-C<sub>3</sub>N<sub>4</sub> S-scheme heterogeneous tight with Mg-N bonds for efficient photo-Fenton degradation: Enhancing both oxygen vacancy and charge migration. *Chemosphere*, *343*, 140285.
- Gao, X., Wu, L., Li, Z., Xu, Q., Tian, W., & Wang, R. (2018). Preparation and characterization of high surface area activated carbon from pine wood sawdust by fast activation with H<sub>3</sub>PO<sub>4</sub> in a spouted bed. *Journal of Material Cycles and Waste Management*, *20*(2), 925-936.



- Garg, K. K., & Prasad, B. (2016). Development of Box Behnken design for treatment of terephthalic acid wastewater by electrocoagulation process: optimization of process and analysis of sludge. *Journal of Environmental Chemical Engineering*, 4(1), 178-190.
- Garshasbi, V., Jahangiri, M., & Anbia, M. (2017). Equilibrium CO<sub>2</sub> adsorption on zeolite 13X prepared from natural clays. *Applied Surface Science*, 393, 225-233.
- Ghaemi, A., Mashhadimoslem, H., & Zohourian Izadpanah, P. (2022). NiO and MgO/activated carbon as an efficient CO<sub>2</sub> adsorbent: characterization, modeling, and optimization. *International Journal of Environmental Science and Technology*, 19(2), 727-746.
- Ghanim, B. M., Pandey, D. S., Kwapinski, W., & Leahy, J. J. (2016). Hydrothermal carbonisation of poultry litter: Effects of treatment temperature and residence time on yields and chemical properties of hydrochars. *Bioresource technology*, 216, 373-380.
- González-Domínguez, J. M., Alexandre-Franco, M., Fernández-González, C., Ansón-Casaos, A., & Gómez-Serrano, V. (2017). Activated carbon from cherry stones by chemical activation: Influence of the impregnation method on porous structure. *Journal of Wood Chemistry and Technology*, 37(2), 148-162.
- Gu, H., Bergman, R., Anderson, N., & Alanya-Rosenbaum, S. (2018). Life cycle assessment of activated carbon from woody biomass. *Wood and Fiber Science*. 50 (3): 229-243, 50(3), 229-243.
- Gueye, M., Richardson, Y., Kafack, F. T., & Blin, J. (2014). High efficiency activated carbons from African biomass residues for the removal of chromium (VI) from wastewater. *Journal of Environmental Chemical Engineering*, 2(1), 273-281.
- Gunawan, T., Wijiyanti, R., & Widiastuti, N. (2018). Adsorption–desorption of CO<sub>2</sub> on zeolite-Y-templated carbon at various temperatures. *RSC advances*, 8(72), 41594-41602.
- Gunawan, T. D., Mariana, Munawar, E., & Muchtar, S. (2022). Preparation and characterization of chemically activated adsorbent from the combination of coconut shell and fly ash. *Materials Today: Proceedings*, 63, S40-S45. <https://doi.org/10.1016/j.matpr.2022.01.023>
- Gunawardene, O. H., Gunathilake, C. A., Vikrant, K., & Amaraweera, S. M. (2022). Carbon Dioxide capture through physical and chemical adsorption using porous carbon materials: A review. *Atmosphere*, 13(3), 397.

- Guo, T., & Bulin, C. (2021). Facile preparation of MgO/graphene oxide nanocomposite for efficient removal of aqueous Congo red: adsorption performance and interaction mechanism. *Research on Chemical Intermediates*, 47(3), 945-971.
- Guo, Y., Zeng, Z., Liu, Y., Huang, Z., Cui, Y., & Yang, J. (2018). One-pot synthesis of sulfur doped activated carbon as a superior metal-free catalyst for the adsorption and catalytic oxidation of aqueous organics. *Journal of Materials Chemistry A*, 6(9), 4055-4067.
- Guo, Y., Zhao, C., & Li, C. (2015). CO<sub>2</sub> adsorption kinetics of K<sub>2</sub>CO<sub>3</sub>/activated carbon for low-concentration CO<sub>2</sub> removal from confined spaces. *Chemical Engineering & Technology*, 38(5), 891-899.
- Gupta, R. K., Ali, E. A., Abd El Gawad, F., Daood, V. M., Sabry, H., Karunanithi, S., & Srivastav, P. P. (2024). Valorization of fruits and vegetables waste byproducts for development of sustainable food packaging application. *Waste Management Bulletin*.
- Hadi, P., Yeung, K. Y., Guo, J., Wang, H., & McKay, G. (2016). Sustainable development of tyre char-based activated carbons with different textural properties for value-added applications. *Journal of environmental management*, 170, 1-7.
- Haeldermans, T., Campion, L., Kuppens, T., Vanreppelen, K., Cuypers, A., & Schreurs, S. (2020). A comparative techno-economic assessment of biochar production from different residue streams using conventional and microwave pyrolysis. *Bioresource technology*, 318, 124083.
- Hakim, A., Tahari, M. N. A., Marliza, T. S., Isahak, W. N. R. W., Yusop, M. R., Hisham, M. W. M., & Yarmoa, M. A. (2015). Study of CO<sub>2</sub> adsorption and desorption on activated carbon supported iron oxide by temperature programmed desorption. *Jurnal Teknologi*, 77(33).
- Hamyali, H., Nosratinia, F., Rashidi, A., & Ardjmand, M. (2022). Anthracite coal-derived activated carbon as an effectiveness adsorbent for superior gas adsorption and CO<sub>2</sub>/N<sub>2</sub> and CO<sub>2</sub>/CH<sub>4</sub> selectivity: Experimental and DFT study. *Journal of Environmental Chemical Engineering*, 10(1), 107007.
- Hamza, U. D., Nasri, N. S., Amin, N., Zain, H. M., & Mohammed, J. (2015). CO<sub>2</sub> adsorption equilibria on a hybrid palm shell-PEEK porous carbons. *Chem Eng Trans*, 45, 301-306.
- Han, J., Zhang, L., Zhao, B., Qin, L., Wang, Y., & Xing, F. (2019). The N-doped activated carbon derived from sugarcane bagasse for CO<sub>2</sub> adsorption. *Industrial Crops and Products*, 128, 290-297.

- Hanif, A., Dasgupta, S., & Nanoti, A. (2016). Facile synthesis of high-surface-area mesoporous MgO with excellent high-temperature CO<sub>2</sub> adsorption potential. *Industrial & Engineering Chemistry Research*, 55(29), 8070-8078.
- Hao, W., Björkman, E., Lilliestråle, M., & Hedin, N. (2013). Activated carbons prepared from hydrothermally carbonized waste biomass used as adsorbents for CO<sub>2</sub>. *Applied Energy*, 112, 526-532.
- He, S., Chen, G., Xiao, H., Shi, G., Ruan, C., Ma, Y., Dai, H., Yuan, B., Chen, X., & Yang, X. (2021). Facile preparation of N-doped activated carbon produced from rice husk for CO<sub>2</sub> capture. *Journal of colloid and interface science*, 582, 90-101.
- He, Y., Zhu, X., Li, Y., Peng, C., Hu, J., & Liu, H. (2015). Efficient CO<sub>2</sub> capture by triptycene-based microporous organic polymer with functionalized modification. *Microporous and Mesoporous Materials*, 214, 181-187.
- Head-Gordon, M., Tully, J. C., Rettner, C. T., Mullins, C. B., & Auerbach, D. J. (1991). On the nature of trapping and desorption at high surface temperatures. Theory and experiments for the Ar-Pt (111) system. *The Journal of chemical physics*, 94(2), 1516-1527.
- Herrera-Barros, A., Bitar-Castro, N., Villabona-Ortíz, Á., Tejada-Tovar, C., & González-Delgado, Á. D. (2020). Nickel adsorption from aqueous solution using lemon peel biomass chemically modified with TiO<sub>2</sub> nanoparticles. *Sustainable Chemistry and Pharmacy*, 17, 100299.
- Hidayat, A., & Sutrisno, B. (2016). Comparison on pore development of activated carbon produced by chemical and physical activation from palm empty fruit bunch. IOP Conference Series: Materials Science and Engineering,
- Hidayu, A., & Muda, N. (2016). Preparation and characterization of impregnated activated carbon from palm kernel shell and coconut shell for CO<sub>2</sub> capture. *Procedia Engineering*, 148, 106-113.
- Hoe, T. K. (2018). The Current Scenario and Development of the Coconut Industry. *94(1108)*, 413-426.
- Hong, S.-M., Lim, G., Kim, S. H., Kim, J. H., Lee, K. B., & Ham, H. C. (2016). Preparation of porous carbons based on polyvinylidene fluoride for CO<sub>2</sub> adsorption: A combined experimental and computational study. *Microporous and Mesoporous Materials*, 219, 59-65.
- Huang, G.-g., Liu, Y.-f., Wu, X.-x., & Cai, J.-j. (2019). Activated carbons prepared by the KOH activation of a hydrochar from garlic peel and their CO<sub>2</sub> adsorption performance. *New Carbon Materials*, 34(3), 247-257.

- Huang, L., Yang, Z., & Wang, S. (2020). Influence of calcination temperature on the structure and hydration of MgO. *Construction and Building Materials*, 262, 120776.
- Huang, S., Wang, Y., Hou, K., Wang, P., He, M., & Liu, X. (2023). Thermodynamic analysis of an efficient pressure-swing CO<sub>2</sub> capture system based on ionic liquid with residual pressure energy recovery. *Journal of Cleaner Production*, 414, 137665.
- Huo, E., Duan, D., Lei, H., Liu, C., Zhang, Y., Wu, J., Zhao, Y., Huang, Z., Qian, M., & Zhang, Q. (2020). Phenols production from Douglas fir catalytic pyrolysis with MgO and biomass-derived activated carbon catalysts. *Energy*, 199, 117459.
- Husein, D. Z., Hassanien, R., & Khamis, M. (2021). Cadmium oxide nanoparticles/graphene composite: Synthesis, theoretical insights into reactivity and adsorption study. *RSC advances*, 11(43), 27027-27041.
- Hussain, R., Mehboob, M. Y., Khan, M. U., Khalid, M., Irshad, Z., Fatima, R., Anwar, A., Nawab, S., & Adnan, M. (2021). Efficient designing of triphenylamine-based hole transport materials with outstanding photovoltaic characteristics for organic solar cells. *Journal of Materials Science*, 56, 5113-5131.
- Hussain, S., Chatha, S. A. S., Hussain, A. I., Hussain, R., Yasir Mehboob, M., Mansha, A., Shahzad, N., & Ayub, K. (2021). A theoretical framework of zinc-decorated inorganic Mg<sub>12</sub>O<sub>12</sub> nanoclusters for efficient COCl<sub>2</sub> adsorption: a step forward toward the development of COCl<sub>2</sub> sensing materials. *ACS omega*, 6(30), 19435-19444.
- Idrees, M., Rangari, V., & Jeelani, S. (2018). Sustainable packaging waste-derived activated carbon for carbon dioxide capture. *Journal of CO<sub>2</sub> Utilization*, 26, 380-387.
- Inoue, S., Hanaoka, T., & Minowa, T. (2002). Hot compressed water treatment for production of charcoal from wood. *Journal of chemical engineering of Japan*, 35(10), 1020-1023.
- Inoue, S., Uno, S., & Minowa, T. (2008). Carbonization of cellulose using the hydrothermal method. *Journal of chemical engineering of Japan*, 41(3), 210-215.
- Iqbaldin, M. M., Khudzir, I., Azlan, M. M., Zaidi, A., Surani, B., & Zubri, Z. (2013). Properties of coconut shell activated carbon. *Journal of Tropical Forest Science*, 497-503.
- Isahak, W. N. R. W., Hasan, S. Z., Ramli, Z. A. C., Ba-Abbad, M. M., & Yarmo, M. A. (2018). Enhanced physical and chemical adsorption of carbon dioxide using

bimetallic copper–magnesium oxide/carbon nanocomposite. *Research on Chemical Intermediates*, 44, 829-841.

Ismail, I. S., Rashidi, N. A., & Yusup, S. (2022). Production and characterization of bamboo-based activated carbon through single-step H<sub>3</sub>PO<sub>4</sub> activation for CO<sub>2</sub> capture. *Environmental Science and Pollution Research*, 29(9), 12434-12440.

Itodo, H. U. a. I. A. U. (2010). Surface Coverage and Adsorption Study of Dye Uptake by Derived

Acid and Base Treated Mango Seed Shells. *Journal of Chemical and Pharmaceutical Research*, 2(3), 673-683.

Jana, I., Naskar, S., Das, M., & Nandi, D. (2018). Dissociative electron attachment to sulfur dioxide: A theoretical approach. *arXiv preprint arXiv:1807.02286*.

Jasni, M., Abdullah, N., Abdullah, S., Razab, M. A., Noor, A. M., Mohamed, M., Yusuf, N. N., Amin, M. M., Rasat, M. M., & Amin, M. M. (2018). Preparation and characterization of activated carbon from cocos nucifera l.(coconut) shell and sugarcane bagasse. *Int. J. Cur. Res. Eng. Sci. Tech*, 1, 416-421.

Jawad, A. H., Abdulhameed, A. S., Wilson, L. D., Syed-Hassan, S. S. A., ALothman, Z. A., & Khan, M. R. (2021). High surface area and mesoporous activated carbon from KOH-activated Dragon fruit peels for methylene blue dye adsorption: Optimization and mechanism study. *Chinese Journal of Chemical Engineering*, 32, 281-290.

Jhaa, G., Pancharatna, P. D., & Balakrishnarajan, M. M. (2023). Topological impact of delocalization on the stability and band gap of partially oxidized graphene. *ACS omega*, 8(5), 5124-5135.

Joshi, S., & Bishnu, K. (2020). Synthesis and Characterization of Sugarcane Bagasse Based Activated Carbon: Effect of Impregnation Ratio of ZnCl<sub>2</sub>. *Journal of Nepal Chemical Society*, 41(1), 74-79.

Kabir Ahmad, R., Anwar Sulaiman, S., Yusup, S., Sham Dol, S., Inayat, M., & Aminu Umar, H. (2022). Exploring the potential of coconut shell biomass for charcoal production. *Ain Shams Engineering Journal*, 13(1). <https://doi.org/10.1016/j.asej.2021.05.013>

Kaithwas, A., Prasad, M., Kulshreshtha, A., & Verma, S. (2012). Industrial wastes derived solid adsorbents for CO<sub>2</sub> capture: A mini review. *Chemical Engineering Research and Design*, 90(10), 1632-1641.

Kakade, P. M., Kachere, A. R., Rondiya, S. R., & Bhosale, S. V. (2021). Graphene oxide assisted synthesis of magnesium oxide nanorods. *ES Materials & Manufacturing*, 12(2), 63-71.

- Kamran, U., Rhee, K. Y., & Park, S.-J. (2019). Effect of triblock copolymer on carbon-based boron nitride whiskers for efficient CO<sub>2</sub> adsorption. *Polymers*, *11*(5), 913.
- Karagöz, S., Bhaskar, T., Muto, A., Sakata, Y., & Uddin, M. A. (2004). Low-temperature hydrothermal treatment of biomass: effect of reaction parameters on products and boiling point distributions. *Energy & fuels*, *18*(1), 234-241.
- Karapinar, D., Creissen, C. E., Rivera de la Cruz, J. G., Schreiber, M. W., & Fontecave, M. (2021). Electrochemical CO<sub>2</sub> reduction to ethanol with copper-based catalysts. *ACS Energy Letters*, *6*(2), 694-706.
- Karbalaei Mohammad, N., Ghaemi, A., Tahvildari, K., & Sharif, A. A. M. (2020). Experimental investigation and modeling of CO<sub>2</sub> adsorption using modified activated carbon. *Iranian Journal of Chemistry and Chemical Engineering*, *39*(1), 177-192.
- Karimi, M., C. Silva, J. A., Gonçalves, C. N. d. P., L. Diaz de Tuesta, J., Rodrigues, A. E., & Gomes, H. T. (2018). CO<sub>2</sub> capture in chemically and thermally modified activated carbons using breakthrough measurements: experimental and modeling study. *Industrial & Engineering Chemistry Research*, *57*(32), 11154-11166.
- Karimi, M., Shirzad, M., Silva, J. A., & Rodrigues, A. E. (2022). Biomass/Biochar carbon materials for CO<sub>2</sub> capture and sequestration by cyclic adsorption processes: A review and prospects for future directions. *Journal of CO<sub>2</sub> Utilization*, *57*, 101890.
- Karishma, S., Kamalesh, R., Saravanan, A., Deivayanai, V., Yaashikaa, P., & Vickram, A. (2024). A review on recent advancements in biochemical fixation and transformation of CO<sub>2</sub> into constructive products. *Biochemical Engineering Journal*, 109366.
- Karyab, H., Ghasemi, M., Ghotbinia, F., & Nazeri, N. (2023). Efficiency of chitosan nanoparticle with polyaluminum chloride in dye removal from aqueous solutions: Optimization through response surface methodology (RSM) and central composite design (CCD). *International Journal of Biological Macromolecules*, *249*, 125977.
- Kassahun, E., Tibebu, S., Tadesse, Y., & Awish, N. (2022). Synthesis optimization of activated carbon driven from scrap tire for adsorbent yield and methylene blue removal under response surface methodology. *Advances in Materials Science and Engineering*, *2022*(1), 2325213.
- Katta, V., Dubey, R., & Joshi, G. (2023). Experimental investigation of activated carbon nanoflakes produced by thermal and chemical activation processes. *Fullerenes, Nanotubes and Carbon Nanostructures*, *31*(1), 10-17.

- Kaveeshwar, A. R., Kumar, P. S., Revellame, E. D., Gang, D. D., Zappi, M. E., & Subramaniam, R. (2018). Adsorption properties and mechanism of barium (II) and strontium (II) removal from fracking wastewater using pecan shell based activated carbon. *Journal of Cleaner Production*, 193, 1-13.
- Khalil, H., Jawaid, M., Firoozian, P., Rashid, U., Islam, A., & Akil, H. M. (2013). Activated carbon from various agricultural wastes by chemical activation with KOH: preparation and characterization. *Journal of Biobased Materials and Bioenergy*, 7(6), 708-714.
- Khalili, S., & Jahanshahi, M. (2021). Selective CO<sub>2</sub> adsorption using N-rich porous carbon derived from KOH-activated polyaniline. *Korean Journal of Chemical Engineering*, 38, 862-871.
- Khalili, S., Khoshandam, B., & Jahanshahi, M. (2015). Optimization of production conditions for synthesis of chemically activated carbon produced from pine cone using response surface methodology for CO<sub>2</sub> adsorption. *RSC advances*, 5(114), 94115-94129.
- Khoshraftar, Z., & Ghaemi, A. (2022). Presence of activated carbon particles from waste walnut shell as a biosorbent in monoethanolamine (MEA) solution to enhance carbon dioxide absorption. *Heliyon*, 8(1).
- Kim, D.-W., Kil, H.-S., Nakabayashi, K., Yoon, S.-H., & Miyawaki, J. (2017). Structural elucidation of physical and chemical activation mechanisms based on the microdomain structure model. *Carbon*, 114, 98-105.
- Kim, M.-J., Choi, S. W., Kim, H., Mun, S., & Lee, K. B. (2020). Simple synthesis of spent coffee ground-based microporous carbons using K<sub>2</sub>CO<sub>3</sub> as an activation agent and their application to CO<sub>2</sub> capture. *Chemical Engineering Journal*, 397, 125404.
- Kim, M., Lee, J. W., Kim, S., & Kang, Y. T. (2022). CO<sub>2</sub> adsorption on zeolite 13X modified with hydrophobic octadecyltrimethoxysilane for indoor application. *Journal of Cleaner Production*, 337, 130597.
- Koçer, A. T., Mutlu, B., & Özçimen, D. (2020). Investigation of biochar production potential and pyrolysis kinetics characteristics of microalgal biomass. *Biomass Conversion and Biorefinery*, 10, 85-94.
- Kong, Y., Shen, X., Cui, S., & Fan, M. (2015). Development of monolithic adsorbent via polymeric sol-gel process for low-concentration CO<sub>2</sub> capture. *Applied Energy*, 147, 308-317.
- Koo-Amornpattana, W., Phadungbut, P., Kunthakudee, N., Jonglertjunya, W., Ratchahat, S., & Hunsom, M. (2023). Innovative metal oxides (CaO, SrO, MgO)

impregnated waste-derived activated carbon for biohydrogen purification. *Scientific Reports*, 13(1), 4705.

- Krishnamurthy, S. (2022). Vacuum swing adsorption process for post-combustion carbon capture with 3D printed sorbents: Quantifying the improvement in productivity and specific energy over a packed bed system through process simulation and optimization. *Chemical Engineering Science*, 253, 117585.
- Kronast, A., Eckstein, S., Altenbuchner, P. T., Hindelang, K., Vagin, S. I., & Rieger, B. (2016). Gated Channels and Selectivity Tuning of CO<sub>2</sub> over N<sub>2</sub> Sorption by Post-Synthetic Modification of a UiO-66-Type Metal–Organic Framework. *Chemistry—A European Journal*, 22(36), 12800-12807.
- Kumar, A., & Jena, H. M. (2015). High surface area microporous activated carbons prepared from Fox nut (*Euryale ferox*) shell by zinc chloride activation. *Applied Surface Science*, 356, 753-761.
- Kumar, S., & Saha, A. (2022). Utilization of coconut shell biomass residue to develop sustainable biocomposites and characterize the physical, mechanical, thermal, and water absorption properties. *Biomass Conversion and Biorefinery*, 1-17.
- Kumar, V., Sharma, N., Panneerselvam, B., Dasarahally Huligowda, L. K., Umesh, M., Gupta, M., Muzammil, K., Zahrani, Y., & Malmtheibi, M. (2024, May 16). Lignocellulosic biomass for biochar production: A green initiative on biowaste conversion for pharmaceutical and other emerging pollutant removal. *Chemosphere*, 360, 142312. <https://doi.org/10.1016/j.chemosphere.2024.142312>
- Kundu, A., Redzwan, G., Sahu, J. N., Mukherjee, S., Gupta, B. S., & Hashim, M. A. (2014). Hexavalent chromium adsorption by a novel activated carbon prepared by microwave activation. *BioResources*, 9(1), 1498-1518.
- Labus, K., Gryglewicz, S., & Machnikowski, J. (2014). Granular KOH-activated carbons from coal-based cokes and their CO<sub>2</sub> adsorption capacity. *Fuel*, 118, 9-15.
- Lam, S. S., Liew, R. K., Cheng, C. K., & Chase, H. A. (2015). Catalytic microwave pyrolysis of waste engine oil using metallic pyrolysis char. *Applied Catalysis B: Environmental*, 176, 601-617.
- Lee, J., Lee, K., Sohn, D., Kim, Y. M., & Park, K. Y. (2018). Hydrothermal carbonization of lipid extracted algae for hydrochar production and feasibility of using hydrochar as a solid fuel. *Energy*, 153, 913-920.
- Leite, A., Saucier, C., Lima, E., Dos Reis, G., Umpierrez, C., Mello, B., Shirmardi, M., Dias, S., & Sampaio, C. (2018, Mar). Activated carbons from avocado seed: optimisation and application for removal of several emerging organic compounds. *Environmental Science and Pollution Research*, 25(8), 7647-7661. <https://doi.org/10.1007/s11356-017-1105-9>



- Leng, L., Xiong, Q., Yang, L., Li, H., Zhou, Y., Zhang, W., Jiang, S., Li, H., & Huang, H. (2021). An overview on engineering the surface area and porosity of biochar. *Science of The Total Environment*, 763, 144204.
- Leng, S., Li, W., Han, C., Chen, L., Chen, J., Fan, L., Lu, Q., Li, J., Leng, L., & Zhou, W. (2020). Aqueous phase recirculation during hydrothermal carbonization of microalgae and soybean straw: A comparison study. *Bioresource technology*, 298, 122502.
- Li, D., Chen, W., Wu, J., Jia, C. Q., & Jiang, X. (2020). The preparation of waste biomass-derived N-doped carbons and their application in acid gas removal: focus on N functional groups. *Journal of Materials Chemistry A*, 8(47), 24977-24995.
- Li, H., Tang, M., Wang, L., Liu, Q., Yao, F., Gong, Z., Li, Y., Lu, S., & Yan, J. (2024). Molecular simulation combined with DFT calculation guided heteroatom-doped biochar rational design for highly selective and efficient CO<sub>2</sub> capture. *Chemical Engineering Journal*, 481, 148362.
- Li, K., Tian, S., Jiang, J., Wang, J., Chen, X., & Yan, F. (2016). Pine cone shell-based activated carbon used for CO<sub>2</sub> adsorption. *Journal of Materials Chemistry A*, 4(14), 5223-5234.
- Li, Q., Liu, S., Peng, W., Zhu, W., Wang, L., Chen, F., Shao, J., & Hu, X. (2020). Preparation of biomass-derived porous carbons by a facile method and application to CO<sub>2</sub> adsorption. *Journal of the Taiwan Institute of Chemical Engineers*, 116, 128-136.
- Li, S., Han, K., Li, J., Li, M., & Lu, C. (2017). Preparation and characterization of super activated carbon produced from gulfweed by KOH activation. *Microporous and Mesoporous Materials*, 243, 291-300.
- Li, X., Tan, C., Jiang, J., Wang, S., Zheng, F., Zhang, X., Wang, H., Huang, Y., & Li, Q. (2021). New construction of electron thermal conductive route for high-efficient heat dissipation of graphene/Cu composite. *Carbon*, 177, 107-114.
- Liang, W., Liu, Z., Peng, J., Zhou, X., Wang, X., & Li, Z. (2018). Enhanced CO<sub>2</sub> adsorption and CO<sub>2</sub>/N<sub>2</sub>/CH<sub>4</sub> selectivity of novel carbon composites CPDA@A-Cs. *Energy & Fuels*, 33(1), 493-502.
- Liew, R. K., Azwar, E., Yek, P. N. Y., Lim, X. Y., Cheng, C. K., Ng, J.-H., Jusoh, A., Lam, W. H., Ibrahim, M. D., & Ma, N. L. (2018). Microwave pyrolysis with KOH/NaOH mixture activation: a new approach to produce micro-mesoporous activated carbon for textile dye adsorption. *Bioresource technology*, 266, 1-10.

- Liew, R. K., Chong, M. Y., Osazuwa, O. U., Nam, W. L., Phang, X. Y., Su, M. H., Cheng, C. K., Chong, C. T., & Lam, S. S. (2018). Production of activated carbon as catalyst support by microwave pyrolysis of palm kernel shell: a comparative study of chemical versus physical activation. *Research on Chemical Intermediates*, 44(6), 3849-3865.
- Liu, G., Dai, Z., Liu, X., Dahlgren, R. A., & Xu, J. (2022, 2022/11/15). Modification of agricultural wastes to improve sorption capacities for pollutant removal from water – a review. *Carbon Research*, 1(1), 24. <https://doi.org/10.1007/s44246-022-00025-1>
- Liu, J., Xuan, D., Lu, Z., Wang, Z., Liu, Q., Li, S., Wang, D., Ye, Y., Wang, D., & Zheng, Z. (2022). A novel perspective on interfacial interactions between polypyrrole and carbon materials for improving performance of supercapacitors. *Applied Surface Science*, 573, 151626.
- Liu, J., Yang, X., Liu, H., Jia, X., & Bao, Y. (2021). Mixed biochar obtained by the co-pyrolysis of shrimp shell with corn straw: co-pyrolysis characteristics and its adsorption capability. *Chemosphere*, 131116.
- Liu, W., Lin, Y., Jiang, L., Ji, Y., Yong, J., & Zhang, X. (2022). Thermodynamic exploration of two-stage vacuum-pressure swing adsorption for carbon dioxide capture. *Energy*, 241, 122901.
- Liu, Z., Zhang, F.-S., & Wu, J. (2010). Characterization and application of chars produced from pinewood pyrolysis and hydrothermal treatment. *Fuel*, 89(2), 510-514.
- Lu, C.-M., Liu, J., Xiao, K., & Harris, A. T. (2010). Microwave enhanced synthesis of MOF-5 and its CO<sub>2</sub> capture ability at moderate temperatures across multiple capture and release cycles. *Chemical Engineering Journal*, 156(2), 465-470.
- Luhadiya, N., Kundalwal, S., & Sahu, S. (2021). Investigation of hydrogen adsorption behavior of graphene under varied conditions using a novel energy-centered method. *Carbon Letters*, 31(4), 655-666.
- Luo, Y., Street, J., Steele, P., Entsminger, E., & Guda, V. (2016). Activated carbon derived from pyrolyzed pinewood char using elevated temperature, KOH, H<sub>3</sub>PO<sub>4</sub>, and H<sub>2</sub>O<sub>2</sub>. *BioResources*, 11(4), 10433-10447.
- Lupul, I., Yperman, J., Carleer, R., & Gryglewicz, G. (2015). Tailoring of porous texture of hemp stem-based activated carbon produced by phosphoric acid activation in steam atmosphere. *Journal of Porous Materials*, 22(1), 283-289.
- Lv, G., Li, S., Zhang, H., Zhu, C., Cheng, J., & Qian, P. (2024). CO<sub>2</sub> adsorption by Cr, Mn, Fe, Co, Ni doped MgO (100) surfaces: A first-principles study. *Separation and Purification Technology*, 128613.

- Ma, X., Li, L., Chen, R., Wang, C., Li, H., & Li, H. (2018). Highly nitrogen-doped porous carbon derived from zeolitic imidazolate framework-8 for CO<sub>2</sub> capture. *Chemistry—An Asian Journal*, 13(16), 2069-2076.
- Ma, X., Li, L., Chen, R., Wang, C., Li, H., & Wang, S. (2018). Heteroatom-doped nanoporous carbon derived from MOF-5 for CO<sub>2</sub> capture. *Applied Surface Science*, 435, 494-502.
- Mabuza, M., Premlall, K., & Daramola, M. O. (2022). Modelling and thermodynamic properties of pure CO<sub>2</sub> and flue gas sorption data on South African coals using Langmuir, Freundlich, Temkin, and extended Langmuir isotherm models. *International Journal of Coal Science & Technology*, 9(1), 45.
- Madzaki, H., Ghani, W., Yaw, T. C. S., Rashid, U., & Muda, N. (2018a). Carbon dioxide adsorption on activated carbon hydrothermally treated and impregnated with metal oxides. *Jurnal Kejuruteraan*, 30(1), 31-38.
- Madzaki, H., Ghani, W. A. W. A. K., Yaw, T. C. S., Rashid, U., & Muda, N. (2018b). Carbon dioxide adsorption on activated carbon hydrothermally treated and impregnated with metal oxides. *Jurnal Kejuruteraan*, 30(1), 31-38.
- Mahmood, T., Ali, R., Naeem, A., Hamayun, M., & Aslam, M. (2017). Potential of used *Camellia sinensis* leaves as precursor for activated carbon preparation by chemical activation with H<sub>3</sub>PO<sub>4</sub>; optimization using response surface methodology. *Process Safety and Environmental Protection*, 109, 548-563.
- Majd, M. M., Kordzadeh-Kermani, V., Ghalandari, V., Askari, A., & Sillanpää, M. (2022). Adsorption isotherm models: A comprehensive and systematic review (2010– 2020). *Science of The Total Environment*, 812, 151334.
- Maleki, F., Ghaemi, A., & Mir Mohamad Sadeghi, G. (2023). Synthesis and characterization of waste Styrofoam hypercrosslinked polymer as an adsorbent for CO<sub>2</sub> capture. *Environmental Progress & Sustainable Energy*, 42(1), e13954.
- Mamtani, K., Shahbaz, K., & Farid, M. M. (2021). Glycerolysis of free fatty acids: A review. *Renewable and Sustainable Energy Reviews*, 137, 110501.
- Maniarasu, R., Rathore, S. K., & Murugan, S. (2021). Potential of using biomass based activated carbon for carbon dioxide capture. *IOP Conference Series: Materials Science and Engineering*, 1130(1), 02022. <https://doi.org/10.1088/1757-899X/1130/1/012022>
- Manmuanpom, N., Thubsuang, U., Dubas, S. T., Wongkasemjit, S., & Chaisuwan, T. (2018). Enhanced CO<sub>2</sub> capturing over ultra-microporous carbon with nitrogen-

active species prepared using one-step carbonization of polybenzoxazine for a sustainable environment. *Journal of environmental management*, 223, 779-786.

- Manzar, M. S., Khan, G., dos Santos Lins, P. V., Zubair, M., Khan, S. U., Selvasembian, R., Meili, L., Blaisi, N. I., Nawaz, M., & Aziz, H. A. (2021). RSM-CCD optimization approach for the adsorptive removal of Eriochrome Black T from aqueous system using steel slag-based adsorbent: Characterization, Isotherm, Kinetic modeling and thermodynamic analysis. *Journal of Molecular Liquids*, 339, 116714.
- Maroto-Valer, M. M., Tang, Z., & Zhang, Y. (2005). CO<sub>2</sub> capture by activated and impregnated anthracites. *Fuel Processing Technology*, 86(14-15), 1487-1502.
- Masoumi, S., & Dalai, A. K. (2020). Optimized production and characterization of highly porous activated carbon from algal-derived hydrochar. *Journal of Cleaner Production*, 263, 121427.
- Mathimani, T., & Mallick, N. (2019). A review on the hydrothermal processing of microalgal biomass to bio-oil-Knowledge gaps and recent advances. *Journal of Cleaner Production*, 217, 69-84.
- Melouki, R., Ouadah, A., & Llewellyn, P. L. (2020). The CO<sub>2</sub> adsorption behavior study on activated carbon synthesized from olive waste. *Journal of CO<sub>2</sub> Utilization*, 42, 101292.
- Miar, M., Shiroudi, A., Pourshamsian, K., Oliaey, A. R., & Hatamjafari, F. (2021). Theoretical investigations on the HOMO–LUMO gap and global reactivity descriptor studies, natural bond orbital, and nucleus-independent chemical shifts analyses of 3-phenylbenzo [d] thiazole-2 (3 H)-imine and its para-substituted derivatives: Solvent and substituent effects. *Journal of Chemical Research*, 45(1-2), 147-158.
- Misran, E., Sarah, M., Dina, S., Harahap, S., & Nazar, A. (2020). Activated carbon preparation from bagasse and banana stem at various impregnation ratio. *Journal of Physics: Conference Series*,
- Mochizuki, T., Kubota, M., Matsuda, H., & Camacho, L. F. E. (2016). Adsorption behaviors of ammonia and hydrogen sulfide on activated carbon prepared from petroleum coke by KOH chemical activation. *Fuel Processing Technology*, 144, 164-169.
- Mohammad, N. K., Ghaemi, A., & Tahvildari, K. (2019). Hydroxide modified activated alumina as an adsorbent for CO<sub>2</sub> adsorption: experimental and modeling. *International Journal of Greenhouse Gas Control*, 88, 24-37.

- Mopoung, S., Moonsri, P., Palas, W., & Khumpai, S. (2015). Characterization and properties of activated carbon prepared from tamarind seeds by KOH activation for Fe (III) adsorption from aqueous solution. *The scientific world journal*, 2015.
- Nakason, K., Panyapinyopol, B., Kanokkantapong, V., Viriya-empikul, N., Kraithong, W., & Pavasant, P. (2018). Characteristics of hydrochar and hydrothermal liquid products from hydrothermal carbonization of corncob. *Biomass Conversion and Biorefinery*, 8(1), 199-210.
- Nandiyanto, A. B. D., Girsang, G. C. S., Maryanti, R., Ragadhita, R., Anggraeni, S., Fauzi, F. M., Sakinah, P., Astuti, A. P., Usdiyana, D., & Fiandini, M. (2020). Isotherm adsorption characteristics of carbon microparticles prepared from pineapple peel waste. *Communications in Science and Technology*, 5(1), 31-39.
- NASA. *NASA Climate Change: Vital Signs of the Planet*. Retrieved July 17 from <https://climate.nasa.gov/vital-signs/carbon-dioxide/?intent=121>
- Nazir, G., Rehman, A., & Park, S.-J. (2021). Valorization of shrimp shell biowaste for environmental remediation: Efficient contender for CO<sub>2</sub> adsorption and separation. *Journal of Environmental Management*, 299, 113661.
- Nille, O. S., Patil, A. S., Waghmare, R. D., Naik, V. M., Gunjal, D. B., Kolekar, G. B., & Gore, A. H. (2021). Valorization of tea waste for multifaceted applications: a step toward green and sustainable development. In *Valorization of agri-food wastes and by-products* (pp. 219-236). Elsevier.
- Nizamuddin, S., Mubarak, N., Tiripathi, M., Jayakumar, N., Sahu, J., & Ganesan, P. (2016). Chemical, dielectric and structural characterization of optimized hydrochar produced from hydrothermal carbonization of palm shell. *Fuel*, 163, 88-97.
- Nor, M., A'liah, N. A., Engku Ariff, E. E., Nik Omar, N. R., Zainol Abidin, A. Z., Muhammad, R. M., Rahim, H., Nazmi, M. S., & Sulaiman, N. H. (2020). Total productivity and technical efficiency of coconuts in Malaysia. *Economic and Technology Management Review*, 15.
- Nowrouzi, M., Younesi, H., & Bahramifar, N. (2018). Superior CO<sub>2</sub> capture performance on biomass-derived carbon/metal oxides nanocomposites from Persian ironwood by H<sub>3</sub>PO<sub>4</sub> activation. *Fuel*, 223, 99-114.
- Nyamful, A., Nyogbe, E. K., Mohammed, L., Zainudeen, M., Darkwa, S., Phiri, I., Mohammed, M., & Ko, J. (2020). Processing and characterization of activated carbon from coconut shell and palm kernel shell waste by H<sub>3</sub>PO<sub>4</sub> activation. *Ghana journal of science*, 61(2), 91-104.

- Oginni, O., Singh, K., Oporto, G., Dawson-Andoh, B., McDonald, L., & Sabolsky, E. (2019). Effect of one-step and two-step H<sub>3</sub>PO<sub>4</sub> activation on activated carbon characteristics. *Bioresource Technology Reports*, 8, 100307.
- Olivares-Marín, M., Garcia, S., Pevida, C., Wong, M., & Maroto-Valer, M. (2011). The influence of the precursor and synthesis method on the CO<sub>2</sub> capture capacity of carpet waste-based sorbents. *Journal of environmental management*, 92(10), 2810-2817.
- Om Prakash, M., Gujjala, R., Panchal, M., & Ojha, S. (2020). Mechanical characterization of arhar biomass based porous nano activated carbon polymer composites. *Polymer Composites*, 41(8), 3113-3123.
- Onawumi, O., Sangoremi, A., & Bello, O. (2021). Preparation and characterization of activated carbon from groundnut and egg shells as viable precursors for adsorption. *Journal of Applied Sciences and Environmental Management*, 25(9), 1707-1713.
- Onochie, U., Obanor, A., Aliu, S., & Igbojaro, O. (2017). Proximate and ultimate analysis of fuel pellets from oil palm residues. *Nigerian Journal of Technology*, 36(3), 987-990.
- Örkün, Y., Karatepe, N., & Yavuz, R. (2012). Influence of temperature and impregnation ratio of H<sub>3</sub>PO<sub>4</sub> on the production of activated carbon from hazelnut shell. *Acta Physica Polonica-Series A General Physics*, 121(1), 277.
- Ouyang, J., Zhou, L., Liu, Z., Heng, J. Y., & Chen, W. (2020). Biomass-derived activated carbons for the removal of pharmaceutical micropollutants from wastewater: A review. *Separation and Purification Technology*, 253, 117536.
- Pacze niak, T., Rydel-Ciszek, K., Chmielarz, P., Charczuk, M., & Sobkowiak, A. (2018). Electrochemical Reaction Gibbs Energy: Spontaneity in Electrochemical Cells. *Journal of Chemical Education*, 95(10), 1794-1800.
- Pali, H. S., Sharma, A., Kumar, M., Annakodi, V. A., Singh, N. K., Singh, Y., Balasubramanian, D., Deepanraj, B., Truong, T. H., & Nguyen, P. Q. P. (2023). Enhancement of combustion characteristics of waste cooking oil biodiesel using TiO<sub>2</sub> nanofluid blends through RSM. *Fuel*, 331, 125681.
- Pallarés, J., González-Cencerrado, A., & Arauzo, I. (2018). Production and characterization of activated carbon from barley straw by physical activation with carbon dioxide and steam. *Biomass and Bioenergy*, 115, 64-73.
- Panda, D., Kumar, E. A., & Singh, S. K. (2020). Introducing mesoporosity in zeolite 4A bodies for Rapid CO<sub>2</sub> capture. *Journal of CO<sub>2</sub> Utilization*, 40, 101223.

- Park, D., Hong, S.-H., Kim, K.-M., & Lee, C.-H. (2020). Adsorption equilibria and kinetics of silica gel for N<sub>2</sub>O, O<sub>2</sub>, N<sub>2</sub>, and CO<sub>2</sub>. *Separation and purification technology*, 251, 117326.
- Park, J. H., Hong, M. W., Yoon, H. C., & Yi, K. B. (2022). Effects of MgCl<sub>2</sub> loading on ammonia capacity of activated carbon for application in temperature swing adsorption, pressure swing adsorption, and pressure-temperature swing adsorption process. *Korean Journal of Chemical Engineering*, 39(10), 2775-2782.
- Peng, A.-Z., Qi, S.-C., Liu, X., Xue, D.-M., Peng, S.-S., Yu, G.-X., Liu, X.-Q., & Sun, L.-B. (2019). N-doped porous carbons derived from a polymer precursor with a record-high N content: Efficient adsorbents for CO<sub>2</sub> capture. *Chemical Engineering Journal*, 372, 656-664.
- Peng, P., Anastasopoulou, A., Brooks, K., Furukawa, H., Bowden, M. E., Long, J. R., Autrey, T., & Breunig, H. (2022). Cost and potential of metal-organic frameworks for hydrogen back-up power supply. *Nature Energy*, 7(5), 448-458.
- Picone, A., Volpe, M., Malik, W., Volpe, R., & Messineo, A. (2024). Role of reaction parameters in hydrothermal carbonization with process water recirculation: Hydrochar recovery enhancement and energy balance. *biomass and bioenergy*, 181, 107061.
- Plaza, M., Pevida, C., Martín, C. F., Feroso, J., Pis, J., & Rubiera, F. (2010). Developing almond shell-derived activated carbons as CO<sub>2</sub> adsorbents. *Separation and Purification Technology*, 71(1), 102-106.
- Poomsawat, S., & Poomsawat, W. (2021). Analysis of hydrochar fuel characterization and combustion behavior derived from aquatic biomass via hydrothermal carbonization process. *Case Studies in Thermal Engineering*, 27, 101255.
- Prabhu, S. V., Varadharajan, V., Mohanasundaram, S., Manivannan, S., Khaled, J. M., Goel, M., & Srihari, K. (2023). A comparative study on process optimization of betalain pigment extraction from *Beta vulgaris* subsp. *vulgaris*: RSM, ANN, and hybrid RSM-GA methods. *Biomass Conversion and Biorefinery*, 1-19.
- Prakash, M. O., Raghavendra, G., Ojha, S., & Panchal, M. (2021). Characterization of porous activated carbon prepared from arhar stalks by single step chemical activation method. *Materials Today: Proceedings*, 39, 1476-1481.
- Pramanik, P., Patel, H., Charola, S., Neogi, S., & Maiti, S. (2021). High surface area porous carbon from cotton stalk agro-residue for CO<sub>2</sub> adsorption and study of techno-economic viability of commercial production. *Journal of CO<sub>2</sub> Utilization*, 45, 101450.

- Prathiba, R., Shruthi, M., & Miranda, L. R. (2018). Pyrolysis of polystyrene waste in the presence of activated carbon in conventional and microwave heating using modified thermocouple. *Waste Management*, 76, 528-536.
- Principe, I. A., & Fletcher, A. J. (2020). Adsorption selectivity of CO<sub>2</sub> over CH<sub>4</sub>, N<sub>2</sub> and H<sub>2</sub> in melamine–resorcinol–formaldehyde xerogels. *Adsorption*, 26(5), 723-735.
- Purdue, M. J., & Qiao, Z. (2018). Molecular simulation study of wet flue gas adsorption on zeolite 13X. *Microporous and Mesoporous Materials*, 261, 181-197.
- Raganati, F., Alfe, M., Gargiulo, V., Chirone, R., & Ammendola, P. (2018). Isotherms and thermodynamics of CO<sub>2</sub> adsorption on a novel carbon-magnetite composite sorbent. *Chemical Engineering Research and Design*, 134, 540-552.
- Raganati, F., & Ammendola, P. (2024). CO<sub>2</sub> Post-combustion Capture: A Critical Review of Current Technologies and Future Directions. *Energy & Fuels*.
- Raganati, F., Miccio, F., & Ammendola, P. (2021). Adsorption of carbon dioxide for post-combustion capture: a review. *Energy & Fuels*, 35(16), 12845-12868.
- RAHMAN, M. H. A. (2020). Rice Husk Activated Carbon with NaOH Activation: Physical and Chemical Properties. *Sains Malaysiana*, 49(9), 2261-2267.
- Rahman, M. M., Muttakin, M., Pal, A., Shafiullah, A. Z., & Saha, B. B. (2019). A statistical approach to determine optimal models for IUPAC-classified adsorption isotherms. *Energies*, 12(23), 4565.
- Raj, T., Chandrasekhar, K., Morya, R., Pandey, A. K., Jung, J.-H., Kumar, D., Singhania, R. R., & Kim, S.-H. (2022). Critical challenges and technological breakthroughs in food waste hydrolysis and detoxification for fuels and chemicals production. *Bioresource technology*, 360, 127512.
- Rajewski, J., & Dobrzyńska-Inger, A. (2021). Application of response surface methodology (RSM) for the optimization of chromium (III) synergistic extraction by supported liquid membrane. *Membranes*, 11(11), 854.
- Ramalho, P., Soares, O., Figueiredo, J., & Pereira, M. (2023). Catalytic reduction of NO over copper supported on activated carbon. *Catalysis Today*, 418, 114044.
- Ramezanipour Penchah, H., Ghaemi, A., & Jafari, F. (2021). Piperazine-modified activated carbon as a novel adsorbent for CO<sub>2</sub> capture: Modeling and characterization. *Environmental Science and Pollution Research*, 1-10.



- Ranjan, D. (2023). Nanomaterials originated from microbes for the removal of toxic pollutants from water. In *Environmental Applications of Microbial Nanotechnology* (pp. 347-363). Elsevier.
- Rasam, S., Moraveji, M. K., Soria-Verdugo, A., & Salimi, A. (2021). Synthesis, characterization and adsorbability of Crocus sativus petals hydrothermal carbonized hydrochar and activated hydrochar. *Chemical Engineering and Processing-Process Intensification*, 159, 108236.
- Rashidi, N. A., & Yusup, S. (2017). Potential of palm kernel shell as activated carbon precursors through single stage activation technique for carbon dioxide adsorption. *Journal of Cleaner Production*, 168, 474-486.
- Ravanchi, M. T., & Sahebdehfar, S. (2021). Catalytic conversions of CO<sub>2</sub> to help mitigate climate change: Recent process developments. *Process Safety and Environmental Protection*, 145, 172-194.
- Ravi, K., Singh, M., Neogi, S., Grafouté, M., & Biradar, A. V. (2022). Hierarchical porous nitrogen-doped carbon supported MgO as an excellent composite for CO<sub>2</sub> capture at atmospheric pressure and conversion to value-added products. *Journal of CO<sub>2</sub> Utilization*, 65, 102222.
- Rehman, A., Nazir, G., Rhee, K. Y., & Park, S.-J. (2022). Valorization of orange peel waste to tunable heteroatom-doped hydrochar-derived microporous carbons for selective CO<sub>2</sub> adsorption and separation. *Science of the Total Environment*, 849, 157805.
- Rehman, A., & Park, S.-J. (2018). Comparative study of activation methods to design nitrogen-doped ultra-microporous carbons as efficient contenders for CO<sub>2</sub> capture. *Chemical engineering journal*, 352, 539-548.
- Reza, M. T. (2022). Investigation of hydrothermal carbonization and chemical activation process conditions on hydrogen storage in loblolly pine-derived superactivated hydrochars. *International Journal of Hydrogen Energy*, 47(62), 26422-26434.
- Reza, M. T., Rottler, E., Herklotz, L., & Wirth, B. (2015). Hydrothermal carbonization (HTC) of wheat straw: Influence of feedwater pH prepared by acetic acid and potassium hydroxide. *Bioresource technology*, 182, 336-344.
- Roberts, J. R., Gracely, E. J., & Schoffstall, J. M. (1997). Advantage of high-surface-area charcoal for gastrointestinal decontamination in a human acetaminophen ingestion model. *Academic emergency medicine*, 4(3), 167-174.
- Rodríguez Correa, C., Ngamyang, C., Klank, D., & Kruse, A. (2018). Investigation of the textural and adsorption properties of activated carbon from HTC and pyrolysis carbonizates. *Biomass Conversion and Biorefinery*, 8, 317-328.

- Rostamian, R., Heidarpour, M., Mousavi, S. F., & Afyuni, M. (2015). Preparation, characterization and sodium sorption capability of rice husk carbonaceous adsorbents. *Fresen. Environ. Bull*, 24, 1649-1658.
- Saha, D., & Kienbaum, M. J. (2019). Role of oxygen, nitrogen and sulfur functionalities on the surface of nanoporous carbons in CO<sub>2</sub> adsorption: a critical review. *Microporous and Mesoporous Materials*, 287, 29-55.
- Şahin, Ö., Saka, C., Ceyhan, A. A., & Baytar, O. (2015). Preparation of high surface area activated carbon from *Elaeagnus angustifolia* seeds by chemical activation with ZnCl<sub>2</sub> in one-step treatment and its iodine adsorption. *Separation Science and Technology*, 50(6), 886-891.
- Sakanaka, Y., Hiraide, S., Yamane, Y., Miyahara, M. T., & Watanabe, S. (2023). Thermal management in vacuum pressure swing adsorption processes using phase change materials. *Chemical engineering journal*, 141262.
- Saleem, J., Shahid, U. B., Hijab, M., Mackey, H., & McKay, G. (2019, 2019/12/01). Production and applications of activated carbons as adsorbents from olive stones. *Biomass Conversion and Biorefinery*, 9(4), 775-802. <https://doi.org/10.1007/s13399-019-00473-7>
- Saleh, T. A. (2022). *Surface Science of Adsorbents and Nanoadsorbents: Properties and Applications in Environmental Remediation*. Academic Press.
- Salgado, M. d. F., Abioye, A. M., Junoh, M. M., Santos, J. A. P., & Ani, F. N. (2018). Preparation of activated carbon from babassu endocarp under microwave radiation by physical activation. *IOP Conference Series: Earth and Environmental Science*,
- Sandeep, B. G. (2021). Reduction of greenhouse gas emission by carbon trapping concrete using carbon cure technology. *Applied Journal of Environmental Engineering Science*, 7(3), & al./Appl. J. Envir. Eng. Sci. 7 N° 3 (2021) 2306-2317.
- Sangare, D., Chartier, A., Moscossa-Santillan, M., Gökalp, I., & Bostyn, S. (2022). Kinetic studies of hydrothermal carbonization of avocado stone and analysis of the polycyclic aromatic hydrocarbon contents in the hydrochars produced. *Fuel*, 316. <https://doi.org/10.1016/j.fuel.2022.123163>
- Sangian, H. F., & Widjaja, A. (2018, 2018/02/01). The Effect of Alkaline Concentration on Coconut Husk Crystallinity and the Yield of Sugars Released. *IOP Conference Series: Materials Science and Engineering*, 306(1), 012046. <https://doi.org/10.1088/1757-899X/306/1/012046>

- Sarwar, A., Ali, M., Khoja, A. H., Nawar, A., Waqas, A., Liaquat, R., Naqvi, S. R., & Asjid, M. (2021). Synthesis and characterization of biomass-derived surface-modified activated carbon for enhanced CO<sub>2</sub> adsorption. *Journal of CO<sub>2</sub> Utilization*, *46*, 101476.
- Seema, H., Kemp, K. C., Le, N. H., Park, S.-W., Chandra, V., Lee, J. W., & Kim, K. S. (2014). Highly selective CO<sub>2</sub> capture by S-doped microporous carbon materials. *Carbon*, *66*, 320-326.
- Sees, M. D., Hamid, U., Otulana, Y., & Chen, C.-C. (2023). Comparison of Heterogeneous Langmuirian Models for Mixed-Gas Adsorption Equilibria. *Industrial & Engineering Chemistry Research*, *62*(18), 7160-7174.
- Serafin, J., Narkiewicz, U., Morawski, A. W., Wróbel, R. J., & Michalkiewicz, B. (2017). Highly microporous activated carbons from biomass for CO<sub>2</sub> capture and effective micropores at different conditions. *Journal of CO<sub>2</sub> Utilization*, *18*, 73-79.
- Sevilla, M., Parra, J. B., & Fuertes, A. B. (2013). Assessment of the role of micropore size and N-doping in CO<sub>2</sub> capture by porous carbons. *ACS applied materials & interfaces*, *5*(13), 6360-6368.
- Shahkarami, S., Dalai, A. K., & Soltan, J. (2016). Enhanced CO<sub>2</sub> adsorption using MgO-impregnated activated carbon: impact of preparation techniques. *Industrial & Engineering Chemistry Research*, *55*(20), 5955-5964.
- Sharma, A., Jindal, J., Mittal, A., Kumari, K., Maken, S., & Kumar, N. (2021). Carbon materials as CO<sub>2</sub> adsorbents: A review. *Environmental Chemistry Letters*, *19*, 875-910.
- Sharma, R., Jasrotia, K., Singh, N., Ghosh, P., Srivastava, S., Sharma, N. R., Singh, J., Kanwar, R., & Kumar, A. (2020). A comprehensive review on hydrothermal carbonization of biomass and its applications. *Chemistry Africa*, *3*, 1-19.
- Shayeganfar, F., Beheshtiyani, J., Neek-Amal, M., & Shamsavari, R. (2017). Electro-and opto-mutable properties of MgO nanoclusters adsorbed on mono-and double-layer graphene. *Nanoscale*, *9*(12), 4205-4218.
- Shen, Q., Zhu, X., Peng, Y., Xu, M., Huang, Y., Xia, A., Zhu, X., & Liao, Q. (2024). Structure evolution characteristic of hydrochar and nitrogen transformation mechanism during co-hydrothermal carbonization process of microalgae and biomass. *Energy*, *295*, 131028.
- Shen, Y., Zhang, N., & Fu, Y. (2019). Synthesis of high-performance hierarchically porous carbons from rice husk for sorption of phenol in the gas phase. *Journal of Environmental Management*, *241*, 53-58.

- Shi, J., Cui, H., Xu, J., & Yan, N. (2022). Carbon spheres synthesized from  $\text{KHCO}_3$  activation of glucose derived hydrochar with excellent  $\text{CO}_2$  capture capabilities at both low and high pressures. *Separation and Purification Technology*, 294, 121193.
- Shi, S., & Liu, Y. (2021). Nitrogen-doped activated carbons derived from microalgae pyrolysis by-products by microwave/KOH activation for  $\text{CO}_2$  adsorption. *Fuel*, 306, 121762.
- Shkir, M., AlAbdulaal, T., Manthrammel, M. A., & Khan, F. S. (2023). Novel MgO and Ag/MgO nanoparticles green-synthesis for antibacterial and photocatalytic applications: A kinetics-mechanism & recyclability. *Journal of Photochemistry and Photobiology A: Chemistry*, 115398.
- Shoab, M., & Al-Swaidan, H. M. (2015). Optimization and characterization of sliced activated carbon prepared from date palm tree fronds by physical activation. *biomass and bioenergy*, 73, 124-134.
- Sing, K. S. (1985). Reporting physisorption data for gas/solid systems with special reference to the determination of surface area and porosity (Recommendations 1984). *Pure and applied chemistry*, 57(4), 603-619.
- Singh, I., El-Emam, A. A., Pathak, S. K., Srivastava, R., Shukla, V. K., Prasad, O., & Sinha, L. (2019). Experimental and theoretical DFT (B3LYP, X3LYP, CAM-B3LYP and M06-2X) study on electronic structure, spectral features, hydrogen bonding and solvent effects of 4-methylthiadiazole-5-carboxylic acid. *Molecular Simulation*, 45(13), 1029-1043.
- Singh, J., Bhunia, H., & Basu, S. (2019). Adsorption of  $\text{CO}_2$  on KOH activated carbon adsorbents: Effect of different mass ratios. *Journal of environmental management*, 250, 109457.
- Skoulou, V., & Zabaniotou, A. (2007). Investigation of agricultural and animal wastes in Greece and their allocation to potential application for energy production. *Renewable and Sustainable Energy Reviews*, 11(8), 1698-1719.
- Song, X., Wang, L. a., Gong, J., Zhan, X., & Zeng, Y. (2020). Exploring a new method to study the effects of surface functional groups on adsorption of  $\text{CO}_2$  and  $\text{CH}_4$  on activated carbons. *Langmuir*, 36(14), 3862-3870.
- Soni, B., & Karmee, S. K. (2020). Towards a continuous pilot scale pyrolysis based biorefinery for production of biooil and biochar from sawdust. *Fuel*, 271, 117570.
- Stemann, J., Putschew, A., & Ziegler, F. (2013). Hydrothermal carbonization: process water characterization and effects of water recirculation. *Bioresource technology*, 143, 139-146.

- Sun, Y., Gao, B., Yao, Y., Fang, J., Zhang, M., Zhou, Y., Chen, H., & Yang, L. (2014). Effects of feedstock type, production method, and pyrolysis temperature on biochar and hydrochar properties. *Chemical Engineering Journal*, 240, 574-578.
- Sütçü, H. (2019). Production and characterization of activated carbons from *Rhododendron ponticum* L. by physical and chemical activation. *Biomass Conversion and Biorefinery*, 1-7.
- Taheri, F. S., Ghaemi, A., Maleki, A., & Shahhosseini, S. (2019). High CO<sub>2</sub> adsorption on amine-functionalized improved mesoporous silica nanotube as an eco-friendly nanocomposite. *Energy & Fuels*, 33(6), 5384-5397.
- Tahir, M. Y., Sillanpaa, M., Almutairi, T. M., Mohammed, A. A., & Ali, S. (2023). Excellent photocatalytic and antibacterial activities of bio-activated carbon decorated magnesium oxide nanoparticles. *Chemosphere*, 312, 137327.
- Tahmasebpour, M., Iranvandi, M., Heidari, M., Azimi, B., & Pevida, C. (2023). Development of novel waste tea-derived activated carbon promoted with SiO<sub>2</sub> nanoparticles as highly robust and easily fluidizable sorbent for low-temperature CO<sub>2</sub> capture. *Journal of Environmental Chemical Engineering*, 11(5), 110437.
- Tamilarasan, P., & Ramaprabhu, S. (2012). Polyaniline–magnetite nanocapsules based nanocomposite for carbon dioxide adsorption. *International Journal of Greenhouse Gas Control*, 10, 486-493.
- Tan, I., Ahmad, A., & Hameed, d. B. (2008). Preparation of activated carbon from coconut husk: optimization study on removal of 2, 4, 6-trichlorophenol using response surface methodology. *Journal of hazardous materials*, 153(1-2), 709-717.
- Tan, I. A. W., Abdullah, A. Z., Lim, L. L. P., & Yeo, T. H. C. (2017). Surface Modification and Characterization of Coconut Shell-Based. *Journal of Applied Science & Process Engineering*, 4(2), 186-194.
- Tan, Y. J., Li, M., Gunawan, G. A., Nyantakyi, S. A., Dick, T., Go, M.-L., & Lam, Y. (2020). Amide–amine replacement in indole-2-carboxamides yields potent mycobactericidal agents with improved water solubility. *ACS Medicinal Chemistry Letters*, 12(5), 704-712.
- Thubsuang, U., Manmuanpom, N., Chokaksornsans, N., Sommut, C., Singhawat, K., Payaka, A., Wongkasemjit, S., & Chaisuwan, T. (2023). Efficient CO<sub>2</sub> adsorption on porous carbon with nitrogen functionalities based on polybenzoxazine: high-pressure adsorption characteristics. *Applied Surface Science*, 607, 155120.

- Tiwari, D., Bhunia, H., & Bajpai, P. K. (2018). Development of chemically activated N-enriched carbon adsorbents from urea-formaldehyde resin for CO<sub>2</sub> adsorption: Kinetics, isotherm, and thermodynamics. *Journal of environmental management*, 218, 579-592.
- Tolkou, A. K., Trikalioti, S., Makrogianni, O., Trikkaliotis, D. G., Deliyanni, E. A., Kyzas, G. Z., & Katsoyiannis, I. A. (2023). Magnesium modified activated carbons derived from coconut shells for the removal of fluoride from water. *Sustainable Chemistry and Pharmacy*, 31, 100898.
- Travis, W., Gadipelli, S., & Guo, Z. (2015). Superior CO<sub>2</sub> adsorption from waste coffee ground derived carbons. *RSC advances*, 5(37), 29558-29562.
- Tun, H., & Chen, C.-C. (2021). Isothermic heat of adsorption from thermodynamic Langmuir isotherm. *Adsorption*, 27(6), 979-989.
- Ullah, S., ur Rehman, A., Najam, T., Hossain, I., Anjum, S., Ali, R., Shahid, M. U., Shah, S. S. A., & Nazir, M. A. (2024). Advances in metal-organic framework@ activated carbon (MOF@ AC) composite materials: Synthesis, characteristics and applications. *Journal of Industrial and Engineering Chemistry*.
- Vall, M., Hultberg, J., Strømme, M., & Cheung, O. (2019). Carbon dioxide adsorption on mesoporous magnesium carbonate. *Energy Procedia*, 158, 4671-4676.
- Van Tran, T., Bui, Q. T. P., Nguyen, T. D., Ho, V. T. T., & Bach, L. G. (2017). Application of response surface methodology to optimize the fabrication of ZnCl<sub>2</sub>-activated carbon from sugarcane bagasse for the removal of Cu<sup>2+</sup>. *Water science and technology*, 75(9), 2047-2055.
- Vega, E., Lemus, J., Anfruns, A., Gonzalez-Olmos, R., Palomar, J., & Martin, M. J. (2013). Adsorption of volatile sulphur compounds onto modified activated carbons: effect of oxygen functional groups. *Journal of hazardous materials*, 258, 77-83.
- Verougstraete, B., Gholami, M., Gomez-Rueda, Y., Pérez-Botella, E., Schoukens, M., Van Assche, T. R., & Denayer, J. F. (2024). Advancements and challenges in electric heating for enhanced temperature swing adsorption processes. *Separation and purification technology*, 128522.
- Viegas, C., Nobre, C., Mota, A., Vilarinho, C., Gouveia, L., & Gonçalves, M. (2021). A circular approach for landfill leachate treatment: Chemical precipitation with biomass ash followed by bioremediation through microalgae. *Journal of Environmental Chemical Engineering*, 9(3), 105187.
- Walton, K. S., Abney, M. B., & LeVan, M. D. (2006). CO<sub>2</sub> adsorption in Y and X zeolites modified by alkali metal cation exchange. *Microporous and Mesoporous Materials*, 91(1-3), 78-84.

- Wan Isahak, W. N. R., Ramli, Z. A. C., Mohamed Hisham, M. W., & Yarmo, M. A. (2013). Magnesium oxide nanoparticles on green activated carbon as efficient CO<sub>2</sub> adsorbent. *AIP Conference Proceedings*,
- Wang, C., Li, L., Shi, J., & Jin, H. (2021). Biochar production by coconut shell gasification in supercritical water and evolution of its porous structure. *Journal of Analytical and Applied Pyrolysis*, *156*, 105151.
- Wang, J., Chen, S., Xu, J.-y., Liu, L.-c., Zhou, J.-c., & Cai, J.-j. (2021). High-surface-area porous carbons produced by the mild KOH activation of a chitosan hydrochar and their CO<sub>2</sub> capture. *New Carbon Materials*, *36*(6), 1081-1090.
- Wang, L., Rao, L., Xia, B., Wang, L., Yue, L., Liang, Y., DaCosta, H., & Hu, X. (2018). Highly efficient CO<sub>2</sub> adsorption by nitrogen-doped porous carbons synthesized with low-temperature sodium amide activation. *Carbon*, *130*, 31-40.
- Wang, L., Yao, Y., Tran, T., Lira, P., PE, S. S., Davis, R., Sun, Z., Lai, Q., Toan, S., & Luo, J. (2023). Mesoporous MgO enriched in Lewis base sites as effective catalysts for efficient CO<sub>2</sub> capture. *Journal of Environmental Management*, *332*, 117398.
- Wang, L., Zhang, Y.-s., Jiang, H.-r., & Wang, H. (2020). Carbonyl-incorporated aromatic hyper-cross-linked polymers with microporous structure and their functional materials for CO<sub>2</sub> adsorption. *Industrial & Engineering Chemistry Research*, *59*(36), 15955-15966.
- Wang, Q., Wu, Z., Tay, H. H., Chen, L., Liu, Y., Chang, J., Zhong, Z., Luo, J., & Borgna, A. (2011). High temperature adsorption of CO<sub>2</sub> on Mg–Al hydrotalcite: effect of the charge compensating anions and the synthesis pH. *Catalysis Today*, *164*(1), 198-203.
- Wang, S.-C. (2021). Fine Activated Carbon from Rubber Fruit Shell Prepared by Using ZnCl<sub>2</sub> and KOH Activation. *Applied Sciences*, *11*(9), 3994.
- Wang, S., Nam, H., & Nam, H. (2020). Preparation of activated carbon from peanut shell with KOH activation and its application for H<sub>2</sub>S adsorption in confined space. *Journal of Environmental Chemical Engineering*, *8*(2), 103683.
- Wang, S., Xu, S., Gao, S., Xiao, P., Jiang, M., Zhao, H., Huang, B., Liu, L., Niu, H., & Wang, J. (2021). Simultaneous removal of SO<sub>2</sub> and NO<sub>x</sub> from flue gas by low-temperature adsorption over activated carbon. *Scientific Reports*, *11*(1), 11003.
- Wang, Z., Goyal, N., Liu, L., Tsang, D. C., Shang, J., Liu, W., & Li, G. (2020). N-doped porous carbon derived from polypyrrole for CO<sub>2</sub> capture from humid flue gases. *Chemical engineering journal*, *396*, 125376.

- Waters, C. L., Janupala, R. R., Mallinson, R. G., & Lobban, L. L. (2017). Staged thermal fractionation for segregation of lignin and cellulose pyrolysis products: An experimental study of residence time and temperature effects. *Journal of Analytical and Applied Pyrolysis*, 126, 380-389.
- Weber, S., Grande, P. M., Blank, L. M., & Klose, H. (2022). Insights into cell wall disintegration of *Chlorella vulgaris*. *PLoS One*, 17(1), e0262500.
- Wei, M., Marrakchi, F., Yuan, C., Cheng, X., Jiang, D., Zafar, F. F., Fu, Y., & Wang, S. (2022). Adsorption modeling, thermodynamics, and DFT simulation of tetracycline onto mesoporous and high-surface-area NaOH-activated macroalgae carbon. *Journal of hazardous materials*, 425, 127887.
- Weng, J., Wei, M.-M., Wu, S.-J., Liu, Y.-Q., Li, S.-R., Ye, Y.-Y., Wang, M., & Wang, D. (2019). High-value utilization of Citrus peel: efficient extraction of essential oil and preparation of activated carbon. *BioResources*, 14(2), 3899-3913.
- Wongcharee, S., Aravinthan, V., Erdei, L., & Sanongraj, W. (2018). Mesoporous activated carbon prepared from macadamia nut shell waste by carbon dioxide activation: Comparative characterisation and study of methylene blue removal from aqueous solution. *Asia-Pacific Journal of Chemical Engineering*, 13(2), e2179.
- Wu, L., Shang, Z., Wang, H., Wan, W., Gao, X., Li, Z., & Kobayashi, N. (2018). Production of activated carbon from walnut shell by CO<sub>2</sub> activation in a fluidized bed reactor and its adsorption performance of copper ion. *Journal of Material Cycles and Waste Management*, 20(3), 1676-1688.
- Wu, L., Sitamraju, S., Xiao, J., Liu, B., Li, Z., Janik, M. J., & Song, C. (2014). Effect of liquid-phase O<sub>3</sub> oxidation of activated carbon on the adsorption of thiophene. *Chemical engineering journal*, 242, 211-219.
- Wu, R., Ye, Q., Wu, K., Wang, L., & Dai, H. (2021). Highly efficient CO<sub>2</sub> adsorption of corn kernel-derived porous carbon with abundant oxygen functional groups. *Journal of CO<sub>2</sub> Utilization*, 51, 101620.
- Xia, Y., Mokaya, R., Walker, G. S., & Zhu, Y. (2011). Superior CO<sub>2</sub> adsorption capacity on N-doped, high-surface-area, microporous carbons templated from zeolite. *Advanced Energy Materials*, 1(4), 678-683.
- Xing, W., Liu, C., Zhou, Z., Zhang, L., Zhou, J., Zhuo, S., Yan, Z., Gao, H., Wang, G., & Qiao, S. Z. (2012). Superior CO<sub>2</sub> uptake of N-doped activated carbon through hydrogen-bonding interaction. *Energy & Environmental Science*, 5(6), 7323-7327.



- Yadavalli, G., Lei, H., Wei, Y., Zhu, L., Zhang, X., Liu, Y., & Yan, D. (2017). Carbon dioxide capture using ammonium sulfate surface modified activated biomass carbon. *Biomass and Bioenergy*, 98, 53-60.
- Yağmur, H. K., & Kaya, İ. (2021). Synthesis and characterization of magnetic ZnCl<sub>2</sub>-activated carbon produced from coconut shell for the adsorption of methylene blue. *Journal of molecular structure*, 1232, 130071.
- Yanai, T., Tew, D. P., & Handy, N. C. (2004). A new hybrid exchange–correlation functional using the Coulomb-attenuating method (CAM-B3LYP). *Chemical physics letters*, 393(1-3), 51-57.
- Yang, C., Wang, Y., Fan, H., de Falco, G., Yang, S., Shangguan, J., & Bandoz, T. J. (2020). Bifunctional ZnO-MgO/activated carbon adsorbents boost H<sub>2</sub>S room temperature adsorption and catalytic oxidation. *Applied Catalysis B: Environmental*, 266, 118674.
- Yang, F., Li, W., Zhong, X., Tu, W., Cheng, J., Chen, L., Lu, J., Yuan, A., & Pan, J. (2022). The alkaline sites integrated into biomass-carbon reinforce selective adsorption of acetic acid: In situ implanting MgO during activation operation. *Separation and purification technology*, 297, 121415.
- Yang, F., Wang, J., Liu, L., Zhang, P., Yu, W., Deng, Q., Zeng, Z., & Deng, S. (2018). Synthesis of porous carbons with high N-content from shrimp shells for efficient CO<sub>2</sub>-capture and gas separation. *ACS Sustainable Chemistry & Engineering*, 6(11), 15550-15559.
- Yang, G., Liu, H., Li, Y., Zhou, Q., Jin, M., Xiao, H., & Yao, H. (2022). Kinetics of hydrothermal carbonization of kitchen waste based on multi-component reaction mechanism. *Fuel*, 324, 124693.
- Yang, J., Yue, L., Hu, X., Wang, L., Zhao, Y., Lin, Y., Sun, Y., DaCosta, H., & Guo, L. (2017). Efficient CO<sub>2</sub> capture by porous carbons derived from coconut shell. *Energy & Fuels*, 31(4), 4287-4293.
- Yang, T., & Lua, A. C. (2006). Textural and chemical properties of zinc chloride activated carbons prepared from pistachio-nut shells. *Materials chemistry and physics*, 100(2-3), 438-444.
- Yang, Z., Zhang, G., Xu, Y., & Zhao, P. (2019). One step N-doping and activation of biomass carbon at low temperature through NaNH<sub>2</sub>: An effective approach to CO<sub>2</sub> adsorbents. *Journal of CO<sub>2</sub> Utilization*, 33, 320-329.
- Yek, P. N. Y., Liew, R. K., Osman, M. S., Lee, C. L., Chuah, J. H., Park, Y.-K., & Lam, S. S. (2019). Microwave steam activation, an innovative pyrolysis approach to convert waste palm shell into highly microporous activated carbon. *Journal of environmental management*, 236, 245-253.

- Yek, P. N. Y., Peng, W., Wong, C. C., Liew, R. K., Ho, Y. L., Mahari, W. A. W., Azwar, E., Yuan, T. Q., Tabatabaei, M., & Aghbashlo, M. (2020). Engineered biochar via microwave CO<sub>2</sub> and steam pyrolysis to treat carcinogenic Congo red dye. *Journal of hazardous materials*, 395, 122636.
- Yong, Z. J., Bashir, M. J., Ng, C. A., Sethupathi, S., Lim, J. W., & Show, P. L. (2019). Sustainable waste-to-energy development in Malaysia: Appraisal of environmental, financial, and public issues related with energy recovery from municipal solid waste. *Processes*, 7(10), 676.
- Yorgun, S., & Yıldız, D. (2015). Preparation and characterization of activated carbons from Paulownia wood by chemical activation with H<sub>3</sub>PO<sub>4</sub>. *Journal of the Taiwan Institute of Chemical Engineers*, 53, 122-131.
- You, X., Yang, L., Zhou, X., & Zhang, Y. (2022). Sustainability and carbon neutrality trends for microalgae-based wastewater treatment: a review. *Environmental Research*, 209, 112860.
- Yu, H., Wang, W., Lin, F., Li, K., Yan, B., Song, Y., Huang, C., & Chen, G. (2021). A facile and green strategy to synthesize N/P co-doped bio-porous carbon with high yield from fungi residue for efficient VOC adsorption. *Separation and Purification Technology*, 276, 119291.
- Yuan, X., Tong, J., Zeng, G., Li, H., & Xie, W. (2009). Comparative studies of products obtained at different temperatures during straw liquefaction by hot compressed water. *Energy & fuels*, 23(6), 3262-3267.
- Yue, L., Xia, Q., Wang, L., Wang, L., DaCosta, H., Yang, J., & Hu, X. (2018). CO<sub>2</sub> adsorption at nitrogen-doped carbons prepared by K<sub>2</sub>CO<sub>3</sub> activation of urea-modified coconut shell. *Journal of colloid and interface science*, 511, 259-267.
- Yusup, S., Khan, Z., Ahmad, M. M., & Rashidi, N. A. (2014). Optimization of hydrogen production in in-situ catalytic adsorption (ICA) steam gasification based on Response Surface Methodology. *biomass and bioenergy*, 60, 98-107.
- Zaccariello, L., Battaglia, D., Morrone, B., & Mastellone, M. (2022). Hydrothermal carbonization: a pilot-scale reactor design for bio-waste and sludge pre-treatment. *Waste and Biomass Valorization*, 13(9), 3865-3876.
- Zaini, M. A. A., Zhi, L. L., Hui, T. S., Amano, Y., & Machida, M. (2021). Effects of physical activation on pore textures and heavy metals removal of fiber-based activated carbons. *Materials Today: Proceedings*, 39, 917-921.
- Zhang, H., Yan, Y., & Yang, L. (2010). Preparation of activated carbon from sawdust by zinc chloride activation. *Adsorption*, 16(3), 161-166.

- Zhang, Y., Song, X., Xu, Y., Shen, H., Kong, X., & Xu, H. (2019). Utilization of wheat bran for producing activated carbon with high specific surface area via NaOH activation using industrial furnace. *Journal of Cleaner Production*, 210, 366-375.
- Zhao, W., Huang, Z., Shen, H., Li, X., Zhao, S., Xie, B., & Xia, S. (2024). Density functional theory study of CO<sub>2</sub> adsorption on metal (M= Li, Al, K, Ca) doped MgO. *Molecular Catalysis*, 553, 113708.
- Zhao, W., Yang, Z., Liu, S., & Ren, A. (2019). Composition and combustion dynamics analysis of typical crop straws. *Journal of Agro-Environment Science*, 38(4), 921-927.
- Zhao, Y., Shen, Y., & Bai, L. (2012). Effect of chemical modification on carbon dioxide adsorption property of mesoporous silica. *Journal of colloid and interface science*, 379(1), 94-100.
- Zhou, K., Li, L., Ma, X., Mo, Y., Chen, R., Li, H., & Li, H. (2018). Activated carbons modified by magnesium oxide as highly efficient sorbents for acetone. *RSC advances*, 8(6), 2922-2932.
- Zhu, D., Yang, H., Chen, X., Chen, W., Cai, N., Chen, Y., Zhang, S., & Chen, H. (2021). Temperature-dependent magnesium citrate modified formation of MgO nanoparticles biochar composites with efficient phosphate removal. *Chemosphere*, 274, 129904.
- Zubbri, N. A., Mohamed, A. R., Lahijani, P., & Mohammadi, M. (2021). Low temperature CO<sub>2</sub> capture on biomass-derived KOH-activated hydrochar established through hydrothermal carbonization with water-soaking pre-treatment. *Journal of Environmental Chemical Engineering*, 9(2), 105074.
- Zubkova, V., Strojwas, A., Bielecki, M., Kieush, L., & Koverya, A. (2019). Comparative study of pyrolytic behavior of the biomass wastes originating in the Ukraine and potential application of such biomass. Part 1. Analysis of the course of pyrolysis process and the composition of formed products. *Fuel*, 254, 115688.
- Zulkurnai, N., Ali, U. M., Ibrahim, N., & Manan, N. A. (2017). Carbon dioxide (CO<sub>2</sub>) adsorption by activated carbon functionalized with deep eutectic solvent (DES). IOP Conference Series: Materials Science and Engineering,

## LIST OF PUBLICATIONS AND PAPERS PRESENTED

### Journal Article Publication

1. **Azmi, N. Z. M.**, Buthiyappan, A., Patah, M. F. A., Rashidi, N. A., & Raman, A. A. A. (2024). Enhancing the CO<sub>2</sub> Adsorption with Dual Functionalized Coconut Shell-Hydrochar using Chlorella Microalgae and Metal Oxide: Synthesis, Physicochemical Properties & Mechanism Evaluations. *Journal of Cleaner Production*, 142736.
2. **Azmi, N. Z. M.**, Buthiyappan, A., Raman, A. A. A., Patah, M. F. A., & Sufian, S. (2022). Recent advances in biomass based activated carbon for carbon dioxide capture—A review. *Journal of Industrial and Engineering Chemistry*, 116, 1-20.
3. **Azmi, N. Z. M.**, Raman, A. A. A., Rashidi, N. A., Patah, M. F. A., & Buthiyappan, A. (2023, December). Activated Hydrochar Derived from Coconut Shell and Microalgae through Hydrothermal Carbonisation for the CO<sub>2</sub> Adsorption. In *IOP Conference Series: Earth and Environmental Science* (Vol. 1281, No. 1, p. 012018). IOP Publishing.
4. Zhang, X. G., Buthiyappan, A., **Mohd Azmi, N. Z.**, & Abdul Raman, A. A. (2024). Towards circular carbon economy: recent developments and techno-economic assessment of integrated carbon dioxide capture and utilisation. *Chemical Papers*, 1-10.
5. **Mohd Azmi, N. Z.**, Buthiyappan, A., Ng, W. S., & Abdul Raman, A. A. (2023, December). Green Solution for Pollution Remediation: Biomass-Based Adsorbent Impregnated with Aluminum Oxide. In *International Conference on Advanced Materials and Engineering Materials* (pp. 67-76). Singapore: Springer Nature Singapore. Scopus indexed

## **Paper Presented**

1. Activated Hydrochar Derived from Coconut Shell and Microalgae through Hydrothermal Carbonisation for the CO<sub>2</sub> Adsorption. 6<sup>th</sup> International Conference on Clean Energy and Technology (CEAT) 2023, 7-8<sup>th</sup> June 2023, Bayview Hotel Georgetown Penang, Malaysia.
2. Evaluation of Biochar Derived Through Hydrothermal Carbonization and Pyrolysis of Microalgae. 6<sup>th</sup> International Conference on Sustainable Energy, Infrastructure & Environment (ICSEIE) 2024, 14-15<sup>th</sup> October 2024, Putrajaya, Malaysia.

Universiti Malaysia